2015

Intensity based interrogation of optical fibre sensors for industrial automation and intrusion detection systems

Gary Andrew Allwood
Edith Cowan University

2015

Intensity based interrogation of optical fibre sensors for industrial automation and intrusion detection systems

Gary Andrew Allwood
Edith Cowan University

Edith Cowan University

Copyright Warning

INTENSITY BASED INTERROGATION OF OPTICAL FIBRE SENSORS FOR INDUSTRIAL AUTOMATION AND INTRUSION DETECTION SYSTEMS

Gary Allwood

This thesis is presented in fulfilment of the requirements for the degree of
Doctor of Philosophy

School of Engineering
Faculty of Health, Engineering, and Science
Edith Cowan University

October 2, 2015

USE OF THESIS

The Use of Thesis statement is not included in this version of the thesis.

ABSTRACT

In this study, the use of optical fibre sensors for intrusion detection and industrial automation systems has been demonstrated, with a particular focus on low cost, intensity-based, interrogation techniques. The use of optical fibre sensors for intrusion detection systems to secure residential, commercial, and industrial premises against potential security breaches has been extensively reviewed in this thesis. Fibre Bragg grating (FBG) sensing is one form of optical fibre sensing that has been underutilised in applications such as in-ground, in-fence, and window and door monitoring, and addressing that opportunity has been a major goal of this thesis. Both security and industrial sensor systems must include some centralised intelligence (electronic controller) and ideally both automation and security sensor systems would be controlled and monitored by the same centralised system. Optical fibre sensor systems that could be used for either application have been designed, developed, and tested in this study, and optoelectronic interfaces for integrating these sensors with electronic controllers have been demonstrated. The versatility of FBG sensors means that they are also ideal for certain mainstream industrial applications.

Two novel transducers have been developed in this work; a highly sensitive low pressure FBG diaphragm transducer and a FBG load cell transducer. Both have been designed to allow interrogation of the optical signal could occur within the housing of the individual sensors themselves. This is achieved in a simple and low cost manner that enables the output of the transducers to be easily connected to standard electronic controllers, such as programmable logic controllers. Furthermore, some of the nonlinear characteristics of FBG sensors have been explored with the aim of developing transducers that are inherently decoupled from strain and temperature interference. One of the major advantages of optical fibre sensors is their ability to be both time division and wavelength division multiplexed. The intensity-based interrogation techniques used here complement this attribute and are a major consideration when developing the transducers and optoelectronic circuits. A time division multiplexing technique, using

transmit-reflect detection and incorporating a dual bus, has also been developed. This system architecture enables all the different optical fibre transducers on the network to have the same Bragg wavelength and hence the number of spare replacement transducers required is minimal. Moreover, sensors can be replaced in an online control system without disrupting the network. In addition, by analysing both the transmitted and reflected signals, problems associated with optical power fluctuations are eliminated and the intensity of the sensor signals is increased through differential amplification.

Overall, the research addresses the limitations of conventional electrical sensors, such as susceptibility to corrosive damage in wet and corrosive environments, and risk of causing an explosion in hazardous environments, as well as the limitations of current stand-alone optical fibre sensor systems. This thesis supports more alert, reliable, affordable, and coordinated, control and monitoring systems in an on-line environment.

DECLARATION

I certify that this thesis does not, to the best of my knowledge and belief:

(i) incorporate without acknowledgement any material previously submitted for a degree or diploma in any institution of higher education;

(ii) contain any material previously published or written by another person except where due reference is made in the text; or

(iii) contain any defamatory material.

I also grant permission for the Library at Edith Cowan University to make duplicate copies of my thesis as required.

Signature.....

Date.....

ACKNOWLEDGEMENTS

I wish to acknowledge the ongoing guidance and assistance of my principle supervisor Assoc. Prof. Steven Hinckley and my associate supervisor Dr Graham Wild. They have both dedicated their time to ensure my research has progressed by motivating and challenging me to excel. Their support throughout my PhD candidature has been outstanding and will always be remembered and appreciated.

I would also like to acknowledge the technical and moral support of Dr Steven Richardson, Dr Alex Lubansky, Dr Octavian Bass, and Assoc. Prof. Ute Muller, whom have willingly given up their time to assist me in my work. I must also thank Mr Trevor Bloch for his financial investment, validating the significance of my research in industry.

I'd especially like to acknowledge my family for their support and patience throughout the last four years and for not giving up on me. Specifically, my mother for her ongoing belief in my ability and my partner for sacrificing many of life's luxuries so that I may complete my doctorate.

Finally, I'd like to dedicate this work to my daughter, who at the age of four has only ever known her father as a PhD student, and to my unborn son, who will be with us in a few months. They have both inspired me to push through the hard times and taught me to enjoy the little things in life.

Contents

LIST OF PUBICATIONS FROM WORK CONTAINED IN THIS THESIS

Allwood, Wild, Lubasnsky, & Hinckley (2015). *A highly sensitive fiber Bragg grating Diaphragm Pressure Transducer.* Accepted for publication in Optical Fiber Technology.

Allwood, Wild, & Hinckley (2015). *Fiber Bragg grating sensing in mainstream industrial processes.* Submitted to IEEE Industrial Applications.

Allwood, Wild, & Hinckley (2015). *Optical fiber sensors in intrusion detection system: A review and forecast.* Submitted to IEEE Sensors.

Allwood, Wild, & Hinckley (2015). *Universal Signal Conditioning Technique for Optical Fiber Sensors in PLC and SCADA Applications.* Submitted to IEEE Transaction on Industrial Electronics.

Allwood, Wild, & Hinckley (2013). *Optical fiber Bragg grating based intrusion detection systems for homeland security.* Proc. Sensor Applications Symposium (SAS 2013).

Allwood, Wild, & Hinckley (2012). *A comparison of InGaAs and Ge photonic power converters for long wavelength power-over-fibre.* Proc. Conference on Optoelectronic and Microelectronic Materials and Devices (COMMAD 2012).

Allwood, Wild, & Hinckley (2012). *Wavelength division multiplexing of a fibre Bragg grating sensor using transmit-reflect detection system.* Proc. 37th Australian Conference on Optical Fibre Technology (ACOFT 2012).

Allwood, Wild, & Hinckley (2012). *In-Ground Optical Fibre Bragg Grating Pressure Switch for Security Applications.* Proc. 3rd Asia-Pacific Optical Sensors Conference 2012 (APOS 2012).

Allwood, Wild, & Hinckley (2011). *Programmable logic controller optical fibre sensor interface module*. Proc. SPIE 2011.

Allwood, Wild, & Hinckley (2011). *A comparison of silicon and germanium photovoltaic power conversion for power-over-fibre*. Proc. SPIE 2011.

Allwood, Wild, & Hinckley (2011). *Programmable Logic Controller Based Fibre Bragg Grating In-ground Intrusion Detection System*. Proc. 2011 Australian Security Congress (SECAU 2011).

Allwood, Wild, & Hinckley (2011). *Fibre Optic Acoustic Sensing for Intrusion Detection Systems*. Proc. Acoustics 2011.

LIST OF ADDITIONAL PUBLICATIONS

Allwood, Wild, & Hinckley (2011). *Power over fibre: Material properties of homojunction photovoltaic micro-cells*. Proc. IEEE 6th International Symposium on Electronic Design, Test and Application (DELTA 2011).

Wild, Allwood, & Hinckley (2010). *Distributed sensing, communications, and power in optical fibre smart sensor networks for structural health monitoring*. Proc. Sixth International Conference on Intelligent Sensors, Sensor Networks and Information Processing (ISSNIP 2010).

Allwood, Wild, & Hinckley (2010). *Photovoltaic micro-cell for distributed power in sensor networks*. Proc. Conference on Optoelectronic and Microelectronic Materials and Devices (COMMAD 2010).

Allwood, Wild, & Hinckley (2010). *Photovoltaic micro-cell design for distributed power-over-fibre optimized for 850nm & 980nm*. Proc. 19th Australian Institute of Physics Congress (AIP 2010).

Allwood, Wild, & Hinckley (2010). *Power-over-fibre for distributed optical fibre smart sensor networks*. Proc. 35th Australian Conference on Optical Fibre Technology (ACOFT 2010).

ABBREVIATIONS

AE	Acoustic Emission
AIP	American Institute of Physics
AOCS	All Optical Control System
BODTR	Brillioun Optical Time-Domain Reflectometry
CAGR	Compound Annual Growth Rate
DCS	Distributed Control System
DMM	Digital Multimeter
DP	Decentralised Peripheral
DSO	Digital Storage Oscilloscope
EMI	Electromagnetic Interference
FAR	False Alarm Rate
FBG	Fibre Bragg Grating
FFP	Fibre Fabry-Perot
FOS	Fibre Optic Sensor
FPGA	Field programmable Gate Array
FSIM	Fibre Sensor Integrated Monitor
FWHM	Full Width Half Maximum
GTE	General Telephone & Electronics
HART	Highway Addressable Remote Transducer
HMI	Human Machine Interface
HVAC	Heating Ventilation and Air Conditioning
IDS	Intensiometric Detection System
IEEE	Institute of Electrical and Electronic Engineers
IOP	Institute Of Physics
LPG	Long Period Grating

MM	Multimode
NAR	Nuisance Alarm Rate
NBN	National Broadband Network
NCAP	Network Capable Application Processor
OFS	Optical Fibre Sensing
OSA	Optical Spectrum Analyser
OTDR	Optical Time-Domain Reflectometry
PA	Process Automation
PCC	Photovoltaic Power Converter
PCF	Photonic Crystal Fibre
PIDS	Physical Intrusion Detection System
PLC	Programmable Logic Controller
PM	Polarisation Maintaining
POD	Probability Of Detection
PODTR	Polarisation Optical Time-Domain Reflectometry
PZT	Piezo-Electric Transducer
RTU	Remote Terminal Unit
SCADA	Supervisory Control And Data Acquisition
SCC	Security Control Centre
SFBG	Superstructured Fibre Bragg Grating
SLD	Superluminescent Diode
SM	Single Mode
SPIE	Society for Photo-Instrumentation Engineers
STIM	Smart Transducer Interface Module
TDM	Time Division Multiplexing
TRDS	Transmit Reflect Detection System
WDM	Wavelength Division Multiplexing

Chapter 1

Introduction

In this chapter, an overview of the project is given, along with a relevant background to fibre optic sensing in the process control and security industries. The main aim, significance, status and problems associated with the project are also discussed, and the chapter concludes with the objectives and research questions.

1.1 Overview

The use of optical fibres in communication applications has increased dramatically in recent years due to their ability to offer faster transmission rates and immunity to electromagnetic interference (EMI) [1]. In particular, the roll-out of the National Broadband Network (NBN) within Australia, will ensure the growth will continue for years to come, and the number of trained technicians and installers of optical fibre systems is increasing significantly because of this demand. These changes in communication standards also have a knock-on effect in optical fibre sensing (OFS) systems, in that optical fibre components have become cheaper and there are more qualified fibre installation technicians. More importantly, many of the common problems associated with optical fibre systems have been solved. These include packaging the fibres correctly so that they are environmentally rugged, and that relatively simple techniques are available for quality testing, as well as splicing and repairing of the fibres.

It is well understood that electronic sensors have limited capabilities in certain con-

ditions, such as harsh environments, where there is risk of sparks causing an explosion, in extreme temperatures and pressures [2], or high EMI, such as overhead transmission lines [3]. These are the areas where fibre optic sensors (FOS) offer an attractive alternative due to their small size and weight, immunity to EMI, and needing no power supply [4]. Similarly, FOS could replace electronic sensors in more mainstream applications because of other desirable attributes: low cost, high sensitivity, and passive nature [5]. Provided the sensors have similar physical properties to electronic sensors, such that they can be easily installed and removed, are as rugged as their electronic counterparts, and the complexity and cost of OFS systems is comparable to equivalent electrical systems, optical fibre systems could potentially replace many electrical systems in the future.

The distributed FOS market was $585M in 2013 and projected to be US$1.458bn in 2018 with one of the major applications being process control [6]. The global process automation market revenue is expected to grow from $86.1bn in 2012, to $124.3bn in 2018, at an estimated compound annual growth rate (CAGR) of 6.05% from 2013 to 2018. Also, the process instrumentation market is expected to grow from $26.5bn in 2012, to $36.7bn in 2018, with a CAGR of 5.07% [7]. Nevertheless, in general, FOS are underutilised in security and process control applications as simpler traditional sensing techniques, based on well established industrial standards, are preferred.

Where FOS are used in these applications, usually, the sensors are on the end of an optical fibre, where the fibre is simply used as the data transmission medium. This method completely eliminates many of the advantages of the fibre itself. Hence distributed or quasi-distributed OFS techniques should be implemented to take advantage of the fibre attributes and become the common practice for smart sensor networks of the future.

Current state-of-the-art OFS work is primarily based on optical fibre Bragg gratings (FBGs) which are embedded within the fibre itself and do not require an external power supply. Whilst this technology has many advantages, it is underutilised in some applications, as there are significant problems that need to be addressed in order to

make it a cost effective solution.

FBG sensors exhibit all of the benefits associated with FOS, not least their ability to be multiplexed [8]. Many different FBG sensors have been developed with almost all measurands being manipulated to cause either a change in the effective refractive index or in the grating period of the FBG, or both. These measurands include temperature, strain, level, flow, and pressure [9]. Most of these variables can be measured using a bare fibre FBG, although the sensitivity and dynamic range of these sensors would be essentially fixed without the development of appropriate transducers. By designing proper mechanical systems in conjunction with FBG sensing technology, highly sensitive instruments with the desired attributes for any given application can be obtained. Furthermore, by manipulating the optical response of the FBG it is possible to use simpler interrogation techniques rather than being forced to use expensive solid state optical interrogators.

The main problem is the complexity and cost associated with combining optical systems with existing electrical systems. Hence, current commercial FOS interrogators are expensive standalone systems that require knowledge of optical engineering. Moreover, it is currently impossible to perform optical actuation; hence there is always a need to convert back from the optical domain to the electrical domain.

The solution, as outlined in this thesis, is to develop OFS and interrogation systems that are directly compatible with current electronic controllers. Programmable Logic Controllers (PLCs) are used in a wide variety of industries from factory assembly lines to controlling lifts in buildings, and controlling large mine sites, as well as commercial security applications. In addition, low cost microcontrollers are now widely used in customised home automation and security systems. The development of optical fibre based sensing systems that are compatible with current electronic systems is essential to ensuring the benefits associated with optical fibre sensors penetrate these mainstream applications.

It is the intention here, to develop new optical sensing and interrogation techniques and integrate them seamlessly with existing control systems to create an almost en-

tirely optical control system, by connecting the OFS directly to PLCs, for industrial applications, and microcontrollers for residential applications.

1.2 Background

A FOS is a transducer which uses light either inside of, or from, an optical fibre to measure a physical dimension by converting it into an optical dimension. The challenge is often, the conversion of the optical dimension into the electrical dimension for easy interpretation through a computer.

FOS have been reported since the late 1970s and are used for a wide variety of applications from static and dynamic strain sensing to chemical and biological sensing. Within the scope of OFS, there are a number of well developed techniques from interferometry and interference to fibre grating technologies. Each of the techniques have their own benefits and associated problems, which will be discussed throughout the literature review section of this thesis. All optical fibre sensors have common advantages over other sensing methodologies, which include greater sensitivity, reduced size and weight, and immunity to electromagnetic interference. However, FBG sensors are particularly versatile and as such a multitude of different transducers have been reported in the literature since they were first invented by Morey, Meltz and Glenn in 1989.

A FBG is a spectrally reflective component written into the core of the fibre that uses the principle of Fresnel reflection. The grating consists of alternating regions of high and low refractive indices. The periodic grating acts as a filter, reflecting a narrow wavelength range, centred about a peak wavelength. This wavelength is known as the Bragg wavelength. Any measurand that has the ability to affect either the refractive index or the grating period, or both, can be measured using a FBG as a sensor. Specifically, a FBG is sensitive to strain and temperature.

Although OFS techniques are currently used in a large variety of applications, this study will focus on residential, commercial and industrial security applications, as well as FOS in the process control industry. Further, the main body of this work focuses on

the application of FBG technology in relation to these applications.

1.2.1 Security

The most obvious form of security for a domestic or commercial property is a physical barrier, such as a wall with barbed wire or broken glass on top. However, this method is not always practical, nor aesthetically pleasing. A slightly more subtle approach is to utilise a fence as a physical barrier, although it would be necessary to know if an intruder has breached the fence. Moreover, for residential applications, a fence may also not be appropriate, and therefore window and door locks may be used to prevent an intruder from entering. Again, it would be desirable to know if an intruder has attempted to break in. In addition, advanced security systems may be able to detect the presence of a potential intruder before a security breach has occurred. This is the role of intrusion detection sensors.

There are a number of different methods currently used, whether electronic or optical in nature, for detection of unwanted intruders which include in-ground intrusion detection, breaching of a perimeter fence, window and door breach detectors, as well as surveillance cameras. The intention for in-ground techniques is to detect the presence of an intruder by sensing the vibrations made by a person walking. A perimeter fence is used to prevent an intruder accessing a forbidden area; sensors are therefore required for detecting a breach of the perimeter by either climbing over or cutting through the fence. Electrical reed switches are commonly used to detect window and door breaches, however, as discussed later in this thesis, optical fibre based reed switches can also be realised. Optical fibre based acoustic glass break detectors are also discussed.

In general, FOS are greatly underutilized in security applications. Where they are used, older optical fibre sensing techniques are typically used, such as scattering and interferometry. Here, it will be demonstrated that FBG sensors offer an attractive alternative with the sensor information easily connected to a standard electronic controller or a security control centre (SCC).

1.2.2 Process Control

Most automated industrial processes use Distributed Control Systems (DCSs) or PLCs for automated control. Both systems are very similar, although DCSs were generally preferred in the past, depending on the application, as they were more sophisticated than PLCs and could control much larger plants. However, PLCs have recently tended to be more common as they have much of the functionality of DCSs, such as distributed I/O racks, etc, but are generally cheaper to install and maintain. PLCs, in conjunction with a human machine interface (HMI), form the basis of Supervisory Control And Data Acquisition (SCADA) systems, combined with communication infrastructure and Remote Terminal Units (RTUs). RTUs basically convert different sensor measurands in to digital data that are sent back to the PLC or supervisory system.

PLCs are also found in niche residential control applications, where they can be used to control a variety of systems within the home. In particular, PLCs can be used to control conventional residential security systems or as the basis for home automation systems. However, microcontrollers are more commonly used as they are simpler to implement and modify, as well being significantly lower in cost.

Whilst a large range of FOS are used in the process control industry, currently, industrial FOS either convert the optical signal to an electrical signal locally at the sensor, or use an RTU before the data are sent back to the PLC. This method eliminates many of the desired properties of the optical fibre itself as the data are transmitted over copper cables. This thesis will concentrate on the use of FBG sensors in the process control industry, specifically the interrogation of the optical signal and its conversion into the optical domain for seamless integration with electronic controllers.

1.3 Aims

The main aim of this project is to investigate the use of FOS in process control and security applications, expand on existing OFS technology through the development of new, novel transducers and interrogation techniques, and attempt to bridge the gap between the emerging sensing technologies and the conventional approaches taken in industry.

1.4 Significance

The primary significance of creating an entirely optical control system for both security and process control applications is the advantageous properties of light and optical fibres, including [1];

- greater sensitivity,
- reduced size and weight,
- environmental ruggedness,
- reduced cost,
- signal security, since the signal is confined to the fibre,
- speed of transmission,
- compatibility with optical communication and telemetry systems, and,
- immunity to electromagnetic interference.

Moreover, almost all traditional sensors can now be replaced by FOS. These include; temperature, strain, vibration, level, pressure, chemical, electrical and magnetic field, rotation, and acceleration, among others [4].

1.5 Status

Traditional sensing techniques have previously been preferred as they have been proven to be robust, fulfilled requirements in terms of sensitivity, and were cost effective. However, as more diverse sensing application emerge, more sophisticated technology is required. Additionally, as the technology has matured, the cost of optical components has significantly reduced. Furthermore, optical fibres are now commonly used for communication, meaning existing fibres can be used for sensing and providing power.

1.6 Motivations

The primary motivations behind this type of work are to achieve more intelligent, robust and safer systems with reduced risk of tampering, as well as, reduced risk of damage to machinery and personnel, at a reduced cost, in addition to increased redundancy resulting in less downtime.

1.7 Objectives

1.7.1 Primary Objectives

- To develop new FBG based transducers for process control applications that are compatible with electronic controllers.
- To create an in-ground FBG based acoustic physical intrusion detection system.
- To create an in-ground FBG pressure switch .
- To create a FBG perimeter fence detector.
- To show that optical fibre reed switches are effective for securing windows and doors.
- To perform intensity based multiplexing of an array of sensors.

1.7.2 Secondary Objective

- To create a simple generic optical fibre sensing interface module with many sensors, combining both wavelength division multiplexing (WDM) and time division multiplexing (TDM).

1.8 Research Questions

1.8.1 Primary Research Questions

1. Can highly sensitive, low cost transducers with on-board optical interrogation be developed?

2. Can the acoustic emissions of an intruder's footsteps be detected using an in-ground FBG IDS and what flooring materials are best suited for this?

3. Are FBG based perimeter fence sensors and FBG based reed switches effective at detecting intruders and what are the limitations?

1.8.2 Secondary Research Question

1. Are FBG sensors a viable and cost effective solution for advanced sensing in process control and security applications?

1.9 Thesis Outline

This thesis consists of twelve chapter. Chapters 1, 2 and 3 include a general introduction, theory and literature review. The literature review itself, whilst being one continuous chapter, is separated into three distinct sections of which two have been submitted as review articles in relevant journals.

Chapters 4 and 5 focus on FBG sensing for intrusion detection applications. Chapter 4 shows acoustic vibrations from potential intruders can be detected through a number

of different flooring materials. Chapter 5 describes the developments of a complete FBG based physical intrusion detection system (PIDS). The experimental results show FBG sensors can be used as in-ground, fence mounted, and in window and door sensors and interrogated using a transmit-reflect detection system (TRDS).

Chapters 6 and 7 consists of experimental work performed on the development of specific transducers utilising low cost interrogation techniques for mainstream industrial applications. Chapter 6 details development of a highly sensitive rubber diaphragm transducer, with the results submitted to the Optical Fiber Technology journal. Since the study was performed, it has become the basis for future work, in collaboration with an industry partner, for the development of real-time monitoring of ocean wave pressures on large diaphragm pumps in wave energy harvesting. Chapter 7 describes a temperature in-sensitive load cell transducer, which utilises two FBGs in a push-pull configuration for on board optical interrogation. The transducer was specifically designed for easy connection to standard electronic controllers.

Chapter 8 reports results from experimental work on the non-linear characteristics of FBGs. The results suggest advanced transducers could be developed which exploit the non-linearities for direct isolation of temperature and strain.

Chapter 9 specifically details experimental work performed on multiplexing incorporating transmit-reflect detection. The first part of the chapter shows that a FBG sensor signal can be multiplexed using dense wavelength division multiplexing (DWDM) and detected using a TRDS, as a proof of concept. The second part of the chapter describes a time division multiplexing (TDM) technique using a dual bus configuration. This particular method addresses many of the issues of FOS proposed by industry, and is the subject of an ongoing research and development project with field trials expected later in 2015.

Chapters 10 and 11 describe the initial developments towards a low cost optoelectronic interface for FBG sensors with standard industrial controllers. It is demonstrated in Chapter 10 that the change in Bragg wavelength of an arbitrary sensor can be easily converted into a 4-20mA industrial standard and connected to an electronic control

system, with the process variable displayed through a SCADA system. The first part of chapter 11 shows the output of a digital in ground pressure switch can be connected to an industrial controller and the alarm displayed on a human machine interface. Furthermore, the development of a smart FBG optoelectronic interface through an industry standard fieldbus protocol is also demonstrated. The second part of the chapter demonstrates multiple FBG sensor signals, from the transducers developed can be multiplexed over the same fibre using WDM and connected to low cost microcontroller. The individual process variables could then easily be incorporated into a wireless sensor network or simply sent over a wireless network to the main control centre. This work shows the potential for low cost hybrid wireless and FBG sensor networks.

Chapter 12 concludes the thesis with a general discussion of the findings and direction of future work.

Chapter 2

Theory

This chapter outlines the basic theory of FOS, with an emphasis on FBGs. It is intended that the information in this chapter provides enough background information such that the following chapters can be clearly understood. A detailed explanation of wave propagation in fibres and the theory of FBGs is given in many books dedicated to the topics. The chapter also gives an overview of typical control system topologies including industrial standards for sensing. A basic understanding of optics and electronics is assumed.

2.1 Fundamentals of Optical Fibre Transmission

The theory of light propagation in optical fibres is well understood and is documented in a number of texts, not least in [10], and as such will not be covered in this thesis. However, it is important to briefly discuss attenuation in silica fibres, as it defines the wavelength ranges that are used in communications and sensing. There are essentially three transmission windows in silica fibres which decrease in optical loss. The first transmission window is around 850nm, the second is around 1310nm, and the third is around 1550nm. Figure 2.1 displays the three windows, including the C-band and L-band, and illustrates the improvements made in the fabrication of fibres since the early 1980's. The base-line logarithmic curves are due to scattering whilst the peaks are due to absorption, including the final peak around 1800nm which is where intrinsic

absorption occurs.

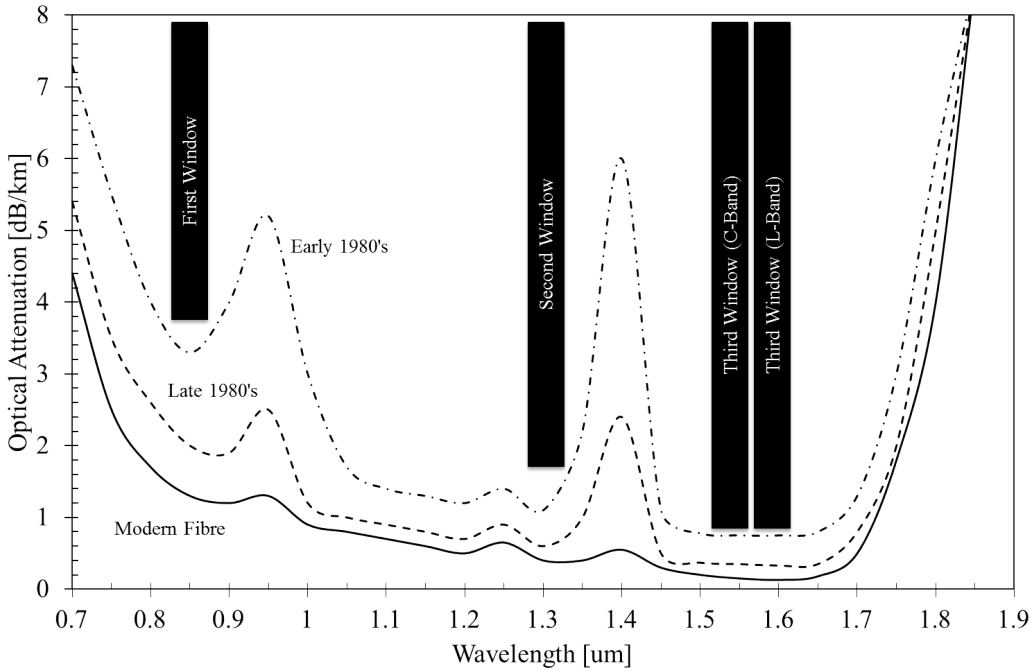

Figure 2.1: Optical transmission loss in optical fibres, showing the three transmission windows and the relative improvements in silica fibres from the 1980's onwards.

2.2 Fundamentals of Optical Fibre Sensing

Nearly all FOS utilize the strain-optic effect [11], whereby an applied strain from an external measurand, such as a pressure wave, causes a change in refractive index of the fibre. This change can be measured in a number of different ways, with the goal in security applications to correlate the change into the magnitude and location of a vibration caused by an intruder.

2.2.1 Interferometry

The theory of interferometry is mature and well understood and will not be explicitly explained here, although, in general for OFS, an optical wave source is split using a

50-50 coupler and directed, either through two separate fibres or in opposite directions through the same fibre, before being recombined at a detector. Any external influence on the fibres will cause the two waves to have a phase imbalance. In security applications, this technique can be used to detect the vibrations from an intruder's footsteps. OFS techniques utilising interferometry come in an array of different configurations. These configurations include: Mach-Zehnder, Fabry-Perot, Michelson, Sagnac, and ring resonance, as shown in figure 2.2. Each of these configurations are discussed in detail in [12].

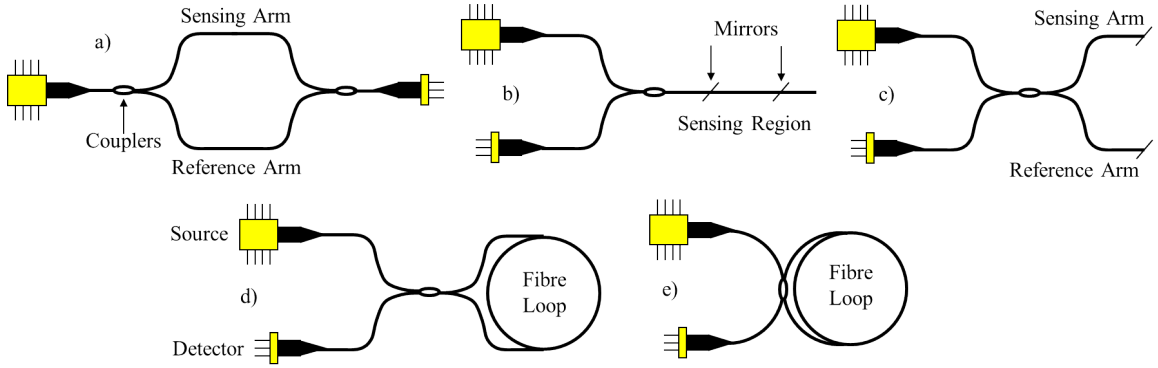

Figure 2.2: Intrinsic optical fibre interferometers: (a) Mach-Zehnder; (b) Fabry-Perot; (c) Michelson; (d) Sagnac; and (e) ring resonator.

2.2.2 Scattering Techniques

FOS can also be achieved by launching light into a fibre and analyzing the different modes of light that leave the optical fibre. This method is called speckle pattern analysis or intermodal interference. In a multimode (MM) fibre, the different modes of the input signal interfere with each other whilst traveling down the optical fibre, which can then be used to create an image or speckle pattern [13]. Any external disturbance acting on the fibre whilst the light travels through it, will cause the image to change, resulting in detection of the disturbance.

Another scattering technique, which is used extensively in distributed sensing is

optical time domain reflectometry (OTDR). When a short light pulse is launched into an optical fibre, some of the light is reflected back off the entire length of the fibre. Three different types of light make up the backscattered light; Rayleigh, Brillouin, and Raman light, which are explained in detail in [14] and depicted in figure 2.3. The vibrations caused by an intruder may change the amplitude, phase and frequency of the reflected signals, which again can be used to determine the location of the intruder.

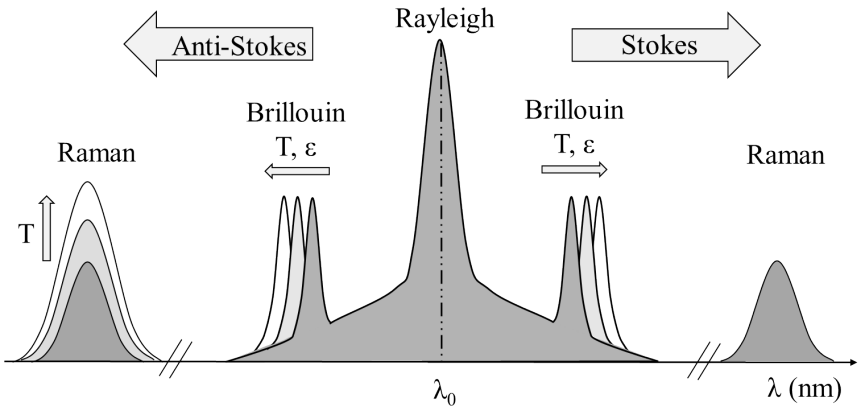

Figure 2.3: Backscattered Rayleigh, Brillouin and Raman light in optical fibres, adapted from [15].

2.2.3 Fibre Bragg Grating Sensors

FBGs [16, 17] are discrete spectrally reflective components which are written into the core of an optical fibre using a high intensity light source. One of the most common techniques is to use a phase mask to create the alternating regions of different refractive indices. Figure 2.4 shows a schematic of the writing process using a phase mask.

The difference in refractive indices results in coupling between forward and backward propagating waves [18,19]. The grating can be modelled as an interference filter whereby Fresnel reflection at each interface and the regular period of the grating, Λ, results in constructive interference in the reflection at a specific wavelength, called the Bragg

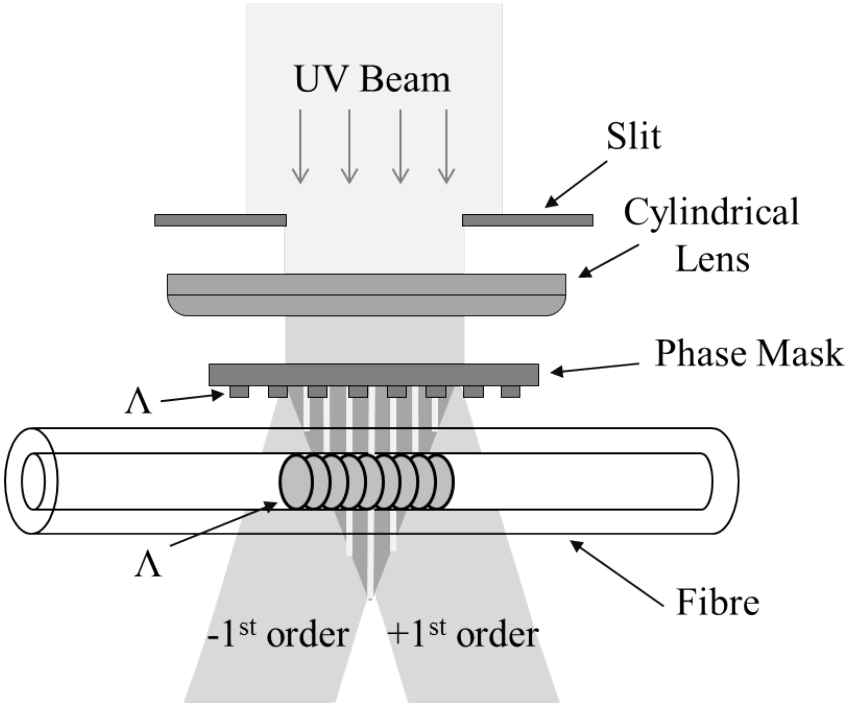

Figure 2.4: A schematic of FBG writing process using a phase mask, adapted from [17]

wavelength, λ_B. The Bragg wavelength is given as,

$$\lambda_B = 2n_{eff}\Lambda, \tag{2.1}$$

where n_{eff} is the effective refractive index of the grating for the guided mode. The refractive index profile can be determined from the following equation [16],

$$n\left(z\right) = n_{eff} + \Delta n cos\left(\frac{2\pi z}{\Lambda}\right) \tag{2.2}$$

where z is the distance along the fibre and Δn is the amplitude of the induced refractive index perturbation.

Any external environmental disturbance that causes a change in the refractive index or period of the grating results in a change in the Bragg wavelength, and as such can be detected by a FBG. The change in Bragg wavelength as a function of induced strain along the z-axis, ϵ and temperature, ΔT is given by [20];

$$\Delta\lambda_B = \lambda_B\left(\left\{1 - \frac{n_{eff}^2}{2}\left[p_{12} - \nu\left(p_{12} + p_{11}\right)\right]\right\}\epsilon + \left[\alpha + \frac{1}{n_{eff}}\left(\frac{dn_{eff}}{dT}\right)\Delta T\right]\right), \tag{2.3}$$

where p_{11} and p_{12} are the strain-optic coefficients, ν is Poisson's ratio, and α is the thermo-expansion coefficient. Equation 2.3 can simplified such that the relative change in Bragg wavelength is;

$$\frac{\Delta\lambda_B}{\lambda_B} = (1 - \rho_e)\,\epsilon + (\alpha + \eta)\,\Delta T, \tag{2.4}$$

where ρ_e is the photo-elastic coefficient and η is the thermo-optic coefficient. Typical values for a silica fibre with a germanium doped core are [21]; $\rho_e = 0.22$, $\alpha = 0.55{\times}10^{-6}/^oC$, and $\eta = 8.6 \times 10^{-6}/^oC$. Hence, the sensitivity of a FBG with a Bragg wavelength of 1550nm to temperature and strain, respectively are [21];

$$\frac{\Delta\lambda_B}{\Delta T} = 14.18pm/^oC, \tag{2.5}$$

$$\frac{\Delta\lambda_B}{\Delta\epsilon} = 1.2pm/\mu\epsilon, \tag{2.6}$$

It is important to note that the strain and temperature terms in equations 2.3 and 2.4 are independent, meaning the two measurands can be isolated through compensation techniques. There have been many different compensation methods proposed. The simplest, for strain isolation, is to ensure the FBG is only loosely bound to the measurand so that it is not subject to strain. An example of a temperature compensation method is shown in figure 2.5.

In the case of transverse strain being applied to the FBG which causes non-uniform deformation of the FBG in the x and y directions as shown in figure 2.6, the reflected Bragg peak splits into two and the shift in wavelengths are given by [22];

$$\frac{\Delta\lambda_{B,x}}{\lambda_B} = \epsilon_z - \frac{n_{eff}^2}{2}\left[p_{11}\epsilon_x + p_{12}\left(\epsilon_y + \epsilon_z\right)\right]; \tag{2.7}$$

$$\frac{\Delta\lambda_{B,y}}{\lambda_B} = \epsilon_z - \frac{n_{eff}^2}{2}\left[p_{11}\epsilon_y + p_{12}\left(\epsilon_x + \epsilon_z\right)\right] \tag{2.8}$$

where ϵ_x, ϵ_y, and ϵ_z are the principal homogeneous strains in the core of the optical fibre, directed along the x, y and z axis, respectively. The separation of the two peaks is

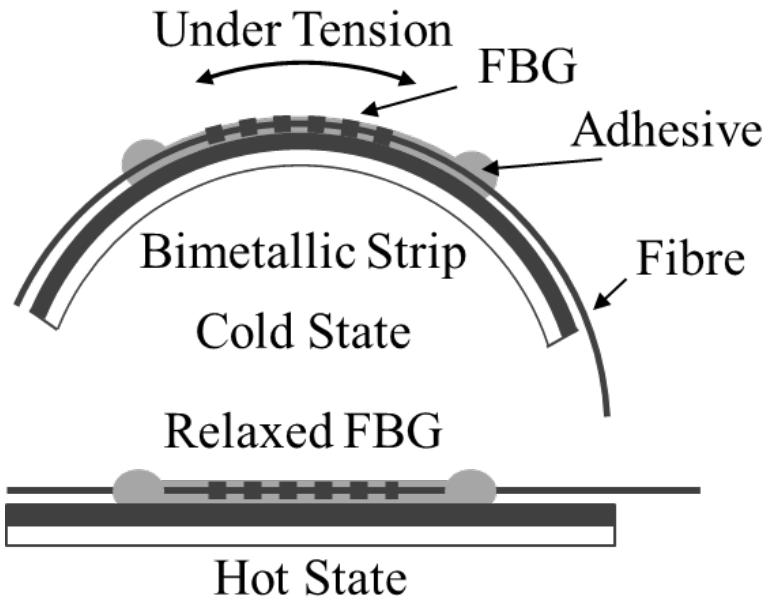

Figure 2.5: The fibre is under high tension in the cold state (top), whereas the strain reduces in the hot state (bottom); hence the temperature induced Bragg wavelength shift moves in opposite directions and cancels out, adapted from [17].

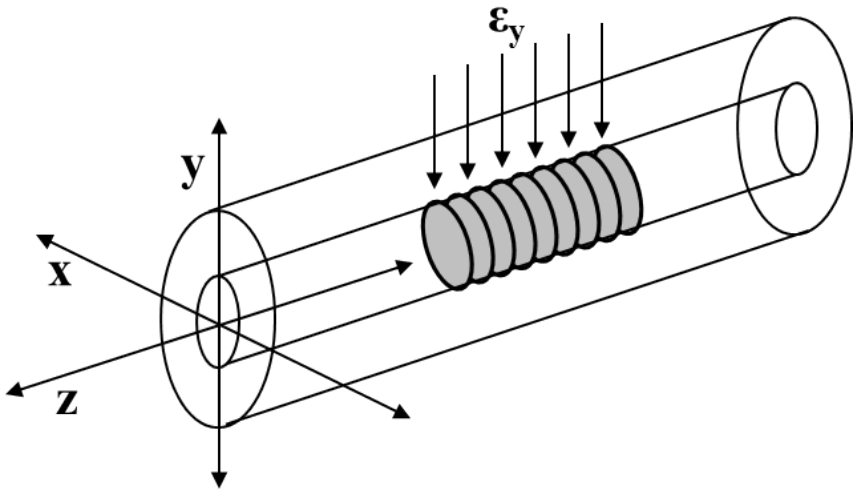

Figure 2.6: A schematic of a FBG subject to a transverse strain in the y-direction, adapted from [22].

proportional to the difference between the transverse strains in the x and y directions, given by;

$$\frac{\Delta\lambda_{B,y} - \Delta\lambda_{B,x}}{\lambda_B} = \frac{n_{eff}^2}{2}\left(p_{12} - p_{11}\right)\left(\epsilon_y - \epsilon_x\right). \tag{2.9}$$

Figure 2.7 shows the fundamental principle of operation for a FBG indicating a typical refractive index profile. A standard FBG reflection spectrum is shown in figure 2.8.

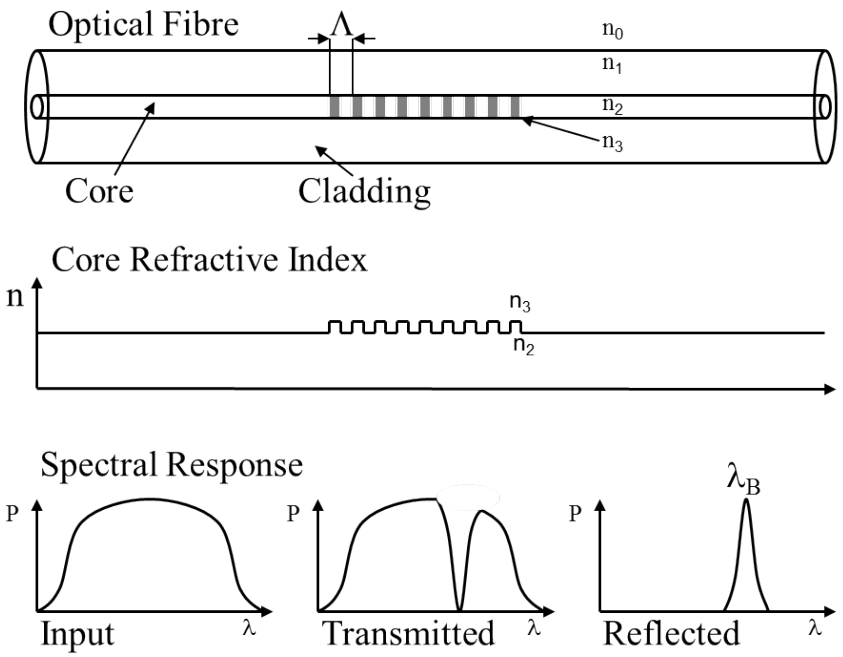

Figure 2.7: Fundamental principle of operation for a fibre Bragg grating.

There are essentially 3 types of gratings which vary in photosensitivity and thus index changes. They are known as type I, II, and IIA with the details of each type given in [17]. In addition, there are different physical types of gratings such as long period gratings (LPGs), chirped gratings, tilted (blazed) gratings, and microstructured FBGs. The structure and refractive index profile of some of the different types, as well as their corresponding reflection spectra, are shown in figure 2.9.

LPGs are similar to standard gratings although they typically have a grating period greater than 100μm. LPGs cause light from the guided mode to be coupled into the

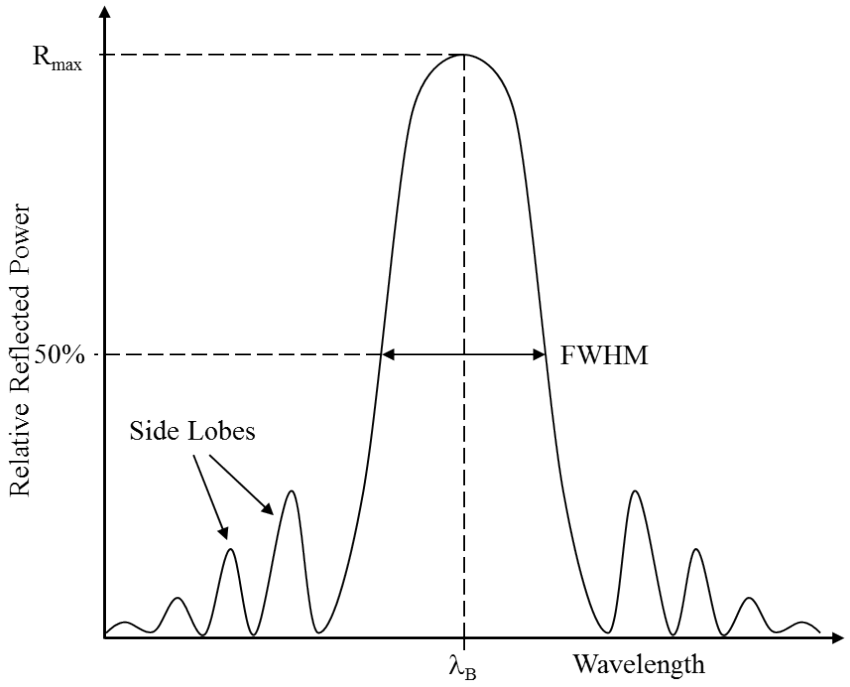

Figure 2.8: The reflected spectrum from a standard FBG showing the Bragg wavelength, λ_B, full width half maximum, FWHM, and side lobes.

cladding modes where it is lost due to scattering and absorption, resulting in a number of troughs in the transmission spectra; a review of LPG sensors is given in [23,24]. Chirped gratings have a varying grating period which usually causes the reflected spectrum to broaden significantly, as such they are often used as bandpass or edge filters [25,26], or interrogators [27]. In tilted gratings, the grating is at an angle with respect to the optical axis, causing the light to be coupled outside of the core of the fibre [28]. Generally, tilted gratings are used in optical interrogators as spectrometers [29]. The first microstuctured FBG had the cladding diameter reduced around the FBG so that the evanescent wave could interact with the surrounding medium [30,31]. Nowadays, there are many different types of microstructured fibres with an array of different cross sectional areas which can improve the way the evanescent wave interacts with the medium inside the holes [32]. Examples of some microstructured fibres are shown in figure 2.10.

Essentially all of the different types of gratings produce different reflected and trans-

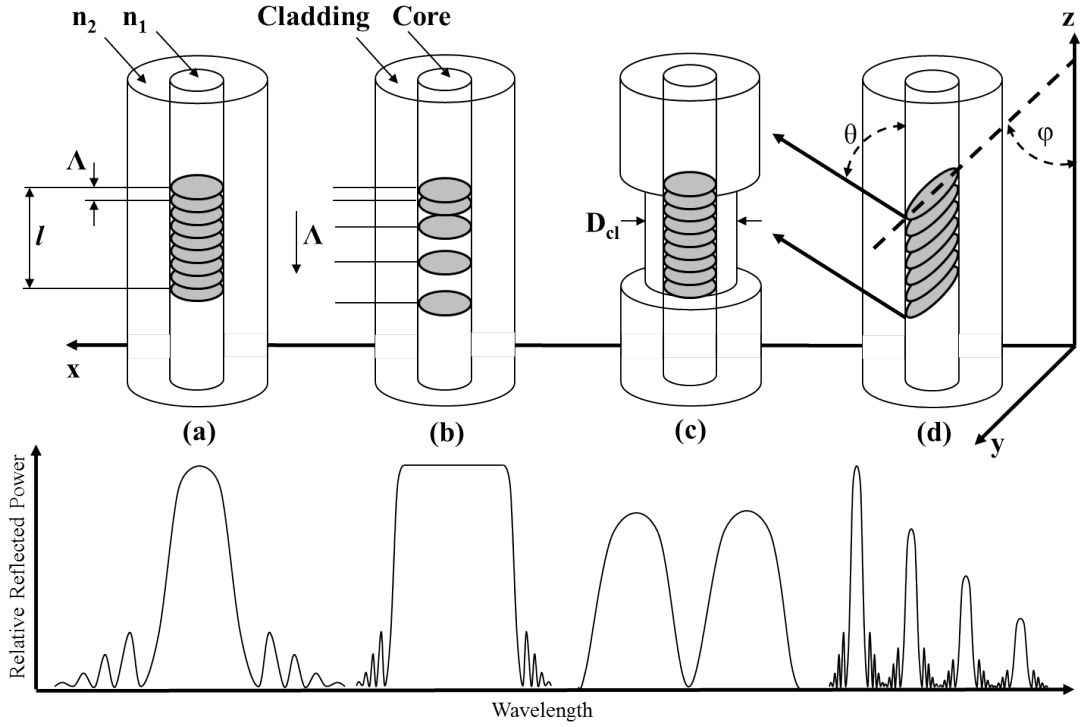

Figure 2.9: Different fibre gratings; (a) standard, (b) chirped, (c) micro-structured, and (d) tilted, with their corresponding reflection spectra below.

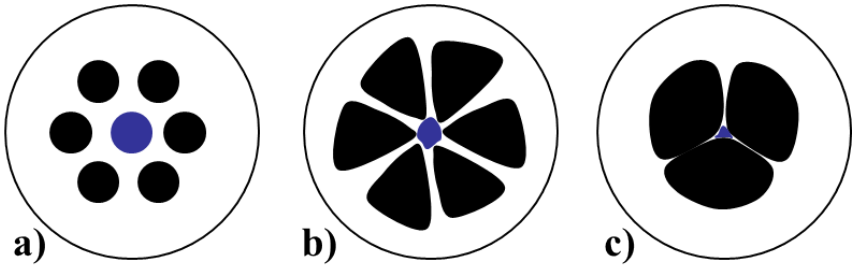

Figure 2.10: Microstructured optical fibres; (a) solid core, (b) grapefruit, and (c) three-hole suspended core, adapted from [32].

mitted spectrum profiles. The profiles can be manipulated and controlled for a given application. Usually, the non-linear characteristics of FBG reflected or transmitted spectra are suppressed, in the form of side lobe suppression through apodisation, or removed externally through signal processing. However, non-linear refractive index pro-

files within FBGs which change the properties of the reflected spectra in desired ways have been reported. Specifically, a superstructured FBG (SFBG) with two reflection bands which have complementary chirps, is demonstrated in [33]. The SFBG acts as a tunable photonic bandpass filter.

Photonic bandgap engineering in FBGs has also been proposed to customize the reflected spectra. A physical defect in the FBG is created through post processing fabrication. This can be achieved by localised heat treatment in specific areas of the FBG. The result is transmission troughs within the reflected spectrum of the FBG [34], as shown in figure 2.11.

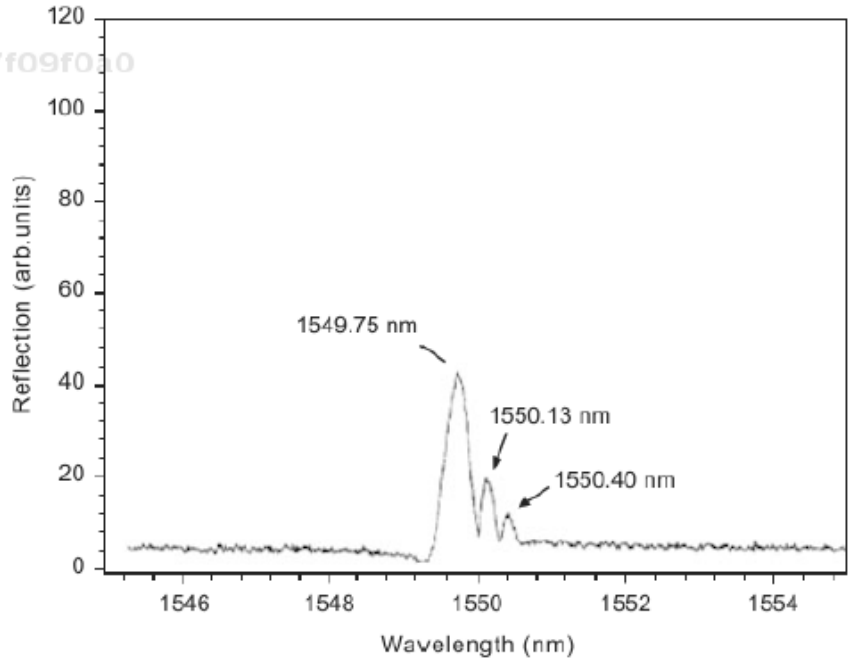

Figure 2.11: Reflection spectrum of a FBG after a localicalised heat treatment at two points [34].

Likewise, localised physical deformation of the FBG can also be used to control the reflection and transmission peaks, such as that proposed in [35]. In this case, lateral load is applied to a small section of the FBG only producing a dip in the reflected spectra which shifts in wavelength with increasing load. However, microstructured FBGs

(MSFBG) offer the greatest flexibility. In MSFBGs, different parts of the fibre cladding around the FBG is removed, so that the evanescent field interacts with the surrounding medium in unique ways [36]. An example of a multi-defect MSFBG, with its corresponding reflected spectra for different refractive indicies, is shown in figure 2.12 [37, 38].

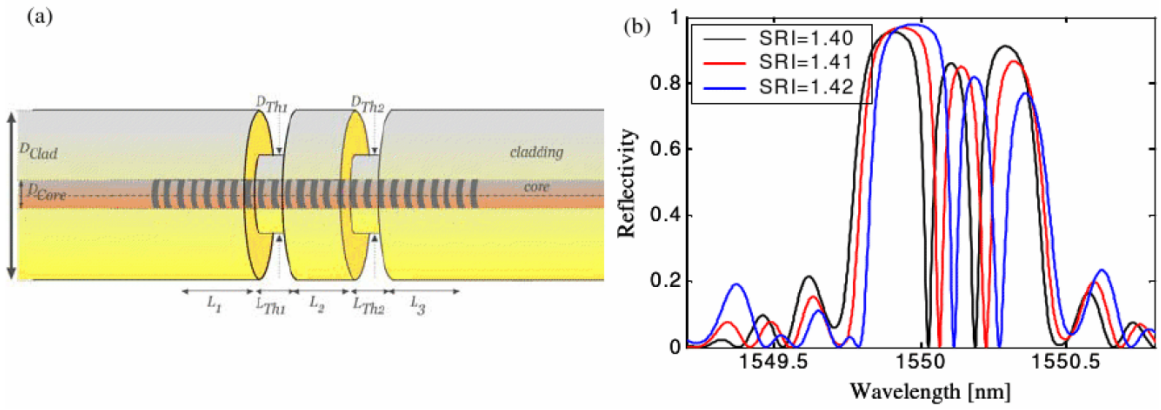

Figure 2.12: (a) Schematic diagram of a multi-defect MSFBG, and (b) numerical reflected spectra from a multi-defect MSFBG for different surrounding refractive indicies [31, 37].

2.3 Intensity Based Interrogation

The type of interrogation technique used in FOS systems has a significant impact on the versatility and cost of each system. The type of interrogation determines the number of sensors that can be utilized in any single distributed sensing, system and whether Time Division multiplexing (TDM) or Wavelength Division Multiplexing (WDM) can be used. Commercial interrogators [39] offer a range of specifications, including the number of sensors and the type of multiplexing used, as well as level of precision and resolution. However, basic models still require knowledge of optical engineering and can be a large portion of the cost of a system, in certain applications. Simple low cost interrogation techniques have been demonstrated [40, 41], and have the potential to enable FOS to penetrate more mainstream applications.

2.3.1 Edge Filter and Power Detection

There are many different interrogation techniques [42], used to detect the Bragg wavelength shift due to an external measurand and convert it from the optical domain into the electrical domain. One of the simplest ways is to transpose the shift into the optical power. In other words, rather than trying to measure a shift in the wavelength directly, convert the shift into a power change, which can easily be detected using a photoreceiver or optical power meter. Edge filter detection [43], is one of the simplest techniques and hence one of the most cost effective. In edge filter detection methods, the shift in the FBG spectrum is detected by use of a spectrally-dependent filter which results in a change in intensity at the detector. The FBG is illuminated by a broadband source, such as a superluminescent diode (SLD). As the Bragg wavelength spectrum of the FBG shifts across the filter, it causes the transmitted intensity to vary as the filter's transmittance varies as a function of wavelength.

A reference FBG can be used as an edge filter for a sensing FBG, where the total reflected intensity has a linear response across the region where the reference Gaussian spectrum is approximately linear, i.e. where both FBG reflected spectra overlap from $20 - 80$ percent. The slope of the filter, or full-width half-maximum (FWHM) of the reference FBG spectrum, determines the sensitivity and dynamic range of the interrogation system [25]. Figure 2.13 shows the basic principle of operation of a linear edge filter, utilizing an optically mismatched FBG.

In power detection methods [9], the shift in the FBG wavelength is detected by using a spectrally-dependent source, which results in a change of intensity at the detector. There are two power detection methods, linear edge source, and the narrow bandwidth source. In narrow bandwidth source based power detection [9], the laser source is centred about the 3dB point of a FBG that is then intensity modulated by the strain induced wavelength shift. That is, the reflected optical power is varied as the linear edge of the FBG is shifted in the spectrum. Either the reflected component or the transmitted component from the FBG can be used. An optical switch can be created by optically

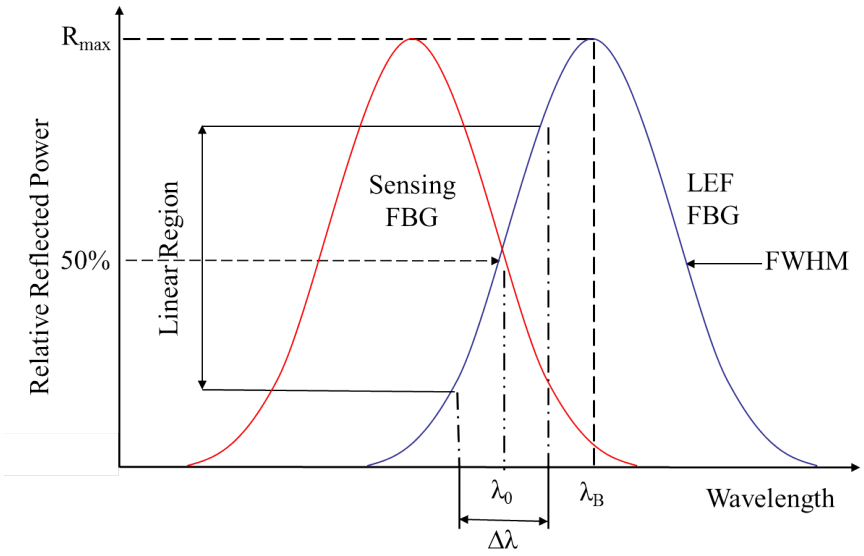

Figure 2.13: Principle of operation of a linear edge filter utilizing an optically mis-matched FBG.

mis-matching a FBG with the laser source. When the Bragg wavelength and the laser wavelength are mis-matched the output is off. An external influence can be used to shift the Bragg wavelength so that the signal overlap, resulting in an on signal. Figure 2.14 shows the principle of operation of this type of optical switch.

2.3.2 Transmit-Reflect Detection

In power detection methods both the transmitted and reflected components occur simultaneously. As the Bragg wavelength of the FBG shifts due to an external measurand, the FBG's 3dB point is also shifted. For a light source tuned to the 3dB point, the amount of optical power reflected from (and transmitted through) the FBG will therefore change, either positive or negative, depending on which edge of the FBG was used, as the measurand varies. Since the transmitted and reflected components vary in opposite directions, they can be differentially amplified to increase the overall signal. Figure 2.15 shows the principle of operation of transmit-reflect detection. A review of FBG sensors and interrogation techniques is given in [44].

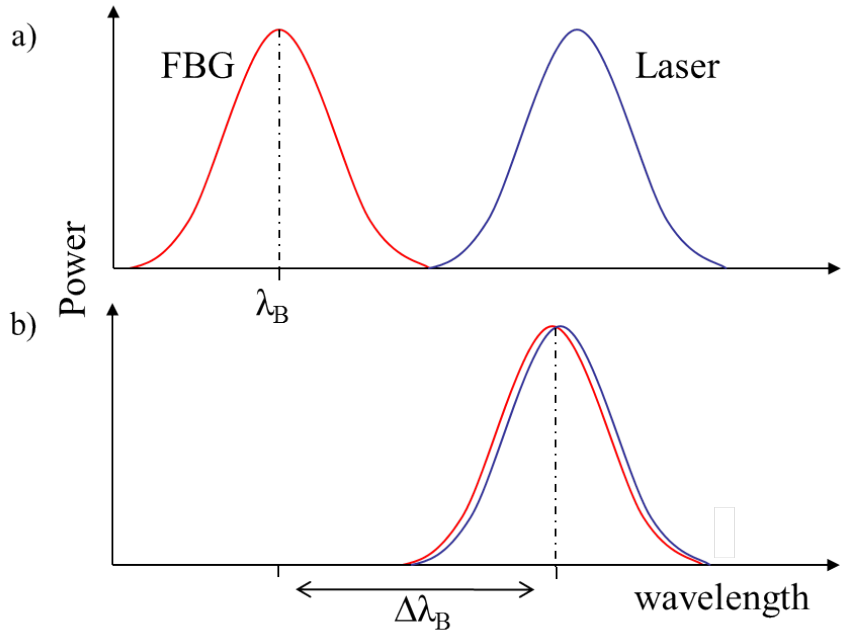

Figure 2.14: Principle of operation of a FBG optical switch; (a) shows the FBG and laser profiles are separated resulting in minimum reflected intensity and hence the switch is in the off state, (b) shows the FBG and laser profiles are matched resulting in maximum reflected intensity and hence the switch is in the on state.

2.4 Industrial Control System Architectures and Networking Standards

A brief description of some of the possible current electronic controllers and networking protocols that may be used in hybrid OFS systems is given below. This is by no means a comprehensive or complete list as there are many different types and vendors, although it should provide a basis for further discussion regarding some of this issues with respect to integrating FOS with current industrial controllers.

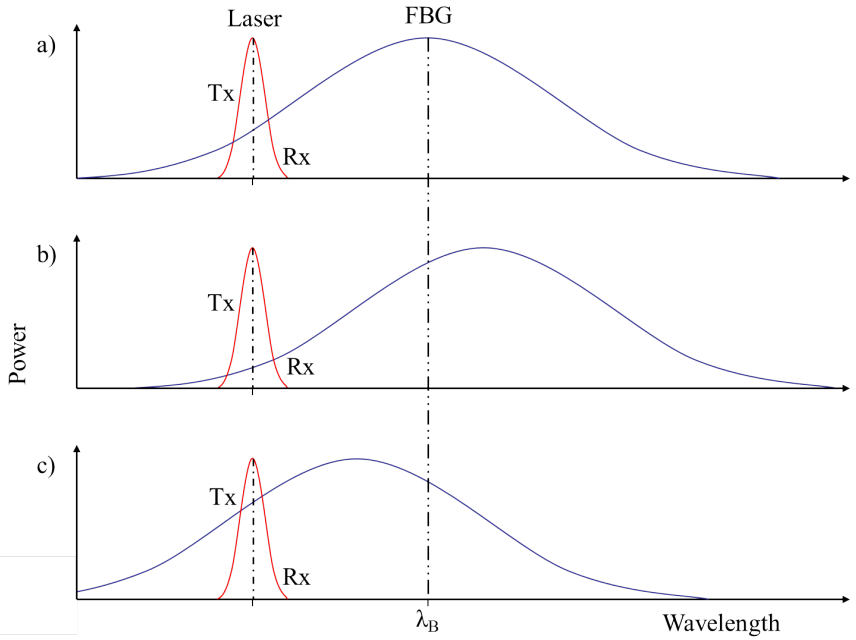

Figure 2.15: Principle of operation of transmit-reflect detection; (a) the reflected and transmit intensities are approximately equal, (b) as the Bragg wavelength of the FBG increases, most of the intensity of the laser is transmitted and a small portion is reflected, (c) as the Bragg wavelength of the FBG decreases, most of the intensity of the laser is reflected and a small portion is transmitted.

2.4.1 Industrial Controllers

Programmable Logic Controllers (PLCs) and Distributed control Systems (DCSs) are the standard intelligence for instrumentation and control systems utilised in process control, and are used in a wide variety of industries from car manufacturing to building management systems, as well as controlling machinery in large mine sites [45]. PLCs often form the basis of many automated industrial processes and are essentially the heart of a Supervisory Control And Data Acquisition (SCADA) system. A PLC is an electro-mechanical computer specifically designed to take in information from a multitude of sensors in real world industrial processes, and react to those sensing inputs by controlling actuators in such a way as defined by the control logic [46]. For example, a PLC may

receive data corresponding to the pressure of a fluid in a pipeline and then react to that signal by sending a command to the field to open a valve, stop a pump, sound an alarm, or any other action, depending on what is required. Both PLCs and DCSs were both originally developed to replace physical relay systems and designed to fulfill certain criteria:

1. Be environmentally rugged and survive in an industrial surrounding,
2. Be easily programmed and maintained by plant personnel and technicians, and
3. Be reusable.

Nowadays, both PLCs and DCSs can perform much more than basic logic operations and are used to perform complex functions as required by any particular process. PLCs are usually preferred over DCSs for smaller systems where a single PLC may be used to control a specific area of a plant, whereas DCSs are usually used for extremely large processes.

2.4.2 Embedded Controllers

Embedded controllers such as Raspberry Pi [47] or Arduino microcontrollers [48] are being used more and more frequently in very small scale control systems. There are educational kits that are used in high school activities, as well as hobby kits for an array of residential applications, such as home automation and robotics. This is because they are extremely low cost, small in size and easily programmed using open source software.

2.4.3 Bus Topologies

Ethernet is a high speed networking technology now used extensively in homes and offices to enable computers to communicate with each other and share resources. Used in conjunction with a router, Ethernet enables easy access to the internet. Depending on the transmission medium and Ethernet controller used in a network, it is now possible

to have bit rates as high as 10 Gbit/s. Ethernet on its own, however, is not practical for most industrial processes as it is not time specific and does not guarantee real-time transfers, i.e. transfers that occur at precise times or intervals. However, there is nothing to stop additional protocols or a master system to be added to Ethernet to control when the data is sent [49].

There is a large assortment of bus topologies used in industrial control systems with a wide variety of communications including Modbus, CANbus, Foundation FieldBus, etc. A detailed review of the history of fieldbus technologies is given in [50]. One of the most widely used is Profibus (process-field-bus) Decentralised Peripheral (DP) which is based on RS485, in conjunction with Profibus Process Automation (PA), which uses Manchester Bus Powered (MBP) transmission. Profibus DP is used to operate actuators and sensors, utilising high speed communication, up to 12Mbit/s, and providing an array of diagnostics about each node on the bus. Profibus PA is used for remote I/O and operates at a much slower data transmission rate of 31.25kbit/s. PA has the main advantage of providing power to sensors over the same communication cable [51].

Although many bus topologies exist, one of the most promising for the optoelectronic PLC interface application is Profinet [52]. Profinet is a type of industrial Ethernet and is in essence Profibus over Ethernet. This means it has all the advantages of Ethernet, such as extremely fast data rates with almost no limitation on the number of slave devices; however, Profinet is also time specific, which is essential for process control applications. Therefore, the PLC can still poll each device and receive each packet of data in a predetermined order in a specific time period. This is possible since the PLC is aware of all slaves on the network at all times, and hence is capable of scheduling the data packets from each. A schematic of the Profinet communication architecture is shown in figure 2.16.

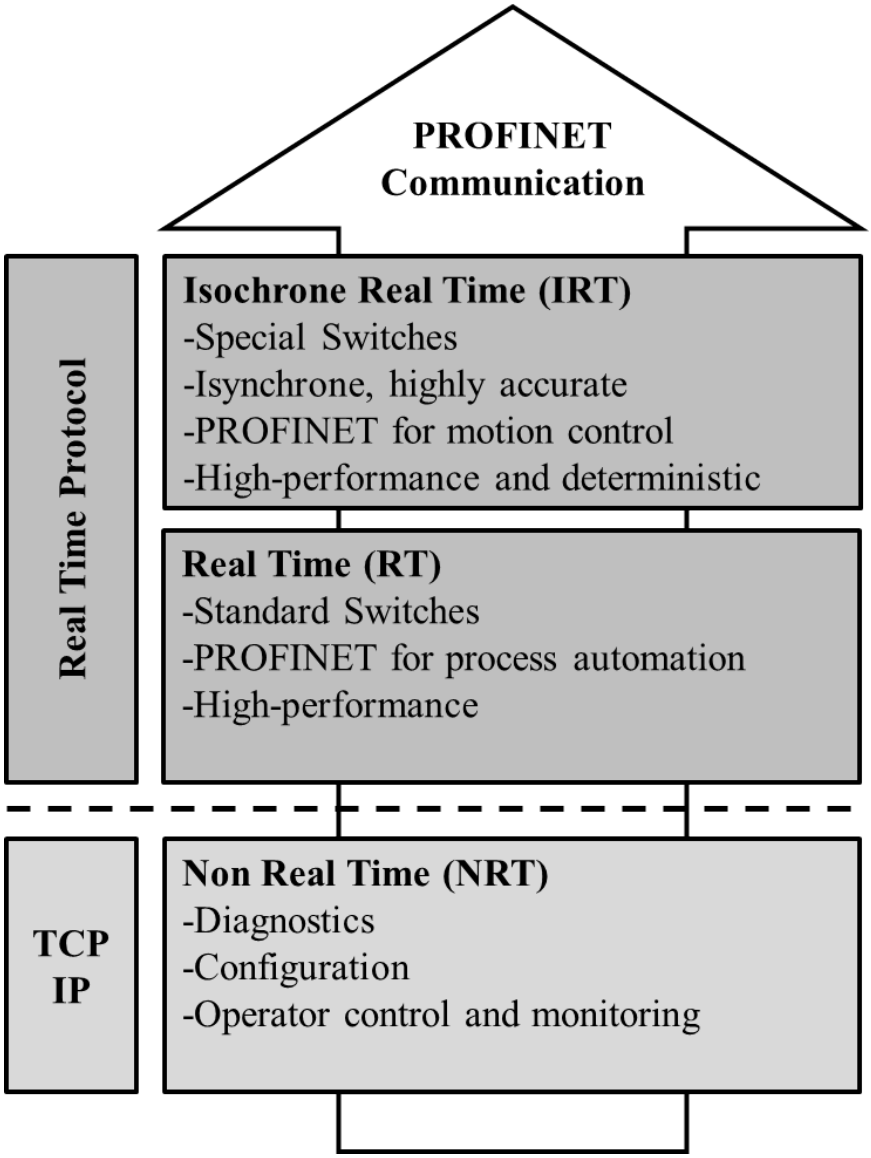

Figure 2.16: Profinet Communication architecture.

2.4.4 Traditional Sensing Techniques

Whilst sensors in most control systems transfer data over smart communication networks such as Profibus PA, traditional sensing methods are still extensively used. One of the traditional analogue input sensing standards is 4-20mA [53]. The analogue range of a sensor sent to a PLC is between 4mA and 20mA, where 4mA corresponds to 0% and 20mA corresponds to 100% of the measurand. The main advantage of this method is

that a loss of power can easily be detected, due to the fact that a 0% reading does not correspond to 0mA. Also the use of a current reading rather than a voltage reading minimises the risk of interference from noise in the signal. The highway addressable remote transducer (HART) protocol [54], shown in figure 2.17, is one of a number of smart instrumentation protocols designed for collecting data from instruments, sensors, and actuators by digital communication techniques.

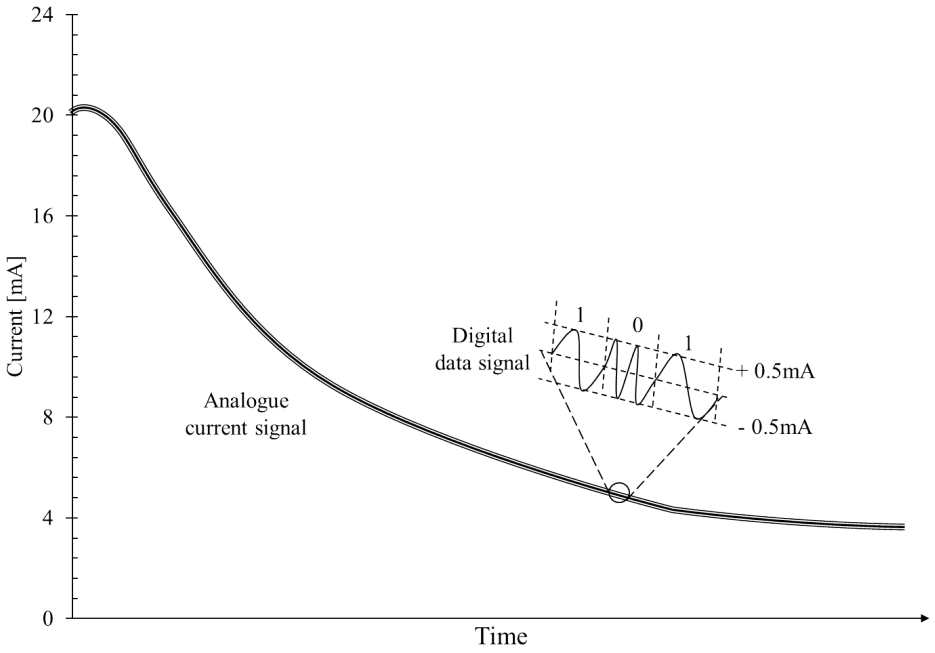

Figure 2.17: The HART protocol showing digital transmission superimposed on the 4-20mA analog signal.

This protocol was originally developed by Rosemount and is regarded as an open standard, available to all manufacturers. With the HART protocol data is superimposed on a 4 to 20mA signal enabling the devices to communicate digitally whilst the analog signal transmission occurs at the same time.

Chapter 3

Literature Review

This chapter gives an overview of the sources of literature used, and gives a brief summary of relevant research literature. This includes a review of optical fibre sensors for security applications, fibre Bragg grating sensors used in process control applications, and fibre Bragg grating interrogators. It is intended that the review follows a chronological order within each section, except in certain cases where similar work is referenced together.

3.1 Significant Journals

A number of journals are strongly related to the specific topic. These journals are available in full text, and will be used as primary reading sources. The primary journals include;

- Journal of Lightwave Technology (IEEE),
- Photonics Technology Letters (IEEE),
- Sensors Journal (IEEE),
- Optical Engineering (SPIE),
- Optics Express (OSA),
- Optical Fiber Technology (Elsevier),

- Sensors and Actuators A: Physical (Elsevier),
- Applied Physics Letters (AIP),
- Measurement Science and Technology (IOP),
- Photonic Sensors (Springer), and
- Sensors (MDPI)

3.2 Databases

A number of databases have been used in the sourcing of literature. These databases have contributed to improving the efficiency of sourcing relevant literature by relating similar articles. The most significant databases include;

- The International Society for Optical Engineering (SPIE) Digital Library.
- The Institute of Electrical and Electronic Engineers (IEEE) Xplore Digital Library.
- The Institute of Physics (IOP) Electronic Journals.
- The Optical Society of America (OSA) Digital Library

3.3 Authors and Research Groups

A number of key authors and research groups have been identified:

Prof. Yun-Jiang Rao is an expert in the field of optoelectronics and has co-authored many journal and conference articles across a range of sensing techniques, including optical time domain reflectometry (OTDR) and FBG sensors.

The optoelectronic division from the University of Sannio, headed by Prof. Andrea Cusano, is one of the most significant FBG research groups, particularly for industrial applications.

Some of the most significant authors in the field of FOS networks and multiplexing techniques and FBG interrogation methods are Dr Rosa Ana Perez-Herrera, Prof. Manuel Lopez-Amo and J.M. Lopez-Higuera from the Department of Electric and Electronic Engineering, Universidad Publica de Navarra, Spain and Prof. Jos Migue Lopez-Higuera from the Photonics Engineering Group, Department of Electronics Technology, Systems and Automation, Universidad de Cantabria.

A significant study of commercial FBG interrogation techniques has been undertaken by Dr Theo Verbruggen from the Energy Research Centre of the Netherlands.

Moreover, Dr Mohamed Mahmoud's work on all optical control systems from Sheffield Hallam University is particularly relevant.

Other noteworthy authors belong to research groups, including but not limited to;

- Optoelectronics Research Centre, University of Southampton,
- Photonics Research Group, Aston University,
- School of Engineering, Sheffield Hallam University,
- Department of Electrical and Computer Engineering, Brigham Young University,
- Department of Mechanical and Aeronautical Engineering, University of California, and
- Institute of Optoelectronics, Military University of Technology, Warszawa.

3.4 Literature Summary

This literature summary will examine the individual areas that contribute to the overall scope of the topic. These include the types of optical sensors used in the different aspects of security applications, such as in-ground intrusion detection and perimeter fences. The use of fibre Bragg gratings for different measurands in the process control industry is reviewed. Furthermore, the wide variety of FBG interrogation techniques is reviewed.

3.5 Status

Almost all traditional sensing applications can now be replaced by optical fibre sensors. These include level, temperature, pressure, strain, vibration, chemical, electrical and magnetic field, rotation, and acceleration measurements among others [16, 17]. This transition from electrical and mechanical sensing to fibre optic sensing techniques has occurred because fibre optic sensors have many advantageous properties including greater sensitivity, reduced size and weight, environmental ruggedness, and immunity to electromagnetic interference [1].

Nevertheless, in general, optical fibre sensors are underutilised in process control and security applications as simpler traditional sensing techniques based on industrial standards are preferred. The use of optical fibre systems is increasing in industry, however, for both information transmission and more diverse sensing applications, since these systems are generally more secure than direct wire, immune to electromagnetic interference, and offer faster data transmission rates [55].

Where fibre optic sensors are used in process control applications, older optical fibre sensing technology, such as scattering and interferometry, are typically used [56]. Usually, the sensors are on the end of an optical fibre, where the fibre is simply used as the data transmission medium. This method completely underutilises many of the advantages of the fibre itself.

3.6 History

The first intrinsic fibre optic sensor for detecting dynamic strain was reported in 1977 by Nelson et al. [57]. The bending of an optical fibre was shown to modulate the amount of power transmitted through the fibre. This bending loss modulation represented a source of disturbance within the fibre transmission.

In the same year, Cole et al. [58] and Bucaro et al. [59] both reported optical fibres immersed in water could be used as opto-acoustic sensors. Both groups used a similar

technique, immersing a fibre within a fluid and then transmitting an acoustic wave through the fluid. The acoustic wave alters the refractive index of the fibre which in-turn changes the path length of the optical beam resulting in a phase shift with respect to a reference beam.

The following year, in 1978, the first fibre Bragg grating was fabricated by Ken Hill [60], using visible laser light that propagated through the core of the fibre. The setup involved the establishment of a standing wave. However, this technique was complicated and it wasn't until 1989 when Meltz, Morey, and Glenn [61] demonstrated a much easier technique using the interference pattern of ultraviolet laser light to create the periodic regions of alternating refractive index externally from the side of the fibre. After demonstrating their transverse holographic fabrication method for FBGs, Morey et al. [62] suggested FBGs could be used to detect a number of different measurands such as temperature, strain, and pressure.

Initially, FBGs were used as spectral transduction elements, meaning that the information was an absolute quantity encoded on the wavelength. The advantage of this technique was that the FBGs were immune to optical power fluctuations. As such, they can be implemented in Wavelength Division Multiplexing (WDM) or Time Division Multiplexing (TDM) systems [63]. Unfortunately, these systems require spectral decoding of the sensor signals, which can be costly and processor intensive. A more efficient alternative is to use FBGs in an intensity based edge filter detection system [64], where the intensity information from the FBG can easily be correlated to the change in the measurand, i.e. the relative spectral shift in the FBG filter results in an optical power change.

The disadvantage of intensity based detection systems is that input optical power fluctuations are reintroduced into the system and the detection accuracy may be reduced. However, the simplicity of detection and reduced cost, since spectral decoding is not required, greatly outweigh the corresponding disadvantages in certain applications, e.g. the output of a digital intensity signal. Hence, these systems would be preferred in process control applications. Essentially, an FBG detects a change in a measurand

as a result of experiencing a strain in an optical fibre, which then alters the reflected wavelength from the FBG. As such, FBGs can be used for a number of different sensing techniques.

3.7 Optical Fibre Sensors in Intrusion Detection Systems: A Review and Forecast

There is a large array of different sensing techniques used for intrusion detection, from glass break detectors, magnetic door and window detectors to surveillance cameras and infra-red trip wires, as well as in perimeter fence and in-ground pressure sensors [65]. A single security setup for a property, whether it is domestic or commercial, may utilize a number of these techniques in creating a complete security system. Moreover, modern systems usually incorporate an inherent level of intelligence for real-time monitoring of sensors via a security control centre. This intelligence is essential for reducing the number of false alarms and increasing the effectiveness of the security system in both detection and prevention of potential intruders. The intelligence can be in the form of a simple processing unit or, more commonly, from a PLC, and may also be integrated with the building automation system [66]. Traditionally, wired security systems were considered the most reliable and affordable solution for intrusion detection. The main advantage of wired systems is that they can be easily connected to a monitoring service via a telephone line. However, these system could be vulnerable to tampering if the wires themselves were not appropriately protected, requiring professional installation.

With the advances in wireless technology in recent years, wireless security systems have become very popular as they can be easily setup, do not require cabling, and can be remotely armed. The disadvantage however, with these systems is that each sensor may require an external power supply. If batteries are used, they may need to be replaced or charged regularly, especially for surveillance cameras which may only last 24 hours before needing to be charged [67].

Optical fibre security systems offer some unique advantages with respect to the other methods. One of the main advantages is that the optical fibre itself can act as both the transmission medium and the sensor. It is well recognized that FOS have many desirable attributes; being small, light weight, environmentally rugged, and have increased sensitivity with respect to traditional sensing techniques [5]. These attributes are ideal for advanced security systems.

There are essentially three broad OFS techniques used for security applications, specifically physical intrusion detection systems (PIDS);

1. interferometry,

2. scattering, and

3. fibre Bragg grating based detection.

Older OFS techniques for security applications utilize scattering and interferometry. Whilst these techniques may be effective for certain specific applications; they have their own drawbacks that are discussed throughout this paper.

Current state-of-the-art OFS for intrusion detection is primarily based on the use of FBGs [68]. FBGs are specifically sensitive to temperature and pressure variations, however; the signal from a FBG can be manipulated so as to act as a sensor for a large array of environmental disturbances. FBGs have been shown to measure changes in level, weight, and flow, as well as, more esoteric measurands such as magnetic field and tilt [44]. The versatility of FBGs makes them ideal for security applications.

Here, a review of the different optical fibre based techniques used for intrusion detection since the late 1980s through to the present state-of-the-art practices is provided. A comparison of the advantages and disadvantages of each system is discussed in reference to the core sensing and interrogation method, as well as the networking capability and the effectiveness of the system as a whole for securing a property against security breaches.

3.7.1 The History of Fibre Optic Sensors for Intrusion Detection Systems

Published in the 1981 Carnahan Conference on Crime Counter Measures was a paper by Montgomery and Dixon [69] which describes the developments of fibre optics as a transmission medium, as pressure, sound, magnetic field, temperature, light, and motion sensors, as well as intrusion detection sensors through fibre breakage. The article discusses the use of fibre optic cables concealed in wire fences or embedded in glass panes for detection of intruders who break the wires or glass. It also mentions that General Telephone and Electronics (GTE) Corporation is developing fibre optic security fences based on the detection of sound near the fence. However, the paper doesn't go into detail regarding the specific demodulation techniques under development. In addition, fibre optic seal collars are described where a bundle of optical fibres in a loop are used to secure a enclosure. The ends of the large bundle of optical fibres are imaged and form a particular pattern. If the seal is broken and replaced by another bundle, the pattern formed would be different.

In 1983, the first scientific paper on FOS, which specifically described a technique for intrusion detection applications, other than fibre breakage, was reported by Rowe [70]. The paper detailed work performed at GTE from 1978 which investigated the feasibility of an optical fibre based in-ground intrusion detection sensor. The study stated that while there was only a small change in the amplitude of the signal due to micro-bending of the fibre from an intruder, there was a significant rotation of the speckle pattern that was analyzed. Hence a method for converting the change in polarization into a measurable electronic output for practical applications was put forward. The technique simply splits the horizontal and vertical polarized components and uses a difference amplifier to convert the signal into a usable voltage. The results show an intruder can clearly be detected when the cable is buried in different types of gravel and at different depths. It was suggested that a threshold detector should be used to minimize the number of false alarms such that only those signals that exceed the threshold value

trigger an alarm. In addition, the study showed rain caused no observable effect whilst an attempt to uncover the fibre was clearly detectable.

In 1984, Robertson and Rarick [71] reported the progress of the U.S. Army Belvoir Research and Development Center into optical fibre technology for physical security. The paper generally focused on the use of fibres as a transmission medium, although the report does describe the development of a fibre optic pressure mat based on micro-bending for the detection of intruders.

From these first advancements came a number of fibre optic security based systems in the following years. In their early work, Leung et al. [72, 73] reported their in-line security sensor system, which was also based on intermodal interference. Their initial results showed that a cable buried at a depth of 30cm was capable of detecting vibrations from a 60kg person walking 3m from the fibre. They also discussed the improved sensitivity of a distributed sensor system containing 8 fibres which had a resolution of 10m over a distance of 2.5km. They used a system with a cable buried at two different depths and characterized low sensitivity and high sensitivity systems and discussed the trade-off between sensitivity and false alarm rate (FAR) [73]. Later, the same group investigated the performance of an optical fibre multi-sensor network using frequency domain multiplexing. Although the system was ineffective due to cross talk, which caused phase errors, it was an important step in attempting to solve problems associated with multi-sensor networks [74].

In the 1988 Carnahan Conference on Security Technology, three papers were published on the use of fibre optic cables in PIDS [75]. Whilst all of these papers focus on the use of the fibre as a data transmission medium, it is worth noting the gradual increase in fibre optic technology for security applications through the 1980s. The report by Nason et al. [76], details the progression of the stand-alone security systems in the 1970's through to the centralized monitoring systems in the 1980's. This centralization meant that alarm and video data needed to be sent over much further distances at greater speed, meaning fibre optic systems were then a viable solution. The paper by Schwalm [77] reports the development of fibre optic components such as splitters, cou-

plers, multiplexers, switches, and sensors, such as in fence intrusion detection sensors, as well as, cables, light sources, and detectors. The ongoing development of each of these components was the driving force behind the growing demand of fibre optic systems in security applications.

Cogdell [78] suggested, with the use of multiplexing, that multiple FOS can be contained within one optical fibre which could then be processed away from a protected area, forming the basis of a perimeter defense system. This advancement came from a novel transduction mechanism for monitoring DC measurands. The non-linear displacement to strain mechanism meant it was possible for a single interferometer to be used to monitor a number of sensors.

Hazen et al. [79] performed a study which tested several different detection methods for use as buried pressure sensors. The first method, bending loss, was not sensitive enough when buried in the ground but was better suited to applications where the fibre experienced a significant strain, such as on a perimeter fence. The second method, speckled pattern variation, now referred to as intermodal interference, was the most sensitive method available. However, this mechanism was also extremely sensitive to external factors such as ambient conditions. Therefore, a focus was placed on the polarization of single-mode (SM) fibres which occurred when pressure was applied to the FOS. Interestingly, in order to solve a number of issues the team decided to use two independent channel detection systems with two analyzers at about 45 degrees from each other. This may be one of the first cases of using parallel fibre optic systems to eliminate detection problems.

In the same year, Kotrotsios and Parriaux [80] reported a fibre optic alarm system which measured the difference in transit time of separate modes launched down the fibre. They claimed this technique increased the dynamic range of the system with respect to reflection based techniques. They also showed that the resolution of the system could be improved by using a Michelson interferometer to analyze the difference in the modes.

Skogmo and Black [81] described a fibre optic barrier integrity monitor, similar to earlier work using the fibre as a breakage sensor. The integrity of a barrier, such as a

fence or wall, was monitored by threading optical fibres into the barrier and launching light into the fibres. If there was a loss of light signal, then a breach had occurred. This method was extremely simple, using the optical fibre as a breach switch.

Griffiths [82] discussed the developments in optical fibres as intrusion detection sensors focusing on the trade-off between high probability of detection (POD) and low FAR for the different approaches taken. He states fibre optic continuity sensors, such as those embedded within a barbed steel tape and attached to a fence or wall, are the most reliable sensors and offer very low FAR and extremely high POD. An alarm is triggered if the fibre is cut, broken or severely distorted acting as a digital breach switch. Speckle pattern sensors can be embedded in the ground or in a fence to monitor low frequency pressure disturbances or high frequency vibrations such as acoustic signals, although the effectiveness of the system depends on the signal processing and alarm thresholds implemented, and therefore the ratio of POD to FAR. Attenuation sensors are also described for monitoring fibre optic transmission lines. If an attempt is made to tap into the line then there is a loss in signal strength and hence an alarm can be triggered. Which of these techniques is implemented depends on the specific application and the overall requirements of the security system.

Five years later, Griffiths [83] reviewed the developments in, and applications of, fibre optic intrusion detection sensors. He described intrusion detection as the elusive question, where optical fibres were the answer. The paper makes a correlation between the developments of fibre optic technology and supporting technology. Parallel developments in electronic components such as laser diodes as well as connectors, splicers and hand tools have rapidly increased the use of FOS, whilst minimizing installation and repair times. Two forms of OFS methods were outlined: continuity and disturbance. Continuity is a method whereby a receiver continuously receives a low power optical signal and an alarm is triggered if the light path is broken as previously detailed. Disturbance refers to an analogue signal where the variation in light intensity or distribution of reflected light signals represents a certain value of a measurand. A number of different applications in physical security are mentioned. These include taut wire sys-

tems where an alarm is triggered if the wire is broken, fibre optic door contact, where the door contact breaks a light path using a magnet as a switch. This is the basic idea behind an optical fibre reed switch. Furthermore, a fibre optic mesh is detailed, where two or more fibres are woven together forming a mesh barrier, including a robust form used as an underwater barrier. A buried pressure sensor is also described using speckle pattern detection. Moreover, Griffiths describes the progress and advancements made by integrated systems. These high tech security systems communicate simultaneously and control all levels of surveillance and alarm handling. Figure 3.1 shows a schematic of typical network architecture illustrating the integration of sensors and control.

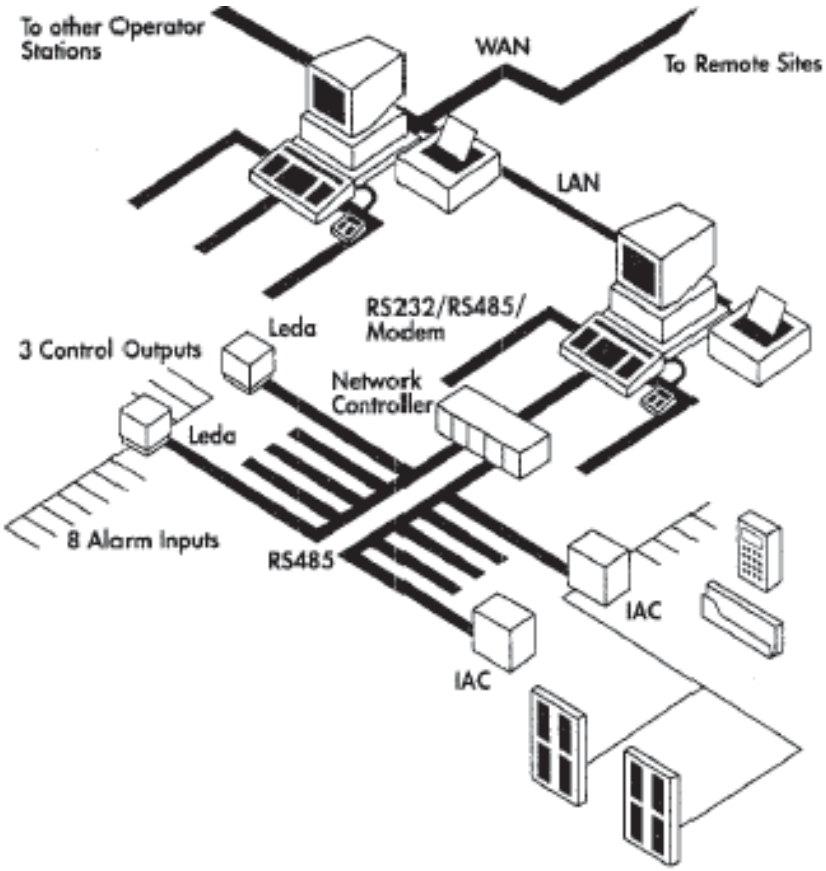

Figure 3.1: typical network architecture illustrating the integration of sensors and control [83].

Bryson and Hawkes [84,85] described a novel fibre optic perimeter protection system.

Their system used multiplexed reflectometric interferometry, originally developed for hydrophones, whereby a vibration from an intruder caused a phase shift in the RF carrier which was demodulated by an optoelectronics unit. The main advantage of this technique was the ability to multiplex a large number of sensors either buried or fence mounted. Interestingly, although their system used reflective x-couplers they proposed the use of FBGs to increase the number of sensors and improve the system. A comprehensive study of the system performance was performed with a comparison of their technique with buried electronic sensors and analysis of different threat signatures from an intruder walking or crawling across the fibre, or a vehicle crossing the fibre, as well as the detection capability in terms of range and effectiveness of reducing false alarms. The paper also described two methods of configuring the system to facilitate the large amount of processing power required. The system could be either connected to a separate control system via a standard computer interface, acting as a black box, or a stand-alone man-machine interface could be implemented using commercially available alarm software or customized software in which different sections of an PIDS are overlaid on an aerial photograph.

Park and Taylor [86] reported an in-ground PIDS based on an all-fibre Michelson interferometer. They showed that this method is capable of detecting a person on foot and a vehicle passing over the fibre, and that the amount of pressure applied is proportional to the phase change received. Two years later, in 1998 [87], the same group reported an OTDR system with a resolution of 400m over a 6km length of fibre.

Bush et al. [88] produced an extensive report on their buried fibre intrusion detection sensor. Their system incorporated a low cost depolarized Sagnac interferometer. They detailed the advantages associated with this method which included high sensitivity and low FAR, as the interferometer was extremely good at distinguishing between singular events and background disturbances. The report describes their system in detail, including the physical layout and the optoelectronic circuit used. The results from their field tests show their system can detect an intruder performing different types of walking and crawling methods with the aim of bypassing the system.

In 1997, two papers were produced by the Institute of Optoelectronics at the Military University of Technology in Poland. These papers would be the first of many, based on fibre optic perimeter detection systems, produced by their research group over the following decade. One of the papers by Ciurpapinski and Maciejak [89] describes a perimeter disturbance localization system based on a Mach-Zender interferometer coupled with a Sagnac interferometer. The other paper by Szustakowski and Ciurpapinski [90] is a review article describing various optical fibre based sensing techniques such as OTDR, Rayleigh interferometers, continuous wave interferometers, and frequency domain sensors based on fluorescent properties of silica fibres. However, the paper is only an overview of these methods and suggests much of the work in each of the areas is ongoing and needs further research.

From 2001 to 2008, Szustakowski et al. [91–97] reported a new generation of fibre optic perimeter sensors in Sagnac loop configuration. They showed their system could be used for both in-ground and fence mounted perimeter detection. The system uses a digital signal processor to distinguish between disturbances from animals, intruders, and the environment. The various disturbances were catalogued in a look-up library, significantly reducing the number of false alarms. Their group reported a number of different configurations using Sagnac and Michelson interferometry, as well as discussing the precision of each system, and their ability to classify various events.

Interestingly, all of their recent work focuses on a security system based on intermodal interference or modalmetric detection, as they now refer to it [98–100]. The technique is almost identical to the earlier work on intermodal interference except they have performed a much more detailed analysis of the integrity of the system. Using highly sensitive focal plane array cameras for analyzing the output from the MM fibre, they verified the most appropriate optical power for the source and the most effective configuration in terms of lengths of sections of SM fibre and the type of connections used between the SM and MM fibres. In addition, an analysis of the frequency response of the system was made. The focus of their study was the protection of museum collections as their system was particularly sensitive to touch and vibrations.

The group then combined the modalmetric sensor with an interferometer, in which one arm of a Mach-Zender interferometer contains the modalmetric sensor, forming a hybrid system with improved response time [101]. Finally, they proposed that the system could used to monitor the integrity of fibre optic data cables [102].

The Senstar-Stellar Corporation, established in 1981, are one of the world's leading companies providing perimeter security in a large array of different industries and sectors. From 2001, Maki et al. [103–106] described one of their technology solutions, IntelliFIBER^{TM}, a fibre optic micro-bend sensor cable system used for perimeter intrusion detection. Their technology supports three different cable types: 2-core MM fibre allowing for signal loopback, 4-core for additional networking capabilities, and 4+2-core comprising of four optical cables and 2 copper cables for powering the electronic processors. The additional copper cables within the same housing eliminates the cost associated with running separate cables and produces a generally more robust cable overall. As the company offers a solution to end users, the system was rigorously tested and offers a 95% POD and low FAR from the environment due to adaptive signal processing algorithms. The success of their OFS system has been enhanced by the simultaneous development and integration of their digital processor electronics technology, Intelli-FLEX.

Crickmore et al. [107, 108] developed a complete land and sea based security system using interferometric FOS with the interrogation again based on Michelson interferometry, essentially identical to Bryson and Hawkes' [84] technique, with some additional components such as fibre amplifiers. For land based detection, they used a combination of discrete and distributed sensors. Whilst distributed sensors in buried cables formed a continuous sensing region, discrete accelerometers were also used as they are typically much more sensitive. The accelerometer developed is based on the mandrel principle and is shown in figure 3.2. Any vertical motion of the mass, transfers pressure to the optical fibre wrapped around the rubber, which in turn causes a change in its length which can then be detected by the interferometer. The distributed sensors could detect footsteps up to 5m from the cable whereas the discrete sensors could discriminate sig-

nals from noise up to 15m from the sensor. This combination of discrete and distributed sensors made it easier to characterize the various targets.

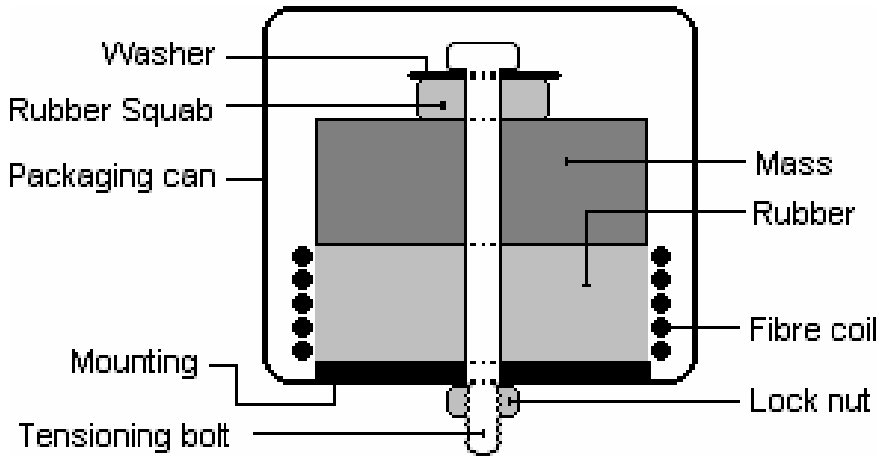

Figure 3.2: Accelerometer design [108].

The system used both wavelength division multiplexing (WDM) and time division multiplexing (TDM) to maximize the number of sensors. Moreover, the system was designed to be interfaced with an open architecture processing system capable of detecting and tracking targets and displaying them on a map on a PC. Figure 3.3 shows the output displays.

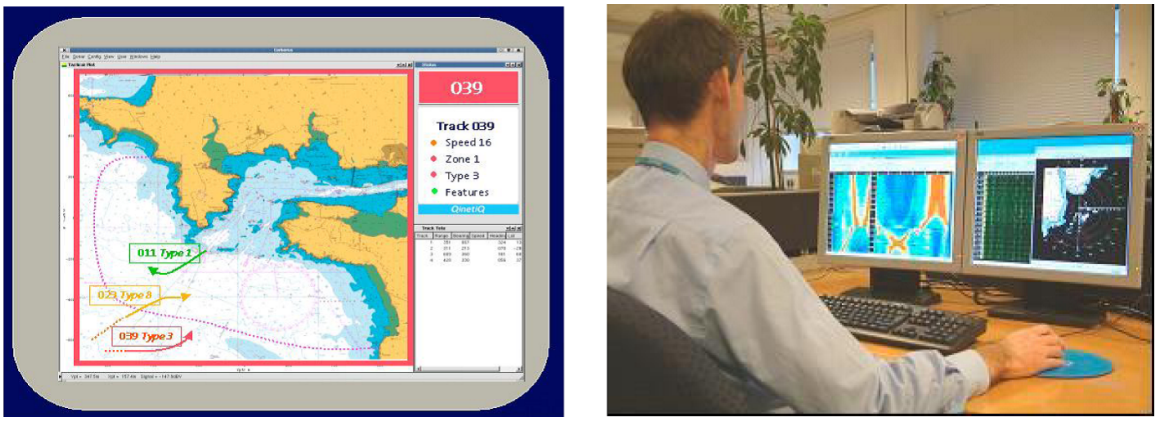

Figure 3.3: Fibre optic hydrophone security system output displays [107].

Whilst also based on interferometry, the in-ground detection method developed by Kezmah et al. [109] seems to be a cheap, effective technique as it does not require

expensive optoelectronic demodulation schemes. The two arms of the interferometer are embedded within the same fibre casing, although they both have a different buffer layer. This means that the disturbance caused by an intruder differs significantly from each arm, altering the returning signal by a number of periods. The main advantage of this technique, other than reduced cost, is that the optoelectronic unit is simple and therefore completely programmable, meaning the sensitivity of the signal can be adjusted depending on the specific environment and the level of external noise. The internal design and layout are shown in figure 3.4.

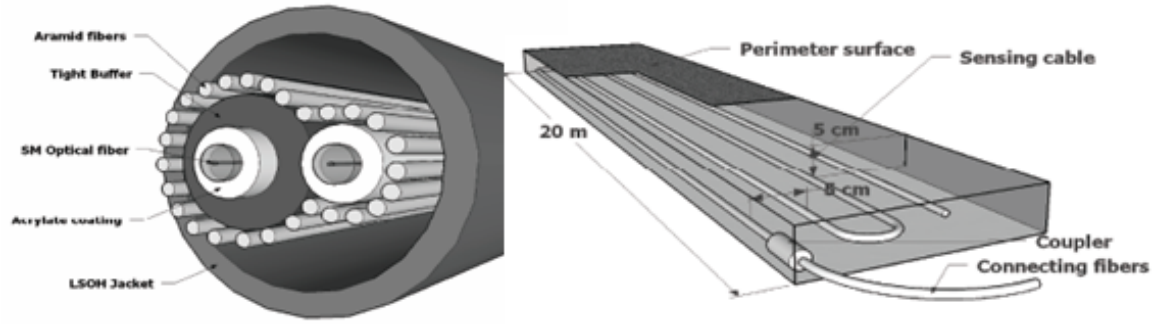

Figure 3.4: Two arm sensing cable [109].

Similarly, Mahmoud and Katsifolis [110] designed a fence based perimeter system, where two sensing fibres and an insensitive lead-out fibre are embedded in a single fibre casing as shown in figure 3.5. Their system utilizes a Microstrain locator developed by Future Fiber Technologies (FFT) and is based on a bidirectional Mach Zehnder sensing system which is capable of locating an intruder anywhere along the sensing arms. Their study focused primarily on event classification in order to increase the POD and reduce both the nuisance alarm rate (NAR) and the FAR [111, 112]. This is achieved using complex algorithms that suppress continuous nuisance alarms such as rainfall and wind, as well as recognizing events and classifying them in to groups, such as cutting events and climbing events. The system demonstrates the effectiveness of an artificial neural network as a robust classification system that can independently detect and classify an array of intrusion and nuisance events. It is worth noting that FFT is currently a world

leader in the design, development, and implementation of optical fibre based security systems with offices in America, Australia, Europe, India, and the Middle-East.

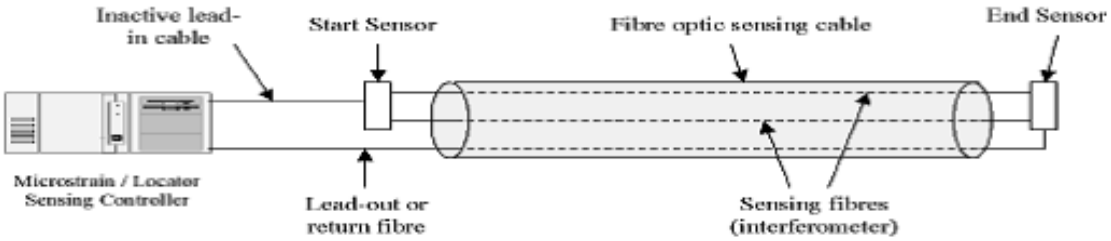

Figure 3.5: Mach-Zender interferometer encased in a single fibre [110].

A study by Yan et al. [113] focused solely on improved signal processing. They formulated an event classification algorithm for vibrations in a perimeter security system which analyzes both static and dynamic signals. A multiclass classification tree of support vector machines based on wavelet packet decomposition was used to recognize vibration signals with a 94.6% recognition rate from nine different events.

Lan et al. [114] developed a fence mounted disturbance sensor for security application which was also in Mach Zehnder configuration. A schematic of the configuration is shown in figure 3.6. Although their design worked effectively at detecting an intruder attempting to climb the fence, environmental disturbances made intrusion recognition difficult and further research on recognition algorithms was required.

McAulay and Wang [115] used a Sagnac interferometer sensor system for intrusion detection. They showed that by having two loops of different lengths it was possible to not only detect an intruder but also ascertain their location. Although they stated their system could be used as perimeter defense for an area with a circumference of up to 100km, they did not mention how precisely an intruder's location can be determined.

From 2008 to 2012, Kumagai et al. [116–118] produced three intrusion detection papers describing their system which is based on Sagnac interferometry incorporating polarization maintaining fibre. Their fence mounted system was specifically designed to be less sensitive to small vibrations from environmental disturbances as it was installed in the perimeter fence of a facility on the coast of Japan. The results compared the

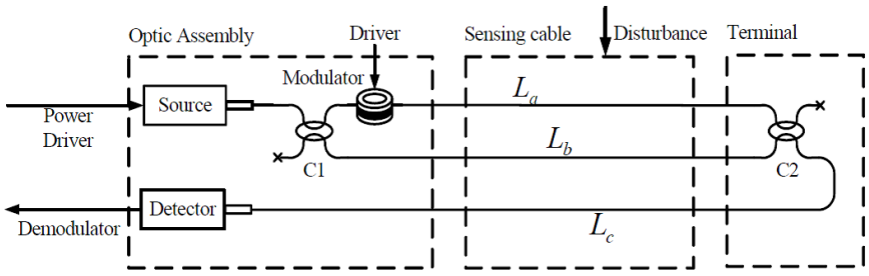

(a) Optical Circuit.

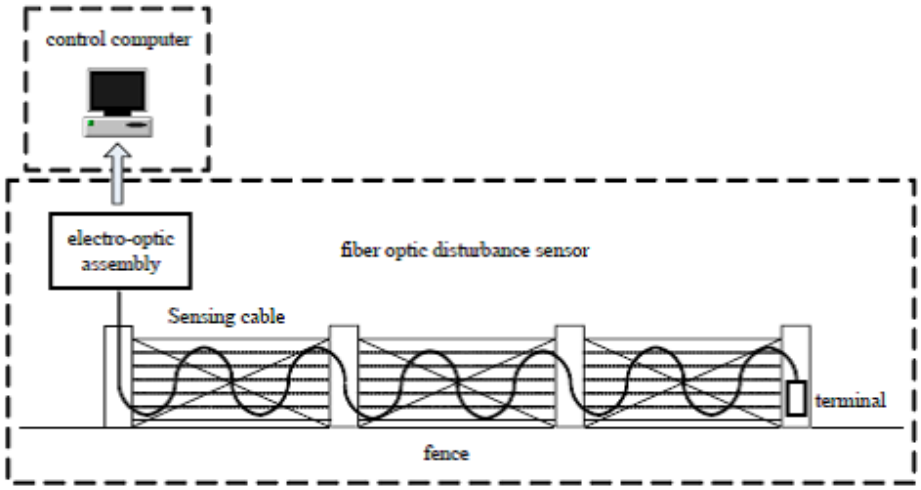

(b) Physical Layout.

Figure 3.6: Fence mounted perimeter system [114].

detection rate of intruders with the number of false alarms produced by increasing wind velocity. With the aid of a camera that was triggered to record when an alarm was triggered, their system had a 100% detection rate with a very low number of false alarms even with wind speeds of up to 45ms^{-1}.

Li et al. [119] developed a fibre optic perimeter PIDS based on Mach-Zehnder and Sagnac interferometry. Their system used a hybrid of TDM and WDM. A pulsed broadband source was split into 6 channels using a WDM. Each of the signals were then put through a 1 x 20 splitter where each of the 20 ports had a different optical delay line, resulting in 120 discrete optical sensing units. Each of the sensing units could be separated by up to 500m meaning the whole system could cover a maximum distance of

60km. As their system utilized state of the art signal processing and data acquisition, over a six month period, it had a FAR of less than 4%.

In 2013, Wu et al. [120] reported a WDM Sagnac PIDS that has a resolution of $\pm 25m$ over a 50km fibre cable. The system uses a single Sagnac loop with two different wavelengths simultaneously launched into it with four detectors used to demodulate the signals.

Speckle pattern analysis, as implemented by Rowe [70], can also be used as technique for fence mounted intruder detection. Choi [121], Arnaoudov et al. [122], and Kwon et al. [123] all reported similar perimeter fence sensing systems based on this technique. The method uses MM fibre that produces a speckled pattern when light is launched into it. Any disturbance caused by an intruder changes the pattern which, after signal processing, can be represented as a fluctuation in voltage. All three groups report effective results although each of their systems require extensive signal processing to remove external noise caused by the environment. Arnaoudov et al. [122] facilitate the signal processing using a microcontroller and produced a relatively simple hand held sensor module, whereas Kwon et al. [123], use a PC based system running a National Instruments LabVIEW program for signal processing.

Many groups have reported the use of OTDR for intruder detection. OTDR is based on Rayleigh backscattering from the fibre itself, and is good for extremely long distances, from 1km to 100km. However, an intruder's location can usually only be localized to approximately the nearest 100m. Blackmon and Pollock [124] described their system which is based on ODTR using a laser source with a very long coherence length for improved sensitivity and resolution. Their system, known as Blue Rose, is in operation at the Naval Undersea Warfare Center in Newport, USA. The Blue Rose system uses standard single-mode optical fibre with an elastomeric coating which is low cost, and can be used for long perimeter and border security applications. Vdovenko and Gorskov [125] reported work on a simulation of a phase sensitive coherent OTDR response to different disturbances which correlates well with earlier work by their group on phase sensitive fibre reflectometers [126, 127].

From as early as 2003, Choi, Juarez, and Taylor [128] described their buried PIDS that specifically used phase sensitive ODTR (ϕ-ODTR) which was designed to enhance coherent effects that are caused by the presence of an intruder or from seismic disturbances. Their simulation results predicted a 35m resolution and a 90m resolution over a range of 10km and 90km, respectively.

From 2005, Juaraz et al. [129–133] reported their physically realized system which used a narrow linewidth laser ($< 3kHz$). The orthogonal polarizations of the backscattered light were sent to separate receivers. The waveforms were then subtracted from previously stored traces to show any localized phase discrepancies produced by the vibrations of an intruder. Their results showed detection of footsteps up to 4.5m from the fibre and vehicles traveling near the fibre, consistently over a distance of 12km.

Using the same technique, Madsen et al. [134] showed that the signals received from a person walking and a car traveling nearby can easily be distinguished after signal processing, as shown in figure 3.7a and 3.7b. The advancements made in signal processing and data acquisition significantly improved the probability of detecting an intruder whilst, at the same time, reduced the risk of false alarms that may have arisen from the laser's centre frequency drifting. They also stated their system was sensitive enough to determine the weight of an intruder, as well as showing the amplitude of the signal detected by a vehicle was proportional to the distance it is from the sensor [135]. Furthermore, their system could perform real-time processing utilizing a field programmable gate array (FPGA) and incorporating LabVIEW software for visual monitoring and control of the perimeter sensor [136]. The system was, however, limited by the amount of memory on the FPGA unit. This type of work is extremely important in realizing advanced security systems that can anticipate potential intrusions before they occur, by recognizing the difference between animal, human and vehicle signatures, and reducing the number of false alarms.

The optical fiber sensors group from the University of Electronic Science and Technology of China (UESTC) [137] reported a distributed PIDS using a combination of ϕ-ODTR and polarization optical time domain reflectometry (PODTR). Both the phase

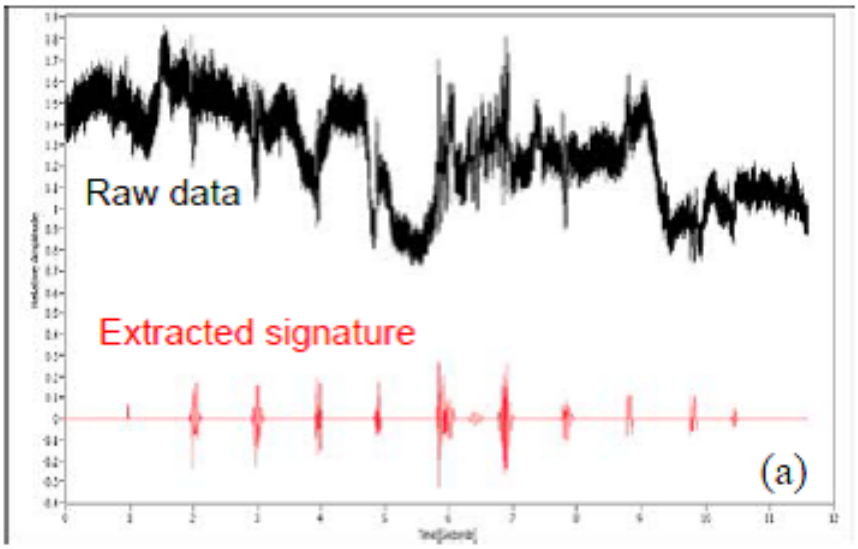

(a) Intruder on foot.

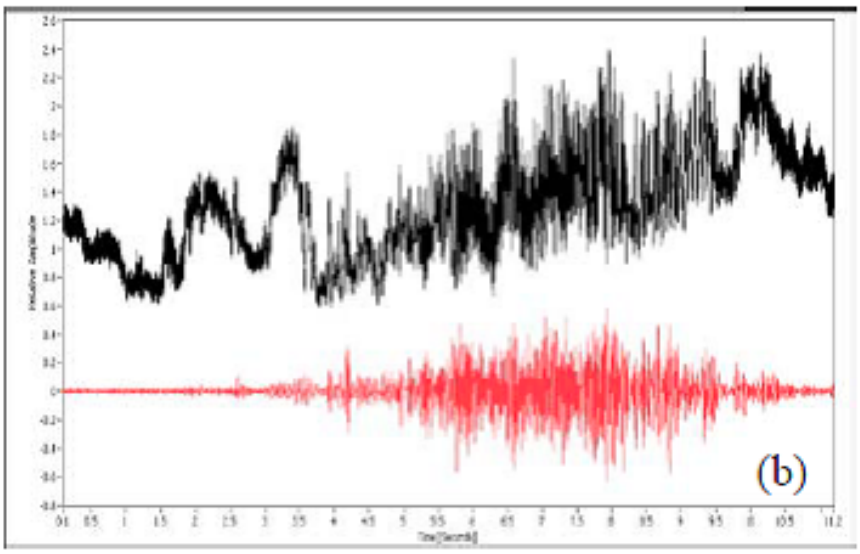

(b) Car traveling on a nearby road.

Figure 3.7: A ϕ-ODTR trace of an intruder on foot and a car traveling on a nearby road. Both the original signals and post processing signals are shown [134].

and polarization of the transmission light were sensitive to disturbances caused by an intruder; by combining these two techniques their system was extremely reliable. Using a 14km long fibre, the experimental results showed the system had a spatial resolution of 50m with 100% detection rate. Their group also showed a successful ϕ-ODTR PIDS

that was capable of detecting intrusion along the entire length of a 62km cable by using a specifically designed optical fibre which was encased in a fibre reinforced plastic [138]. In 2009, this was reportedly the longest and most sensitive ϕ-ODTR distributed sensing system to date. Their more recent work describes a 106km fence based system using PODTR with bi-directional pump lasers to amplify the signal [139]. Again the group state that at the time of publication this was the longest perimeter fence system using optical fibre based intrusion detection. However, the addition components required add to the complexity and the cost of the system.

From 2011-2013, Wu et al. [140–144] from the same group, reported a FBG based intrusion detection fence system. They reported the progress of their quasi-distributed FBG system by analyzing a number of different algorithms to improve the POD and reduce the NAR. These methods include: autocorrelation characteristics analysis, where the proposed system has a predicted POD of 99.5% and a NAR of 0.5% [140], principal component analysis, which results in a recognition rate of 96.52% for eight type of intrusion methods [141], and 3-layer back-propagation artificial neural network which has a recognition rate of 96.03% [143]. In addition, they stated their system could predict fire threats without any additional components [142]. The fence mounted FBG PIDS is shown in figure 3.8. In 2012, Rao wrote a short review paper on the research performed by the optical fiber sensors group at UESTC [144].

In 2014, the group reported an OTDR PIDS which utilizes multi-scale wavelet decomposition [145]. The report, from a year and a half long trial of a PIDS for a 220km long national borderline fence in China, states the system was successfully implemented but does not state the actual recognition rate. Both the OTDR and FBG based systems use similar intrusion detection process flow which is shown in figure3.9.

Klar and Linker [146] reported a system specifically designed for detecting underground tunneling used for smuggling, using smart underground security fences. The detection system is based on wavelet decomposition of Brillouin optical time domain reflectometry (BODTR) and was capable of detecting tunneling vibrations whilst also being insensitive to above ground noise. The approach was previously used in geotech-

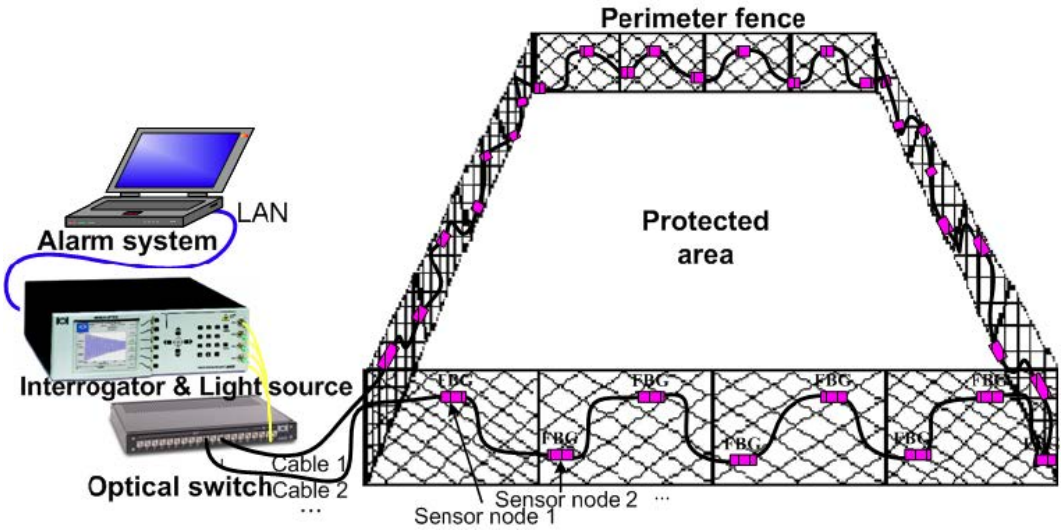

Figure 3.8: FBG based fence PIDS [141].

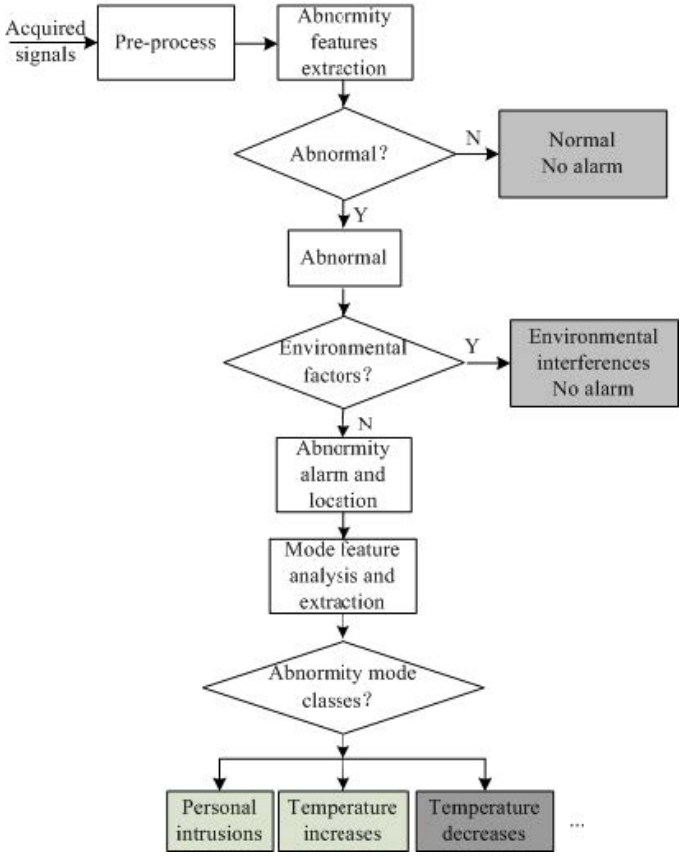

Figure 3.9: process flow for FBG based fence PIDS [140].

nical engineering for monitoring the excavation effects of large underground tunnels for transportation and water systems. The technique was then adapted to detect soil vibration caused by the excavation of much smaller tunnels. The signal processing incorporates a neural network algorithm designed to specifically recognize the wavelet coefficients from tunnel signatures. Their results indicated that their system could detect tunnels as deep as 20m with a diameter of 0.5m or larger.

Likewise, Ferdinand et al. [15] developed a system based on BOTDR. The specific design of the Brillouin analyzer is not detailed, however its characteristics are 1m spatial resolution, over 10km span, $\pm 2.5\mu$m/m strain resolution, and a 3s response time. As the system was developed as a commercial product, a strong focus was placed on the installation technique and the development of a user friendly interface. The field deployed system utilized two separate sensing cables to compare detections and eliminate false alarms.

Jia et al. [147] designed an in-line intrusion sensor system based on interferometry, comprising of a 3dB coupler and a Faraday Rotating Mirror. This technique uses the phase angle of the detection signal to determine the location of the intrusion. Their simulations showed that their system could locate an intrusion within a distance of 128m along a 40km sensing fibre. They claimed by using a Fast Fourier Transform method to calculate the phase angle of the signal, rather than loop structures, their system requires simple signal processing and hence is low cost.

A year later, the same group [148] reported an in-line Sagnac perimeter fence system and a ϕ-ODTR PIDS. Their results showed the properties of walking or running human-beings. They described the gait characteristic, which is the time for an average complete walking cycle, i.e. 2 steps is 1.216s; this includes the step period which is about 0.6s and the foot step down time which is 0.2s. They reported a person running has a step period of about 0.4s with a foot step down period of about 0.2s. Therefore, it was suggested that a signal that has a period of 0.3-0.75s and a duration of 0.15-0.25s must be a human signal, rather than a periodic signal from an animal or a random signal from external noises such as weather fluctuations. Again, these results are significant in pre-empting

an intrusion and the method is effective in determining a human intruder at extremely long distances, up to 40km from the detector. However, there was no reference to how near the person needed to be to the fibre for the signal to be recorded. Also, the person must be walking along the length of the fibre and the study does not include results for a person walking perpendicular to the fibre; hence the term "in-line". Moreover, although the methodology is reported to be much cheaper than others, the cost of interferometric detectors is significant, compared to other techniques. The group later reported work on a high speed data acquisition system specifically developed for a chaotic fibre optic fence system [149]. The system was designed for use on a high speed digital oscilloscope developed using LabVIEW. A real-time sample rate of 1GS/s was reported.

Likewise, Wang et al. [150] reported an improved OTDR system using extensive signal processing. Their technique called complementary correlation OTDR used Golay codes to overcome limitations between the maximum sampling rate and frequency of the transmitted signal. The physical setup was fairly simple as the system analyzed the transmitted and reflected power to determine if an intrusion had occurred. The implementation of Golay codes increased the signal to noise ratio and hence improved the dynamic range of the system.

Two papers by Okazaki et al. [151] and Morshed [152] reported PIDS essentially based on OTDR. However, the focus of the studies is on novel fibres. Okazaki et al. [151] reported a hetero core fibre where a section of the 9μm core was reduced to 3μm, which acted as an intensity based vibration sensor. The technique was specifically used to detect vibrations caused by a potential intruder trying to cut or break a glass window pane, by attaching the fibre sensor to a metallic needle attached to a window. The study reported two configurations of the sensor with a trade-off between sensitivity and physical size between the two of them. Both types were highly sensitive and independent of temperature fluctuations. Morshed [152] reported a very similar technique using a section of multimode fibre joined with FC/PC connectors to a single mode fibre, as the intensity based pressure sensor. The main advantages of this technique were that it was low cost and simple.

Of the four fibre optic based technological approaches; OTDR, speckle patterns (based on non-linear effects), interferometry (including Michelson, Sagnac, and Mach-Zehnder), and FBGs, the latter has seen a great deal of interest in recent years, with significant growth in the security sector in the last decade [153]. However, it has yet to be fully exploited in PIDS. In 2002, Spirin et al. [154] reported a small scale system which is based on OTDR, that also uses low reflective Bragg gratings to segment the fibre. In this way, the system can use a continuous light, source and determine in which section perturbation occurred by analyzing the transmitted and reflected optical power. Although they claimed this was a simple low cost technique, in order to scale up the system many Bragg gratings would be required to maintain the spatial resolution of the system and this would increase the complexity of the signal processing and the overall cost. In fact, the group resorted back to a traditional OTDR system for a large scale test.

In 2005, Zhang et al. [155] demonstrated an in-ground seismic wave sensor for detection of troops and vehicles in military applications. They used a network of FBGs that were fixed to an inert mass attached to a spring. This technique amplified the seismic signal from a potential intruder which was then detected by the FBG. This was the first PIDS to utilize the true reflection characteristics of a distributed network of FBGs. The technique used demodulation or reference gratings to convert the shift in wavelength caused by an intruder in to a change in optical power. An example of a single channel interrogation scheme is shown in figure 3.10.

Four years later, the same group [156] reported significant improvements on their FBG seismic sensor system including: a scanning laser wavelength-based demodulation system, a digital lock in amplifier and FPGA, and a carbon fibre cantilever for overall improved performance. The basic structure of the FBG sensor head which is attached to a spring mass system is shown in figure 3.11. Their results clearly showed the increased sensitivity and reduced response to noise of the FBG based sensor with respect to an electromagnetic sensor.

The study by Jiang et al. [158] expanded on the use of distributed FBG for invasion

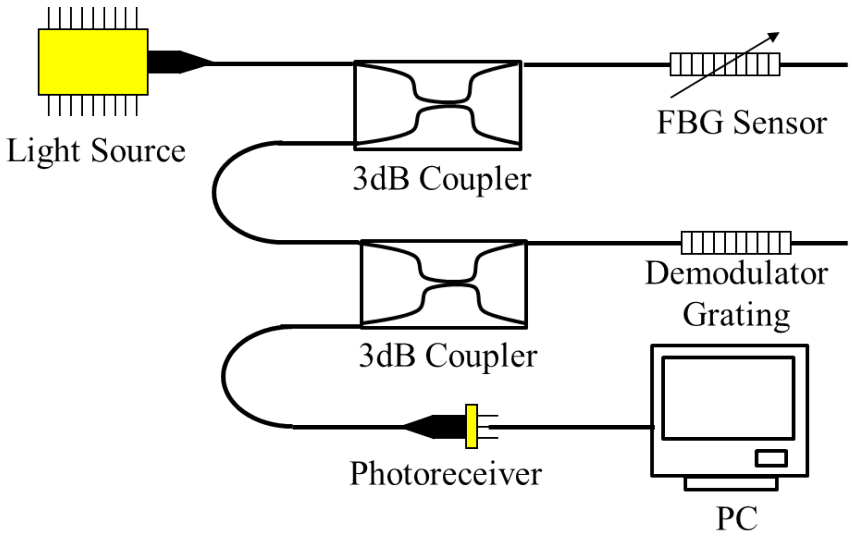

Figure 3.10: Interrogation of FBG based seismic system, adapted from [155].

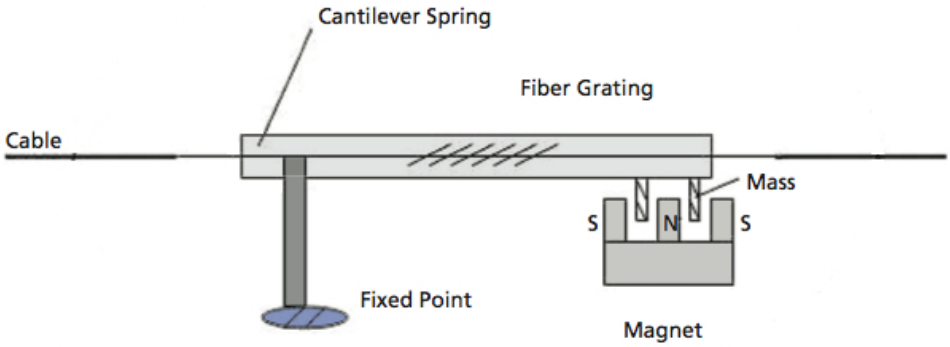

Figure 3.11: Basic structure of FBG seismic sensor head [157].

monitoring. They used Empirical Mode Decomposition and wavelet packet characteristic entropy algorithms to decompose the signals from multiple FBGs to determine the location of an intruder, through in-ground detection and fence detection. Whilst the technique was fairly comprehensive, it was effective at analyzing the vibrational signals from a number of different FBGs and calculating an intruder's location. A graphical user interface (GUI) was developed using LabVIEW, making it possible to monitor the perimeter in real-time. However, it did not allow for determining false alarms and needed to be optimized. Figure 3.12 shows the GUI.

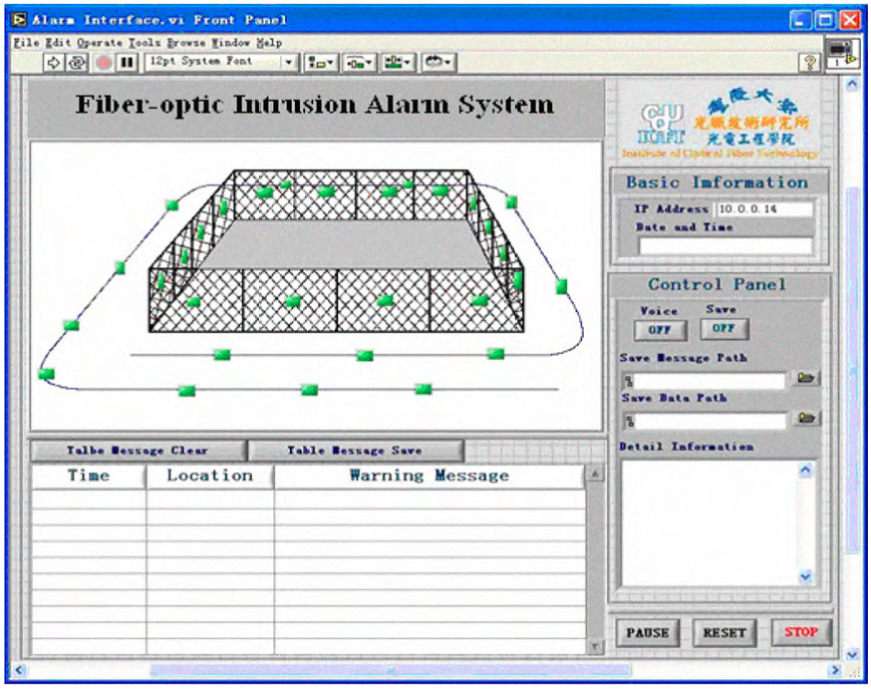

Figure 3.12: Graphical user interface for FBG based intrusion alarm system [158].

Hao et al. [159] reported an armored cable based FBG perimeter intrusion detection sensor. The report detailed the results from an in depth field trial showing the system could resolve nuisance events and uses a commercial FBG interrogator to resolve the signals from an array of sensors. However, it does not detail the design of the sensor and simply states that the armored cable protects the sensor against rodents and is crush resistant.

Most recently, Catalano et al. [68, 160] reported an FBG PIDS for protection of railway assets. They proposed the use of quasi-distributed FBG strain sensors embedded in a pressure mat for perimeter protection and FBG accelerometer sensors for rail track protection. Their results showed an intruder can easily be detected when pressure is applied to the mat or when walking close to accelerometer sensors through detection of acoustic emissions generated from the footsteps. Both sensor networks are integrated into a single system, demonstrating that different FBG sensor arrays can form the basis of an advanced PIDS using the same core technology.

The author's own research on optical fibre based PIDS is based on FBG technology, but specifically focuses on increased flexibility and usability of low cost complete security systems. This includes the development of an FBG based reed switch for monitoring windows and doors [161], a simple FBG fence mounted system, and the implementation of in ground quasi distributed FBG digital and analog pressure sensors in different flooring materials [162, 163] detailed in Chapters 4 and 5. Furthermore, the aim is to achieve seamless integration of FOS with traditional electronic controllers by utilizing simple, but innovative interrogation techniques [164] as discussed in Chapters 10 and 11 of this thesis. This has the potential to increase the penetration of optical fibre PIDS into both mainstream commercial and residential applications. In addition, it has been demonstrated in Chapter 12 that FOS could be integrated into wireless sensor networks for specific applications [165], capitalizing on the benefits of both technological approaches, with the potential of forming advanced, robust PIDS. An example of an PIDS incorporating in-ground FBGs, fence mounted FBGs, and FBG reed switches, is shown in figure 3.13.

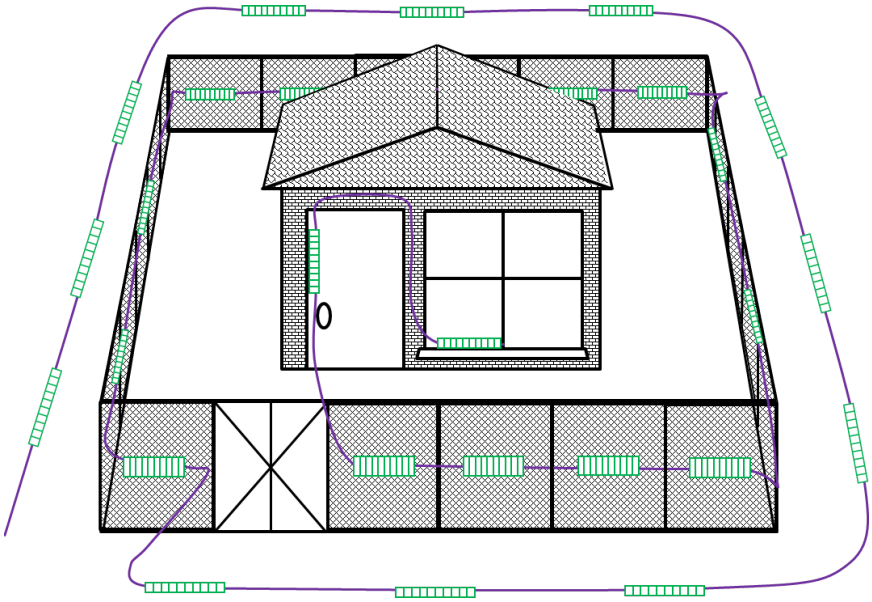

Figure 3.13: A schematic of an PIDS incorporating in-ground FBGs, fence mounted FBGs, and FBG reed switches within a single fibre.

3.7.2 The Future of Optical Fibre Sensors for Intrusion Detection Systems

As discussed throughout this review, the development of all optical fibre based systems for intrusion detection has progressed significantly throughout the last few decades because of the well understood advantageous properties of FOS with respect to physical security applications. ODTR is by far the most cost effective solution for very large perimeter intrusion detection. With the implementation of multiple detection methods, such as phase sensitive and polarization sensitive ODTR in conjunction with the significant advances in signal processing for increased sensitivity and resolution, the use of ODTR PIDS will inevitably increase.

Interferometry based systems may still be utilized in specific applications where high precision is required. However, generally the cost of implementing these systems will mean cheaper alternatives would be favored where possible.

The use of FBG sensing technology is expanding rapidly in many applications, such as structural health monitoring and is now starting to emerge into more mainstream industrial processes. This expansion will aid the growth of FBG sensing in PIDS. It has been clearly demonstrated that the improvement of signal processing techniques has a direct impact on the versatility and effectiveness of FBG based systems to ensure high POD and low FAR. Moreover, as the diversity of FBG sensors for intrusion detection increases, such as FBG based reed switches, FBG based in-ground digital and analog pressure sensors and in fence FBG sensing systems, the penetration of FBG technology in physical security applications will increase. FBGs have the potential to form a complete security system based entirely on a single technology. In addition, as low cost, simpler interrogation techniques become available for seamless integration into electrically based security systems, incorporating surveillance cameras for example, the use of FBGs in PIDS will further increase.

The author has identified two areas that will provide significant opportunity for improvement of optical fibre based PIDS:

1. electrical and optical integration, and

2. improved signal processing for large sensor capacity systems.

The integration of different quasi-distributed sensors with low cost electronic controllers will mean a complex and complete PIDS, utilising digital and analog FOS, and surveillance cameras, can be monitored through one simple supervisory control system. Moreover, surveillance cameras could be powered over optical fibres using photonic power converters, creating an almost entirely optical based system. Large systems, incorporating high numbers of densely packed sensors, will require improved signal processing and data acquisition techniques. Through pattern recognition algorithms, PIDS could pre-empt potential intruders in a non-invasive manner. For example, it may be possible to detect unusual movement of a potential intruder around a facility before a physical breech has occurred. Furthermore, it is worth noting, whichever fibre technology is implemented, and in order to be a successful system, professional installation processes and user friendly interfaces are also an important consideration for the final system design.

3.7.3 Patents for Fibre Optic Intrusion Detection Sensors

It is worth noting that whilst it is stated in this review that the first scientific report of an optical fibre based PIDS was in 1983, there were earlier patent applications. The first patent application for a fibre optic security system was filed in 1978 by Sadler [166]. However, this system was essentially an electronic sensing system connected to a control unit by an optical fibre, although, if the fibre was cut an alarm would be triggered. The first truly fibre optic intruder alarm system patent was filled in 1980 by Butter [167]. His system used a buried multimode optical fibre as the sensing element itself, and analyzed the speckle pattern changes at a detector as a disturbance or intrusion occurred. A FBG perimeter security system patent was filed in 2010 by Lamont [168]. Many more patents based on fibre optic intrusion detection have been filed which will not be detailed in this paper but can be reviewed through Google Scholar, should the reader wish to do so.

3.7.4 Intrusion Detection Conclusion

In conclusion, an historical review of optical fibre based PIDS has been given and the general theory of each of the methods has been summarized. Each of the various techniques has been explained and a detailed discussion of the results outlining the advantages and drawbacks of the proposed systems has been performed. Further, a general forecast of potential research directions has been made including improved integration of optical and electrical systems and improved signal processing for high density quasi-distributed, high performance PIDS of the future.

3.8 Fibre Bragg Grating Sensing in Mainstream Industrial Processes

In 2005, Willsch et al. [169] provided a review of FOS systems in process control, and environmental and structural monitoring. The report highlighted the developments of FBG sensing in wind turbine, aerospace, structural health monitoring, and railway transportation applications, as well as improvements in specific chemical sensors and interrogation techniques. In 2011, the same group reviewed FOS with a focus on research and industry in Germany [170]. The review again highlights the improvements made in FBG technology and its expansion from the laboratory into industrial application through spin-off companies. This is reflective of FBG technology worldwide. Nevertheless, penetration of FBG sensors in to mainstream industrial processes such as the amenities and services sector, mining, and the oil and gas industry has been extremely limited considering the technology has been developing for over 30 years. In fact, this has been highlighted many times, not least by Kersey et al. [8] almost 20 years ago who stated that fibre sensor technology remained in a laboratory-based prototype stage. Whilst there has been some commercial success, this appears to still be the case. There are a number of reasons why their diffusion into these markets has been so slow: from lack of awareness and trust in the technology, to deficits in the physical engineering of

appropriate transducers for rugged environments, as well as the complexity and cost of FBG sensor networks. Moreover, the lack of FBG sensing and interrogation standards, means the technology has only significantly progressed in niche applications, such as structural health monitoring, which will not be covered in detail in this report.

The main focus of researchers over the years with regard to FBG sensing in general, has been to design and produce FBGs with increased sensitivity at different wavelengths, which arguably, for relatively low frequency applications such as the process control industry, is not the most significant factor. Whereas in fact the correct dynamic range, appropriate packaging and networking capabilities are far more significant issues.

In recent years, however, there have been significant developments in two of the areas that have restrained the progress of FBG technology. Firstly, the issue of temperature and strain isolation has been overcome using various techniques reported in the literature, from simply having co-located FBGs that are exposed to the same temperature fluctuations to isolate stress and strain, to more complex methods, such as using tilted or chirped FBGs to distinguish between the different measurands. Secondly, simpler interrogation techniques are being utilised such that the optical signal can easily be transposed into the electrical domain, allowing the optical networks to be interfaced seamlessly with electronic systems. In addition, the production of FBGs has improved significantly through draw tower processes and automated manufacturing [171].

Here, how the FBG market has grown over the past decade and what the predictions are for growth in the industry in the future are explored. The development of the various different types of FBG sensors that have been developed for potential use in mainstream process control industries from past to present are discussed. Moreover, the different interrogation and networking techniques, and their integration with existing control system technology, are reviewed. The section concludes with recommendations for future work that would potentially provide significant opportunity for the advancement of FBG sensor networks in these mainstream industries.

3.8.1 Market Overview

Fibre Optic Sensors

A report released in February 2014 by ElectroniCast, a market and technology forecast consultancy company, states that the global consumption value of FOS will grow from US$1.89bn in 2013 to US$4.33bn in 2018 resulting in an annual growth rate of 18% as shown in figure 3.14 [172]. A similar report released by BCC Reasearch in June 2014 states the same market will grow from US$1.8bn in 2013 to US$2.2bn in 2018, resulting in a compound annual growth rate (CAGR) of 4.5% [173]. This follows BCCs 2011 report which predicted a growth from US$1.2bn in 2011 to US$2.5bn in 2017, a CAGR of 10.5% [174].

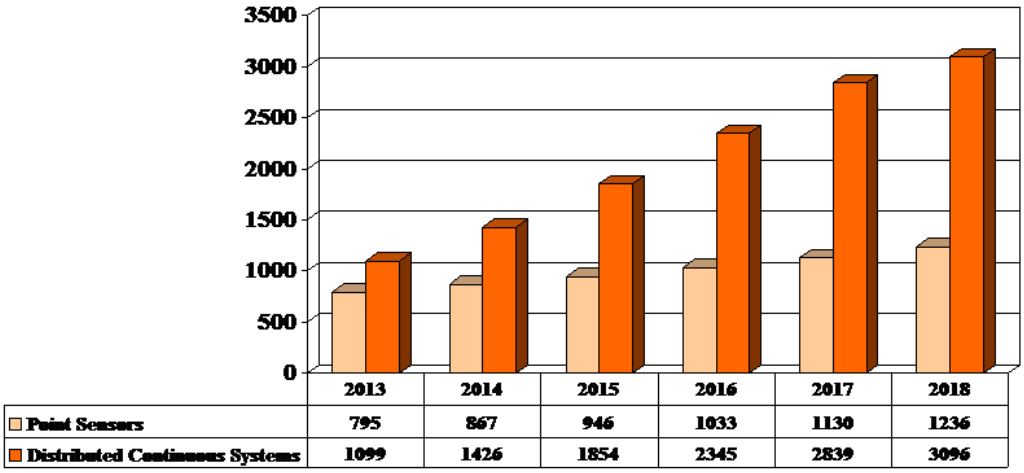

Figure 3.14: Fiber Optic Sensor Global Consumption Market Forecast (Value Basis, US$Billion)

The distributed FOS market was $585M in 2013 and projected to be US$1.458bn in 2018 with one of the major applications being process control, as reported by the Photonics Sensor Consortium in conjunction with Light Wave Venture [6]. Despite some discrepancies in the figures, all of the reports predicted substantial growth in the FOS market, particularly in intrinsic sensors, i.e. those embedded within the fibre.

Automation Industry

The global process automation market revenue is expected to grow from $86.1bn in 2012, to $124.3bn in 2018, at an estimated CAGR of 6.05% from 2013 to 2018. Also, the process instrumentation market is expected to grow from $26.5bn in 2012, to $36.7bn in 2018, with a CAGR of 5.07% [7]. Seamlessly integrating FOS into process control industries has the potential to not only tap into these lucrative markets but also boost them further.

3.8.2 Types of FBG Sensors for Mainstream Industries

The most commonly used sensors in process control industries such as power generation, water treatment and services, mining, and the oil and gas are; temperature, pressure, level, chemical, and flow. FBG sensors have been demonstrated for sensing each of these different measurands.

FBG Temperature Sensors

FBGs are inherently sensitive to temperature as outlined in the theory of this paper, and as such the literature for FBG based temperature sensors is extensive. Some of the key findings will be discussed in this paper. In 1990, Morey et al. [62] were the first to show a FBG temperature sensor. They reported a FBG temperature sensitivity of 6.8pm/^oC at a wavelength of 830nm. Xu et al. [175] reported a FBG temperature sensitivity of 10pm/^oC at a wavelength of 1300nm, in 1994. The following year, Rao et al. [176] reported a FBG temperature sensitivity of 13pm/^oC at a wavelength of 1550nm. Since then Rao has published a number of papers on the progress of FBG technology and applications. Not least, in 1997, Rao et al. [177] devised a FBG temperature sensor system for medical applications. They showed that FBGs could be used for profiling the human body during hyperthermia treatment. They achieved a resolution of 0.1^oC and a precision of $\pm$0.2^oC over a temperature range of 30-60^oC. Recently, Mamidi et al. [178] reported a high temperature FBG sensor with an operating range from 20-550

^oC. Interestingly, they also reported a low cost intensity based interrogation technique using a LPG as a linear edge filter. The system had a resolution of 0.5^oC. Canning et al. [179] presented a review of 4 different types of temperature sensors using gratings with distinct characteristics. Among these, a high temperature sensor with an operating range of up to 1200^oC, was reported.

One of the main applications for FBG based temperature sensors is in electrical power systems and large generators because of their immunity to electromagnetic interference. A number of studies have been performed and are detailed in [180–186].

Perhaps more significant, with respect to FBG temperature measurements, is the research based on techniques for temperature compensation when using FBGs to detect other measurands. In other words, how is it possible to isolate and distinguish between fluctuations in temperature and strain induced changes? Some of these techniques will be discussed in the following sections.

FBG Pressure Sensors

The sensitivity of FBGs to pressure can be a direct result of strain induced in the fibre due to pressure or by a pressure change on a transducer which can cause a positive or negative shift in the Bragg wavelength. Xu et al. [187] reported a FBG pressure sensor in 1993. They showed a wavelength-pressure sensitivity of -3pm/MPa over a range of 70 MPa. This is the commonly excepted value for the pressure sensitivity of a standard bare FBG. This value is far too low for most sensing applications and as such the main focus of research groups was to produce pressure sensors with increased sensitivity. The improvements are detailed in the following paragraphs.

Three years later Xu et al. [187] reported another FBG pressure sensor, having improved the pressure sensitivity by a factor of ten, using mechanical amplification, by mounting the FBG in a hollow glass bubble [188]. Liu et al. reported simultaneous measurement of pressure and temperature using a polymer coated FBG. Their results show a sensitivity of -80pm/Mpa and $88pm/^oC$ at 1540.2nm [189]. They then increased the sensitivity of their sensor to -5.28nm/MPa by embedding the polymer coated FBG in

an aluminum cylinder [190]. In their later work, with the polymer coated FBG embedded in a copper cylinder, they reported a sensitivity of -3.77nm/MPa at 1558nm but with improved thermal stability [191]. The group then reported an ultra thin FBG pressure sensor with the FBG bonded perpendicular to a diaphragm causing the FBG to stretch along the length of the FBG under pressure. They studied the effects of varying the radius and Young's modulus of the diaphragm. When optimized, the sensitivity was as high as 7nm/MPa [192]. More recently the same group also reported a diaphragm based FBG sensor which uses an L-shaped lever and has a sensitivity of 0.244nm/kPa [193]. A schematic of the sensor is shown in figure 3.15.

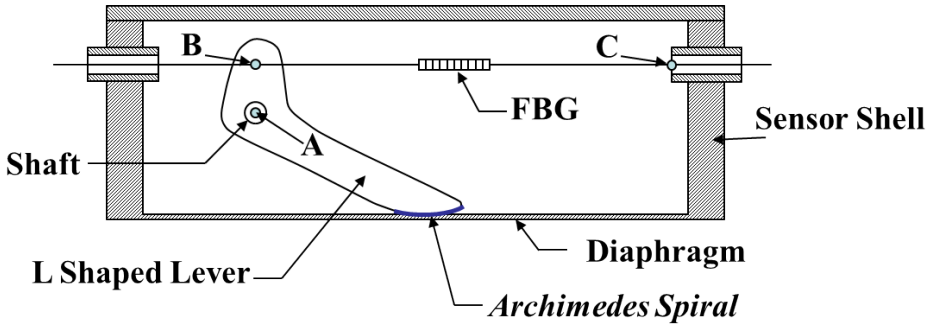

Figure 3.15: Schematic of the ultra high sensitive pressure sensor, adapted from [193].

A FBG pressure sensor embedded within metal bellows was reported by Song et al. [194]. As the metal bellows have a lower spring rate than the fibre a sensitivity of 48pm/kPa was reported.

Again using a polymer filled aluminum casing, Ahmad et al. [195] reported a sensitivity of -8.7nm/MPa. The same group [196] also reported a metal diaphragm based FBG pressure sensor with a sensitivity of -1.67nm/Mpa. Although this is not as sensitive as the polymer based sensors, it can be used in more practical applications as it is more robust and not susceptible to corrosion.

Likewise, Huang et al. [197] reported a diaphragm type FBG pressure sensor with a sensitivity of 1.57pm/kPa across a range from 0-1MPa. By using two FBGs and analysing the difference in the wavelength shift, the temperature sensitivity was ef-

fectively eliminated. The same group [198] also reported a Bourdon tube type FBG pressure sensor designed for pipeline leakage detection. The sensor has a sensitivity of 1.414pm/kPa across a range from 0-1MPa. Temperature compensation is achieved in the same way as their previous sensor. A schematic of the design is shown in figure 3.16.

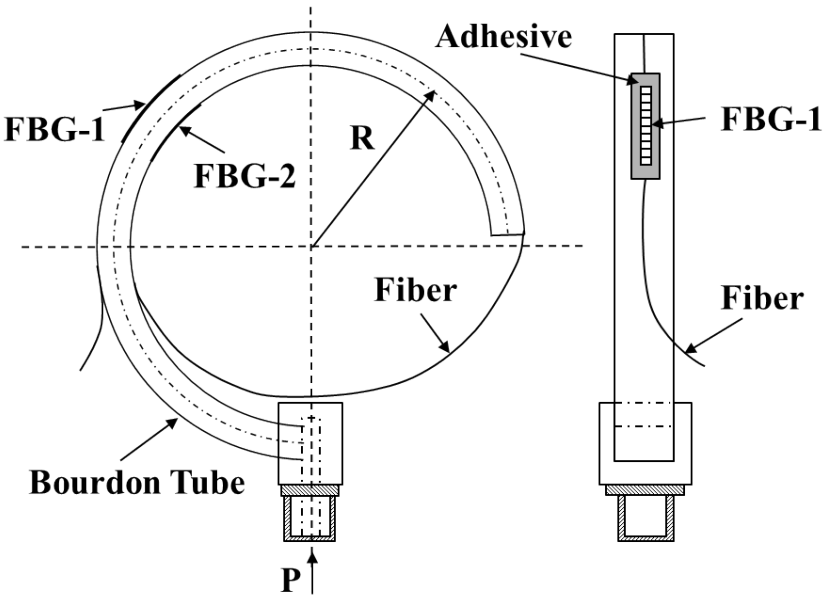

Figure 3.16: The structure of the FBG Bourdon tube pressure sensor, adapted from [198].

Pachava et al. [199, 200] also described a diaphragm type FBG pressure sensor where the FBG is bonded perpendicular to the diaphragm surface with a U-shaped clamp. They report a sensitivity of 31.67nm/MPa. Xiong et al. [201] designed, simulated, and tested a similar sensor to that proposed by Pachava et al. [199, 200], which had a sensitivity of 3.55nm/MPa.

Bock et al. [202] reported a tapered long period Bragg grating pressure sensor with a pressure sensitivity of 51pm/MPa, which was significantly greater than a bare standard FBG. LPGs have the potential to have custom designed sensitivities; however, the manufacturing process is usually expensive and time consuming. In their paper, Bock et al. [202] described a new low cost fabrication technique using a computer assisted

precision arc-discharge apparatus.

In 2010 and 2011, Yan et al. [203, 204] described their pressure sensor sheet which used FBGs fabricated in photonic crystal fibres (PCFs), which were then embedded in polymer foils. Their initial sheet had 5 FBGs within it, whereas their later sheet consisted of 15 FBGs in a mesh layout with a spatial resolution of 10mm. The intention was to develop a large area pressure mat for use in rehabilitation and medical fields. They report a local pressure sensitivity of 9.08pm/kPa and 265pm/kPa, for the small and large sheet, respectively.

A pressure sensor reported by Hsu et al. [205] has a sensitivity of 28pm/MPa and is effectively temperature insensitive. They use a strained FBG and mechanical system that reduces the strain on the FBG as the temperature increases, causing the Bragg wavelength to shift in the opposite direction. The result was a minimal wavelength shift across a temperature from 10 - 60^oC.

Wu et al. [206] described a sensor capable of measuring temperature and hydrostatic pressure simultaneously using a FBG in a standard section of fibre combined with a FBG in a section of grapefruit microstructured fibre. The FBGs showed a similar response to changes in temperature of approximately 11pm/^oC. However, the microstructured FBG was significantly more sensitive to pressure variations having a sensitivity of 13.4pm/MPa, compared to 4pm/MPa for the standard FBG.

Rajan et al. [207] reported a pressure sensor incorporating a vinyl diaphragm and a polymer FBG. The lower Young's modulus of the polymer FBG resulted in a sensitivity of 1.32pm/pa, more than 6 times greater than the most sensitive standard FBG pressure sensor reported to date.

The author details a similar study in chapter 6 of this thesis whereby a standard FBG is bonded to a rubber diaphragm. The pressure sensor results show a sensitivity of 0.116nm/kPa.

FBG Level Sensors

Many FBG level sensors are essentially pressure sensors that determine the level of a liquid based on the pressure applied by the liquid, which is proportional to the height of the liquid. As such, some research groups have developed liquid level sensors through simple modifications of their pressure sensors. Guo et al. [208] described their temperature-insensitive FBG liquid level sensor, which was based on a cantilever beam structure. The particular shape of the structure produced a chirp in the FBG under pressure, which was proportional to the height of the liquid. This chirp broadened the reflected spectrum and resulted in a change in optical power when connected to a photodiode. Changes in temperature caused the Bragg wavelength to shift but did not change the received optical intensity. This is a good example of exploiting nonlinear responses from a FBG to isolate different measurands. Lai et al. [209, 210] also reported a liquid level sensor, whereby a FBG was bonded to a cantilever which is attached to a buoy. The FBG experienced a vertical pressure that compresses it depending on the amount of buoyancy, which corresponds to the level of the liquid. Meng et al. [211] reported a similar simple technique using a cantilever with a float attached to the end. As the liquid caused the float to rise, a strain induced wavelength shift occurred. Dai et al. [212] described their simple technique of measuring liquid level by attaching one end of a FBG to the base of a container and the other end to a float, thus relating the strain to the level of the liquid.

In 2002, Fukuchi et al. [213] described a Bourdon tube based water level sensor. A FBG was attached to the end of the Bourdon tube so that an increase in pressure caused by increased water level would increase the strain on the FBG. Sengupta et al. [214] reported a very similar hydrostatic pressure sensor used for measuring liquid level. Their design was also based on a Bourdon tube with two FBGs attached to the free end of it. The change in hydrostatic pressure induces a strain in one of the FBGs, and not the other, meaning it is effectively temperature insensitive.

There have been some reported techniques for direct liquid level sensing which will

be discussed. Khaliq et al. [215] described their LPG level sensor. The ratio of the amount of the FBG immersed in the liquid to that exposed to air produced a change in transmitted intensity. Yun et al. [216] reported an etched FBG liquid level sensor. Etching the cladding from the FBG increases its response to changes in refractive index. Again the ratio of the amount of the FBG immersed in the liquid to that exposed to air produced a change in intensity. Similarly, Mou et al. [157, 217, 218] demonstrated a semi-immersed FBG that exploited the difference in refractive index of the liquid and air. Their sensor, however, used a tilted FBG rather than an etched FBG or a LPG. Recently, Gu et al. [219] demonstrated a similar technique using a tilted FBG inscribed in a thin core section of a fibre. Their results show high sensitivity and immunity to temperature changes.

FBG Flow Sensors

Recently, there have been a number of studies performed using FBGs as flow sensors. As with all FBG transducers, FBG flow sensors either manipulate a strain or temperature induced wavelength shift to determine the flow rate. Some research groups, such as Zhan et al. [220], have developed flow sensors that act in a similar way to the level sensors, in that a cantilever is used as the basis of the sensor. The force created by the flow of a fluid causes the cantilever to deflect, which in turn changes the induced strain on the FBG. Lu and Chen [221] also used this technique and reported a flow meter with a resolution of $58.1 cm^3/s$ in the forward direction and $166 cm^3/s$ in the backward direction. Yao et al. [222] also used this method, although they used two FBGs; one attached to either side of the cantilever for temperature compensation. Other gas flow sensors exploit changes in temperature, by coating the FBG and adapting the principles of conventional hot-wire-anemometers. That is, monitoring the temperature change as a function of gas flow around the sensor [223]. Cashdollar and Chen [224], and Caldas et al. [225, 226] reported a gas flow meter using this technique, by coating a FBG with silver. Cashdollar and Chen [224] demonstrated a FBG heated with a laser diode and nitrogen gas blown on to it. The results showed that the change in temperature of the

FBG, and hence the shift in Bragg wavelength, related to the gas flow rate. Caldas et al. [225, 226] used a hybrid LPG and FBG setup with 1480nm light launched into the fibre. They presented a working air flow meter with a resolution of 0.8m/s.

Rodriguez-Cobo et al. [227] proposed a novel FBG flow sensor. They demonstrated the use of their fluid flow sensor using an arc-shaped plastic transducer with two FBGs attached to it. The air flow caused one FBG to stretch and the other to compress. Salgado et al. [228] used two strain sensors FBGs to measure the change in circumference and length of a PVC pipe, which they correlated with the flow rate of the fluid in the pipe. Jiang and Gao [229] reported a dual FBG flow sensor using an elastomer transducer with a specifically designed shape to maximize the impact of the fluid flow.

Zamarreno et al. [230] demonstrated a multiplexed 8×8 FBG array for measuring flow rate, followed by a 16×16 FBG array capable of measuring fluid turbulence [231]. The FBG array was orientated perpendicular to the pipe, producing a two dimensional map of the fluid flow. The results showed different patterns for different flow rates.

Additional FBG Sensors

Over the years there have been a number of papers published on the use of FBGs as chemical sensors, from Meltz et al. [232] in 1991 to Lu et al. [233] in 2009. Most techniques are based on the interaction of hydrogels or polymers that swell in the presence of specific chemicals or the interaction of the evanescent field with different chemicals. When a FBG is immersed in a hydrogel, it causes the FBG to expand as the hydrogel swells [234]. Cong et al. [235] specifically show a salinity sensor using this method. Figure 3.17 shows a representation of a FBG chemical sensor immersed in a hydrogel. Frazao et al. [236] reported an etched FBG for salinity measurement through evanescent field interaction. Furthermore, the group demonstrated the use of their sensor for simultaneous measurement of salinity and temperature in a large scale, fully integrated, environmental monitoring system.

FBGs have become the basis of a number of more exotic sensors such as magnetic field sensors, accelerometers, and tilt sensors etc. An example of some of these sensors is given

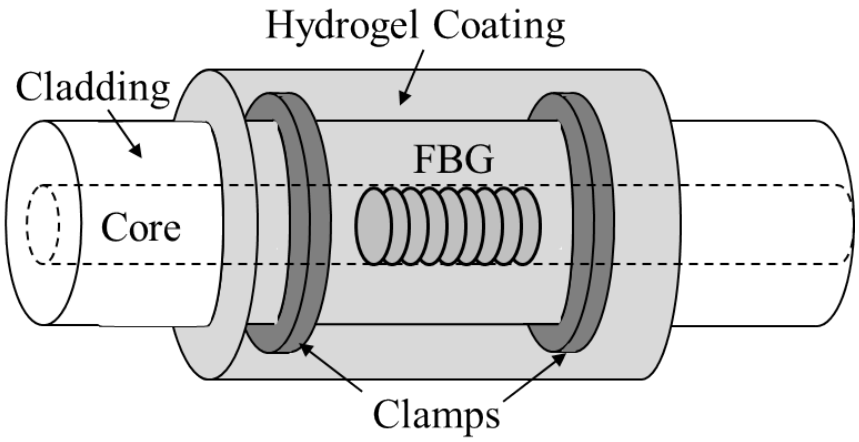

Figure 3.17: A FBG chemical sensor based on mechanical work on stimuli-responsive of a hydrogel, adapted from [234].

below. Madhav et al. [237] demonstrate a FBG bonded to a piece of Nickel can act as a magnetic field sensor. A magnetic field induces a strain on the Nickel which is detected by the FBG. Zhu and Shum [238] report a FBG accelerometer in which a FBG attached to a cantilever is deflected depending on the magnitude of the applied acceleration. Guan et al. [239] described a FBG tilt sensor. Four FBG sensors are attached to four arms that are perpendicular to a pendulum. Each FBG is strained equally when the pendulum is vertical; when the pendulum is tilted each FBG experiences a strain. The system can detect the magnitude and direction of the inclination with respect to the horizontal direction.

3.8.3 FBG Multiplexing and Interrogation Techniques

One of the main advantages of FBG sensors is their ability to be easily multiplexed through TDM and WDM. There are many different multiplexing architectures for quasi distributed sensor systems such as serial bus, dual bus, star, tree, and mesh. Each of these architectures are detailed in [240]. Which architecture is the most appropriate depends on the requirements of the application, such as the number of sensors in a system, and also on cost.

The information from each sensor must be separated and interpreted, which requires an interrogator system to interrogate many FBGs connected in series. Initially, FBG interrogators were large, complex and expensive units; however, since the late nineties, a number of different groups have attempted to minimise and simplify them without loss of functionality.

In 1998, Fallen et al. [241] reported a simple passive system that could simultaneously interrogate several FBG sensors. Half of the reflected light was incident on a ramped grating and the other half was sent to a reference arm. As the ramped grating had a large bandwidth, each reflected signal from multiple FBGs in series would be reflected off different parts of the ramped FBG. In a similar way, Chtcherbakov et al. [242] presented an active interrogation system using a chirped FBG. However, instead of receiving a change in intensity, the signal was converted into a phase change and de-multiplexed using an arrayed-waveguide grating; then the signals were sent to separate detectors.

Ye et al. [243] demonstrated an active interrogation method using polarisation maintaining (PM) fibres, whereby the reflected signals from multiple FBGs firstly passed through a Fabry-Perot filter, separating the different wavelengths, and secondly, passed through a polarisation splitter, which were then sent to two different detectors. The advantages associated with this method were that the transverse strain measurements were inherently temperature independent, and as there were two separate detectors, there was no limitation on the measurable strain due to the gap between the two Bragg wavelengths decreasing below the normal achievable resolution.

Another active interrogation system shown by Abad et al. [244] used a two stage de-modulation similar to that of Ye et al. [243], except they used a LPG rather than a chirped grating for separating the wavelengths and then applied a phase delay to the signals using a delay line. This method only required the use of a single detector as the relative phase difference was not affected by unwanted power fluctuations.

A portable, robust FBG interrogation system was proposed by Roths et al. [245] in 2005. The technique used a tunable FBG that is stretched by a piezo-electric transducer (PZT) and a saw-tooth voltage signal, which acted as an analyser. This approach

had significant merit, as it addressed the issue of reducing the complexity and cost associated with interrogator systems. Unfortunately, the system required fairly extensive calibration and data acquisition software to correct nonlinearities associated with the PZT.

Beccherelli et al. [246] reported an intensity based interrogation method using an integrated optical filter. The technique used a tunable liquid crystal polymer that could select a specific wavelength depending on the voltage. Again, they presented their work as a simple inexpensive option. Likewise, Tsai et al. [247] used an intensity based tunable system incorporating a fibre Fabry-Perot (FFP) filter that was controlled by a voltage from a control I/O board. The FFP filter was tuned with an incremental step of 0.02V, which corresponded to a resolution of 5pm in wavelength. Figure 3.18 shows their experimental setup.

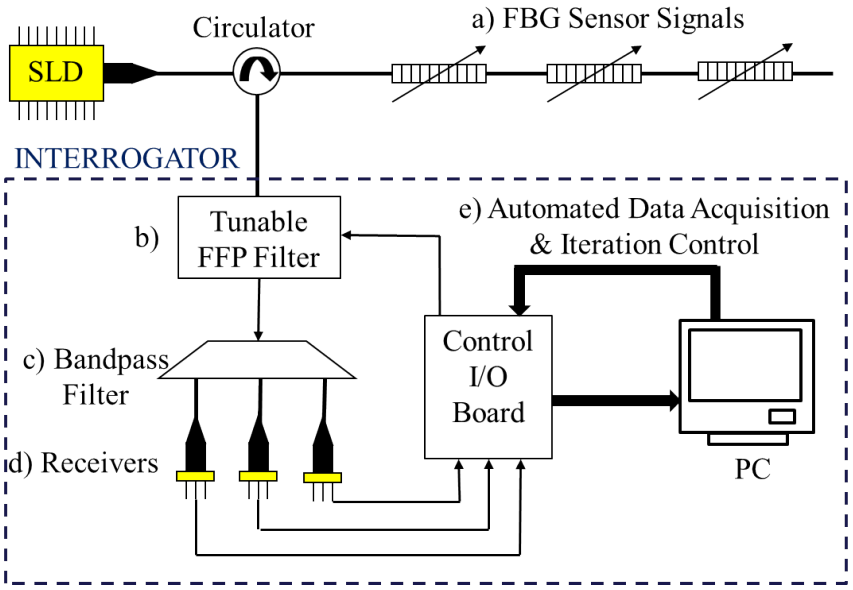

Figure 3.18: Schematic diagram of proposed Bragg grating interrogation system: (a) FBG sensor signal; (b) tunable FFP filter with voltage controlled by a computer; (c) bandpass filter with number of matched-spectral window; (d) number of corresponding photodetectors; and (e) automated data acquisition and iteration control, adapted from [247].

Villatoro et al. [248] also reported a low cost intensity based interrogator. Their system used a two-mode PCF interferometer. The PCF acted as a linear variable filter in the range of 800nm to 1600nm, and could detect wavelength shifts as small as 2pm.

A pertinent study performed by Kunzler et al. [249,250] had many similar objectives to the research that is to be performed here, in that their goal was to produce a small low cost interrogator that could also be networked. Their fibre sensor integrated monitor (FSIM) had the ability to monitor a full array of fibre sensors, including several FBGs at the same time at kilohertz speed. Their unit consisted of a tunable SLD which was swept across a wide range of wavelengths reflecting off any FBGs within the range. Each peak Bragg reflection was recorded and compared against the value of the previous scan. This technique minimised the amount of data processing, meaning the FBG sensors were feasible for sensor networks. The FSIM was a low cost, high speed device which was significantly smaller and less complex than other commercial interrogators. Figure 3.19 shows a comparison of some optical interrogator units with respect to the FSIM.

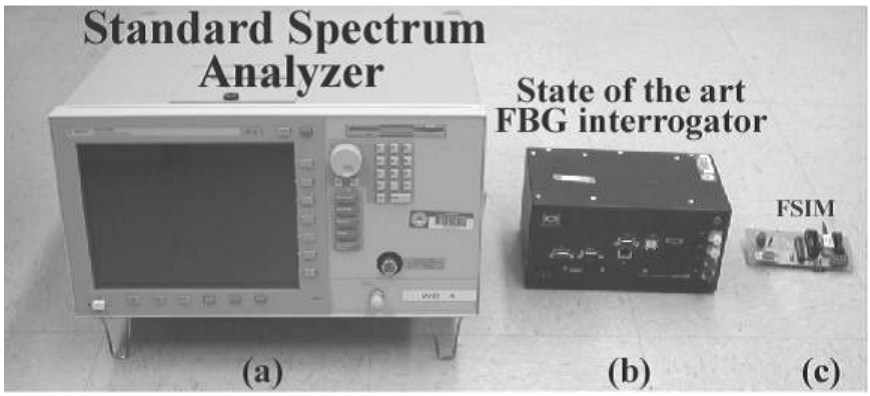

Figure 3.19: A comparison of the sizes of (a) an optical spectrum analyser, (b) a Micron Optics FBG interrogator, and (c) an FSIM handheld prototype [249].

Orr and Niewczas [251] reported a polarization-switching FBG interrogator for simultaneous measurement of magnetic field strength and temperature. The system used a polarisation beam splitter and a fast optical switch to select which polarised signal is sent to the Mach-Zehnder interferometer. The interrogation involves comparing reflec-

tions from both left and right circularly polarised light. In this way, any common noise or drift can be easily cancelled out. As the magnetic field strength is determined from the angle of polarisation, any other measurand that causes a wavelength shift, i.e. temperature, pressure, etc, can be measured simultaneously. Whilst this active technique appears to be effective, the setup is expensive because of its complexity.

Due to the increase in use of FBG networks over the last decade, a number of different commercial interrogator systems have emerged. However, the technology is still relatively new, meaning many of the products on the market do not live up to the manufacturer's claims or customer's expectations, for a number of different reasons including system failure and inaccurate measurements. Furthermore, the lack of a robust measuring system is not only due to problems associated with the interrogator itself, but also with the interrogator software and the sensors [39]. Table 3.1 shows an overview of a number of these interrogators.

It is worth noting that all of the commercial interrogators available are large expensive units. A detailed comparison of the performance of the HBM, Insensys, and Smart Fibres products is given in [39].

3.8.4 Optical Actuation and All Optical Control Systems

An entirely optical control system would be highly advantageous in certain applications. They have the potential to exceed current sensitivity and communication speeds as well as having all the advantages associated with optical systems and none of the drawbacks of electrical systems.

The goal is to create a control loop where the process variable is both detected and modulated in the optical domain, in addition to the controller providing feedback optically, with the final component being actuated via an opto-pneumatic or opto-electric converter. Whilst steps have been made toward achieving this goal, to date a practical complete system has not been realised and currently the best solution is to have minimal electronic signal conversion.

Table 3.1: An overview of commercially available FBG interrogators, adapted from [39]

Supplier	Model	Resolution (pm)	Accuracy (pm)	WDM/TDM
Micron Optics	Sm130-200	0.5	2-5	WDM
HBM	1-DI-101	0.5	2-5	WDM
Welltech	FBG3000-8	1	5	WDM
FOS&S	FOS&S-X1	1	10	WDM
FOS&S	FOS&S-X2	1	10	WDM
FIBERPRO	IS7000	1-2	5	WDM
Technobis	TFT4	1-2	Not Specified	TDM
Technobis	Deminsys	2	Not Specified	WDM
Insnesys	WT-1010	0.8 /2/5	a few $\mu\epsilon$	TDM
Smart Fibres	T4	6	20	TDM

In 1990, Hockaday and Waters [252] showed a technique for direct optical to mechanical actuation. Their method uses lasers to heat a pneumatic or hydraulic fluid causing it to deviate from a central path. The deflection was a result of optical modulation of the fluid viscosity. The deflected jet of fluid produced a direct differential pressure signal that can be controlled without the need of any electronic signal. The differential pressure was used to actuate a valve.

In 2003, Mahmoud [253] discussed the potential of an all optical control system (AOCS) incorporating FBGs. FBGs enable the process variable to be transmitted, modulated, and received on a single fibre optic cable and mimics the two wire 4-20mA electronic signal of an electronic process control loop. He described how FBGs can be used to measure many different process variables such as temperature, strain, and flow, and illustrates an AOCS. Figure 3.20 shows the AOCS, where the process variable is

converted into a frequency via a fast Fourier transform, and then the controller uses a PZT to tune another FBG to provide an optical output. It is stated that the proposed system would need an opto-pneumatic or opto-electric converter to provide actuation. The actuation could then be performed by a technique based on Hockaday and Waters' [252] system or by using a photovoltaic power converter (PPC) [254].

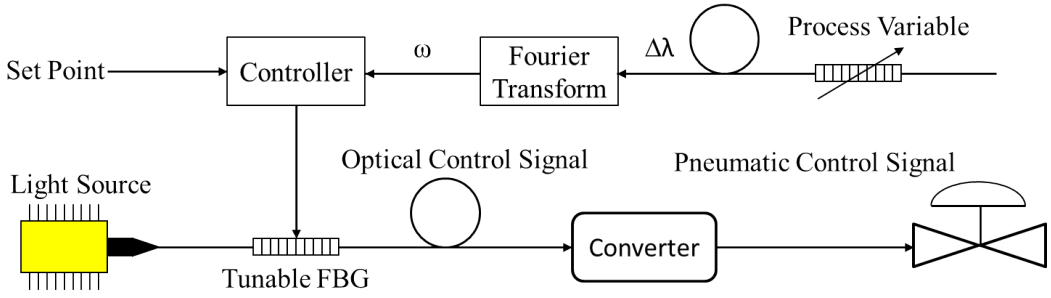

Figure 3.20: All optical control system, adapted from [253].

PPCs are essentially miniature solar cells designed to be responsive to specific wavelengths and connected directly to an optical fibre. GaAs photovoltaic power converters have conversion efficiencies as high as 55% [255]. The only commercially available PPCs are made of GaAs, and can produce up to 0.5W of electrical power. GaAs has been a particularly favourable material for use as a PPC because of its high quantum efficiency, 90%, and relatively high responsivity of approximately 60% at a wavelength of 0.82 microns [256]. In general, experimental evidence shows that the higher the band gap energy of a material, the higher the photovoltage and fill factor, as shown in table 3.2

A GaAs PPC would be transparent to any signals above 0.87μm, making it a useful device in modern optical communication networks. Also, lasers producing light within the GaAs optimum range, 790nm to 850nm, are readily available and can produce up to 5W of power [257]. This is well above the minimum required power to actuate a small solenoid valve, approximately 0.5W. Although only GaAs based PPCs are commercially manufactured, research has shown that both silicon and germanium PPCs could be a viable solution for longer wavelength power conversion, having optical to electrical power

Table 3.2: Caparison of I-V Data of Single Junction PPCs , adapted from [256]

Bandgap/ Type	$\lambda(\mu$ m)	R at λ (A/W) (QE)	J_{sc} (A/cm^2)	V_{oc} (V)	Fill (%)	Eff (%)
1.42eV GaAs	0.82	0.59 (90%)	0.81	1.1	88	57
0.74eV InGaAs	1.55	1.06 (85%)	5.1	0.48	67	34
0.55eV InGaAs	2.1	1.18 (70%)	3.2	0.29	63	22

conversion efficiencies as high as 50% [254]. Furthermore, it has been demonstrated that communication, sensing and power signals can be simultaneously sent over the same fibre without any interference or loss of signal strengths.

3.8.5 Interfacing and Networking FBGs

Ping et al. [258,259] reported a networked FOS system based on the IEEE1451 standard for smart transducer interfaces for sensors and actuators. In their study, a GaAs chip was used as a temperature sensor and connected to a smart transducer interface module (STIM). The STIM was then connected to a PC or PLC, which acted as a virtual network capable application processor (NCAP), via a CAN bus interface module. The system architecture is shown in figure 3.21.

Whilst the work performed by Kunzler et al. [249,250] was predominantly based on their FBG interrogation technique, their FSIM acted as a smart sensor node, having additional functionality such as signal conditioning, data processing, and a bus output locally on-board. Hence, the FSIM was connected to a network of other devices using Ethernet.

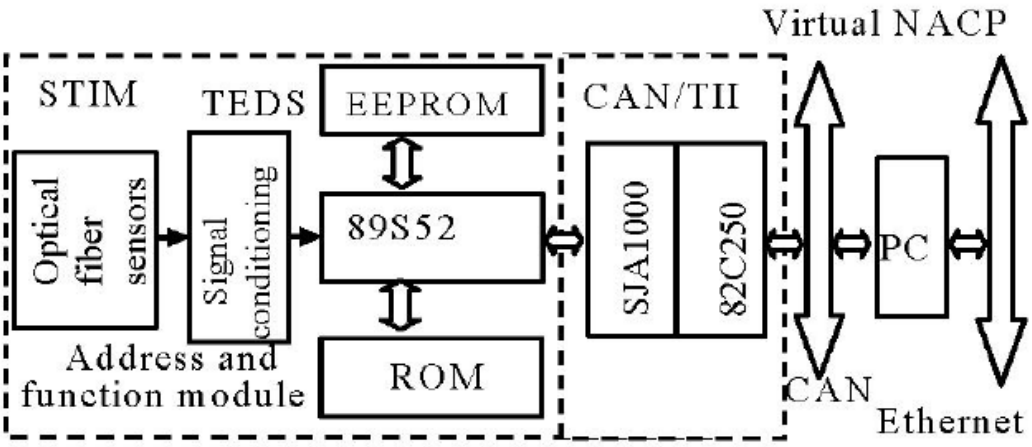

Figure 3.21: System architecture of 'non-NCAP' networked optical fibre sensor based on CAN fieldbus [258].

3.8.6 The Future of FBG sensing in Industry

In order for FOS networks to penetrate into mainstream industrial processes two things must happen. Firstly, appropriate transducers must be developed that satisfy a number of criteria;

- Be environmentally rugged.
- Have appropriate sensitivity.
- Have the correct dynamic range.
- Be easily replaceable without disrupting the network.
- Adhere to engineering standards, either existing or new.

Secondly, FOS networks should be seamlessly integrated with existing control system architectures. Standalone FOS interrogators are expensive and require knowledge of optical engineering. FOS have the potential to replace all of the downstream I/O components from a PLC or DCS in certain applications. However, in the interim, integrating an array of fibre sensors into an existing control system would be a logical

first step. A fibre system that could be connected to a PLC through a simple interface module such that the PLC and operators perceive the FOS as standard electronic sensors would eliminate the need for additional training and therefore reduce costs. This would allow faith in OFS to build up and the use of fibre sensors to become standard engineering practice in mainstream industrial processes. Further, this would pave the way for almost entirely optical control systems of the future.

In addition, interfacing FOS with low cost embedded controllers may have the potential to form smart hybrid systems such as those containing wireless sensor networks and FOS networks. Moreover, the information from the FOS could be sent over a wireless network as proposed in [260]

3.8.7 Industrial Review Conclusion

In Conclusion, a review of FBG sensing technology with respect to their use in mainstream industrial process applications has been performed. The review has focused on the types of sensors that have been developed for industries such as power generation, water treatment and services, mining, and the oil and gas sector has been performed. A market overview was reported, as well as a discussion of some of the factors limiting their penetration into these markets. Furthermore, the author has made recommendations for future work that would potentially provide significant opportunity for the advancement of FBG sensor networks in these mainstream industries.

Chapter 4

Fibre Optic Acoustic Sensing for Intrusion Detection Systems

The following two chapters focus on FOS for physical intrusion detection applications. As discussed in the literature review, there are many different techniques using PIDS, although this work is based on FBG sensor development. The reason FBG technology was chosen was because of the versatility of FBGs to detect different measurands. Typically, detection of potential intruders is either performed through measurement of their acoustic emissions (AEs) or through detection of physical pressure vibrations. Whilst interferometry, OTDR, and intermodal interference methods can detect both of these types of disturbances, they are generally used for large scale applications and require complex signal processing and interrogation techniques. The goal of this work is the development of a PIDS for relatively small scale domestic or industrial applications. In addition, FBGs are inherently more practical for point based sensing, such as the detection of window and door breaches, rather than fully distributed sensing techniques. AEs are stress waves that propagate through a material. AEs can be generated by external sources, specifically impacts, or actively generated by actuators. The vibrations caused by a potential intruder generate AEs that may be detected using in-ground FBG sensors. In this chapter, the detection of acoustic vibrations from potential intruders is examined. AEs generated from a low impact test were detected by a FBG through a variety of flooring materials and interrogated using a TRDS.

4.1 Characterisation of Optical Components

The first step of the experiment was to characterise the spectral response of the FBG and the tunable laser. This is typical of most of the experiments that are detailed throughout this thesis. The characterisation was used to determine the operating point for the FBG AE sensor. The optical circuit uses a broadband SLD (DenseLight DL-BZ1-CS5254A) as the light source, and an optical spectrum analyser (OSA, Anritsu MS9001B1). The loss function of the OSA was used to measure the spectral response of the FBG (Photronix Technologies) and to look at the output of the tunable laser source (Anritsu MG9637A). The laser was tuned to give an output that matched the 3dB point of the FBG used. This ensured that 50 percent of the power was transmitted through the FBG and 50 percent was reflected, forming a TRDS, previously reported [261]. A schematic of the experimental setup is shown in figure 4.1.

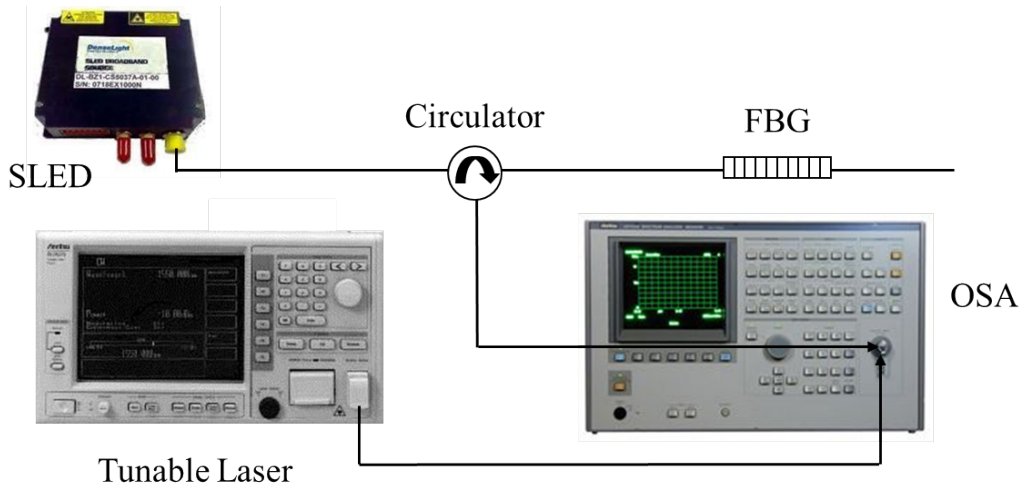

Figure 4.1: Experimental setup for the spectral measurements of the FBG using the SLD (top) or the tunable laser (bottom).

4.2 Acoustic Measurements for Standard Flooring Materials

In the second step of the experimental procedure, the laser output was connected to a circulator (FDK YC-1100-155) so that both the transmitted and reflected signal could be detected. In order to increase the amplitude of the output signal, both outputs could be differentially amplified, as the transmitted and reflected signals would have equal but opposite magnitudes. In a practical system, this would ensure that, whilst the FBG was under no strain, the output would be zero. Any change in signal would then be amplified as the combination of the two signals. The transmitted and reflected signal were connected to a digital storage oscilloscope (DSO, Agilent DSO3062A), which was in turn connected to a PC for transferring the data. Figure 4.2 shows a schematic of the experimental setup.

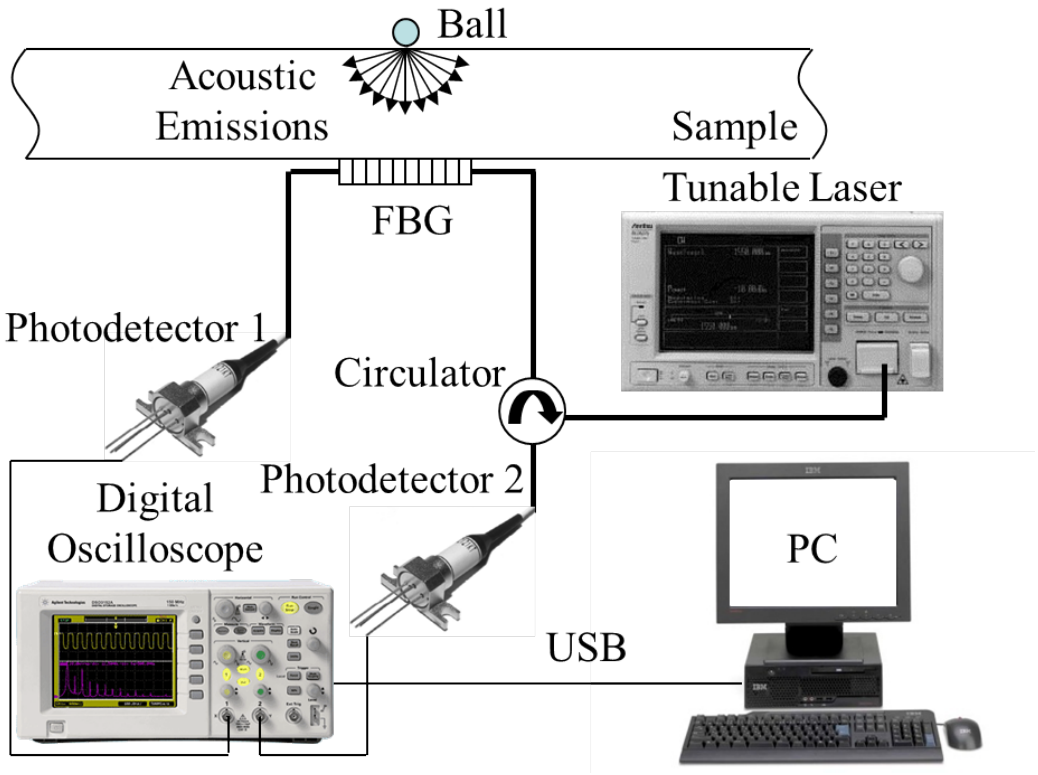

Figure 4.2: Experimental setup for the AE experiments.

The FBG was placed between a piece of underlay and various common flooring materials; a piece of solid timber flooring, a piece of laminate flooring, a ceramic floor tile, and a porcelain composite tile, as well as a sheet of aluminium for comparison. All samples were approximately 1cm thick, 30cm long and 20cm wide, with the exception of the aluminium which was approximately 0.5cm thick.

To test the sensitivity of the system to AEs, a low velocity impact test was performed. Here, a small rubber ball, approximately 2cm in diameter, weighing 5g, was used to generate an AE. The rubber ball was dropped from approximately 0.5 metres above the sample and the acoustic signal was recorded using the DSO. In each case, the ball was initially dropped directly above the FBG, then dropped at the edge of each sample approximately 30cm from the FBG.

Figures 4.3 - 4.7 show the output of the DSO for solid timber, laminate flooring, ceramic tile, porcelain composite tile, and aluminium, respectively, for the low velocity impact test of each sample. Each figure shows the voltage output on the top (10mV/div) for the transmitted (yellow) signal and the reflected (green) signal, as well as the fast Fourier transform (magenta) on the bottom, of the transmitted signal, with respect to time for (a) the ball dropped directly above the FBG and (b) the ball dropped 30cm from the FBG.

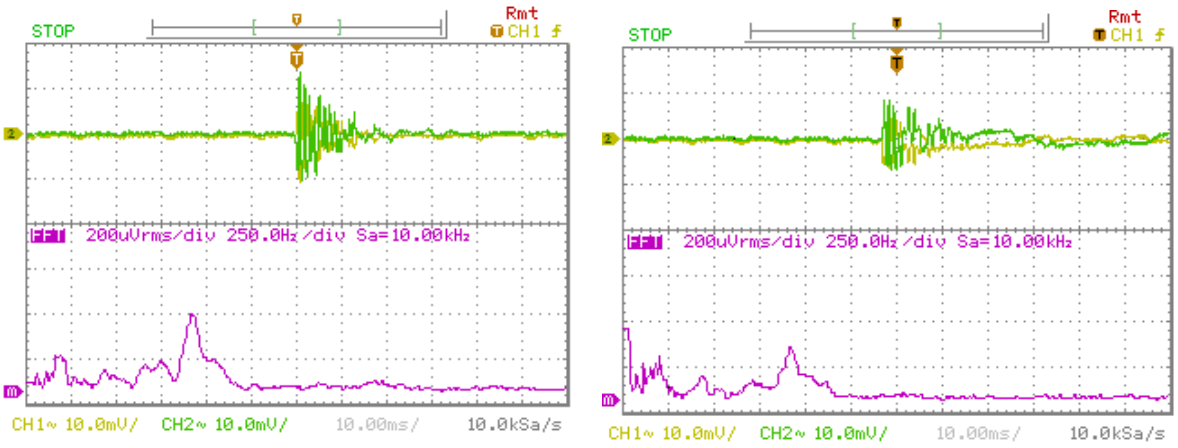

(a) Directly above. (b) 30cm from the FBG

Figure 4.3: Solid timber low velocity impact test.

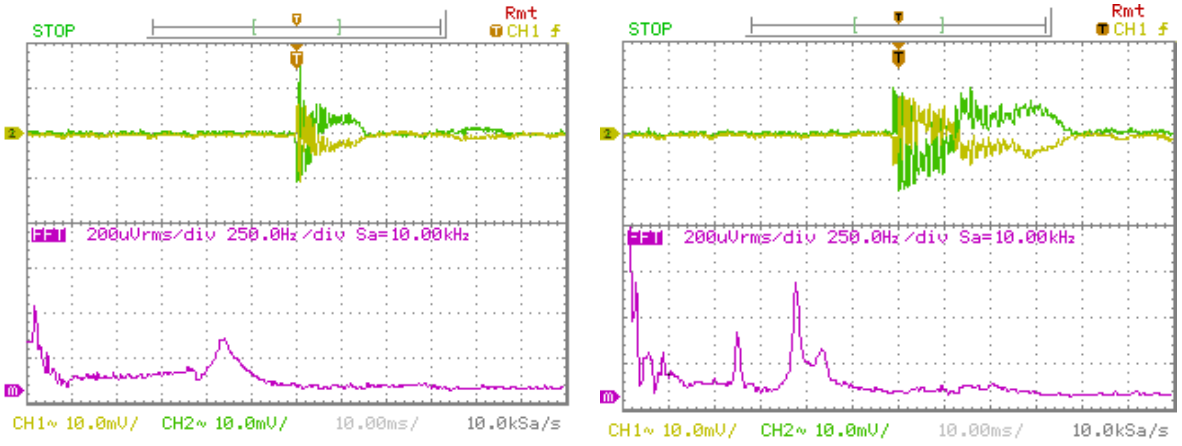

(a) Directly above. (b) 30cm from the FBG

Figure 4.4: Laminate wood low velocity impact test.

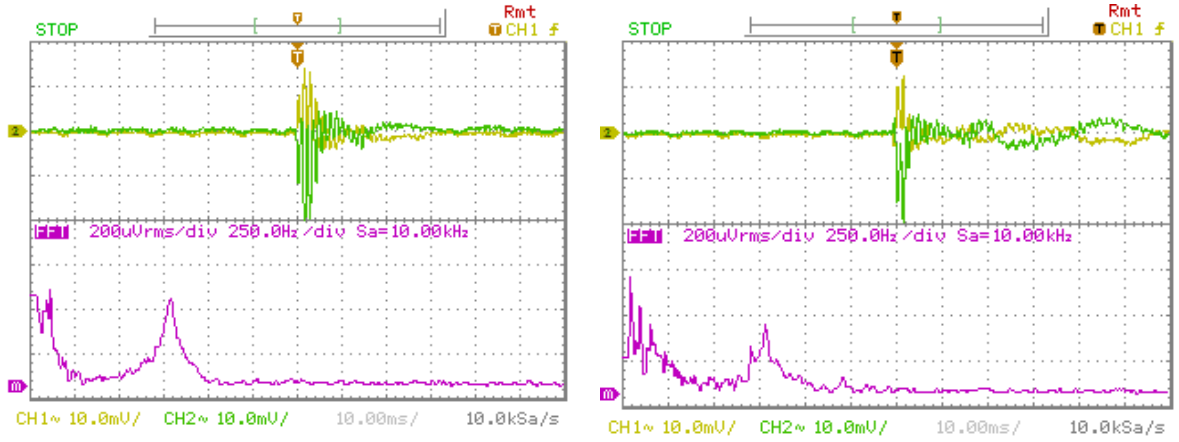

(a) Directly above. (b) 30cm from the FBG

Figure 4.5: Ceramic tile low velocity impact test.

The acoustic signals generated from the low energy impact tests were easily detected through the materials used. Figure 4.3a shows solid timber flooring produced a transmitted and reflected peak signal of approximately 10mV, with the signal being clearly visible for over 10ms when the ball was dropped from directly above the FBG. The results in figure 4.3b are similar except the peak amplitude of the signals is reduced, as expected, although the signal do not fully attenuate until after 30ms. The Fourier transforms are similar displaying the frequency of the acoustic signal was just under

(a) Directly above. (b) 30cm from the FBG

Figure 4.6: Porcelain composite tile low velocity impact test.

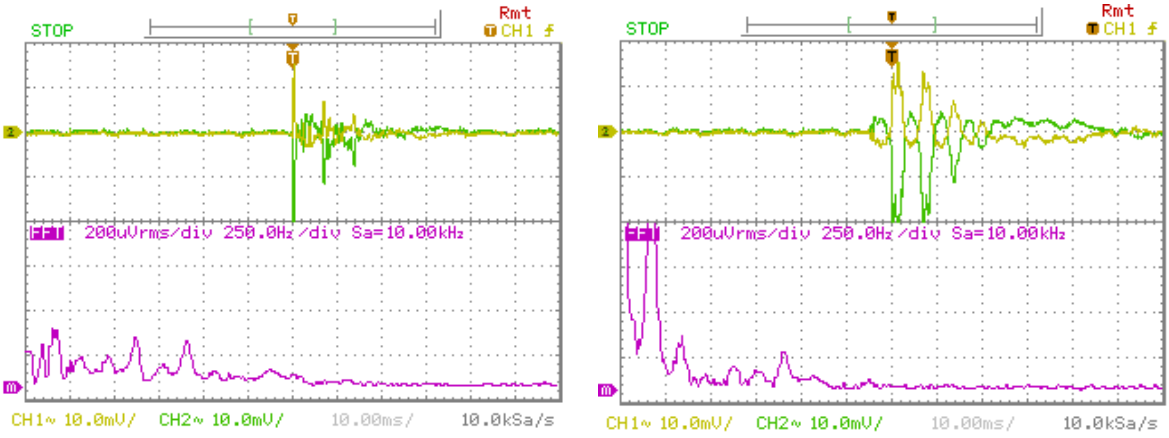

(a) Directly above. (b) 30cm from the FBG

Figure 4.7: Aluminium sheet low velocity impact test.

1kHz.

The results from the laminate flooring were similar to the solid timber flooring in the first instance, although the signals oscillate around a non zero value before attenuating. The frequency of the AE was again just over 1kHz with reduced amplitude. Figure 4.4b shows the individual signals propagate for 40ms with a significant amplitude and the Fourier transform showed there were multiple frequencies propagating through the material and contributing to the recorded signals.

Figure 4.5a shows the ceramic floor tile produced a stronger signal with the peak being approximately 20mV for the reflected and 15mV for the transmitted. The imbalance in the signals suggested that the laser may have drifted slightly from the 3dB point of the FBG or that the performance of one of the detectors was better than the other. The frequency of the AE was again just over 1kHz. Again, when the ball was dropped 30cm from the FBG the signal propagated for longer at a reduced amplitude.

Both figures 4.6a and 4.6b were very similar, with slightly less amplitude in the latter. The porcelain composite tile produced a much cleaner signal with less noise, although the amplitude was only 10mV. The signal also attenuated slower and was visible for over 20ms. Again, the reflected signal was slightly stronger. Interestingly, the frequency of the AE was only approximately 200Hz.

The response of the aluminium sheet was significantly different, producing a sharper spike followed by two more spikes for the first test. The Fourier transform showed that there was more than one acoustic signal detected with similar, small amplitudes. When the ball was dropped 30cm from the FBG much cleaner oscillating signals were produced with successive amplitude of around 10mV. The Fourier transform clearly shows multiple strong frequency peaks. Both the aluminium sheet and the laminate flooring produced better signals when the ball was dropped 30cm from the FBG. In these cases multiple frequencies contributed to the received signals. The different responses of each of the materials to AEs is related to the density and the elastic properties of the materials. In general, the denser the material the faster an acoustic wave travels through it.

The amplitudes of each of the output signals were doubled by differentially amplifying the transmitted and reflected signals. Figure 4.8 shows the differential output from the solid timber sample as an example and illustrates the advantage of using the TRDS. This was performed for all of the signals, although only the solid timber results are shown to validate the technique.

In addition to the AEs generated by the drop test, the high frequency response of the sensor was tested using actively generated acoustic signals from a function generator (Agilent 33250A). The experimental setup is shown in figure 4.9.

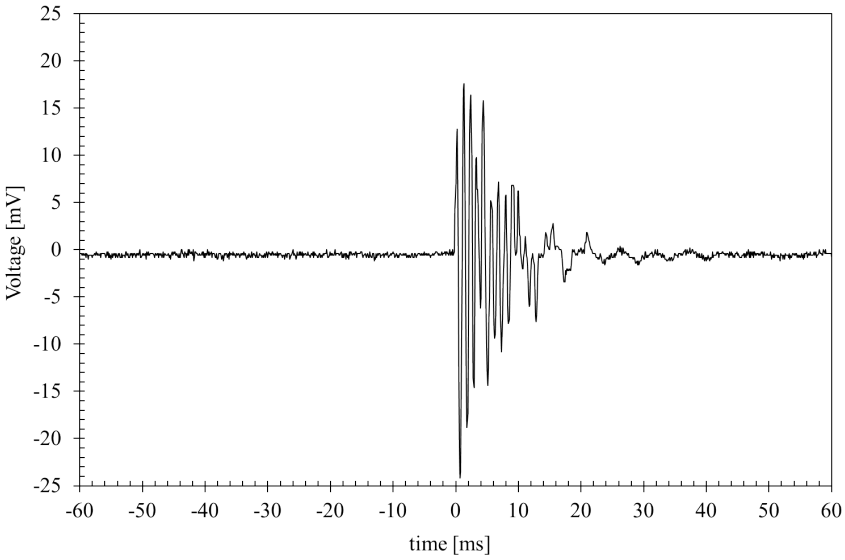

Figure 4.8: Solid timber initial rubber ball test differential output.

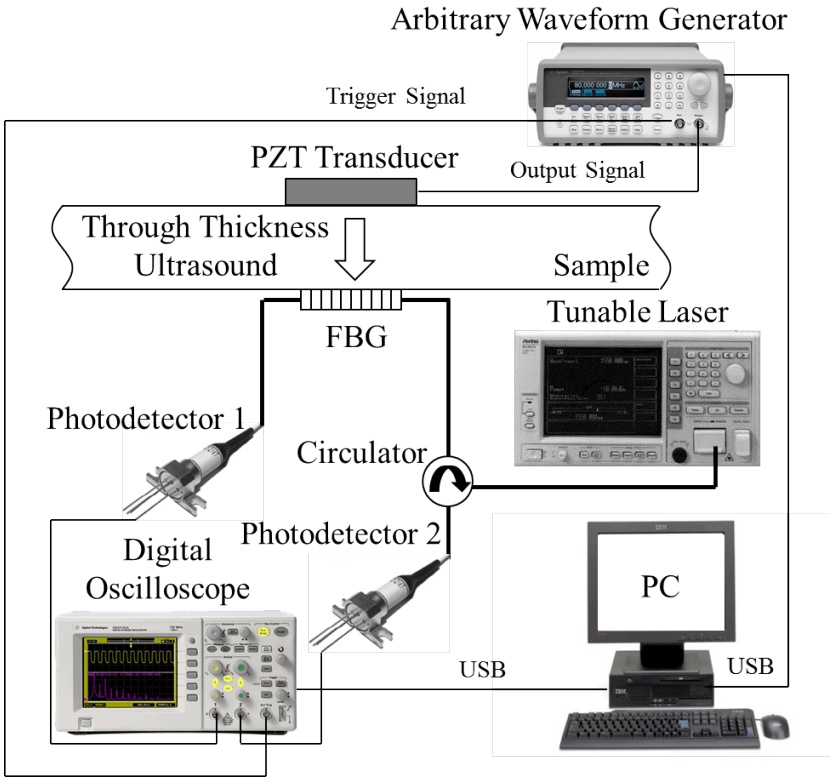

Figure 4.9: Setup for the actively generated acoustic signals.

Figures 4.10 and 4.11 show the high frequency response from the FBG, through the ceramic tile and the sheet of aluminium, respectively. In both cases the differential signal was used to amplify the output to almost 2mV, (4mV/div). There was no observed high frequency response from the other samples.

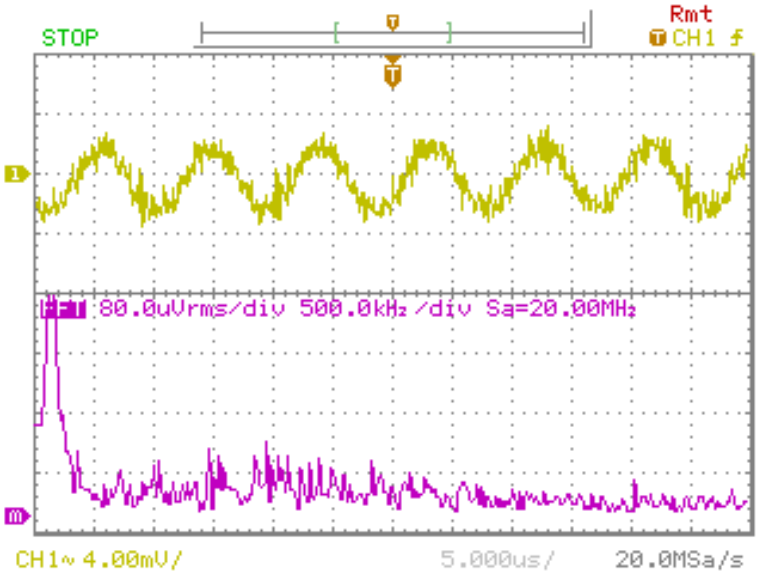

Figure 4.10: Ceramic tile response to 108.5 kHz signal.

The results show that high frequency signals can be detected through a ceramic tile and aluminium, although only very specific frequencies relating to the resonant mode of the transducer were detected. Through the ceramic floor tile a frequency of 108.5kHz was detected with an amplitude of approximately 6mV. Through the aluminium sheet a frequency of 112.2kHz was detected with an amplitude of approximately 4mV. Unfortunately, the output of the frequency generator used was only 10V, which limited the range of results obtainable. Future experiments using equipment with greater electrical output may show high frequency responses to a range of frequencies and a wider variety of materials.

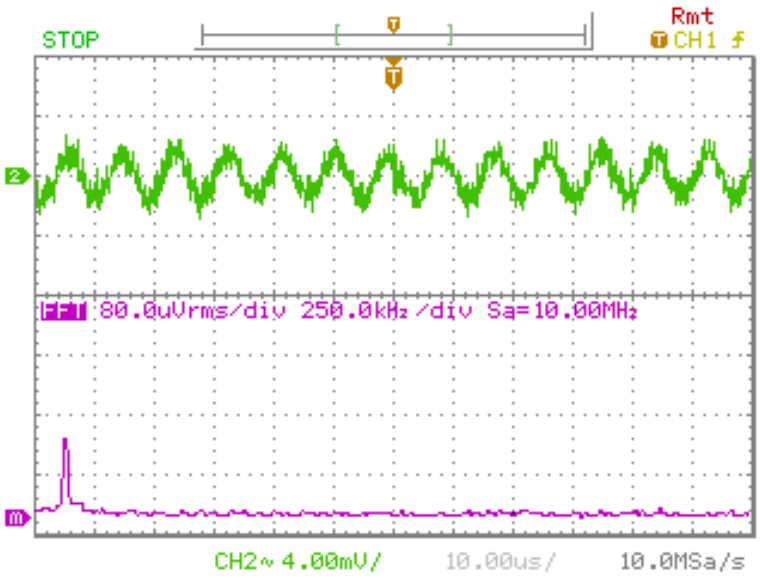

Figure 4.11: Aluminium response to 112.2 kHz signal.

4.3 FBG Embedded in Concrete

Finally, a FBG was embedded into a slab of concrete. To achieve this, a cardboard mould, approximately 30 x 15 x 5cm, was made and standard concrete mix consisting of sand, cement and blue metal (rocks) were mixed together with water and poured onto the mould, so that it was about 2.5cm thick. The fibre was then placed on top of the concrete mix, ensuring the FBG was approximately in the centre with the pig tail ends of the fibre slotted through the two ends of the mould. The remaining concrete was then poured over the fibre so that it was embedded in the concrete approximately 0.5cm deep, then left to set for 48 hours. Given that the sensor embedded within the concrete was significantly less sensitive, a low velocity impact test using a steel ball, approximately 2cm in diameter and weighing 30g, was performed. In addition a standard footstep test was performed, where a 60kg man wearing a common soft soled training shoe, raised his foot approximately 10cm and stepped on to the sample with one foot for approximately 1 second. Figures 4.12 and 4.13 show the output (4mV/div) from the FBG embedded in concrete from the footstep test and a low velocity impact test, respectively.

The results demonstrate that it is possible to detect acoustic signals from a small

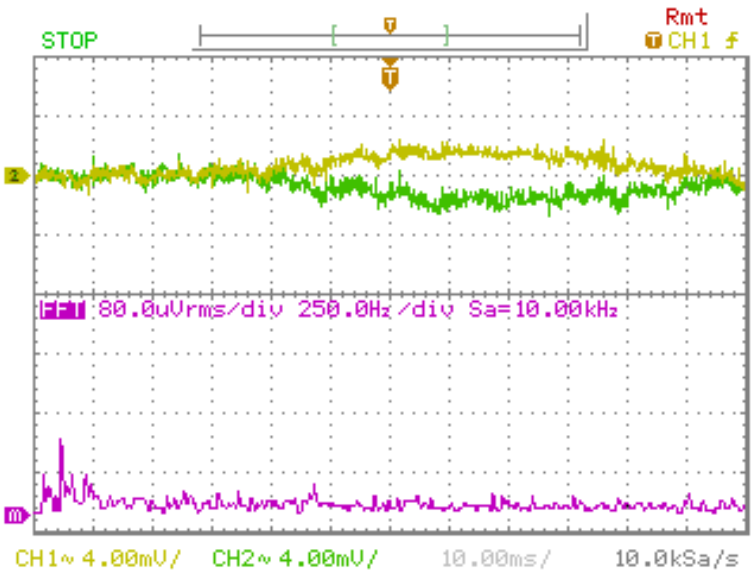

Figure 4.12: Concrete footstep test.

Figure 4.13: Concrete low velocity impact test.

steel ball and a person's footstep, using an FBG embedded in concrete. The frequency of the AE generated from the low velocity impact was approximately 1.4kHz. The relatively low signal size (2mV), for both the low velocity impact test and the footstep test, can be attributed to the small input optical power (0.35mW) from the tunable

laser and the associated photodetectors used. Increasing the output power of the laser or using improved detectors would increase the sensitivity of the system. The low signal to noise ratio may be related to the small strain signal applied to the FBG through the concrete, given that the FBG is bare, and there will be a mismatch between the glass fibre and the concrete in terms of the acoustic impedance. In addition to this, amplification in the electrical domain would also enable the in-ground acoustic sensor to detect smaller signals, such as the AEs from a smaller person. This could have a number of applications not just limited to in-ground intrusion detection. However, embedding FBGs in concrete has its complications as they cannot be moved or replaced easily if they are damaged.

4.4 Spatial Measurements

Later, the spatial resolution of the acoustic signals were investigated using a larger piece of laminate flooring. This sample was approximately 0.5cm thick, 60cm long and 20cm wide. The same drop test was performed using the rubber ball dropped from a height of approximately 0.5m, although the position of the impact was varied in 10cm intervals along the piece of laminate flooring, perpendicular to the FBG. The high output signal can be attributed to the use of highly sensitive InGaAs detectors (Thorlabs DET01CFC) with incorporated transimpedance amplifiers for improved noise performance. The results are shown in figure 4.14.

The results clearly show attenuation of the AE with distance from the FBG. As we would expect, the magnitude of the signal received by the FBG appears to decrease in a logarithmic way, as the intensity of the AE decreases by $1/r^2$, although it is still clearly detectable 0.5m from the FBG, suggesting that real in-ground PIDS could be capable of detecting an intruder's footsteps, even if the intruder did not stand directly on the sensor. These results also demonstrate the ability of improved detectors to significantly improve the amplitude of the output signal whilst still using a relatively low power light source.

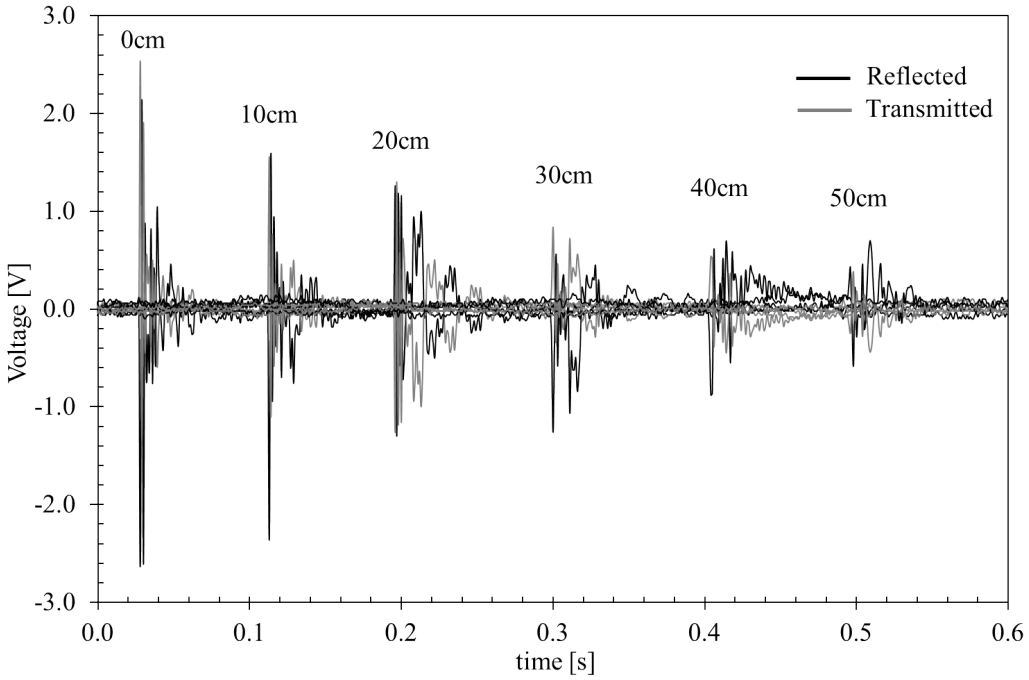

Figure 4.14: Attenuation of the acoustic signal as a function of distance for the laminate flooring, showing the transmitted signal (grey) and the reflected signal (black).

4.5 General Discussion

Although all of the materials used in this study could be effectively utilised in a PIDS, solid timber or laminate flooring would be more practical to implement as these materials require underlay or have an air gap between the floor boards and the solid floor. One of the advantages of using underlay in this study was that the FBG was placed between the underlay and the material, which ensured a good quality signal was detected, as well as protecting the fibres from being damaged. The FBG could also be secured to the underside of a floor board for easy installation of a PIDS.

The acoustic signals generated from a footstep would be significantly greater than a rubber ball, meaning that they would be detected without the need for any additional signal amplification, in all of the materials tested. Only a small amount of additional circuitry will be required for the implementation of a practical PIDS. Specifically, an envelope detector and a comparator will give a direct detection result. As the amplitude

of the AE signal is analog in nature, it could be used to determine the distance an intruder is from the FBG sensor. However, this would require further analysis of the spatial sensitivity of the sensor, as the weight of an intruder would need be taken into consideration. Furthermore, the implementation of improved detectors could mean a real in-ground PIDS could be realised with high POD.

4.6 Chapter Conclusion

FBGs can effectively detect AEs through various materials using a low velocity impact test. The AEs generated by a footstep could also be detected by an FBG embedded 5mm deep in a slab of concrete. The acoustic vibrations caused a strain in the optical fibre, and hence, altered the wavelength reflected by the FBG. This strain induced wavelength shift can then easily be detected by converting this wavelength shift into an intensity change. This is performed using a TRDS, where a laser is tuned to the 3dB point of the FBG, and the optical power transmitted and reflected is modulated by the spectral shift of the FBG. In practice, a comparison of both the reflected and transmitted signals could be made regularly to ensure the laser is tuned to the 3dB point of the FBG using a feedback loop for a temperature controller. The intention is to use FBGs as an in-ground intrusion detection system to detect the AEs generated by an intruder walking within range of the sensors. This type of intrusion detection system can be applied to both external (in soil, etc) and internal (within the foundations or flooring of the home) security systems. The results show that the AEs can clearly be detected through wood, ceramic tiles, aluminium and concrete. This technology could be used as an in-ground intrusion detection method for domestic and commercial security applications.

Chapter 5

Optical Fibre Bragg Grating Based Physical Intrusion Detection Systems

This chapter describes the use of FBG sensors in a complete PIDS. A FBG based in-ground pressure switch for intrusion detection through temporary flooring materials, such as tiles and wooden laminate, is demonstrated. In addition, the use of FBGs as in-fence perimeter breach detectors is shown. Finally, a FBG based reed switch for use in PIDS for doors and windows is reported. The combination of the different intrusion detection techniques illustrate the versatility of FBGs in security applications, showing this single technology can be used to form a complete PIDS. Furthermore, the chapter details the progress made towards a complete FBG sensor network for advanced security applications.

5.1 In-Ground Pressure Switch

Experiments on transverse loading of an FBG have proven to be very positive in terms of using this as a switch with a TRDS [261]. As such, the same setup as the acoustic sensing experiment in Chapter 4 was used, but instead of actively generated acoustic signals and acoustic emissions from drop tests, pressure, in terms of a transverse load, was applied to the various flooring materials in the form of a footstep. This required the

tunable laser (Anritsu MG9637A) and the FBG (Micron Optics OS1100) to be optically mismatched, so that there was a static dc offset from the transmitted and reflected signals, acting as a digital TRDS. Hence, the laser was tuned to be 0.2nm greater than the Bragg wavelength. The two receivers required for the TRDS were incorporated into an intensiometric detection system (IDS) [262] with the required difference and amplification (Gain = 1, relative to 2.5 volts) circuitry included. The difference signal from the IDS was then connected to a DSO to view the change in signal, which was in turn connected to a PC for transferring the data, as shown in Figure 5.1.

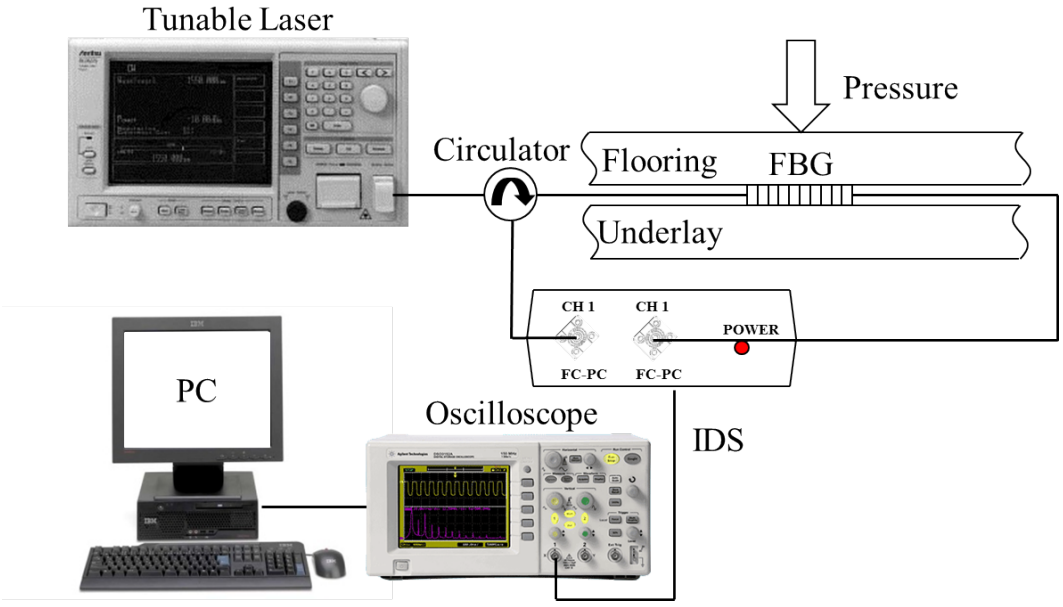

Figure 5.1: Experimental setup for the in-ground FBG pressure switch sensor, showing the optical circuit, and the IDS (containing two photoreceivers and the required difference circuitry).

In the FBG switch experiments, the grating was placed between a piece of underlay and three different flooring samples; a piece of solid wood flooring, a piece of laminate flooring, and a ceramic floor tile. A standard footstep test was performed, where a 60kg person wearing a common soft soled shoe, walked across the sample, stepping on to the sample with one foot. This was repeated for each of the three flooring samples. Prior to the experiments using the IDS, the optical components were characterised as per figure

4.1 in Chapter 4. The Bragg wavelength shift of the FBG embedded below all three materials was recorded using the OSA whilst under load from the 60kg person. The reflected spectra are shown in figure 5.2.

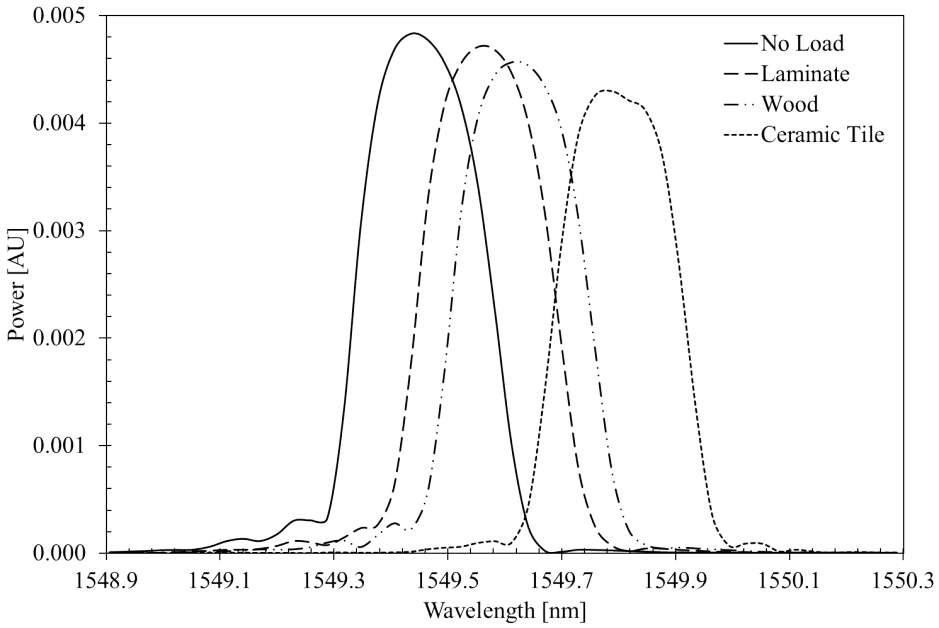

Figure 5.2: Reflected spectra for the FBG with no load and a 60kg load using laminate flooring, wood flooring, and a ceramic floor tile.

The Bragg wavelength shift was 0.12nm, 0.18nm, and 0.36nm for the laminate flooring, wood flooring, and a ceramic floor tile, respectively. This demonstrates the significance of the flooring material and is a result of the coupling between the flooring and the underlay. Catalano et al. [68] reported a wavelength shift of just over 0.6nm for an FBG embedded in a rubber polymer loaded with 60kg, almost double the maximum recorded wavelength shift here. Hence, it is clear that the sensitivity of the in-ground system could be improved by optimising the material in which the FBG is embedded. However, three common flooring materials were specifically chosen here, to reduce the cost of a PIDS and enable easy installation into existing or new properties.

The differential output from the FBG beneath all three materials, whilst being stepped on, is displayed in figures 5.3 - 5.5. The results show there is a significant

increase in dc output when the FBG is stepped on, for all three materials with a variation of at least 0.5V, when using a relatively low power laser (0.35mW).

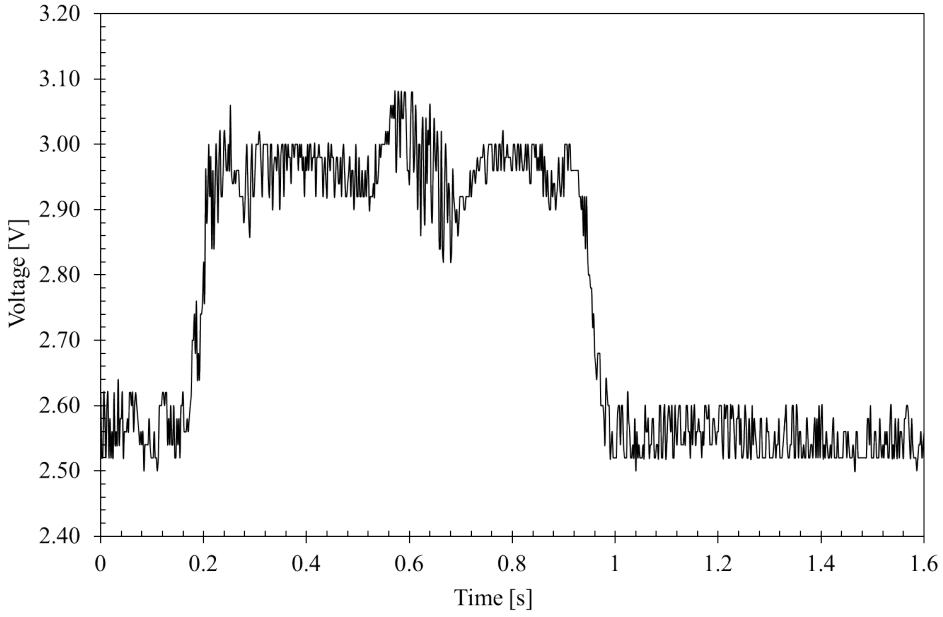

Figure 5.3: In-ground FBG pressure switch signal for the laminate wood flooring.

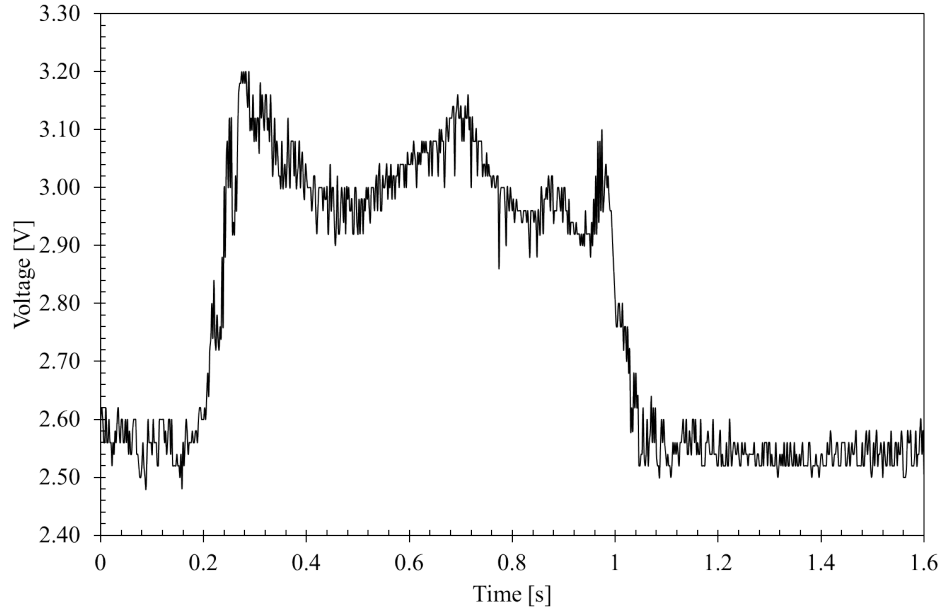

Figure 5.4: In-ground FBG pressure switch signal for the solid wood flooring.

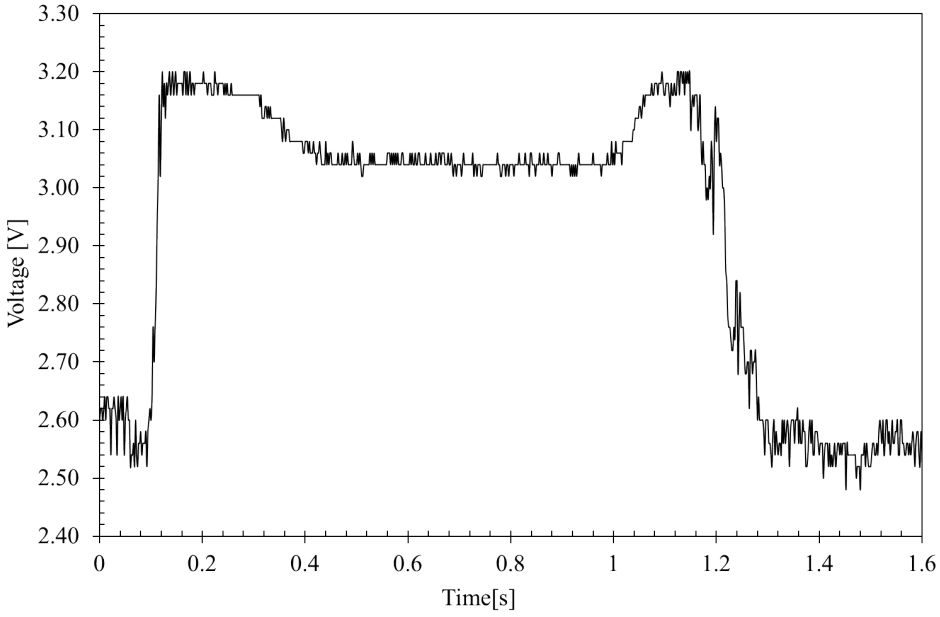

Figure 5.5: In-ground FBG pressure switch signal for the ceramic floor tile.

The ceramic floor tile produced the largest response with a peak increase of 0.6V, which agrees with the optical measurements. The output was also clearer with less noise, and a shorter response time between the minimum and maximum signal. This also agreed with the results from the acoustic measurements. Both wooden flooring materials had similar responses although the laminate wood produced a slightly larger peak output. This also agreed with the AE results although it was counter to the optical measurements. This could be because the optical measurements were performed in a static test, whereas the footstep test was dynamic. Hence, the fluctuation of the Bragg wavelength was not observed during the original test.

The signal to noise ratio for all three samples was relatively high, facilitating the digitizing of the signal via a comparator (relative to a suitable value) and also minimizing any bit errors and hence false alarms. Although the ceramic floor tile produced the best results, embedding FBGs below such tiles may prove difficult and the effect of floor adhesive has not been examined and may produce significantly different results without the underlay. The results show that FBGs embedded below flooring could work

effectively as pressure switches and could easily be configured to trigger an alarm. This type of intrusion detection technique has all of the advantages of other optical security sensors, such as infra-red (IR) trip wires, but is also completely hidden and cannot be seen by indirect methods (such as an IR camera), as it is embedded within the floor itself.

5.2 In-Fence Perimeter Sensor

FBG perimeter fence systems have previously been reported [140–144], although these generally used stand-alone interrogators. Hence an attempt to recreate the results using the TRDS was made so that a complete low cost PIDS could be created using different types of FBG security sensors. A FBG was attached to the centre of a small section of wire fencing, 1.1m x 0.7m. The fencing consisted of 1mm thick steel, woven together forming hexagonal sections which were 5cm in diameter. This was then connected to the optical circuit, as shown in figure 5.6.

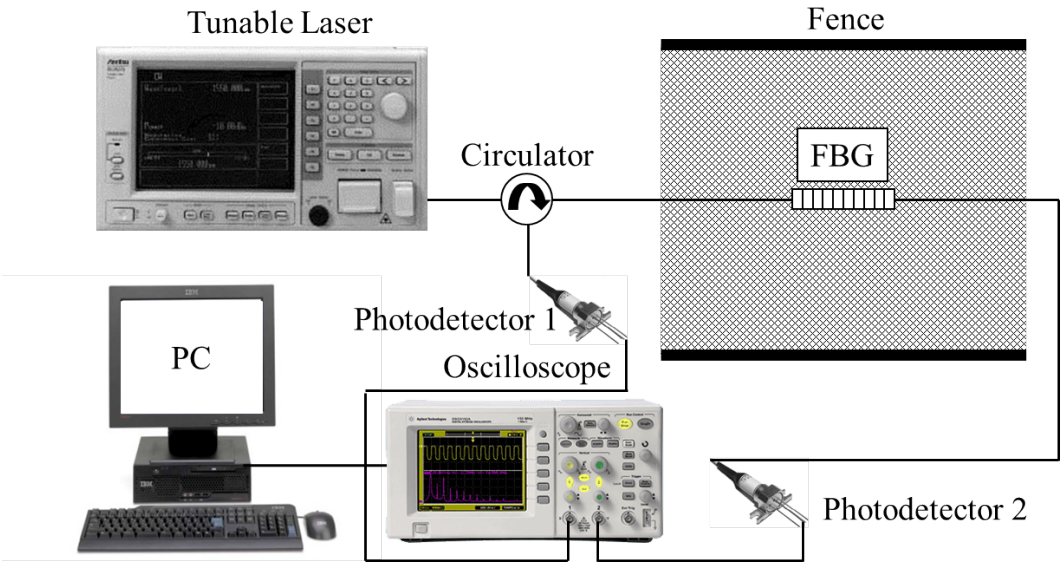

Figure 5.6: Experimental setup for the fence mounted FBG sensor, showing the optical circuit.

A small steel ball, approximately 20g in mass, attached to a 30cm piece of wire, was held horizontal at the top of the fence panel. The ball was released, causing it to swing like a pendulum and strike the fence panel in the centre, so as to mimic a vibration caused by an intruder attempting to climb the fence. The ball and wire were then moved across the fence in 10cm increments before the fence was struck each time. Figures 5.7 to 5.11 display the transmitted and reflected signals received from the FBG attached to the wire fence for the relative positions.

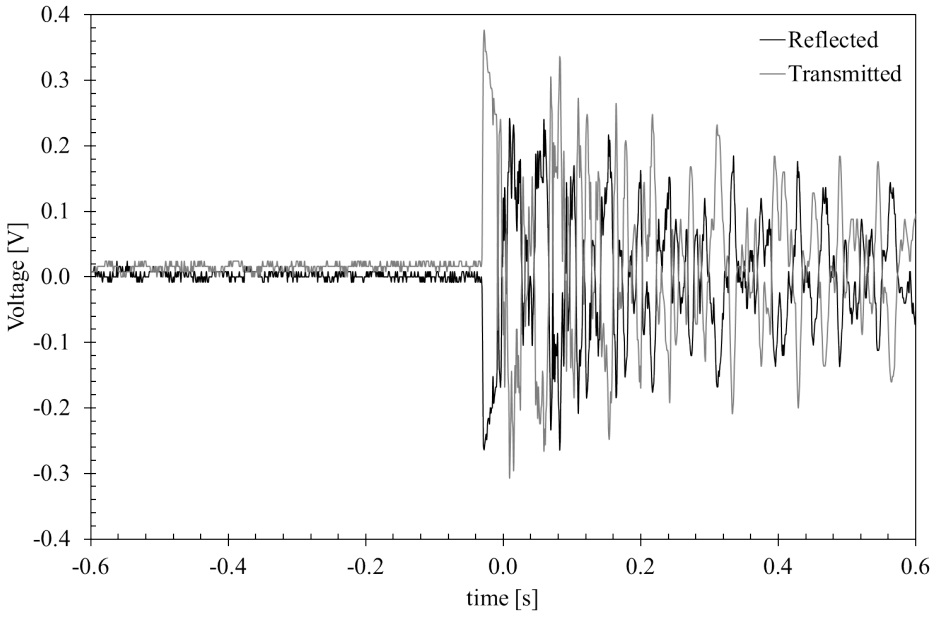

Figure 5.7: Transmitted and reflected signal from the fence mounted FBG with impact at the centre of the fence.

The results clearly shows that a vibration caused by an intruder attempting to climb the fence could be detected without amplification and therefore be used to trigger an alarm. The amplitude of the signal did decrease slightly as the impact was moved further from the FBG; however, the wire structure of the fence panel was quite loose causing it to vibrate significantly wherever the impact occurred. A larger scale test would need to be performed to accurately analyse the spatial performance of the fence mounted FBG sensor. Additional analysis and signal processing may also be required to ensure false

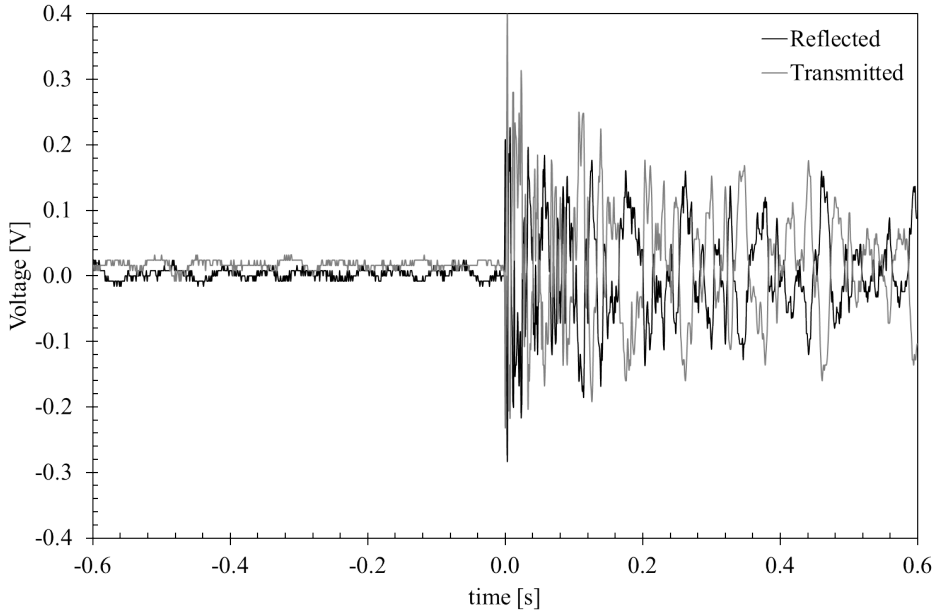

Figure 5.8: Transmitted and reflected signal from the fence mounted FBG with impact 10cm to the right of the FBG.

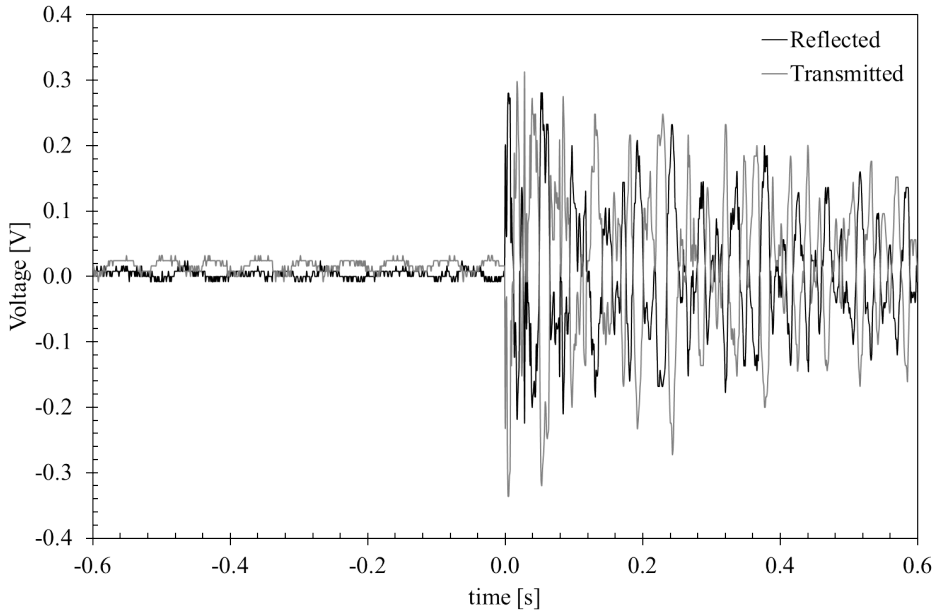

Figure 5.9: Transmitted and reflected signal from the fence mounted FBG with impact 20cm to the right of the FBG.

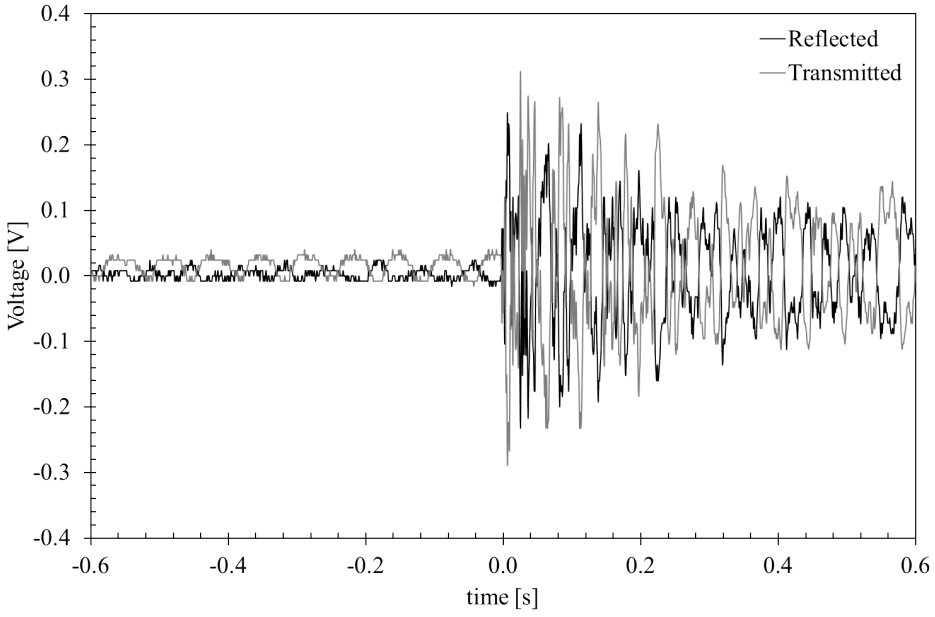

Figure 5.10: Transmitted and reflected signal from the fence mounted FBG with impact 30cm to the right of the FBG.

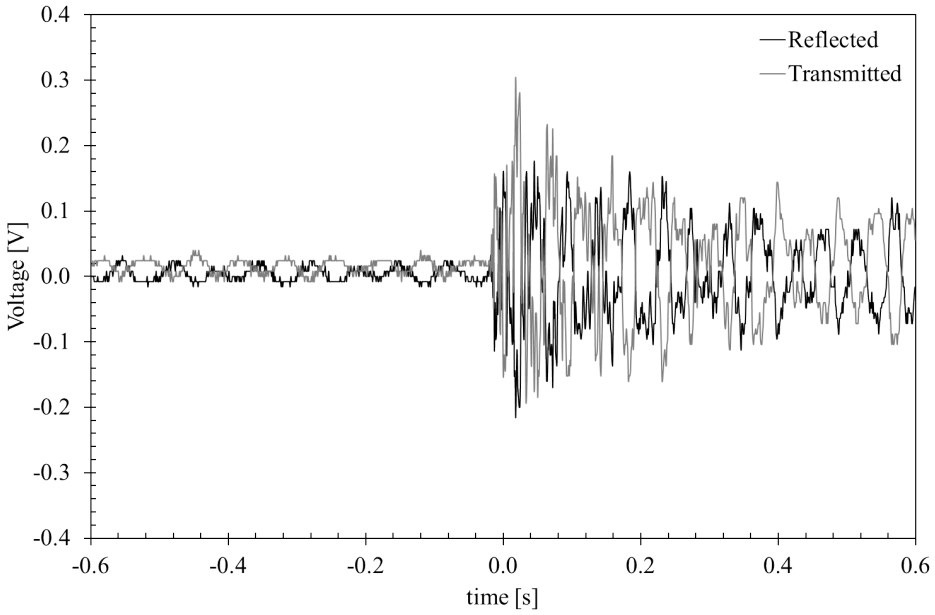

Figure 5.11: Transmitted and reflected signal from the fence mounted FBG with impact 40cm to the right of the FBG.

alarms caused by environmental vibrations such as wind, are minimized, as described in similar studies [111–113]. However, as the signal is relatively strong using the TRDS, this could easily be achieved by setting the trigger value quite high, although analysis of the trade-off between high POD and low FAR would need to be performed.

5.3 Reed Switch

A traditional reed switch is basically an electrical switch which is actuated by a magnetic field. An FBG reed switch has previously been demonstrated using the TRDS [263], whereby an FBG was located between a ferromagnetic (steel) and a diamagnetic (aluminium) metal. As a magnet was placed on the aluminium, the FBG was laterally stressed between the metal layers. However, this technique requires a strong physical contact with the FBG which may not be practical in a real system, and the output response of the transducer is complicated, as a transverse load deforms the FBG differently in the x and y directions. The response of longitudinal strain on FBGs is well documented and easier to induce than transverse strain. Hence, a different FBG reed switch setup was used so as to cause a longitudinal strain in the FBG. The experimental setup for the cantilever based FBG reed switch is illustrated in figure 5.12.

An FBG was placed between two thin strips of steel forming a metal beam to be used as a cantilever. The cantilever was positioned over the edge of a small block with one end held down with a clamp. A small rectangular magnet was placed on top of the free end of the cantilever and another was positioned below the cantilever causing it to deflect. The magnet below was slid from left to right along the direction of the cantilever until it no longer caused the cantilever to deflect, mimicking the opening of a door or window. Both the transmitted and reflected signal were connected to an Arduino microcontroller for data acquisition. The Arduino uses open source software for programming which is extremely easy to code. To display an output voltage of between 0 and 5 volts the program illustrated in figure 5.13 was written.

The reflected spectra as a function of magnet distance from the FBG cantilever

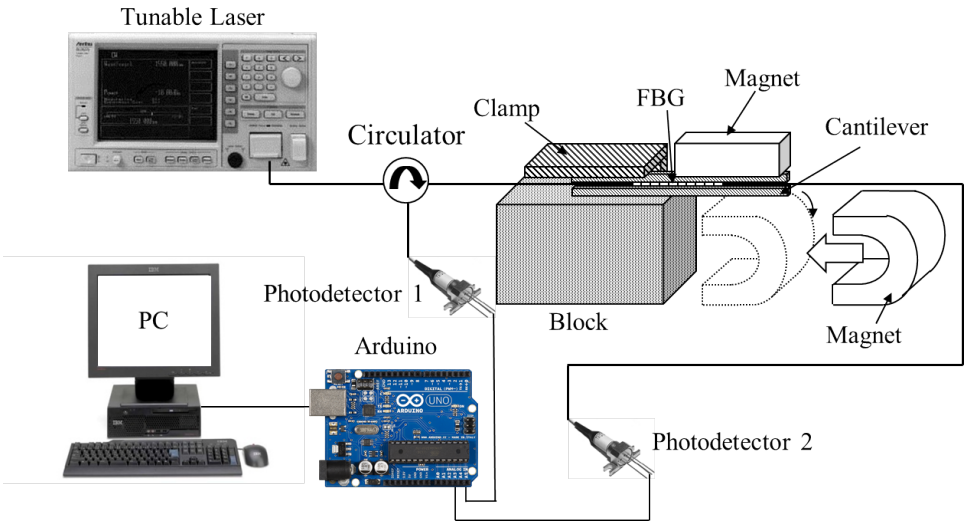

Figure 5.12: Experimental setup for the cantilever based FBG reed switch, showing the magnetic transducer and the optical circuit.

are displayed in figure 5.14a and in figure 5.14b with a constant power offset. The reflected spectra for the reed switch with the magnet positioned directly below it (at 0cm, representing a closed switch) and 5cm to the right of it (representing an open switch) are again shown in figure 5.15. The figure also displays the laser profile indicating its relative position, and the reflected spectrum of the reference FBG (which will be explained below).

The results from the cantilever FBG reed switch are shown in figure 5.16. Again the transmitted, reflected, and difference signal are displayed. In this experiment the power of the laser was only 0.35mW, although highly responsive photodetectors (Thorlabs DET01CFC) were again used.

The nature of the physical interaction between the cantilever and the magnet resulted in a complex output, which will be explained in the following points:

- Initially, the magnet was directly below the FBG, causing the cantilever to deflect. The Bragg wavelength of the FBG was slightly less than the laser wavelength, resulting in most of the light being reflected and minimal light being transmitted; this was the case from 0 to 0.25s.

ReedSwitchArduino

```
// to the pins used:
const int analogInPin1 = A0;  // Analog input pin 0 for the transmitted signal
const int analogInPin2 = A1;  // Analog input pin 1 for the reflected signal

int sensorValue1 = 0;        // value read from Rx
int sensorValue2 = 0;        // value read from Tx

void setup() {
  // initialize serial communications at 9600 bps:
  Serial.begin(9600);
}

void loop() {
  // read the analog in value:
  sensorValue1 = analogRead(analogInPin1);
  sensorValue2 = analogRead(analogInPin2);
  float voltage1 = sensorValue1 * (5.0 / 1023.0);
  float voltage2 = sensorValue2 * (5.0 / 1023.0);
  // print the results to the serial monitor:
  Serial.print("Reflected Voltage = " );
  Serial.print(voltage1);
  Serial.print("\t Transmitted Voltage = ");
  Serial.println(voltage2);

  // wait 100 milliseconds before the next loop
  delay(100);
}
```

Figure 5.13: The data acquisition program for displaying the transmitted and reflected signals between 0 and 5 volts using an Arduino microcontroller.

- As the magnet was moved slowly across the FBG from left to right, the cantilever deflected further causing the Bragg wavelength to increase, such that it matched the laser wavelength, at 0.3s.

- As the magnet was moved further, the cantilever deflection increased to a maximum, shifting the Bragg wavelength to a maximum above the laser wavelength, resulting in minimum reflection and maximum transmission at 0.38s.

- From 0.4s onward, with the magnet being moved further, the deflection of the cantilever started to decrease, causing the Bragg wavelength to decrease. At 0.45s, the Bragg wavelength again matched the laser wavelength, which produced maximum reflection and minimum transmission.

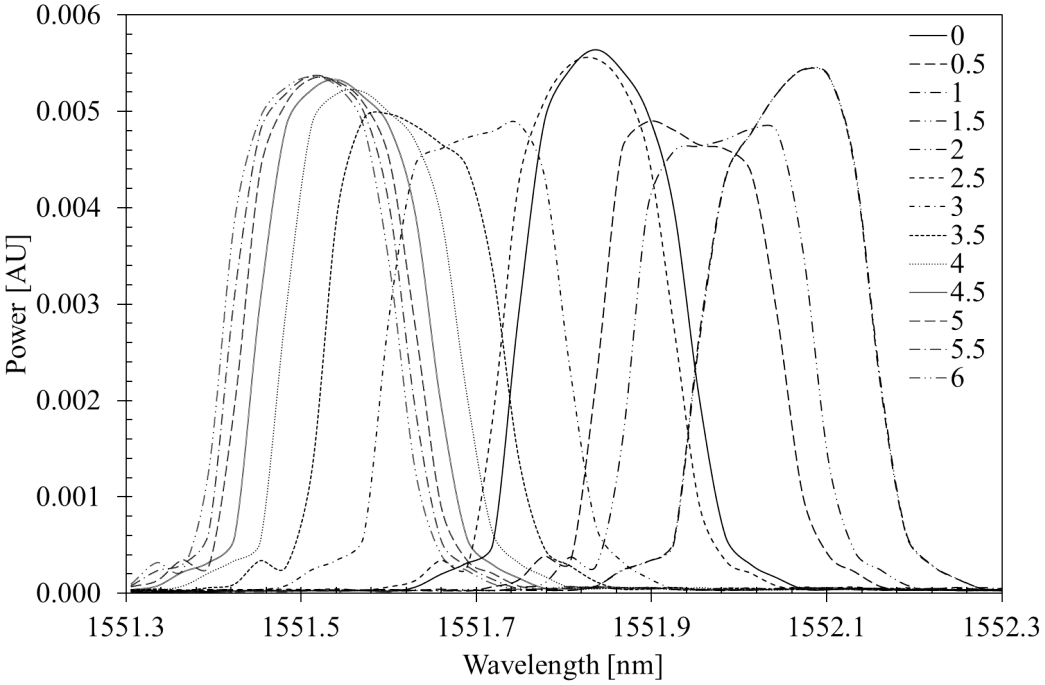

(a) Reflected spectra.

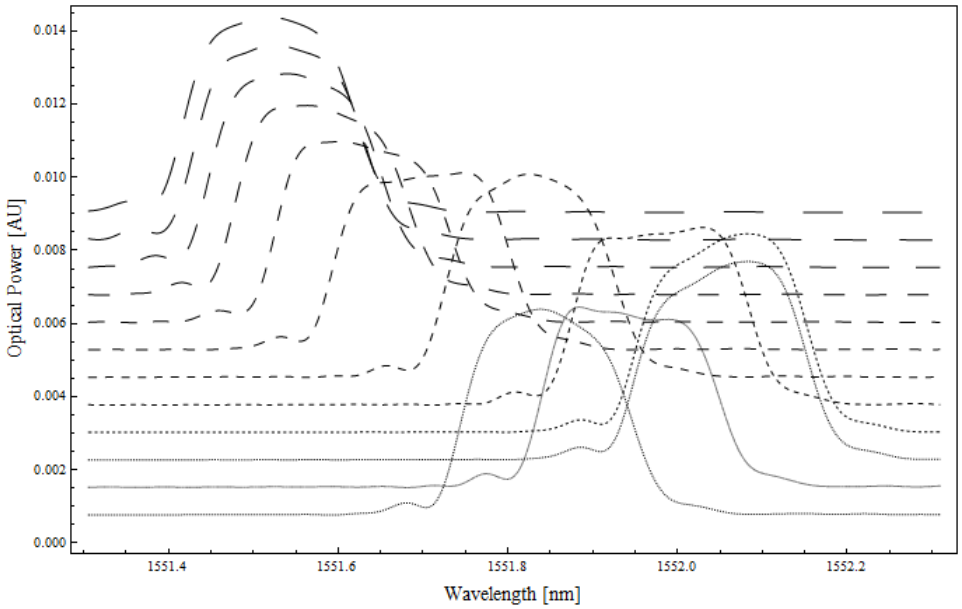

(b) Reflected spectra with a constant power offset for easier viewing.

Figure 5.14: Response of FBG reed switch as a function of magnet distance; increasing dash spacing relates to increased distance in cm.

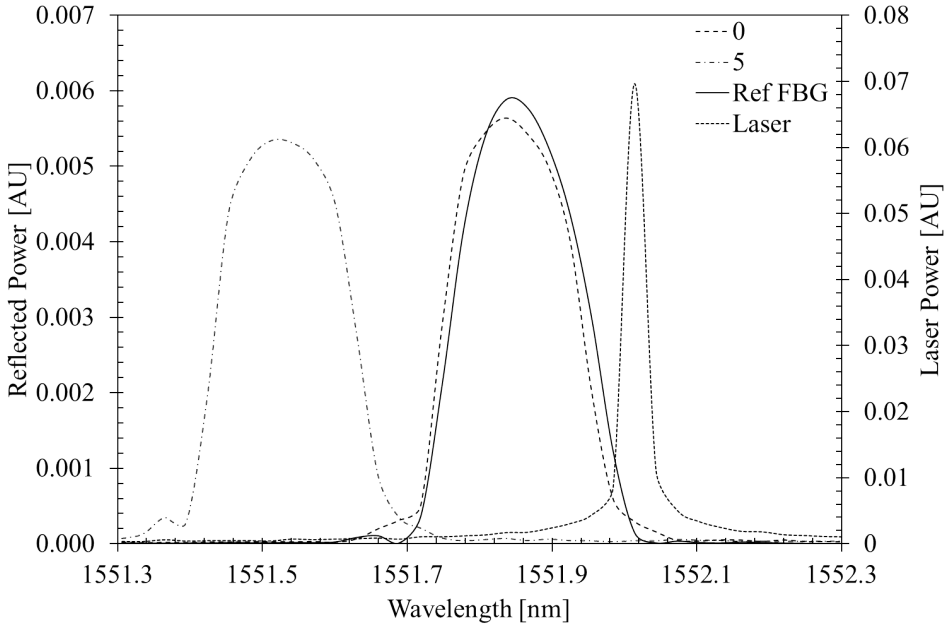

Figure 5.15: Reflected spectra for the reed switch at 0cm and 5cm, and the laser profile, and the reflected signal from the reference FBG.

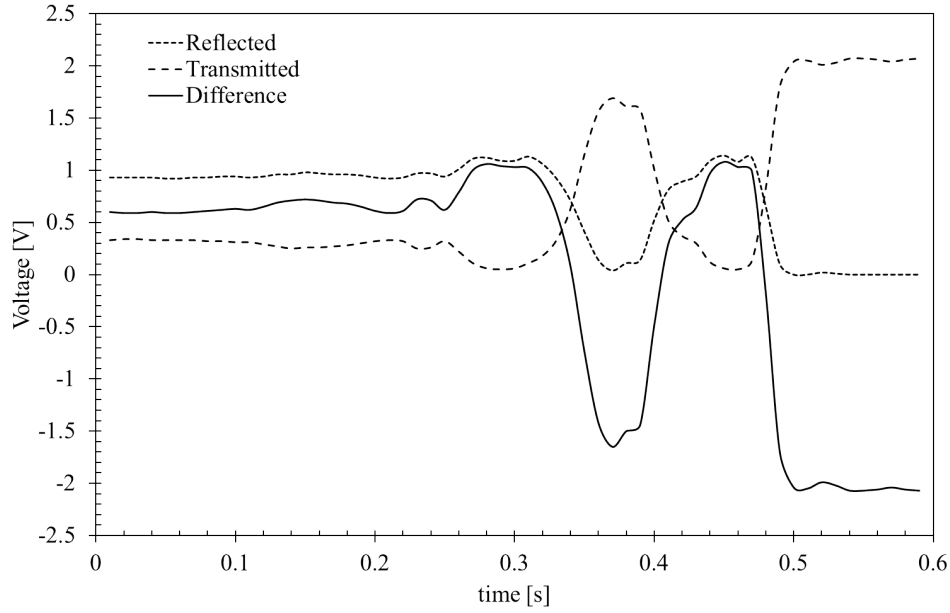

Figure 5.16: Transmitted, reflected, and the difference signals from the FBG reed switch as the magnet is shifted from left to right inducing a longitudinal strain.

- As the magnet is moved further from the cantilever, the deflection continued to decrease, resulting in a decrease in the Bragg wavelength, until there is almost no reflected signal and almost all the light was transmitted.

The full deflection of the cantilever resulted in a Bragg wavelength shift of approximately 0.6nm. In a practical system, the switch would be orientated such that there is only a small interaction between the cantilever and magnet, resulting in a Bragg wavelength shift of only around 0.1nm, producing the results in figure 5.17, which show the last 0.15s of the switch results.

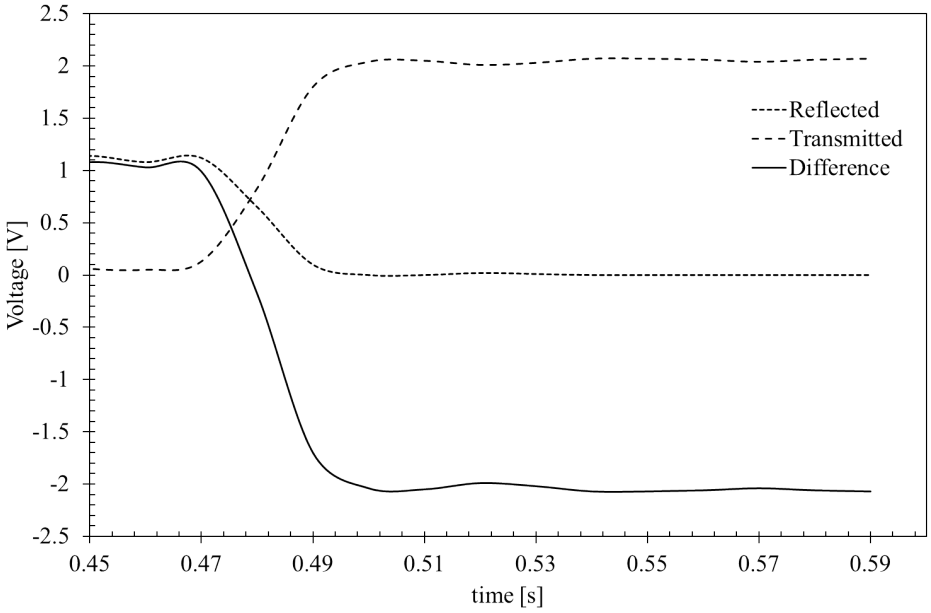

Figure 5.17: Transmitted, reflected, and the difference signals from the FBG reed switch from 0.45s to 0.6s illustrating its 3V switching ability.

It can be clearly seen that the difference signal switches between 1 volts and -2 volts, a 3 volt swing. This change could easily be configured to trigger an alarm in a PIDS. In addition, it is worth noting that the bottom magnet and the cantilever never physically touched, resulting in a non-contact switch. This would be the case if the two parts of the switch were to be fitted inside a window or door, and a frame.

5.4 Optically Matched FBG Interrogation

Whilst implementing the TRDS has the benefits of increased signal amplitude and compensation for source optical power fluctuations, as it stands currently it requires a laser for each FBG sensor. In commercial systems this may not be cost effective, particularly for high density systems, in terms of the number of sensors. Hence, it may be more practical in certain applications to implement multiplexing by using a single broadband source and some sort of demodulation technique. This can come in the form of tunable optical filters; however, these are generally quite expensive and are limited by the tuning speed of the filter. Furthermore, a tunable filter can essentially provide all of the spectral characteristics of the sensors in terms of their intensity with respect to wavelength, which in the case of digital switches, is not required.

The use of a demodulator or reference grating is a far simpler interrogation technique. This technique enables the variation in FBG reflected wavelength to be converted into an intensity change and thus detected using a standard photoreceiver, as with the TRDS. Furthermore, if the FBG sensor and the demodulator grating are co-located, the temperature sensitivity of the FBG can be effectively eliminated.This technique will be discussed in more detail in the following chapters. However, for a simple demonstration, the FBG reed switch was interrogated using this method. Figure 5.18 displays the change in the output intensity of the FBG reed switch using a optical matched reference grating. The results illustrate that the reflected intensity from both FBGs changes with the switch position. The reason the curve appears to have steps is because the resolution of the data acquisition system (PASCO ScienceWorkshop 750 Interface) was limited to $\pm 5mV$.

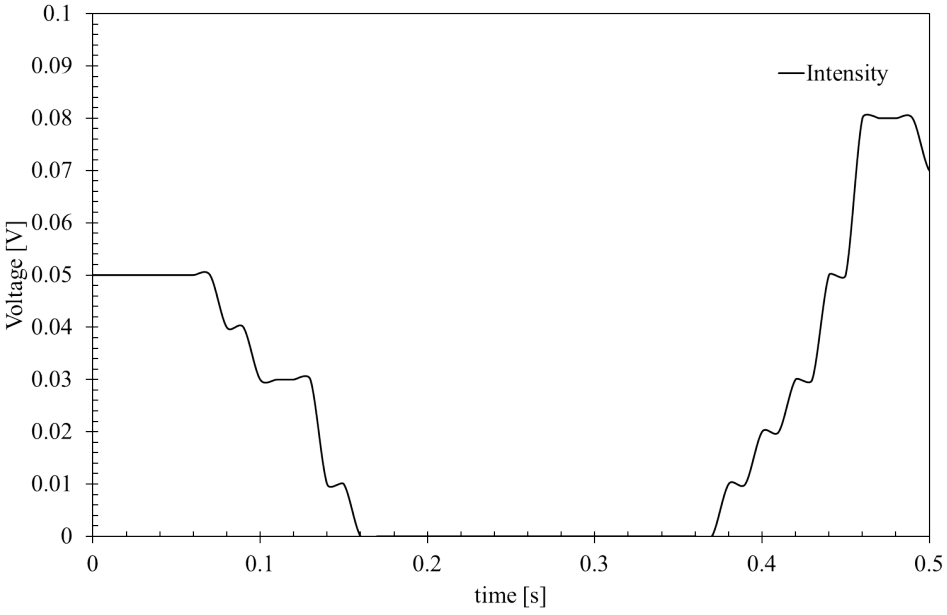

Figure 5.18: The reflected intensity from the reed switch FBG and a matched reference FBG using a SLD.

5.5 Chapter Conclusion

Three different optical fibre sensing techniques based on a TRDS, that contribute to a complete optical fibre based security system, have been demonstrated. The results show FBG sensors have the potential to replace existing electrical pressure mats, perimeter fence sensors, and reed switches used for domestic and commercial PIDS. Furthermore, the different sensors could easily be multiplexed over the same fibre using WDM and interrogated using optically mis-matched FBGs, reducing the cost of the system by utilising a single broadband source.

Chapter 6

A Highly Sensitive Fibre Bragg Grating Diaphragm Pressure Transducer

In this chapter, a highly sensitive diaphragm based pressure transducer for extremely low pressure applications has been developed. The response of the transducer has been modeled using small deformation theory, and the results have been compared to analogous experiments. Furthermore, a simple ultra-low cost interrogation technique has been implemented in an attempt to increase the penetration of FBG sensors into mainstream industrial processes by making them easily compatible with current electronic controllers. By splitting the reflected signal into two, and using one signal as a reference, or by comparing the transmitted and reflected signals, it is possible to overcome issues associated with intensity based interrogation techniques, such as optical power fluctuations [264]. Moreover, the simplicity and reduced cost of the interrogation far outweigh the disadvantages, particularly in quasi-static applications.

6.1 Transducer Design, Modelling and Response

Diaphragm pressure transducers incorporating FBGs bonded to a metallic diaphragm have been designed, tested and reported [198, 201, 265, 266]. Typically, the Young's modulus and physical dimensions of the diaphragm are much greater than that of the

fibre, and in turn, of the grating. Hence, the stress induced wavelength shift is essentially determined by the physical properties of the diaphragm. When considering the use of a rubber diaphragm this is no longer the case. The Young's modulus of the silica fibre is significantly greater than that of the diaphragm, such that the fibre itself is the limiting factor determining the strain induced wavelength shift, particularly in the region of the bonded FBG. However, it is shown that the sensitivity of the transducer is strongly correlated to the radius of the actual diaphragm. Modelling based on small deformation theory supports this hypothesis and agrees with experimental data.

6.1.1 Transducer Design

A common rubber material was used as the elastic body for the diaphragm pressure transducer. A small circular piece of the rubber, with a radius of approximately 14mm, was bonded to a plastic cylinder, while the FBG (Micron Optics OS1100) was bonded near the centre of the rubber diaphragm. The Young's modulus of the rubber and silica fibre used were experimentally determined using a PASCO stress/strain apparatus (AP-8216A), shown in figure 6.1 [267]. As the samples were small and the results were difficult to obtain, three trails were performed and the average Young's moduli were calculated.

Figure 6.1: Experimental setup for determining the Young's modulus of the rubber and silica fibre using the PASCO Scientific stress/strain apparatus.

The results for the rubber sample and silica fibre are displayed in figures 6.2 and 6.3, respectively. The Young's modulus, defined as stress divided by strain, was determined from the slope of the stress/strain graph. For the rubber, it was found to be approximately 1.4MPa. Likewise, the Young's modulus of the silica fibre was measured to be approximately 50GPa. Because of the relative sizes and moduli of the fibre and diaphragm, the fibre was estimated to provide a factor of 200 greater resistance than the diaphragm, and consequently the set up can be considered to be completely controlled by the fibre.

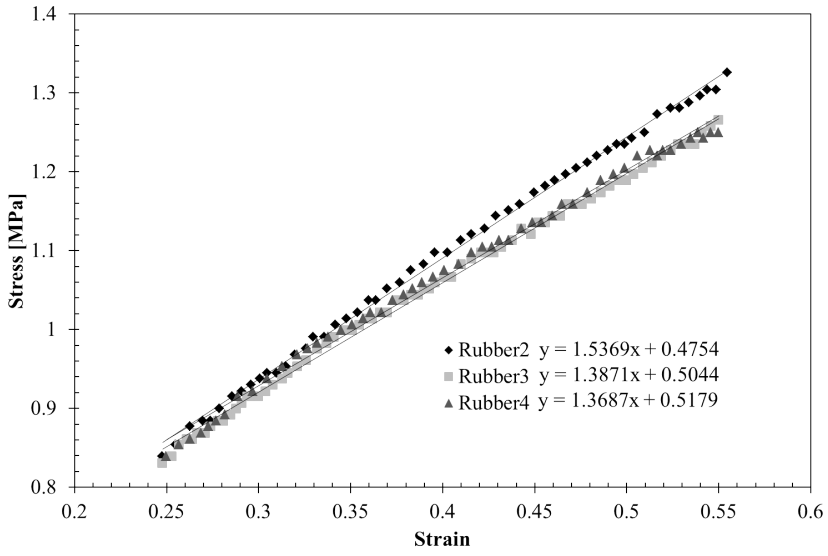

Figure 6.2: Experimental determination of the Young's modulus of the rubber diaphragm in MPa.

6.1.2 Small Deformation

The elastic body of the transducer is a circular flat diaphragm. As pressure is applied to one side of the diaphragm, strain is imposed on the diaphragm, distributed about its centre. Provided the edge of the diaphragm is fixed to a cylinder, and the applied pressure is uniform across the entire diaphragm, the strain at any point on the diaphragm can be calculated using small deformation theory [268]. Small deformation

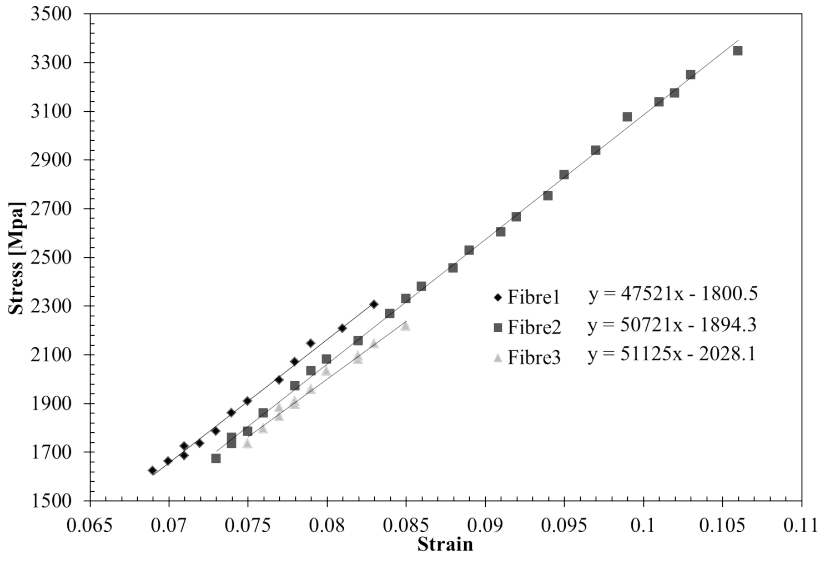

Figure 6.3: Experimental determination of the Young's modulus of the silica fibre in MPa.

theory specifically describes the radial, ϵ_r, and the tangential, ϵ_t, strain at any point on a circular diaphragm as a function of applied pressure, P, given by [269];

$$\epsilon_r = \frac{3\left(1-\nu^2\right)\left(R^2-3r^2\right)}{8Eh^2}P \tag{6.1}$$

$$\epsilon_t = \frac{3\left(1-\nu^2\right)\left(R^2-r^2\right)}{8Eh^2}P \tag{6.2}$$

where E is the Young's modulus of the material, h and R are the thickness and radius of the diaphragm, respectively, and r is the distance from the centre of the diaphragm to a point of measurement. At the centre of the diaphragm the magnitude of the total strain, ϵ_c, is given by;

$$\epsilon_c = \frac{3\sqrt{2}\left(1-\nu^2\right)R^2}{8Eh^2}P \tag{6.3}$$

Figure 6.4 shows the normalized strain distribution curves for a circular diaphragm. The strain distribution curves for the proposed design were also modeled using small deformation theory, as shown in figure 6.5. The parameters used were; Young's Modulus

$E = 50$GPa, Poisson's ratio $\nu = 0.19$ [22], radius $R = 14.0$mm, and the thickness $h = 0.125$mm.

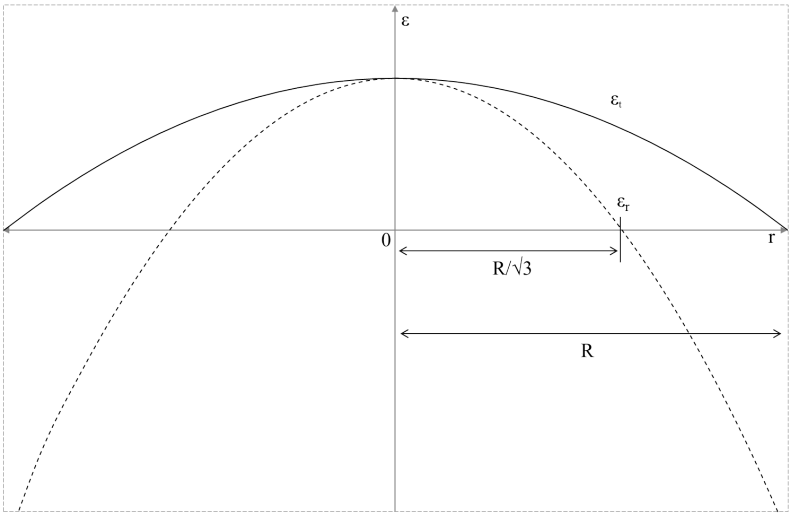

Figure 6.4: Strain distribution curves for a circular diaphragm showing the tangential and radial strain change as a function of r from the centre of the diaphragm. The strain at the centre is where $r = 0$.

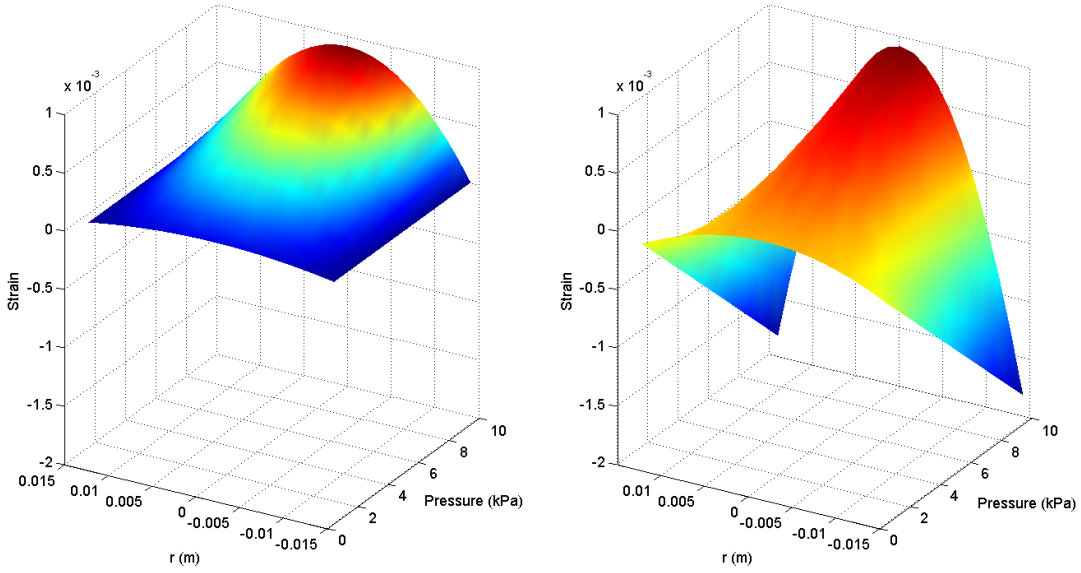

Figure 6.5: (a) Tangential strain and (b) radial strain as a function of distance r, from the centre of the diaphragm, and applied pressure.

6.1.3 Optical Response of Pressure Transducer

The transducer's optical response due to pressure was measured using the setup shown in figure 6.6. The FBG diaphragm transducer was attached to a small rubber tube with a T-junction attached. One outlet of the T-junction was connected to an electronic pressure sensor and data acquisition system, to record the change in pressure. The other outlet was connected to a syringe secured to a translational stage to provide an incremental pressure change. The optical source was a broadband SLD (DenseLight DL-BZ1-CS5254A), which was connected to port 1 of a circulator (AFW CIR-4-12-L-1-2), with the FBG connected to port 2, and an OSA (Thorlabs OSA202), connected to port 3.

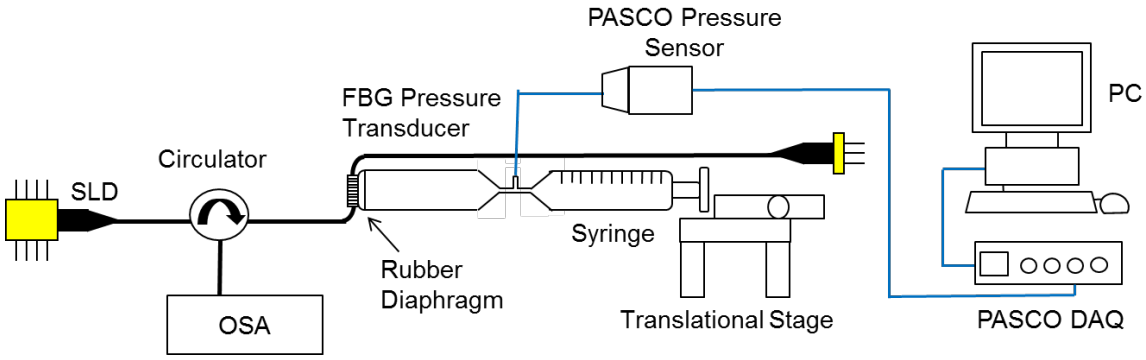

Figure 6.6: Experimental setup for the wavelength shift of the sensing FBG as relative pressure is applied.

The reflected wavelength spectra were recorded and analysed. Figure 6.7 shows the reflected spectra as a function of applied pressure from 4kPa to 10kPa relative to atmospheric pressure in increments of 0.5kPa, with each spectrum having an intensity offset of 0.002 for ease of viewing. The increase in dash spacing corresponds to an increase in pressure. The graph shows there are small fluctuations in peak optical power as the pressure is varied. The shift in wavelength is linear and the shape of the reflected spectrum does not change significantly with increased pressure.

The experiment was repeated three times over a maximum range of 12kPa, with the average transfer function recorded. Figure 6.8 indicates that the Bragg wavelength shift

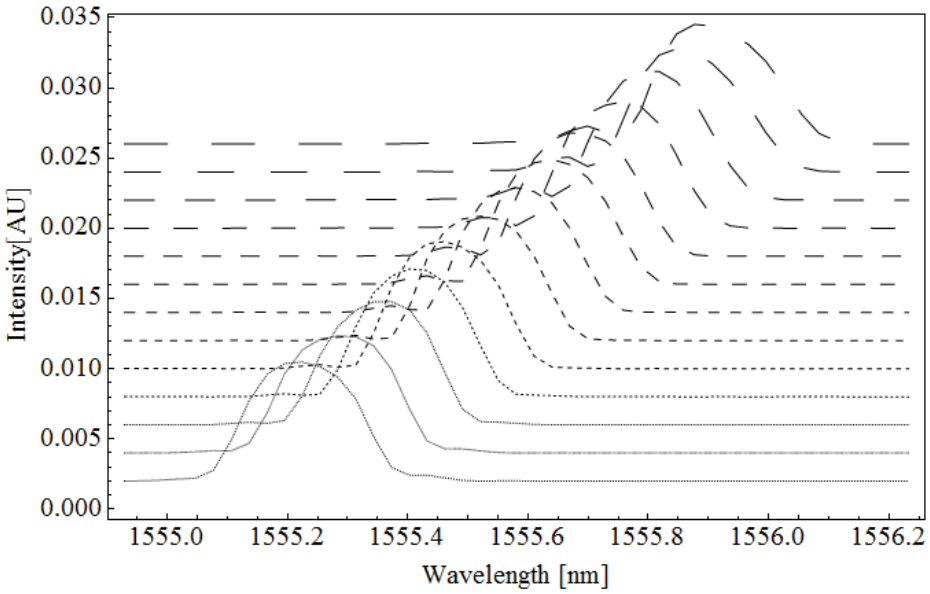

Figure 6.7: Reflected wavelength spectra as a function of pressure from 2kPa to 12kPa relative to atmospheric pressure withe an increasing intensity offset. The increased dash spacing refers to increased pressure.

of the FBG due to applied pressure is linear over the entire pressure range, and that there is a good agreement with all three runs showing the results are highly repeatable. The solid line shows the average transfer function. The pressure transducer has an average sensitivity of 0.116nm/kPa, which compares favorably with the 0.048nm/kPa transducer based on metal bellows, reported by Song et al. [194], and the 0.031nm/kPa diaphragm pressure transducer, reported by Rao et al. [266].

Simulation results for different fibre arc lengths on the diaphragm, based on small deformation theory, are displayed on the same graph as dashed lines. The increasing dash spacing corresponds to radii of 11, 12, and 14.4mm, respectively. The value of 14.4mm represents the maximum available radius of the transducer; however, the data correlates very well with a radius of 11mm. This is because the FBG was not bonded exactly to the centre of the diaphragm, which had the effect of reducing the available radius. Further, this shows than by changing the position of the sensor, and hence

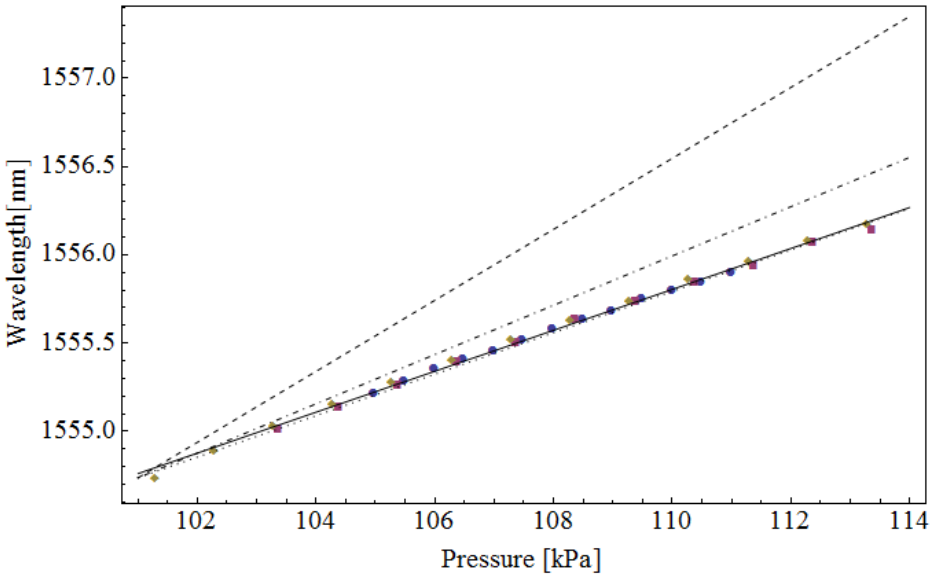

Figure 6.8: Bragg wavelength as a function of applied pressure with repeated measurements and simulation results. The solid line is the average line of best fit for all of the data. The dashed lines show the simulated results, with increased dash spacing corresponding to radii of 11, 12, and 14.4mm.

the length of the fibre across the diaphragm, the sensitivity of the transducer can be modified.

6.2 Intensity Based Interrogation Modeling

Wild and Richardson [270] developed a numerical model for intensity based interrogation of FBGs. Their model can be used to determine the reflected intensity from an FBG using a laser light source (power detection). The same method has been used in this study to model the reflected intensity from two FBGs using a broadband light source. This is because the reflected signals from the FBGs are Gaussian, as is the signal from a laser. Their study also discusses linear edge filter detection which could have been used to approximate the proposed system. The reflected intensity is given by;

$$R = BS_0L_0\sqrt{\frac{\pi}{\alpha_S + \alpha_L}}exp\left[-\frac{\alpha_S\alpha_L}{\alpha_S + \alpha_L}\left(\lambda_S\left(P\right) - \lambda_L\right)^2\right] \tag{6.4}$$

where B is the amplitude of the broadband source, S_0 and L_0 are the reflectivity of the sensing and reference FBG, respectively, λ_S and λ_L are the Bragg wavelengths of the sensing and reference FBGs, respectively, and α_S and α_L are the widths of the FBG Gaussian signals, such that the FWHM, $\Delta\lambda_x$ is given by;

$$\alpha_x = \frac{ln16}{\left(\Delta\lambda_x\right)^2} \tag{6.5}$$

Furthermore, the intensity spectra were simulated and compared to the real intensity spectra for different values of applied pressure. The values used in the simulations were; $P_{11} = 0.121$, $P_{12} = 0.270$ [11], the effective refractive index $n_{eff} = 1.468$ [22], $S_0 = 7.0\mu W/nm$, $L_0 = 8.0\mu W/nm$, $\Delta\lambda_S = 0.203$nm, $\Delta\lambda_L = 0.213$nm, and $\lambda_L = 1555.52$nm.

6.2.1 Experimental Procedure and Results

Using the experimental setup shown in figure 6.6, the reflected spectra from the sensing FBG with no exerted pressure, and that of an optically mis-matched filter FBG, at 19^oC, were recorded, as shown in figure 6.9. The figure shows their relative peak intensity, FWHM and spectral position before pressure is applied to the transducer.

The sensing FBG was then connected to port 2 of the four port circulator, the reference FBG was connected to port 3, and the OSA connected to port 4, so as to record the reflected intensity spectra from both FBGs. The optical circuit is shown in figure 6.10.

Initially, as the two FBG reflected spectra effectively did not overlap, there was no reflected intensity spectra recorded by the OSA, as expected. As pressure was applied to the transducer, and the reflected spectrum from the sensor FBG shifted towards that of the reference FBG, an intensity waveform with increasing amplitude was recorded.

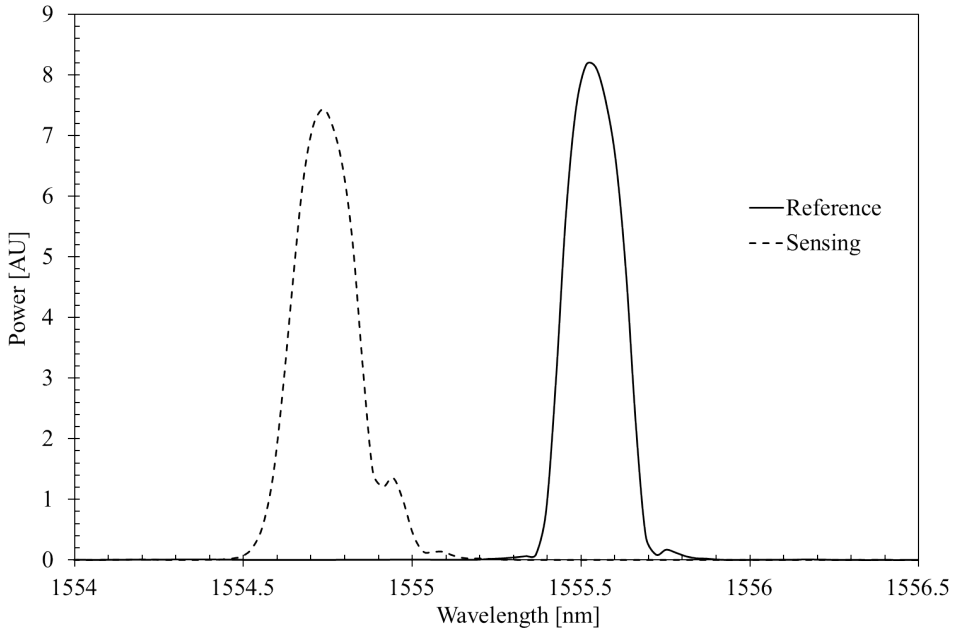

Figure 6.9: Sensing (dashed curve) and reference (solid curve) FBG spectra in the absence of applied pressure.

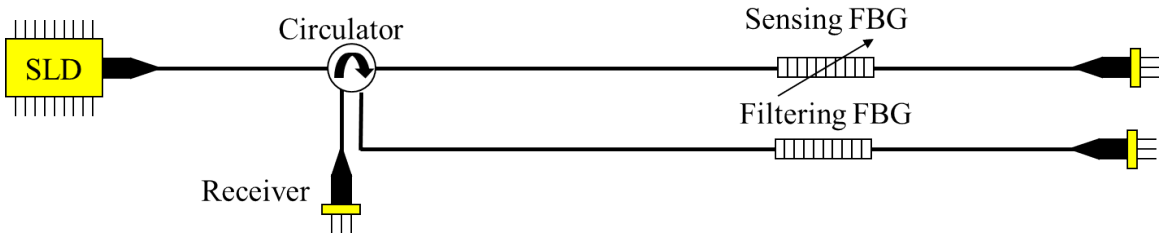

Figure 6.10: A schematic of the optical circuit for the interrogation system.

As the pressure was increased further, the amplitude of the signal reached a maximum and then decreased towards zero again.

The results are shown in figure 6.11 with an increasing intensity offset. The graphs show that as the two signals overlap, a Gaussian like intensity waveform is produced. As pressure is applied, both the FWHM and the amplitude of the reflected signal increase, as well a shift in the peak wavelength from 1555.4nm to 1555.7nm occurs. The maximum intensity occurs where the two separate signals have the same Bragg wavelength, at approximately 1555.52nm, which corresponds to the Bragg wavelength of the reference

FBG, as expected. Figure 6.11a shows the variation in peak intensity, wavelength and FWHM for each individual spectrum. The simulated intensity spectra based on the overlapping of two Gaussian waveforms are shown in figure 6.11b. The results show that the model correlates well with the real data. The only major difference is that the real data waveforms are slightly wider and hence have a larger FWHM.

The variation in total optical intensity, i.e. the integral of the optical intensity reflected from both FBGs, as the pressure is increased, is shown in figure 6.12. The solid line shows the simulated intensity and the recorded intensity is shown with the data points. The reason data appears to be in steps is because of the low resolution of the electronic pressure sensor. The resolution of the sensor was only 0.1kPa. Both the real data and simulated curve show an approximate Gaussian intensity response to pressure, with an approximately linear region from 106kPa to 107kPa, and a maximum intensity at 107.5kPa.

The change in intensity with respect to time was used to calculate the actual pressure response of the FBG pressure transducer using equation 6.4. The pressure variation with respect to time recorded by the electrical pressure sensor and the calculated FBG pressure are shown in figure 6.13. As there are multiple values of pressure for each intensity value, the pressure with respect to time data is split in two, with a small separation in the middle. This is the region where the peak intensity occurs and is essentially due to error in recording the maximum intensity for a specific pressure. The graph shows the FBG pressure sensor is more sensitive and has better resolution than the electronic pressure sensor, demonstrating that a FBG diaphragm pressure transducer has better response than an electrical counterpart and justifies their implementation in low pressure applications.

Finally, the OSA was replaced with a photodetector to convert the intensity into a voltage. This was performed to simply demonstrate that this interrogation technique would enable the output of the optical fibre transducer to be easily connected to an electronic controller. Figure 6.14 shows the output voltage as a function of applied pressure in the linear region. Using this interrogation technique, with reference FBG

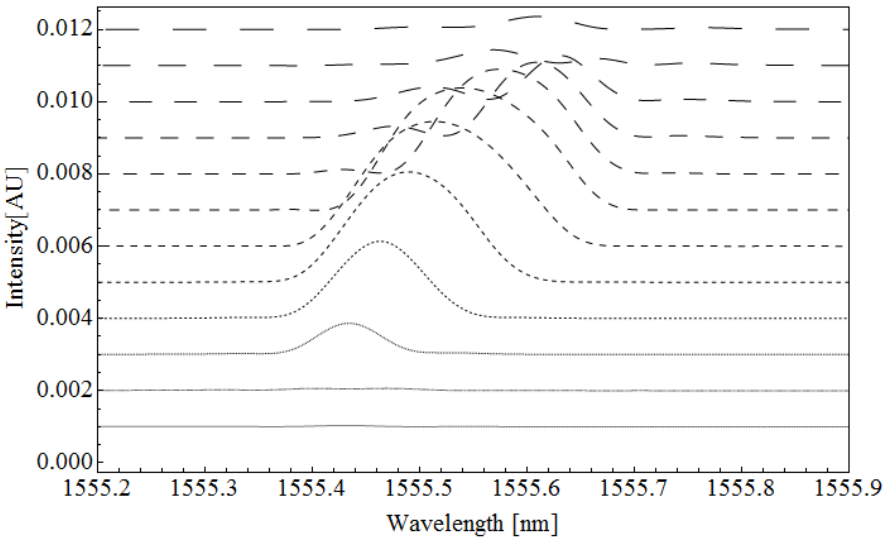

(a) Experimental data shifted by a 0.002 intensity per kPa offset.

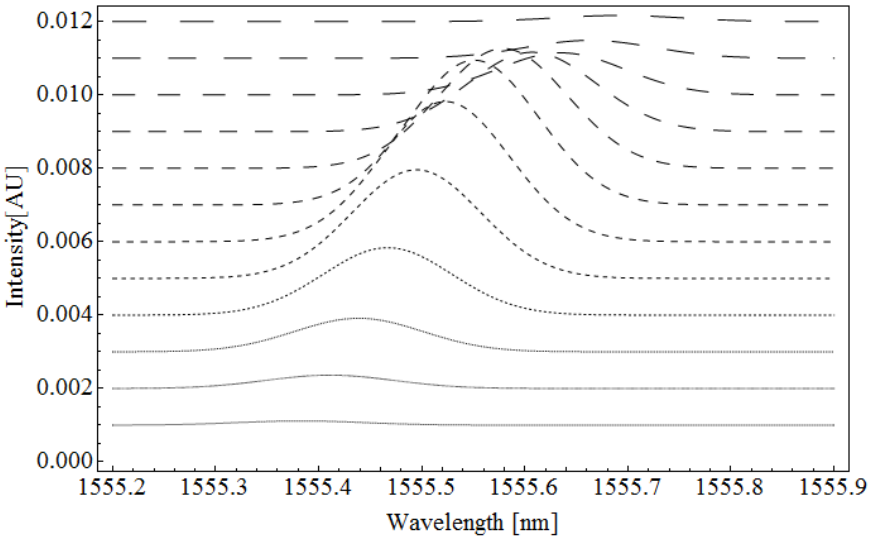

(b) Simulated data shifted by a 0.002 intensity per kPa offset.

Figure 6.11: Real and simulated reflected spectra from the combination of both FBGs as a function of applied pressure. Increased dash spacing corresponds to increased gauge pressure from 3.5kPa to 9kPa in increments of 0.5kPa.

chosen here, the transducer produces a linear output from 106kPa to 107kPa across a voltage range of 1.5V, which corresponds to a sensitivity of 1.41V/kPa. However, the dynamic range of the transducer could be increased by changing the properties of the

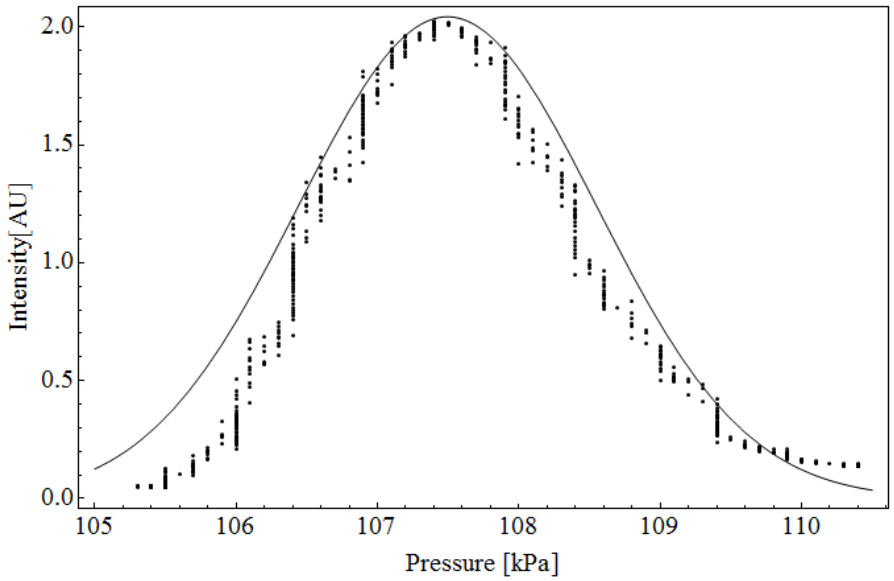

Figure 6.12: Total optical intensity of output signal as a function of applied pressure. The simulated intensity is shown with the solid line and the actual intensity is shown with the data points.

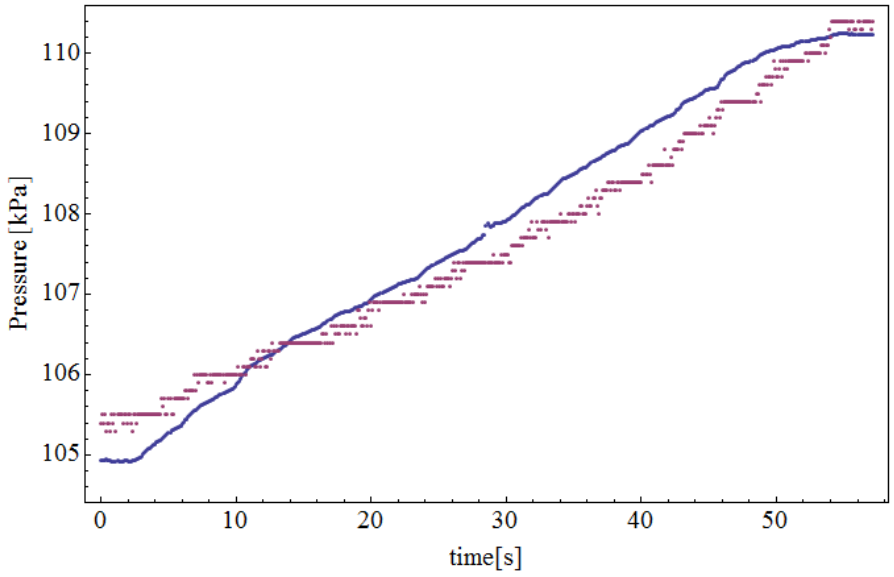

Figure 6.13: Pressure variation with respect to time recorded by the electrical pressure sensor (data points) and the calculated FBG pressure (solid line).

reference FBG.

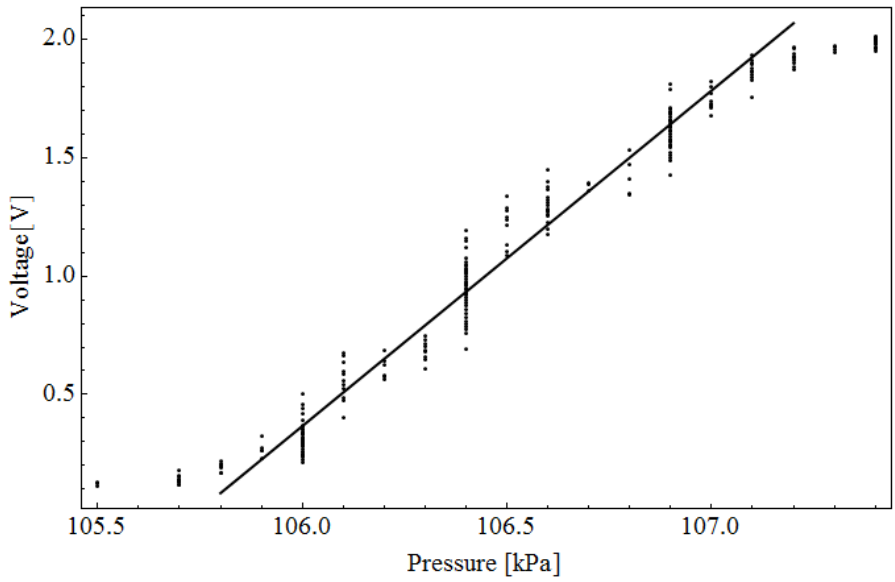

Figure 6.14: Output voltage as function of applied pressure.The data points correspond to the values recorded by the data acquisition system which appear to be in vertical lines due to the low resolution of the pressure sensor. The solid line is the line of best fit based on a linear approximation where the sensitivity is 1.41V/kPa.

Using a chirped grating [25], the FWHM could be significantly increased, although there would be a trade-off between sensitivity and dynamic range. The effect of varying the FWHM of the reference FBG on the sensitivity and dynamic range of the interrogation system, is shown in figures 6.15 and 6.16.

Figure 6.15 shows the simulated reflected spectra as a function of increasing FWHM from 0.1nm to 0.3nm in increments of 0.05nm. The curves illustrate that as the FWHM is increased, the intensity distribution spreads out over a larger area. Hence, in the region where there is a linear approximation the gradient decreases. This essentially means that as the FWHM is increased, the dynamic range of the system is increased, as the minimum recordable intensity is further from the peak pressure point. However, as the gradient decreases, the change in intensity for each increment of pressure decreases, reducing the sensitivity of the interrogation system.

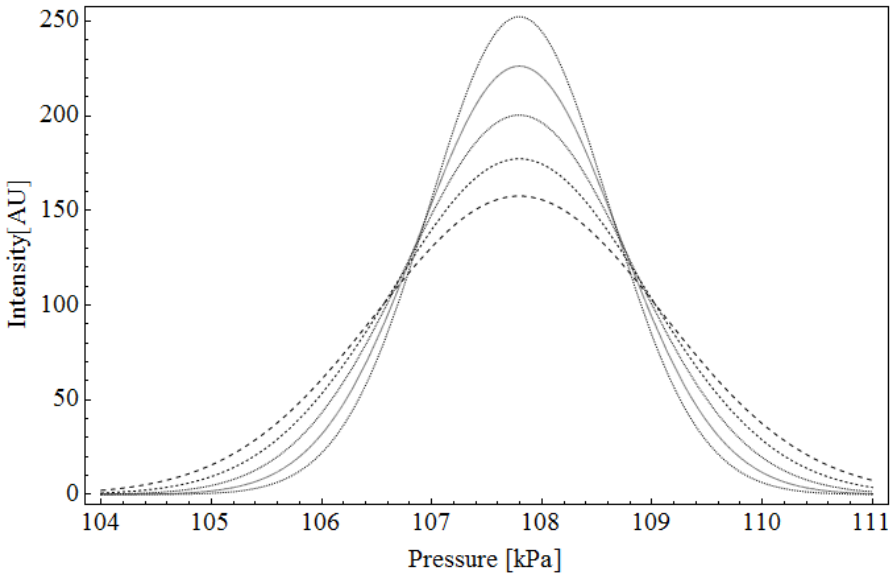

Figure 6.15: Reflected spectra as a function of increasing the FWHM of the reference FBG from 0.1nm to 0.3nm in increments of 0.05nm.

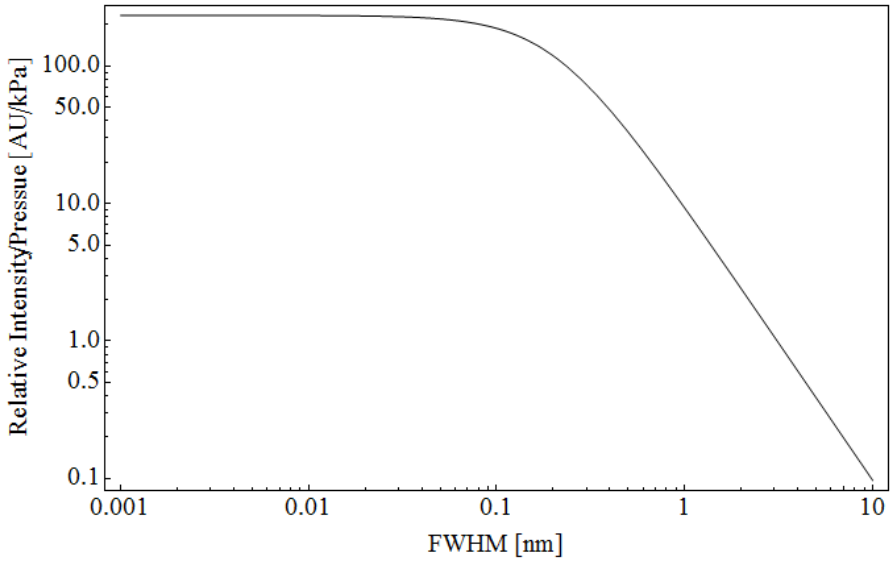

Figure 6.16: Sensitivity of the system as a function of FWHM of the reference FBG.

Figure 6.16 shows how the sensitivity of the system changes with change in FWHM over a large range. For a FWHM less than 0.1nm, there is almost no increase in sen-

sitivity as the FWHM decreases. This suggests that there are other factors limiting the sensitivity in this region, such as the sensitivity of the actual sensor. Also, from approximately 0.3nm onwards, the sensitivity is inversely proportional to the FWHM. Therefore, when optimising the interrogation of a transducer for a specific application, there would be a trade-off between sensitivity and dynamic range.

6.3 Discussion

Using an edge filter based interrogation technique eliminates the need for an expensive solid state interrogator and enables the transducer to be directly connected to an electronic controller, such as a PLC in a plug and play fashion. By packaging the filter and the sensor together, the transducer is effectively temperature insensitive (as the Bragg wavelengths are separated by less than 1nm, meaning the relative shift in Bragg wavelength over a range of 100K is approximately 0.5pm). Furthermore, multiple transducers could be multiplexed by simply connecting both the sensing and filtering fibre in series with the respective fibre's of transducers of this type, provided the FBGs have different Bragg wavelengths. The only additional components required would be a wavelength division de-multiplexer (DeMux), and a photodetector for each transducer.

The error in the measured pressure was $\pm$0.05kPa, whilst the error in the measured wavelength was extremely small as the OSA is a high precision instrument ($\pm$0.3pm). In theory, power detection methods could be used to interrogate the FBG pressure sensor by tuning a laser to the 3dB point of the FBG and analyzing the reflected and/or the transmitted power [261]. However, this would not eliminate problems associated with a shift in Bragg wavelength due to temperature. Also, either multiple sources would be required, or a high speed scanning laser would need to be utilized in order for multiplexing to occur, increasing the cost of the system.

Off-the-shelf FBGs were used as both the sensor and the interrogator in this study. FBGs with specific Bragg wavelengths could be utilized such that the transducers output would be linear for a differential pressure range starting at 0kPa. The use of a chirped

FBG, with a broader reflected spectral range, as the linear edge filter, would enable a transducer with a larger dynamic range to be produced. Furthermore, the properties of each FBG pair could be designed and manufactured early in the development stage to ensure the desired attributes of a specific transducer would be obtained.

6.4 Chapter Conclusion

A highly sensitive diaphragm based FBG pressure transducer has been designed and tested. The results show that the transducer has a sensitivity of 0.116nm/kPa and hence the use of a rubber diaphragm significantly increases the sensitivity of the transducer with respect to metal diaphragms. The design utilizes an on-board interrogator in the form of an optically mismatched FBG acting as a linear edge filter. Both the sensitivity and the dynamic range of the interrogation system can be optimized for a given application by changing the optical properties of the filter, such that increasing the FWHM would increase the operating range of the transducer but decrease the sensitivity. Moreover, the transducer is effectively temperature insensitive as the sensing FBG and filtering FBG are co-located. This technique removes the need for an expensive solid state FBG interrogator and therefore increases the probability of this type of transducer being utilized in mainstream industrial applications. The transducer could be utilized for very low pressure applications such as heating, ventilation, and air conditioning (HVAC), as well as medical engineering. Furthermore, being a passive optical transducer, it would be extremely useful in highly hazardous or in-vivo environments.

Chapter 7

A Temperature Insensitive Fibre Bragg Grating Load Cell with On-Board Intensity Based Interrogation

In this chapter, a dual FBG based load cell in a push-pull configuration is reported. The results show that an output Gaussian waveform reflected from two optically matched FBG sensors produces a linear output voltage as function of applied load within a defined range. The output spectra from both FBGs were explicitly recorded for both loading and unloading of the load cell, as well as the combined output spectrum using a four port circulator. As both FBGs are co-located, the system is effectively temperature insensitive.

7.1 Load Cell Design and Characterisation

The mechanical setup is based on a three point bending system whereby a thin sheet of steel is placed across two steel platforms and held in place by clamps to prevent the edges of the steel plate from pivoting. A small piece of steel was placed in the centre of the sheet before it was loaded with 1kg masses. Two FBGs were bonded to the top and bottom of the sheet, respectively. The reflected spectra from both the top and bottom FBGs were analysed separately whilst loading and unloading the transducer to show

the Bragg wavelength shift. A broadband source (DenseLight DL-BZ1-CS5254A) was used together with a four-port circulator (AFW CIR-4-12-L-1-2) and an OSA (Thorlabs OSA202). The SLD was connected to the first port of the circulator, the FBG was connected to port 2 and the OSA was connected to port 3, as shown in figure 7.1. The reflected spectra were then recorded as a function of applied load, for both loading and unloading of the transducer.

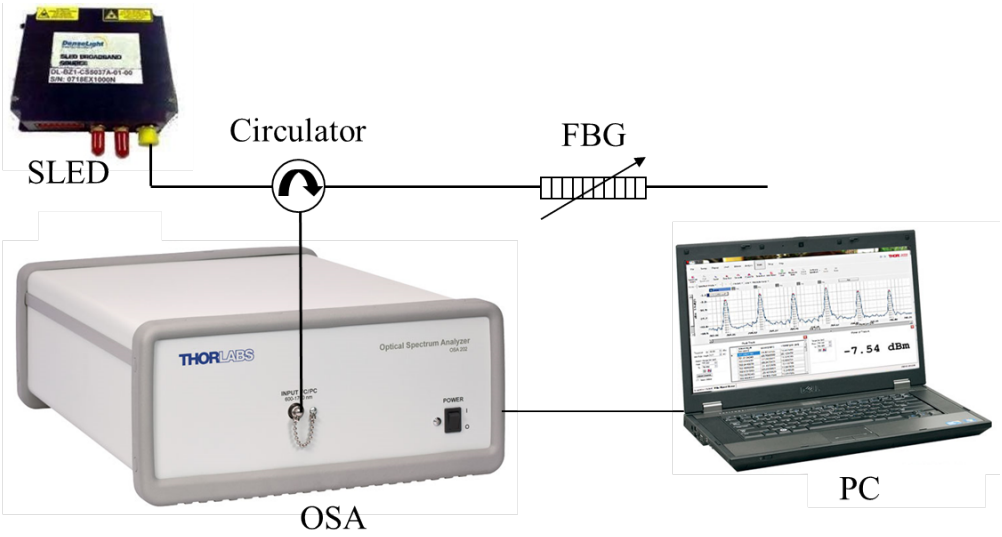

Figure 7.1: Experimental setup for the determination of Bragg wavelength shift as a function of load for the top and bottom FBG.

For intensity based measurements, the top FBG and the bottom FBG were connected to port 2 and port 3 of the circulator, respectively, and the OSA was connected to port 4. As the Bragg wavelength of both FBGs were approximately the same, the reflected spectra overlapped, acting as a linear edge filter for the optical signal, converting the corresponding shifts in wavelength to an optical intensity change. The intensity spectra were recorded as the transducer was loaded and unloaded. The OSA was then replaced by a photodetector (Thorlabs DET01CFC) and the output of the photodetector was connected to a 149.5kΩ resistor so as to give an output voltage of between 0 and 5V. A schematic of the load cell system is shown in figure 7.2.

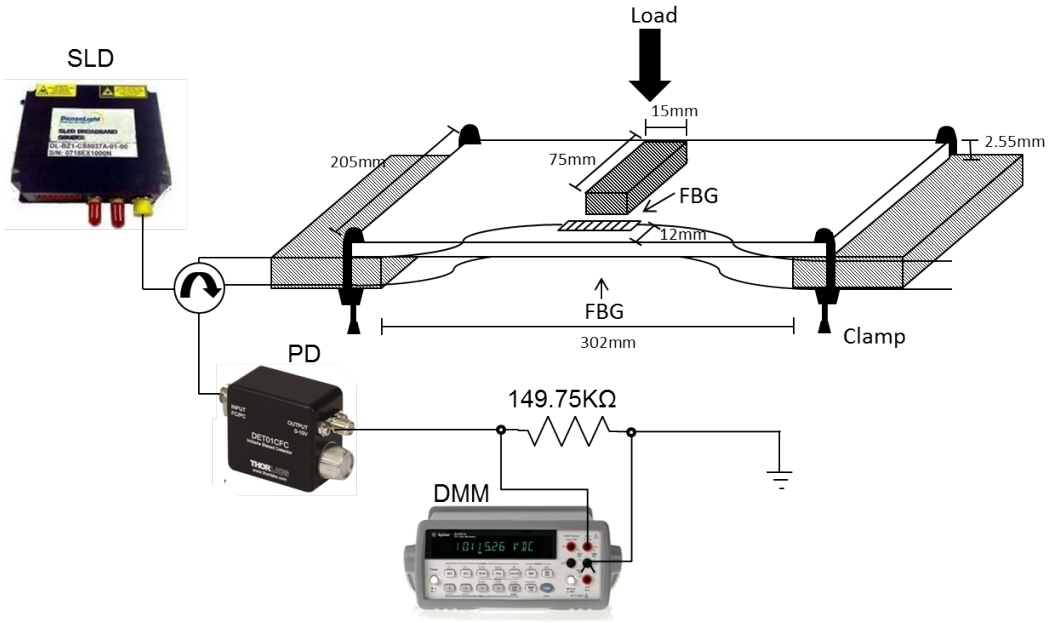

Figure 7.2: Experimental setup for FBG based load cell.

7.2 Spectral Response of Individual FBGs

Figure 7.3a and 7.3b show the reflected spectra from the top FBG for loading and unloading, respectively. As expected, the load caused the top FBG to compress. The Bragg wavelength increased as the load cell was loaded and returned to the original wavelength after it was unloaded. There was no significant change in the shape of the reflected spectra.

Figure 7.4a and 7.4b show the reflected spectra from the top FBG for loading and unloading, respectively. As expected, the load caused the bottom FBG to stretch. The Bragg wavelength reduced as the load cell was loaded and returned to the original wavelength after it was unloaded. There was no significant change in the shape of the reflected spectra.

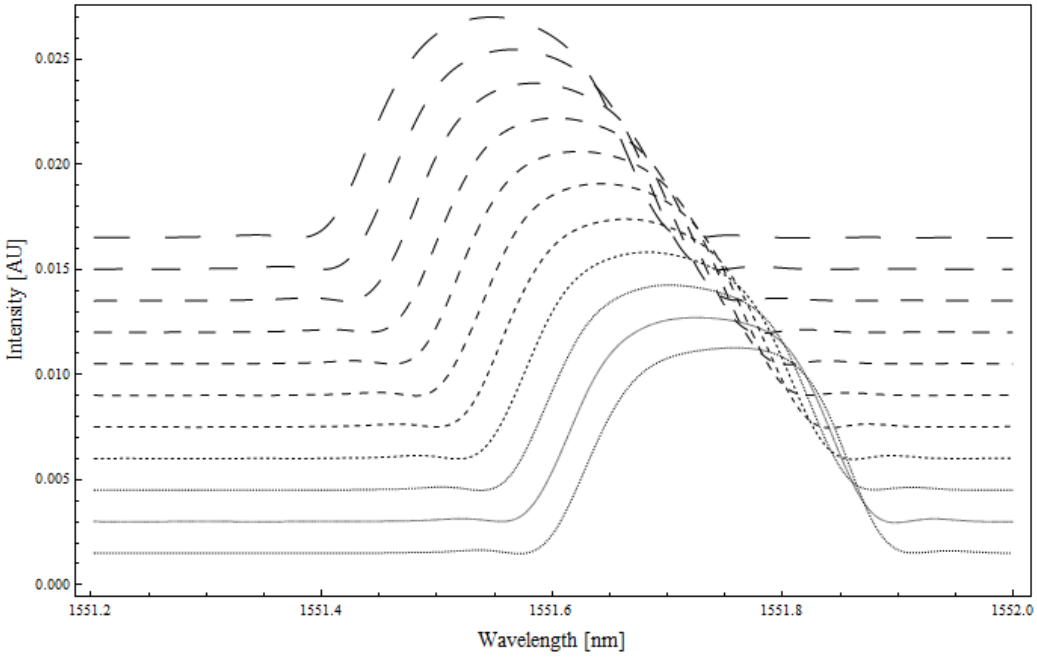

(a) Loading.

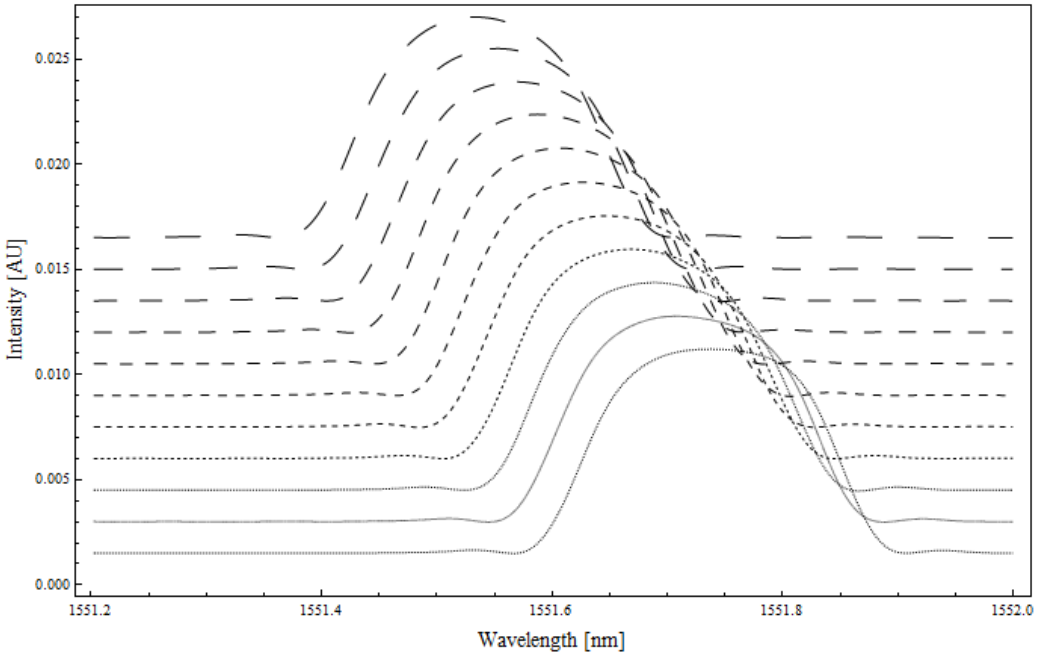

(b) Unloading.

Figure 7.3: Reflected spectra from the top FBG as a function of applied load.

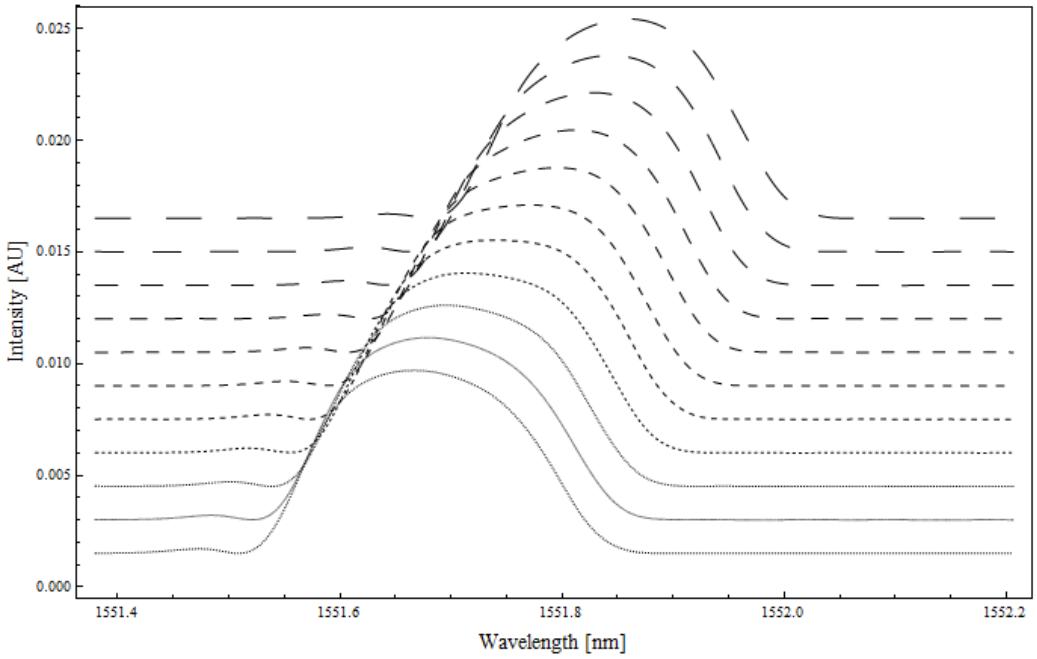

(a) Loading.

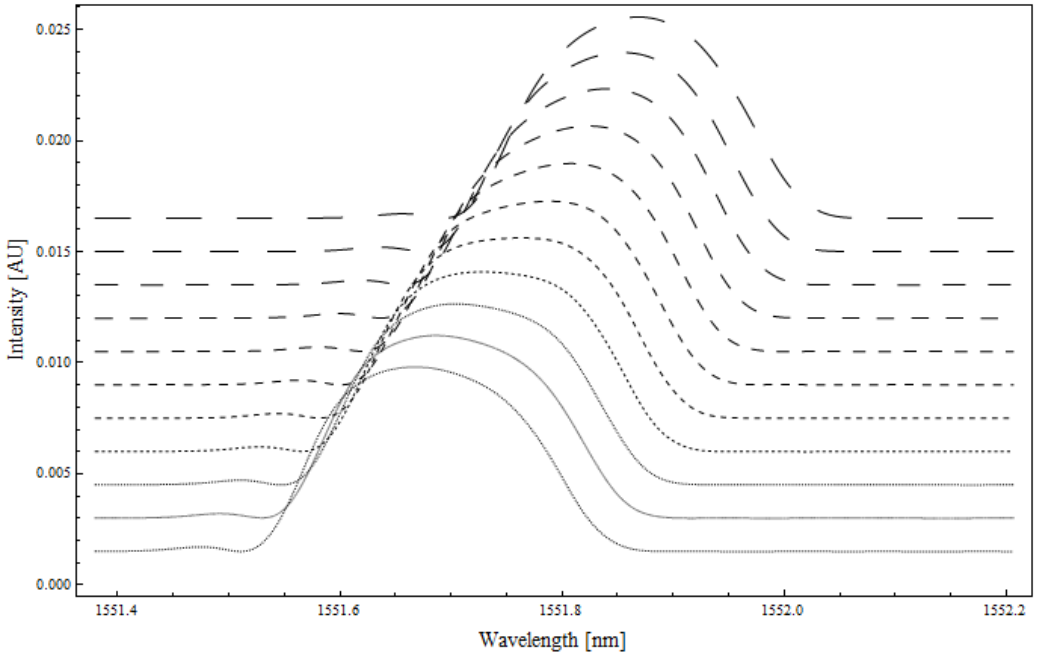

(b) Unloading.

Figure 7.4: Reflected spectra from the bottom FBG as a function of applied load.

7.3 Bragg Wavelength Shift

Figures 7.5 and 7.6 show the Bragg wavelength shift of the top FBG and bottom FBG for loading and unloading of the load cell transducer, respectively. The wavelength shift of both FBGs were recorded as the transducer was unloaded to determine if there was any hysteresis.

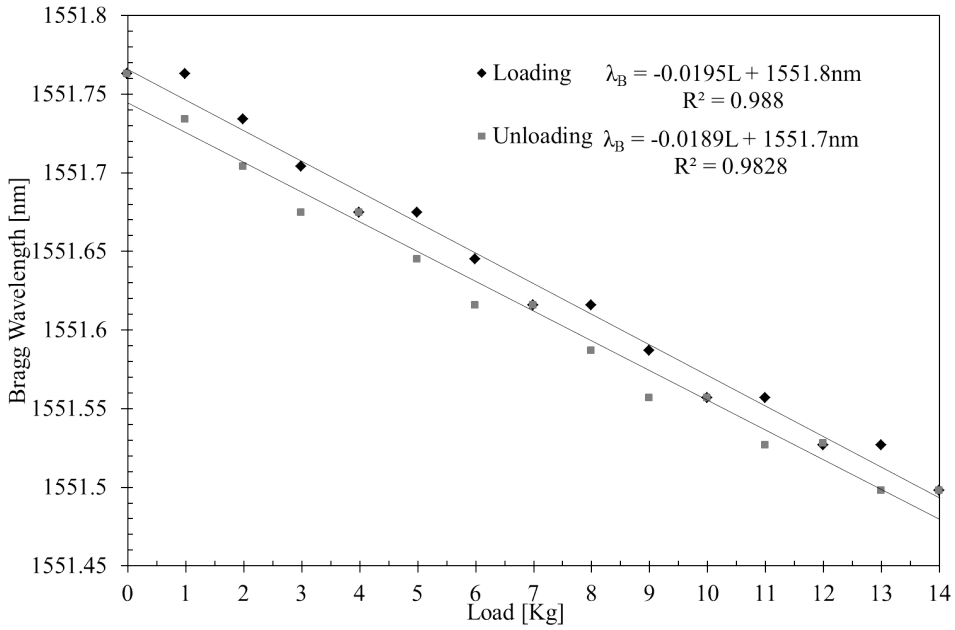

Figure 7.5: Bragg wavelength shift of the top FBG.

The results show that the Bragg wavelength shift was approximately linear for both FBGs for loading and unloading from 0 to 14kg. Although the data can be approximated as linear, there is not a perfect fit because the reflected spectra are Gaussian in shape and hence the convolution of both Gaussians produce a Gaussian intensity profile. There is some evidence of hysteresis for the top FBG across the full range and for the bottom FBG between 4 and 11kg, which is a result of the mechanical deformation of the transducer, although this is relatively small. The Bragg wavelength shift was recorded as -19.2pm/kg for the top FBG and 19.3pm/kg for the bottom FBG. The error in the applied load was small, only ±0.002kg/kg. The error in the recorded wavelength was again extremely small as the precision of the OSA was ±0.3pm. Figure 7.7 shows the linear regression

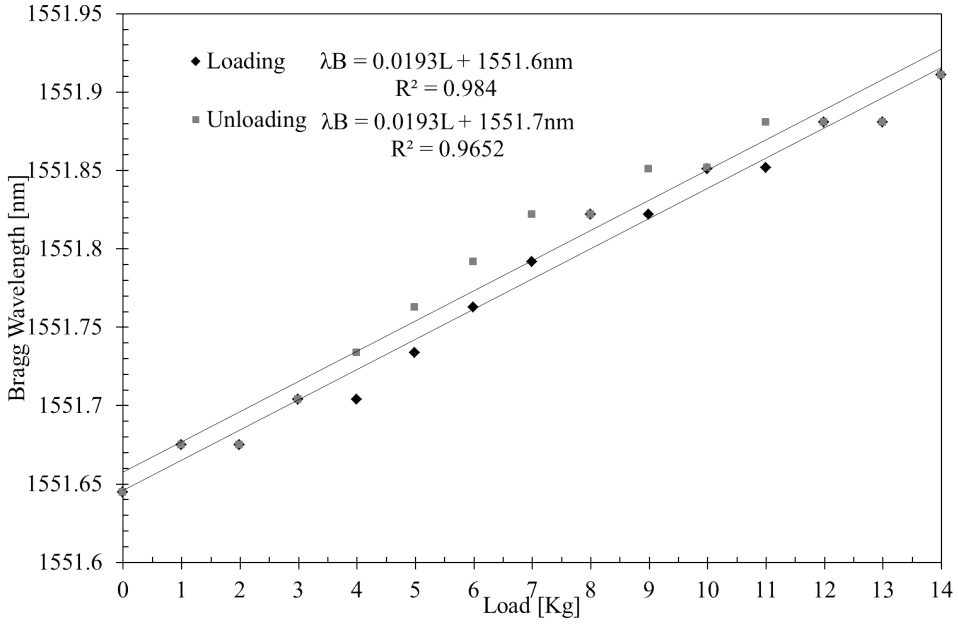

Figure 7.6: Bragg wavelength shift of the bottom FBG.

lines for both FBGs, highlighting the region where the two spectra overlap. Again the reason they do not overlap at a single point is not due to error in the measurements, but to the hysteresis of the transducer.

A cantilever based load cell reported by Benjamin et al. [271] also recorded a linear response for Bragg wavelength shift against load. They reported a Bragg wavelength shift of 0.4nm/kg over a range of 0 to 2kg. However, the sensitivity of the load cell reported here, and those previously reported, depends on the mechanical properties of the transducer rather than the optical properties of the FBG. The maximum obtainable sensitivity would correspond to a flexible bending structure such that the applied load caused the maximum possible strain in the FBG ($1.2pm/\mu\epsilon$). Their cantilever based load cell was interrogated using an OSA; however, an optically mis-matched FBG could have been bonded to the underside of the cantilever. This would form a push-pull configuration similar to that demonstrated here, meaning the output of the transducer could be converted into a voltage in the same way.

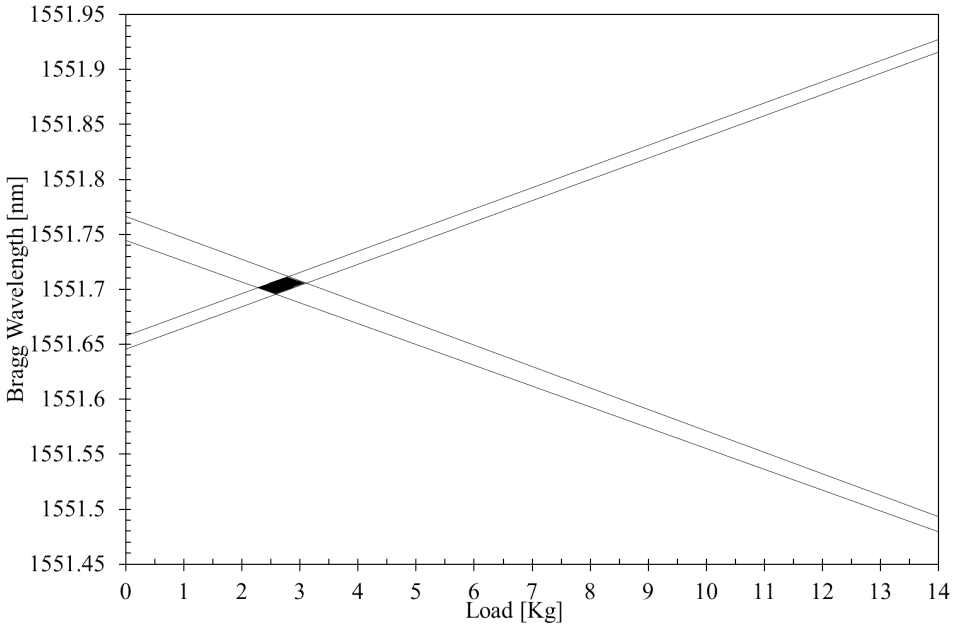

Figure 7.7: Bragg wavelength of both FBG showing the region where the two spectra overlap.

7.4 Intensity Spectra

The intensity spectra as a function of applied load for loading and unloading of the transducer are shown in figure 7.8a and 7.8b, respectively. The results show that the peak intensity occurred at a wavelength of approximately 1551.7nm for both FBGs. This verifies that the peak intensity occurs at a wavelength that is directly between the two Bragg wavelengths and is at a maximum when both Bragg wavelengths are the same. Hence, the maximum intensity is recorded when the transducer is loaded with approximately 3kg, such that both spectra overlap completely. Both intensity spectra firstly increase in width and height as load is applied, before reducing in width and height, until no reflected intensity is recorded. The results demonstrate that the Bragg wavelength shift of both FBGs, caused by changing the load of the transducer, can be transposed into an intensity change localised around a single wavelength.

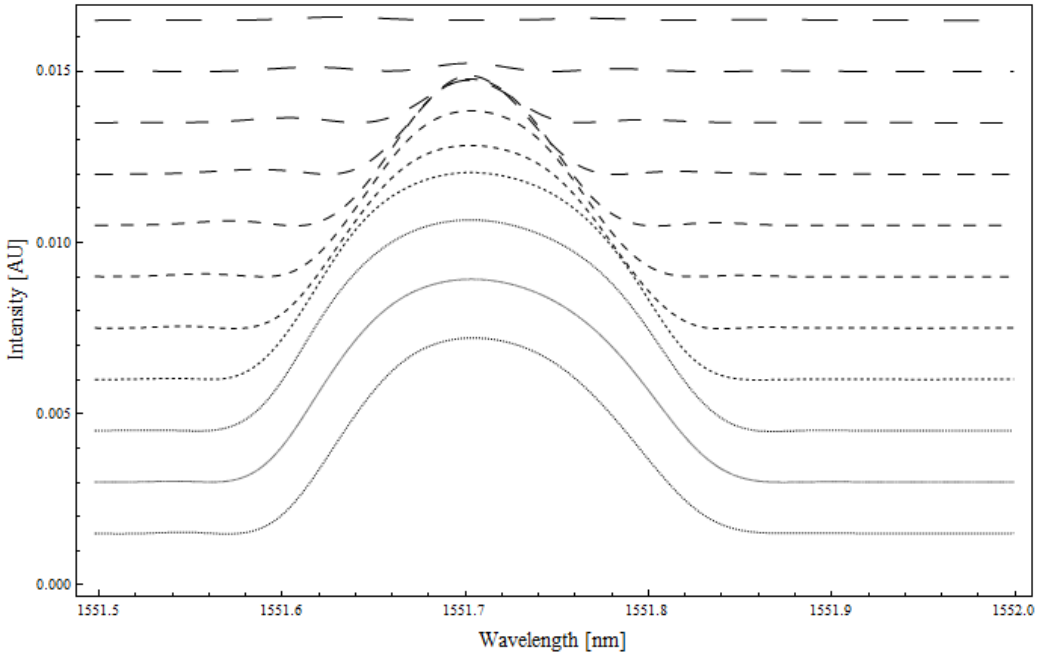

(a) Loading.

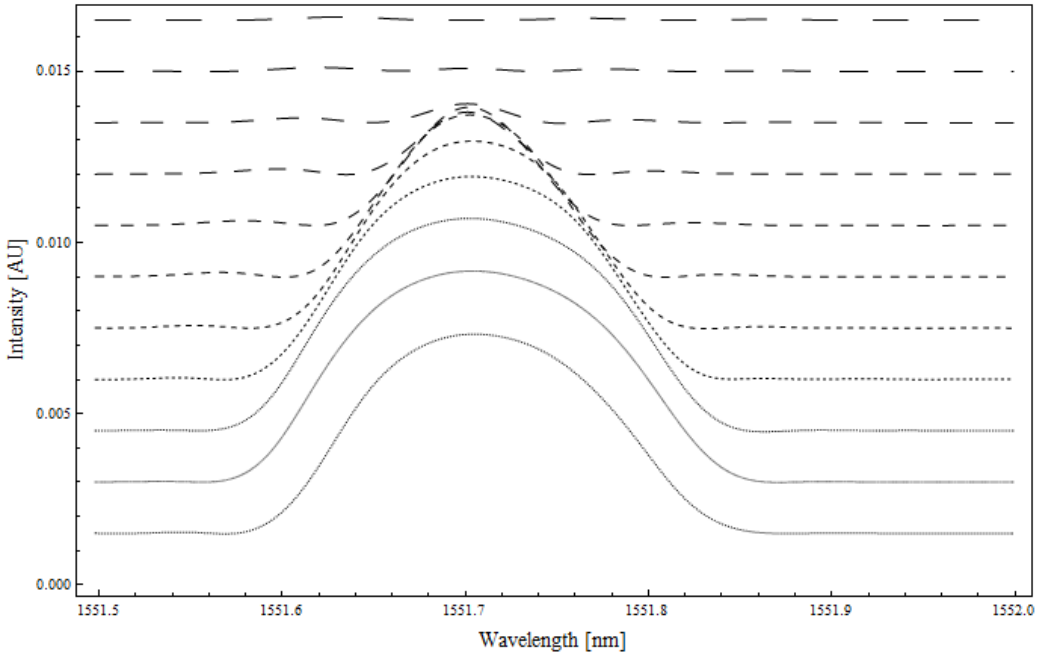

(b) Unloading.

Figure 7.8: Output optical intensity spectra as a function of load.

7.5 Output Voltage

The output voltage from the load cell transducer as a function of loading and unloading is shown in figure 7.9. The results show that the output voltage from the load cell transducer is approximately linear for a load from 4 to 8kg, for both loading and unloading. The error in the recorded voltage was again small ($\pm 0.005V$). Obviously the hysteresis recorded earlier carried through to the voltage measurements, with the maximum difference being approximately 0.5V. This relates to error in the load of up to 0.7kg. Using a $149.5k\Omega$ resistor produced a linear response from 0.5 to 4V across the 4kg range.

This output range would be ideal for connection to a standard industrial controller or microcontroller. In order for a commercially viable load cell to be produced that did not require any pre-loading, the two FBGs would be manufactured such that the bottom FBG had a Bragg wavelength approximately 50pm greater than the top FBG. The dynamic range and sensitivity of the transducer could be changed by changing the dimensions and material of the bending structure. The hysteresis may also be reduced by using different materials and dimensions. Furthermore, this technique eliminates problems associated with the temperature sensitivity of FBGs as the output voltage corresponds to the correlation between the reflection spectra of both FBGs. As the FBGs are co-located, any temperature fluctuations would cause both spectra to shift in the same direction and not alter the output voltage with respect to load. This is far simpler than the load cell temperature compensation technique proposed by Matsumura et al. [272], which required applying a negative strain to the FBG through thermal expansion of the load cell material.

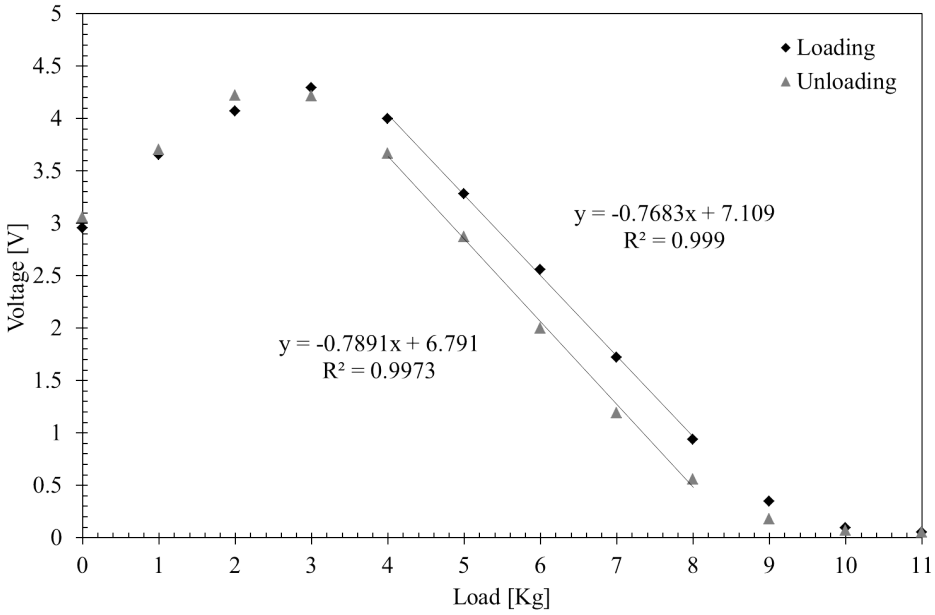

Figure 7.9: Output voltage from the transducer as a function of load whilst loading and unloading.

7.6 Chapter Conclusion

In this chapter, a temperature insensitive FBG load cell with on-board intensity based interrogation is reported. The load cell is based on a three point bending system with a FBG bonded to the top and the bottom of the steel structure. The reflected spectra from each of the FBGs were recorded as the load cell structure was loaded uniformly with masses from 0 to 14Kg. Using a four port circulator and the concept of a linear edge filter detection, the signal was reflected off both FBGs to give a relative intensity change as a function of applied weight. The results show that the output intensity is both linear and repeatable, with respect to the applied weight across a load from 4-8kg, although there is some evidence of hysteresis. Using a photodetector and a load resistor, a linear output voltage was attained from approximately 0.5 to 4V. The transducer was specifically designed so the output could be connected directly to a standard industrial controller or a microcontroller.

Chapter 8

Large Deformation of a Fibre Bragg Grating: Non-Linear Characteristics of the Reflected Spectra

In this chapter, the non-linear characteristics of the reflected spectra from a FBG under excessive stress were analyzed in detail. Firstly, the effect of lateral loading on a FBG with respect to longitudinal loading was examined. Lateral loading uniquely causes the deformation of the reflected Gaussian waveform, resulting in splitting of the primary peak [273]. The results show that the magnitude of the lateral load is related to the separation distance of the additional peaks. Both longitudinal loading and a change in temperature cause the Bragg wavelength to shift with no change in the spectral shape of the reflected spectrum, whereas lateral loading clearly distorts the reflected spectrum. Hence, the potential to produce a pressure, strain or load sensor, due to lateral deformation, that is inherently temperature insensitive, is proposed. Secondly, the FBG was bonded to a rubber diaphragm and stressed outside the anticipated normal operating range of the sensor, resulting in the formation of additional peaks. The results show that as the pressure is increased, more peaks form with increasing intensity. The relationship between the magnitude and separation of the additional peaks is discussed, as well as the change in shape of the primary peak with respect to pressure.

In this work, deformation of the reflected spectra is created through non-destructive methods, meaning the original waveform is obtained when the FBG is no longer subject

to stress. This is achieved through lateral loading of the FBG, using relatively large masses, and by inducing excessive strain on the FBG, using a rubber diaphragm pressure transducer.

8.1 Longitudinal Strain of a Fibre Bragg Grating

The experimental setup for the lateral and longitudinal loading of a FBG is shown in figure 8.1. Initially the FBG was loaded so as to cause a longitudinal strain (in the z-direction along the FBG). The FBG was secured to the optical bench on one side using some small pieces of tape. The other end of the fibre was fed over a pulley and increasing masses were attached to it. The Bragg wavelength was recorded as a function of load from 0 to 0.4kg in increments of 0.05kg. The load was then removed.

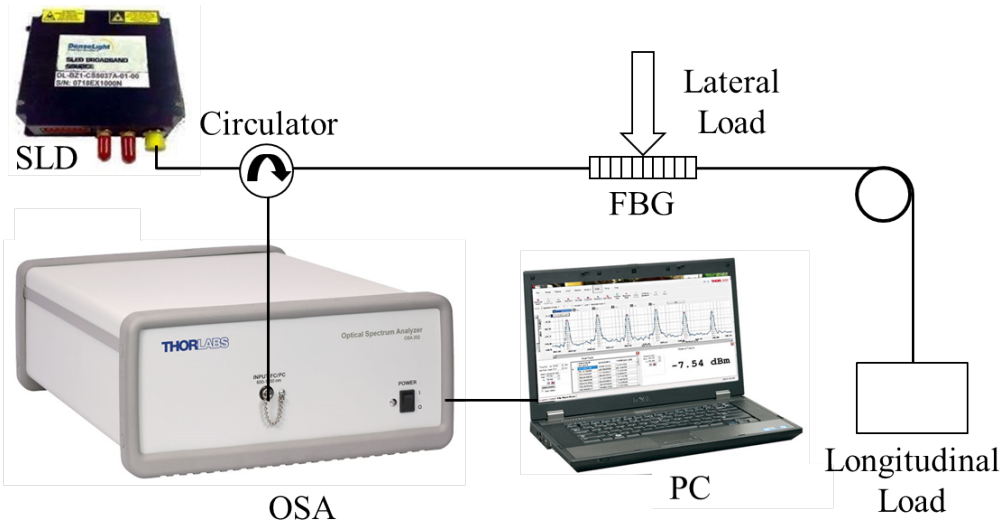

Figure 8.1: The experimental setup for lateral and longitudinal loading of a FBG.

Figure 8.2 shows the reflected spectra of the FBG under longitudinal stain. A constant intensity offset has been applied for easier viewing and increasing dash spacing corresponds to an additional load of 0.05kg. The results do not display any obvious variation in the spectral shape of the reflected spectra as the load is increased.

Figure 8.3 displays the Bragg wavelength shift and variation in optical power of

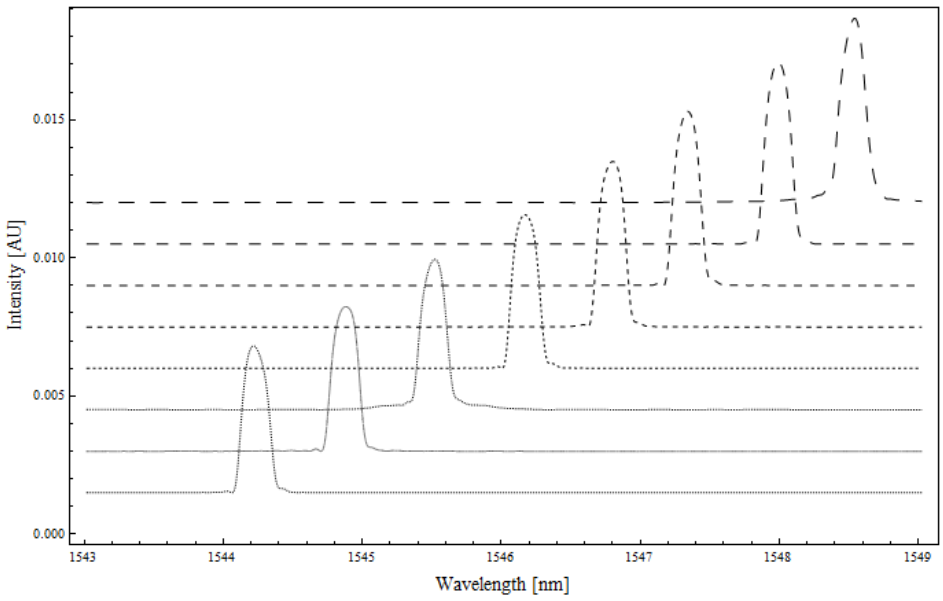

Figure 8.2: Reflected spectra of FBG under longitudinal loading, with constant intensity offset for easier viewing. The increasing dash spacing corresponds to an additional load of 0.05kg.

the reflected spectra under longitudinal loading. As expected, the Bragg wavelength increases linearly with increasing load, resulting in a Bragg wavelength shift of 12.44nm/kg. Based on the standard strain value of 1.2pm/$\mu\epsilon$ for a FBG, this shift corresponds to approximately 10000$\mu\epsilon$/kg or 10$\mu\epsilon$/g.

The results demonstrate that the Bragg wavelength of the FBG can be easily tuned over at least 5nm through longitudinal strain. It would have been interesting to determine the maximum load/strain the fibre and FBG could withstand before the fibre broke; however, in the interest of maintaining the FBG, this was not performed.

There is a small fluctuation in peak optical power which may be attributed to optical power fluctuations from the source, as there is no clear indication that there is a relationship between the peak optical power and the strain induced wavelength shift. The errors associated with the applied masses were relatively small, ($\pm 0.01kg$). The error in the recorded wavelength and peak optical power were also extremely small; $\pm 3.1pm$ at 1550nm and $\pm 1dB$, respectively, as the OSA is a high precision instrument

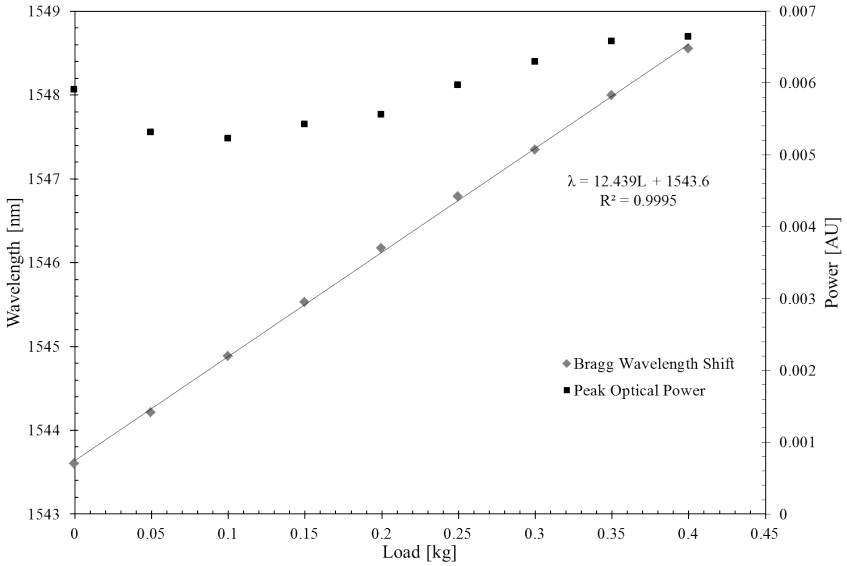

Figure 8.3: Bragg wavelength shift and change in optical power of FBG under longitudinal loading.

8.2 Lateral Loading of a Fibre Bragg Grating

The FBG was then placed on the bench with a support fibre placed parallel to it as proposed in [273]. A small sheet of steel weighing 0.086kg was then placed across the two fibres as a support for the additional load. The system was then loaded from 0 to 4kg in increments of 0.25kg, so as to laterally load the FBG with half of the applied load, as shown in figure 8.4.

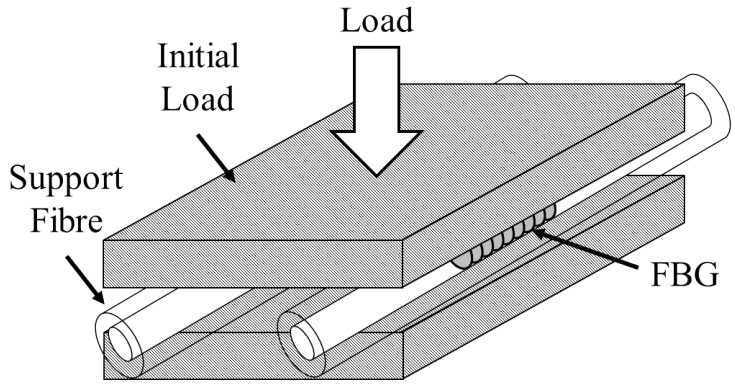

Figure 8.4: The experimental setup for lateral loading of a FBG.

Figure 8.5 shows the reflected spectra of the FBG as a function of applied lateral load. Half of the waveforms have been omitted in figure 8.5a and a constant intensity offset has been applied in figure 8.5b, for easier viewing.

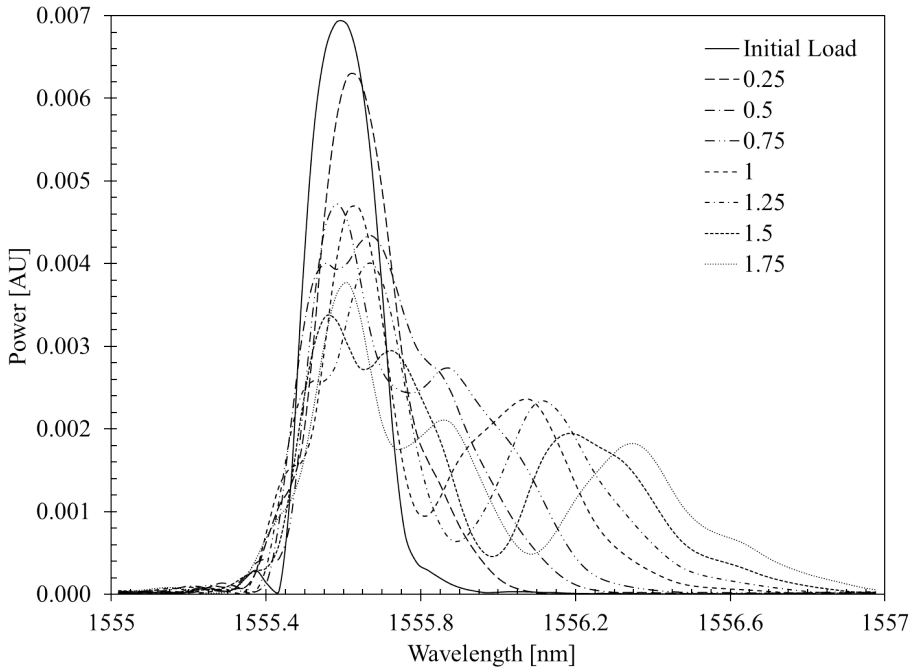

(a) Reflected spectra.

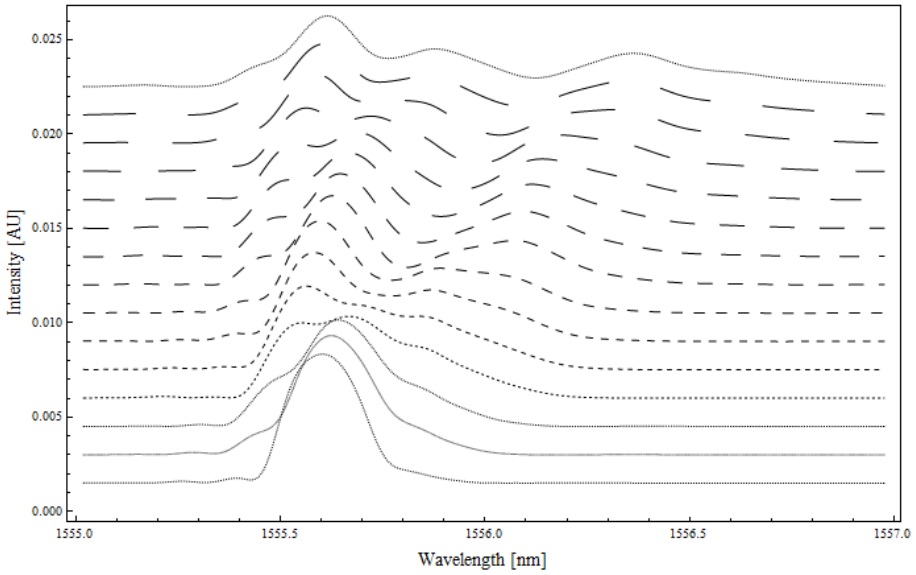

(b) The reflected spectra with constant intensity offset for easier viewing.

Figure 8.5: Spectral response of the FBG under lateral loading.

With an additional load of 0.5kg, the results show the reflected spectrum starts to broaden and deform. After 1.0kg is applied, the waveform is split in two and a secondary peak is clearly visible. However, unlike the results obtained in [273] the results do not exhibit an equal splitting of the FBG peak. This may be due to non-uniform loading caused by the fibres slipping. After 1.5kg is applied, a tertiary peak starts to form. With 1.75kg applied, three peaks are clearly visible. These results appear to strongly agree with those reported by Urna et al. [274], as shown in figure 8.6.

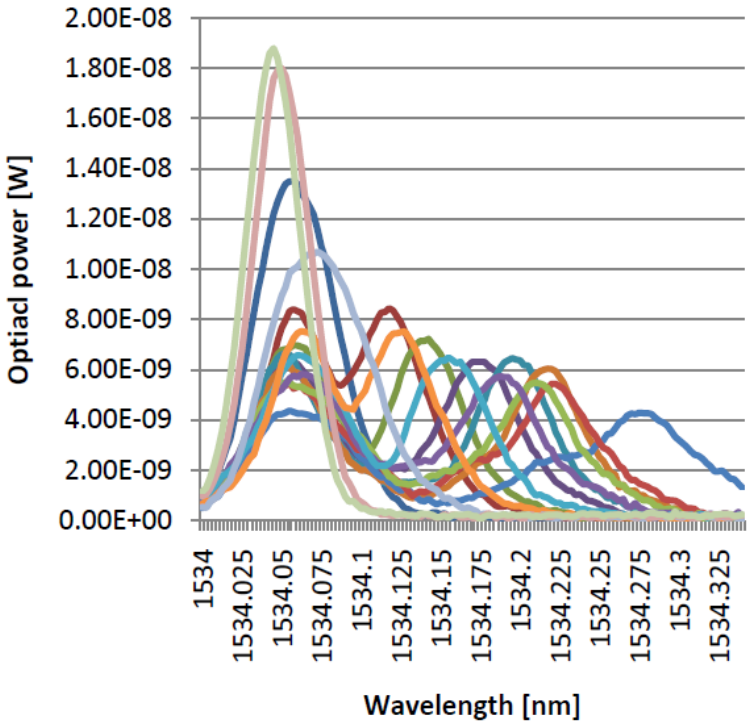

Figure 8.6: Reflected spectra of FBG under lateral loading reported by [274].

However, in their report they state that the increase in lateral deformation only produces a secondary peak, where the distance between the primary and secondary peak correlates to the amount of lateral deformation due to applied pressure. It can be argued that in fact the spectral characteristics of the FBG under large deformation are more complex than previously proposed. The results obtained in [274] appear to show the beginning of the formation of a third peak, agreeing with the results obtained

in this study. Furthermore, the variation in peak optical power of each of the spectral peaks, which is not discussed in [274], approximately agree. This suggests that the change in peak optical power could be an alternative method of interrogating the lateral deformation of the FBG.

8.3 Large Deformation of a Fibre Bragg Grating based Rubber Diaphragm Transducer

Finally, a different FBG bonded to a rubber diagram, which is described in detail in Chapter 6, was stressed outside it's anticipated operating range. Excessive positive and negative pressure was applied to the rubber diaphragm so as to deform the FBG. Pressure from negative 12kPa through to positive 27kPa, relative to atmospheric pressure, was applied and the reflected spectra were recorded.

The reflected spectra for the pressure sensor are shown in figure 8.7. The results show that the peak amplitude of the primary peak increases, then decreases, in parabolic way as the pressure changes. As the pressure is increased, a single-sided side lobe begins to increase in amplitude until additional peaks form. The number of peaks, with increasing amplitude, increase as the pressure increases. As negative pressure is applied relative to atmospheric pressure, so as to bend the diaphragm in the opposite direction, a single sided side lobe on the opposite side begins to increase in amplitude. Again additional peaks begin to form as the negative pressure is increased. It is suggested in [275] that the formation of a single-sided side lobe is due to non-uniform deformation across the FBG. This could be the case as the FBG was not bonded exactly to the centre of the diaphragm. A detailed analysis of the relationship for each of the peaks as a function of applied pressure is given in figures 8.8 - 8.10.

Figure 8.8 shows the Bragg wavelength shift of all of the peaks across the entire pressure range. Although the Bragg wavelength shift of the primary peak can be linearly approximated within the normal operating range of the sensor, it is clear that

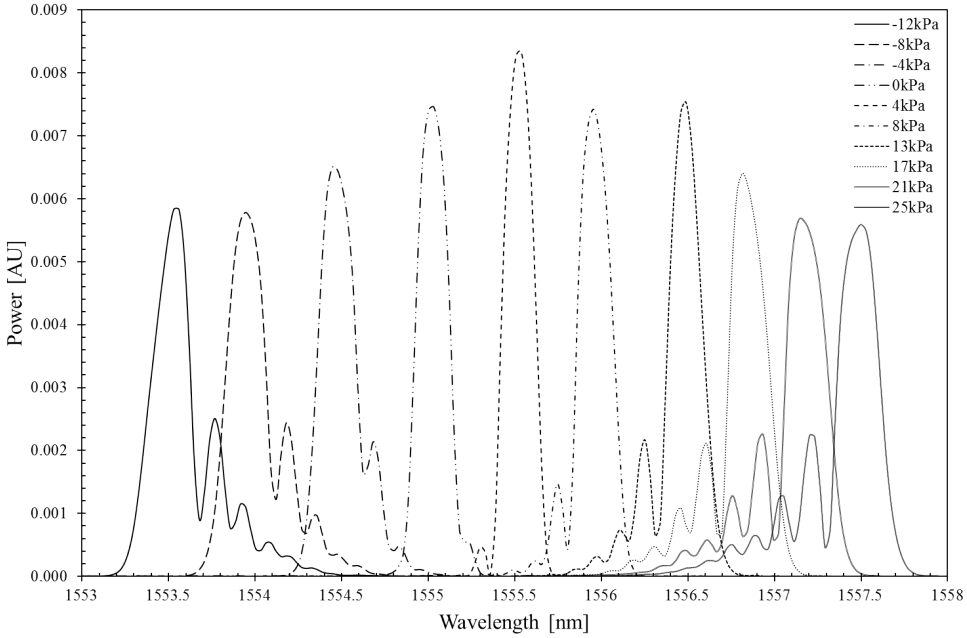

Figure 8.7: Reflected spectra for the pressure sensor under excessive pressure.

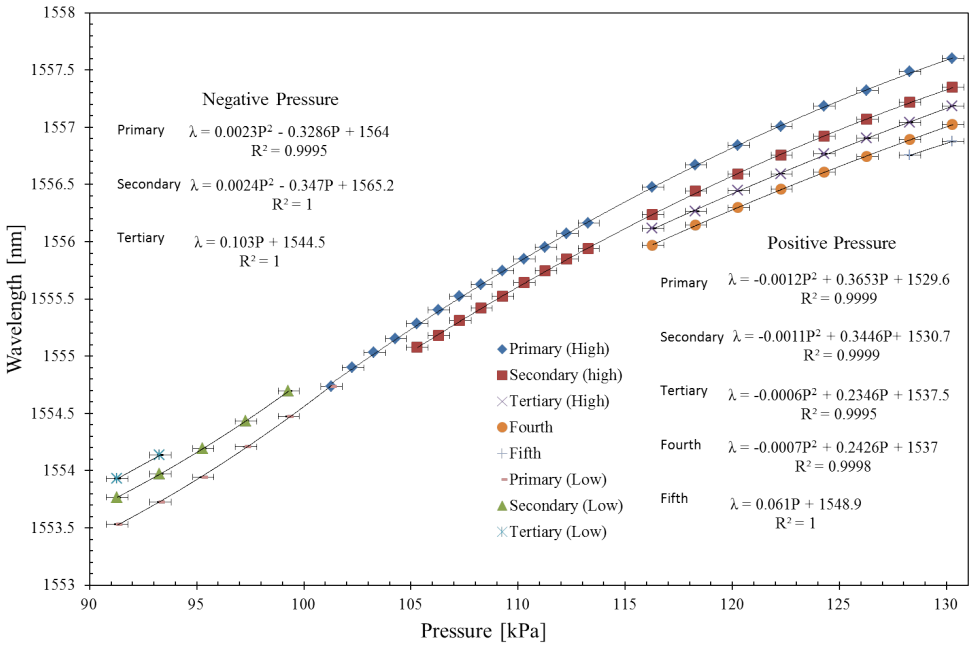

Figure 8.8: Bragg wavelength shift against pressure for all peaks.

it actually has a polynomial response to pressure over a larger range. Likewise, the Bragg wavelength shift of the addition peaks could be approximated as linear although polynomial curves fit the data much better.

Figure 8.9 shows the wavelength difference between the consecutive peaks. Although the data are quite sporatic, linear approximations have been made. The results suggest that the difference between individual peaks increases with pressure, represented positive linear approximations. Although the magnitude of the difference between the successive peaks decreases, i.e. the difference between the primary and secondary peak varies from approximately 0.2nm to 0.25nm whereas the difference between the secondary and tertiary peak varies from 0.12nm to 0.18nm.

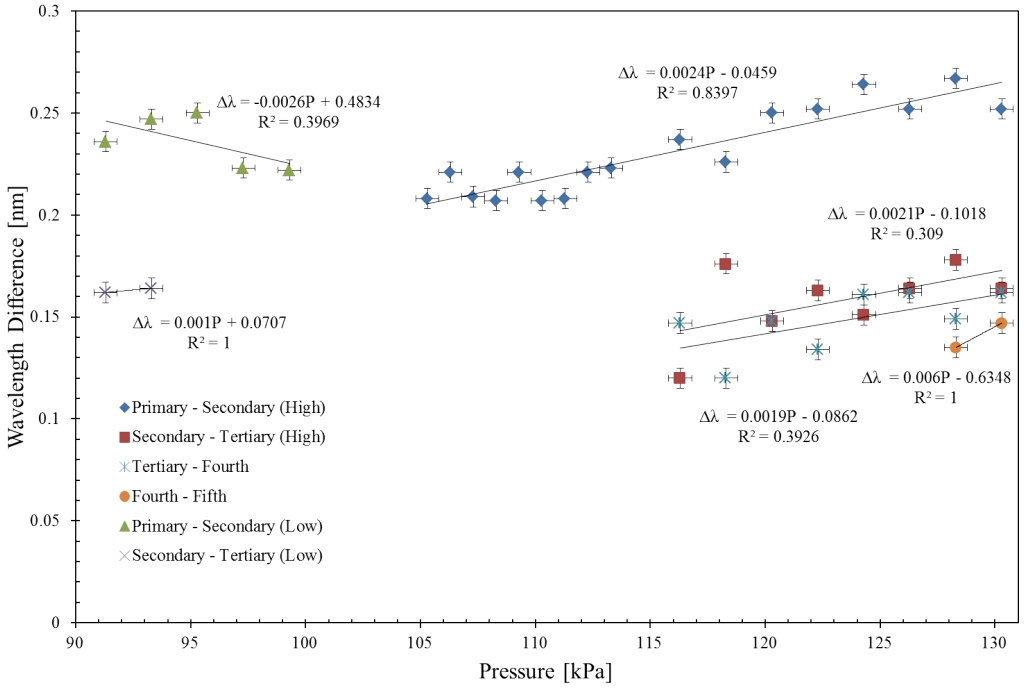

Figure 8.9: Wavelength difference between the consecutive peaks as function of applied pressure.

The variation in peak optical power of all of the peaks in shown in figure 8.10. The results show that as more pressure in applied, both positive and negative relative to atmospheric pressure, the amplitude of the primary peak decreases. Conversely, the

peak optical power of the additional peaks increases with pressure, although this is a non-linear increase. The decrease in the peak intensity of the primary peak is expected as more of the available intensity is spread across the additional peaks, thus it is a form of peak splitting, similar to the results shown in figure 2.11. The errors in the recorded pressures ($\pm 0.5kPa$) in each of the three graphs are due to the low resolution of the pressure sensors.

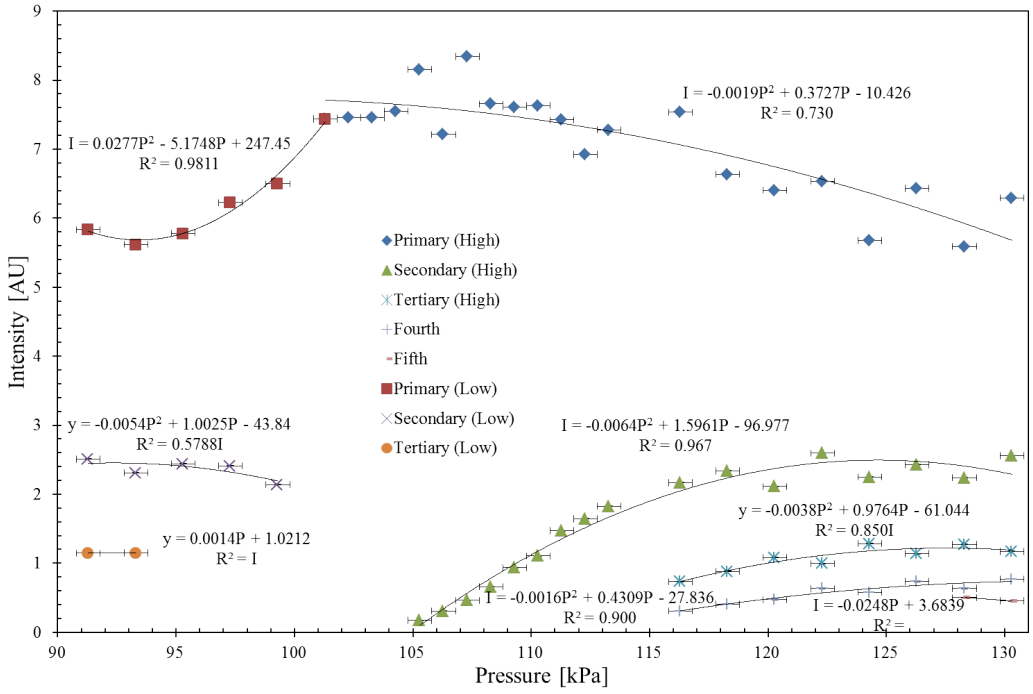

Figure 8.10: Variation in peak optical power as a function of excessive pressure.

8.4 General Discussion

The results in this chapter suggest there may be opportunity to produce pressure transducers that are inherently isolated from temperature and longitudinal strain through examination of their non-linear reflected spectra. This could be achieved by physically observing the changes using an OSA, or by monitoring the differences in the additional peaks using photodetectors and WDM techniques. Furthermore, the transducers may

not need post processing to achieve the complex changes in the reflected spectra, which can be returned to normal through removal of the strain.

8.5 Chapter Conclusion

In this chapter, large deformation of a FBG has been demonstrated. This has been achieved in two ways; firstly, through lateral loading, and secondly through excess pressure applied to a FBG rubber diaphragm transducer. In each case the deformation of the FBG causes significant changes in the shape of the reflected spectra. These changes could by exploited to enable complex sensors to be produced that are inherently insensitive to changes in temperature. Moreover, these techniques offer a non-destructive method of manipulating the reflected spectra, where the original waveform can be obtained through removal of the strain.

Chapter 9 has been excluded from this version of the thesis at the request of the author.

Chapter 10

Universal Signal Conditioning Technique for Optical Fibre Sensors in PLC and SCADA Applications

In this chapter, the output from an arbitrary FBG based optical switch has been directly connected to a standard digital input on a PLC using a TRDS and some simple additional circuitry. The switch was used to drive a digital output, sound an alarm and display the intrusion event on the HMI. In addition, a FBG was used to detect a variation in temperature, causing a change in the Bragg wavelength. A TRDS was used to convert the optical signal into a voltage. The voltage was then converted into a 4-20mA industry standard which was received as an analogue input to a PLC. The true temperature value was then displayed on a HMI to be observed by an operator. The PLC was programmed to display an alarm on the HMI when the temperature exceeds a pre-determined value. This technique enables FOS to become a low cost plug and play option for industrial automation controllers.

10.1 PLC FOS Digital Input Interface

Here, a PLC FOS digital input interface is demonstrated. An in-ground FBG pressure switch, discussed in Chapter 5, was used as an arbitrary digital input signal for a PLC (Siemens S7-300). A bench-top tunable laser (Anritsu MG9637A) was connected to

the FBG (Micron Optics OS1100) via an optical circulator (FDK YC-1100-155). The reflected signal was directed down to the first photoreceiver (Fujitsu FRM3Z231KT) via the optical circulator, and the transmitted signal passed through the FBG and was directed to the second receiver (Fujitsu FRM3Z231KT). The output of the two receivers was differentially amplified using a high speed differential amplifier (AD830ANZ).

A simple comparator circuit was then used to ensure the differentially amplified output voltage would be correctly interpreted by the PLC. The output from the comparator was then connected to a 2 channel digital input module on the I/O rack (Siemens ET200S). The digital input card detects a 1 when the input voltage is above 15V and it detects a 0 when the input voltage is below 5V. The transimpedance amplifier supply and the PIN bias for the two receivers was provided by a $\pm 5V$ DC power supply. The 24V for the comparator circuit would be supplied by the PLC. The PLC FOS digital input interface circuit diagram is shown in figure 10.1.

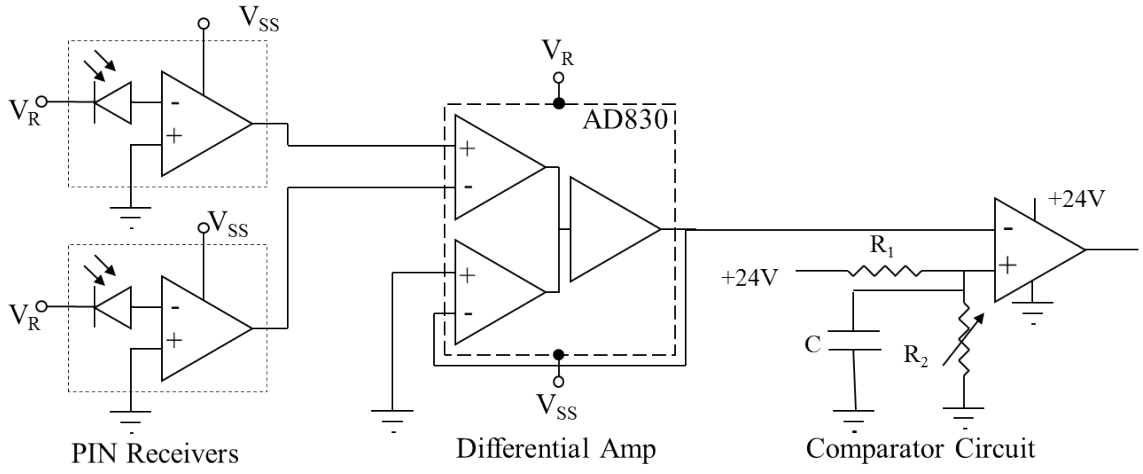

Figure 10.1: Schematic of the PLC FOS digital input interface, including receivers, differential amplifier, and comparator circuit.

The in-ground pressure switch provided the digital signal for the PLC FOS digital input interface, which was connected to the digital input channel on the Siemens S7-300 PLC I/O rack. The experimental setup is shown in figure 10.2.

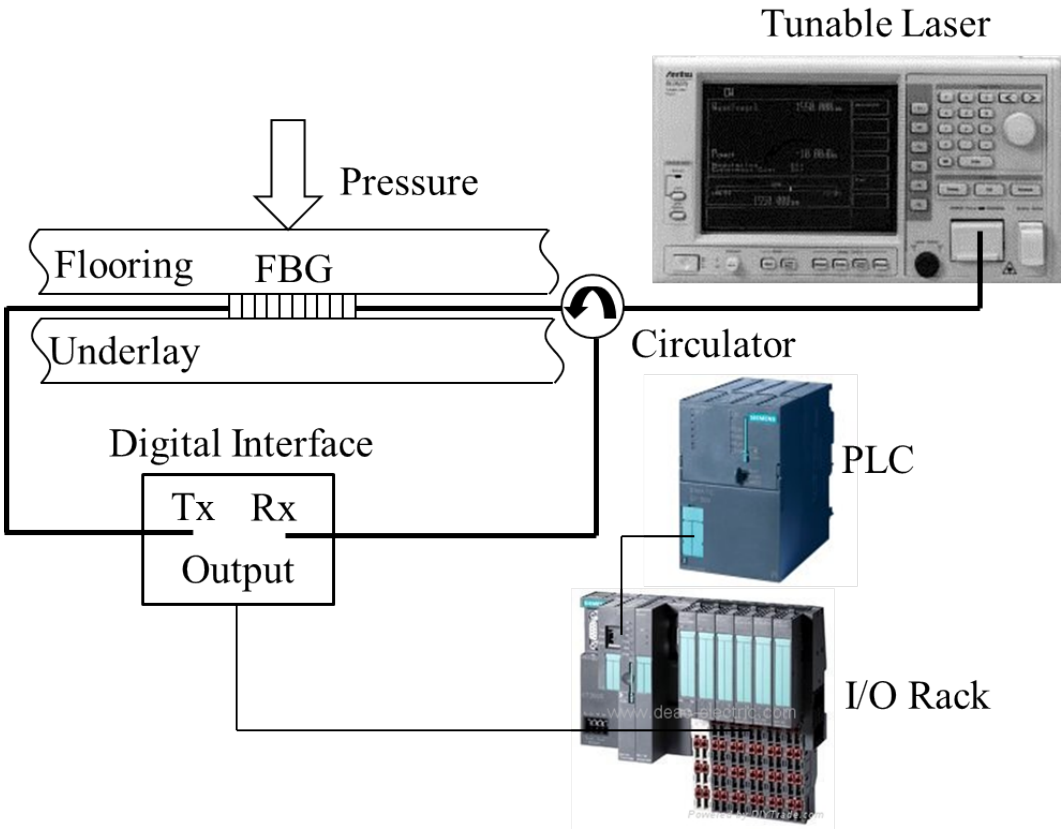

Figure 10.2: Experimental setup for the digital input interface connected to the PLC I/O rack.

The PLC was programmed with a few simple lines of ladder logic to activate a digital output and trigger an alarm in the form of a buzzer. The ladder logic is shown in figure 10.3.

A simple PIDS HMI created using WinCC Flexible software [278] was designed to display the alarm event. Figure 10.4 shows the HMI display when the perimeter is secure and when a security breach has occurred.

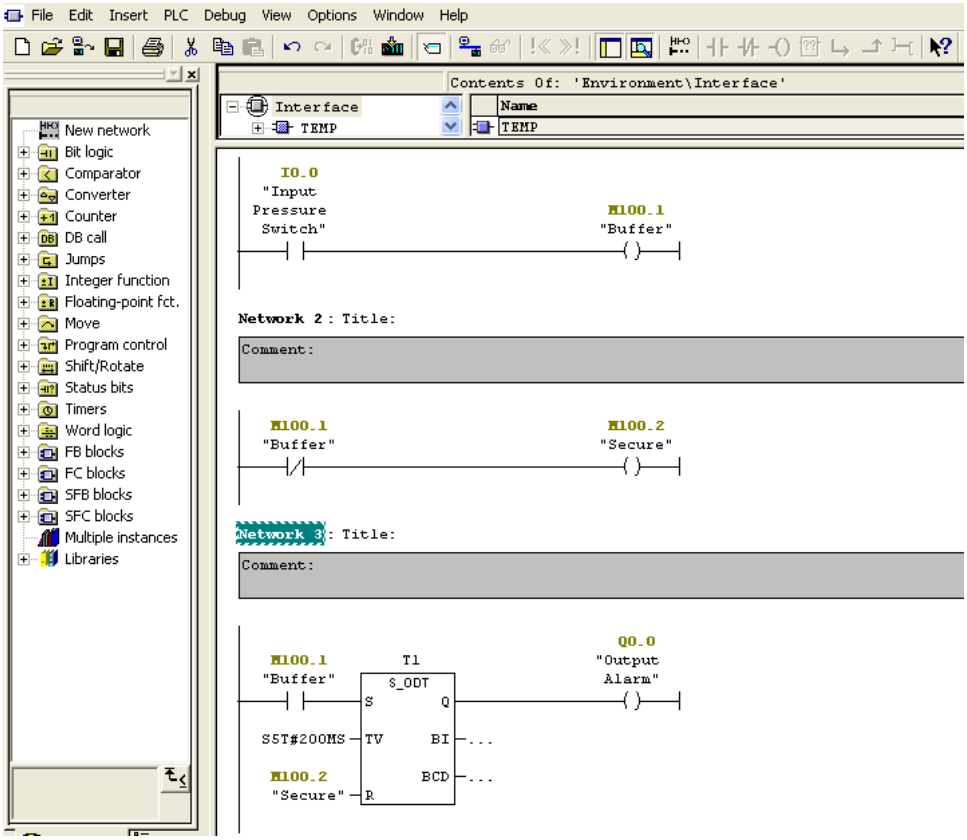

Figure 10.3: Simple ladder logic for turning on an alarm siren when a security breach is detected in the form of an optical fibre in-ground pressure switch.

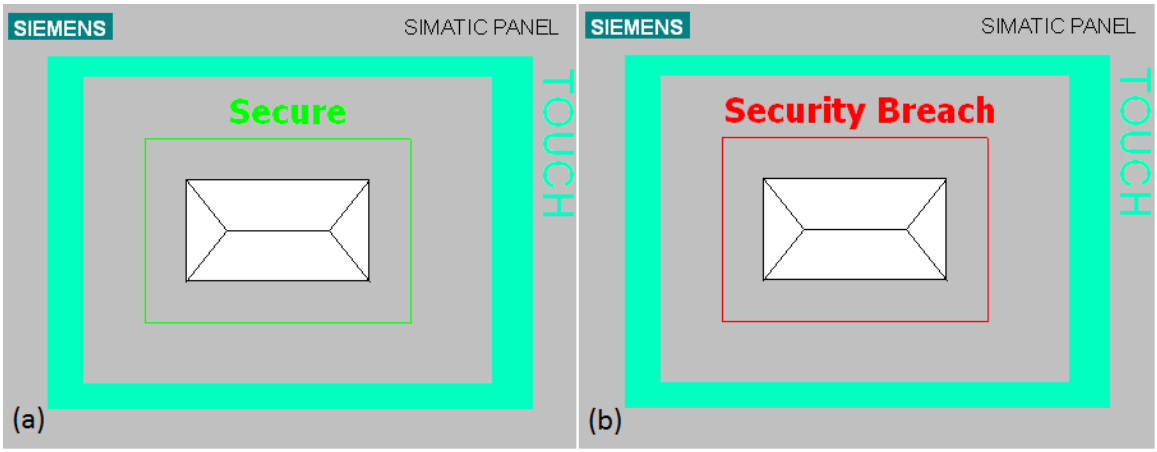

Figure 10.4: A simple HMI display for (a) a secure perimeter and (b) a security breach.

10.2 PLC FOS Analogue Input Interface

Here, a PLC FOS analog input interface is demonstrated. The experimental setup was similar to the previous setup, except a bench-top tunable laser module (Ando AQ 8201-13B) was used instead of the Anritsu MG9637A tunable laser. Again, the output of the two receivers was differentially amplified using a high speed differential amplifier (AD830ANZ). However, an additional 3V DC offset was supplied to the second summing input of the difference amplifier via a voltage divider from the +5V. The DC offset was used due to the requirements of the transconductance amplifier. The transconductance amplifier converts a voltage range of 1 to 5V into 4 to 20mA, as required by the PLC. This requires a bias resistance of 250Ω, giving 4mA at 1V, and 20mA at 5V and therefore a midpoint of 3V. The transimpedance amplifier (current-to-voltage converter) supply, PIN bias for the two receivers, and the supply for the transconductance amplifier (voltage-to-current converter) was provided by a $\pm 5V$ DC power supply. Figure 10.5 shows the circuit diagram of the PLC FOS analogue input interface.

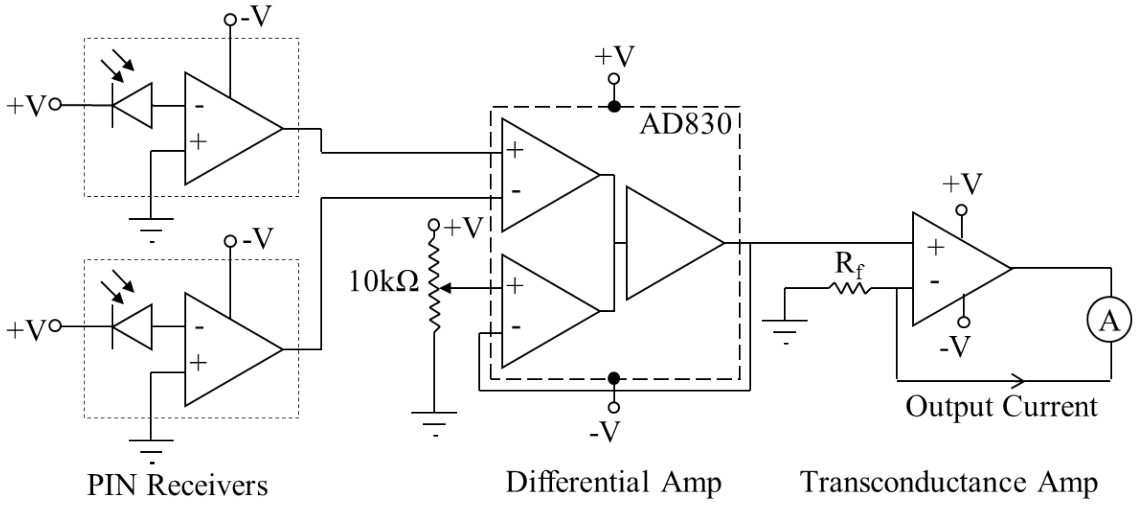

Figure 10.5: Schematic of the PLC FOS analogue input interface, including receivers, differential amplifier, and transconductance amplifier.

Initially, the spectral characteristics of the FBG needed to be measured, and the

tunable laser needed to be set to the correct wavelength, in order to determine the operating point for the FBG sensor. This was achieved in the same way as detailed in figure 4.1. The laser was initially tuned to the minimum reflectivity above the Bragg wavelength to ensure that all the optical power was transmitted through the FBG.

Prior to utilizing the optical input with the two transimpedance amplifiers, two function generators (Agilent 33250A) were used, each set to give a negative voltage, similar to those expected from the transimpedance amplifiers. Initial tests showed the voltage of each receiver varied from -1 to -2V, for zero to maximum optical power (8mW) of the tunable laser. The output of the difference amplifier was then between -1V to 1V, and with the 3V offset it then gave an expected 2V to 4V output voltage to the transconductance amplifier, which corresponded to an expected output current of 8 to 16mA. To test the entire range of the system, the function generator output voltages were varied between -2.5V and 0.5V, to give an output current of 4mA to 20mA, measured using a Digital Multimeter (DMM) (Goldstar DM-331). Figure 10.6 shows the experimental setup used to characterise the transconductance amplifier circuit.

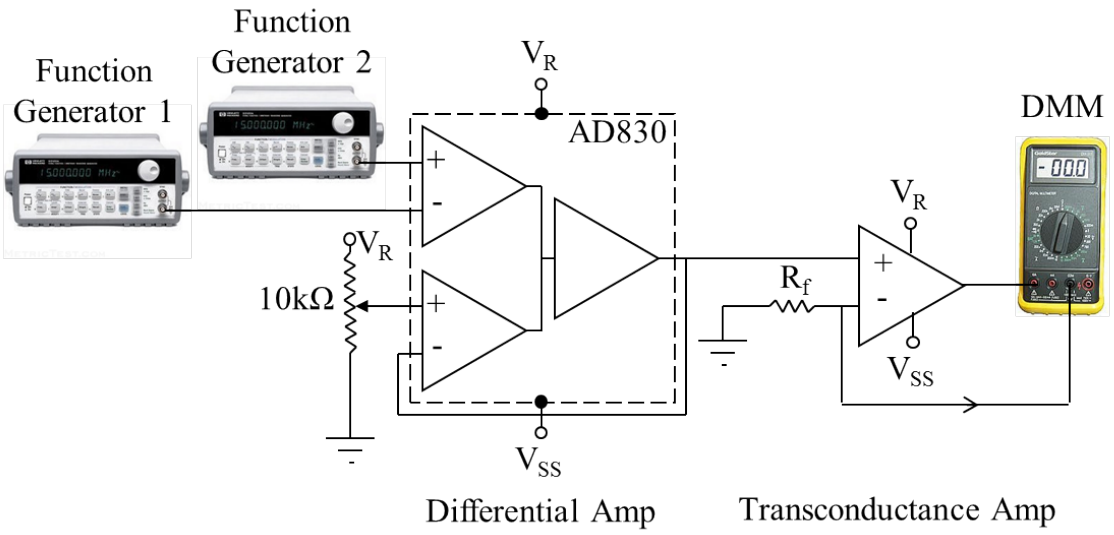

Figure 10.6: Experimental setup to characterise the performance of the transconductance amplifier circuit.

Figure 10.7 shows the transfer function of the transconductance amplifier. As shown, the transfer function is extremely linear, where the gradient is (3.89±0.11)mA/V and the intercept is (12.2 ± 0.5)mA. There is a small discrepancy in the equation coefficient and offset, as we would expect the values for the gradient and intercept to be exactly 4mA/V and 12mA, respectively. The reason for this small inconsistency is most likely due to uncertainties in the voltage offset value, (2.99 ± 0.02)V, and the feedback resistance, R_f $(250 \pm 5)\Omega$, used in the transconductance amplifier circuit. Moreover, there is a small uncertainty in the precision of the DMM, $\pm(1.5\% + 0.02)$mA and $\pm(0.5\% + 0.001)$V, when measuring the current and voltage, respectively.

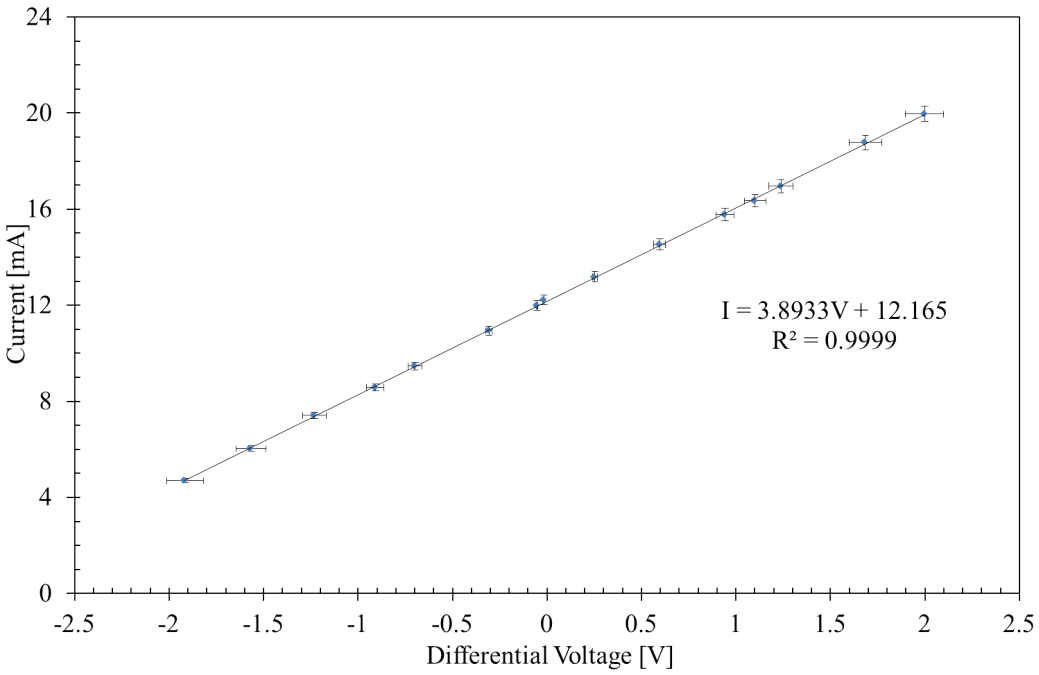

Figure 10.7: The transfer function of the transconductance amplifier, showing the output current as a function of the measured input voltage difference.

For the test experiment to monitor temperature, the FBG and a thermometer were placed in a large beaker of water. The FBG was then connected to the optical circuit as before and the water was then slowly heated using a hotplate (Industrial Equipment and Control PTY CH2093). The transmitted and reflected signals were connected to the

optoelectronic PLC interface and the output current was monitored on a DMM (Escort EDM168A) as a function of the temperature, before being connected to an analogue input channel on the Siemens S7-300 PLC I/O rack. The setup for the temperature measurement is show in Figure 10.8.

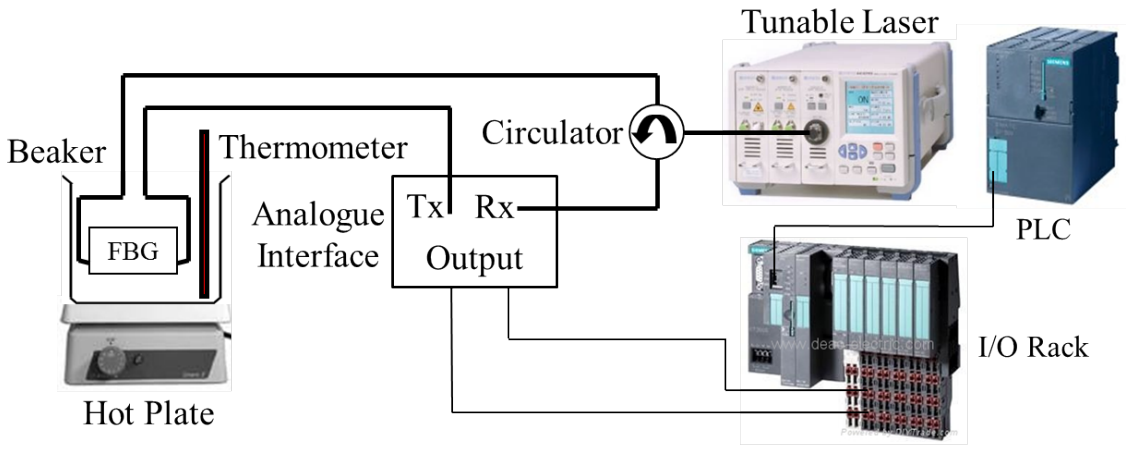

Figure 10.8: Setup for the temperature characterisation experiment.

Figure 10.9 shows the output current from the complete circuit (Fig. 10.5) as a function of the applied temperature to the FBG sensor. The curve is a sigmoid, or half a Gaussian, as we would expect. This is because both the laser and FBG spectra are Gaussian in shape, and when multiplied together, the result is a Gaussian. The amplitude of this Gaussian increases from minimum to maximum. The optical power of the laser was such that the value of the voltage varied from -1.2V to 0.2V, corresponding to a change in current of approximately 6mA, from 6.97mA to 12.81mA. The asymmetry was due to the use of a temporary bare-fibre-connector, adding more loss in the reflected path compared to the transmitted path. With the use of connectorised components, this would no longer be an issue. The straight line between 8.02mA and 12.01mA, where the gradient is $(0.51 \pm 0.01) mA/V$ and the intercept is (3.24 ± 0.95)mA, shows the region where the output current is linear with respect to temperature. Hence, in practice, this particular setup could be used as a temperature sensor with a range from approximately 22-30^{o}C with high precision.

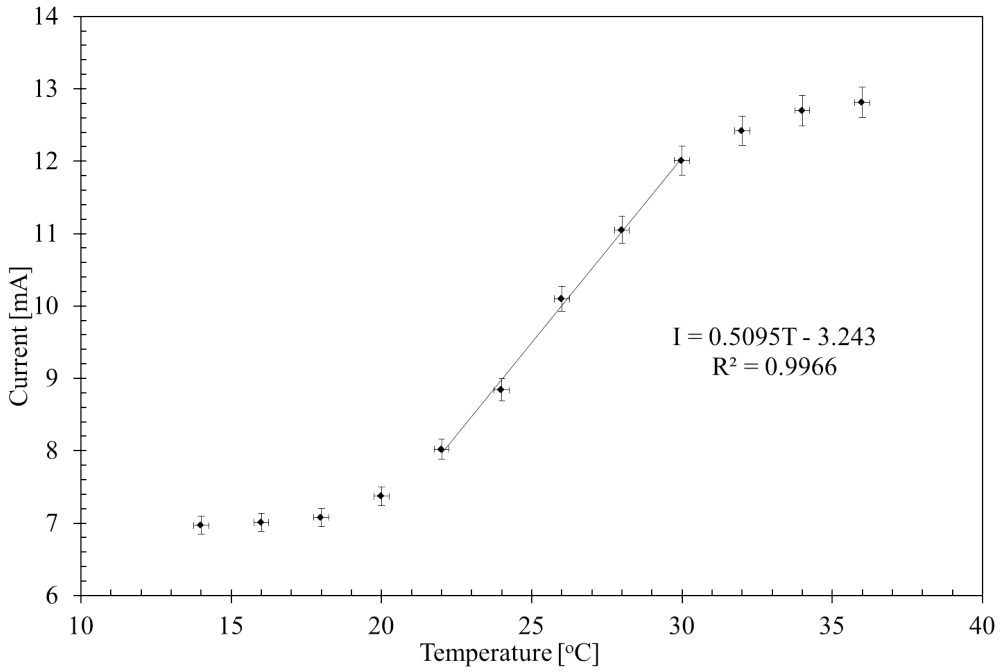

Figure 10.9: Output current as a function of temperature.

The PLC was again programmed in ladder logic and a graphical representation of the input current to the PLC and the output temperature was created using WinCC Flexible software [278]. The direct readout from the analogue input module is converted into 4-20mA, which is then converted into the actual temperature range, in the PLC logic. To achieve the conversion from current to temperature, the data from figure 10.9 in the linear region were plotted with temperature as a function of current. The transfer function, $T(I)$, then became,

$$T = 2.092I + 5.02, \tag{10.1}$$

where I is the current in mA and T is the temperature in ^{o}C. However, because the PLC can be programmed to perform complex operations, all of the data could be converted from current to temperature. Hence, the transfer function was estimated from a multiple regression fit, by selecting a third order polynomial ($R^2 = 0.9855$),

$$T = 0.298I^3 - 8.885I^2 + 89.093I - 274.5. \tag{10.2}$$

This was then used in the PLC software (Sematic Step7) to compute the temperature

across the full dynamic range of the sensor from 14-36°C. Both the current and the temperature were displayed in real-time on bar graphs on the HMI, shown in figure 10.10. Figure 10.10a shows an image of the HMI with the temperature in the normal operating range. Additionally, an alarm was programmed to be displayed when the temperature exceeded 30 degrees Celsius. This event is shown in figure 10.10b.

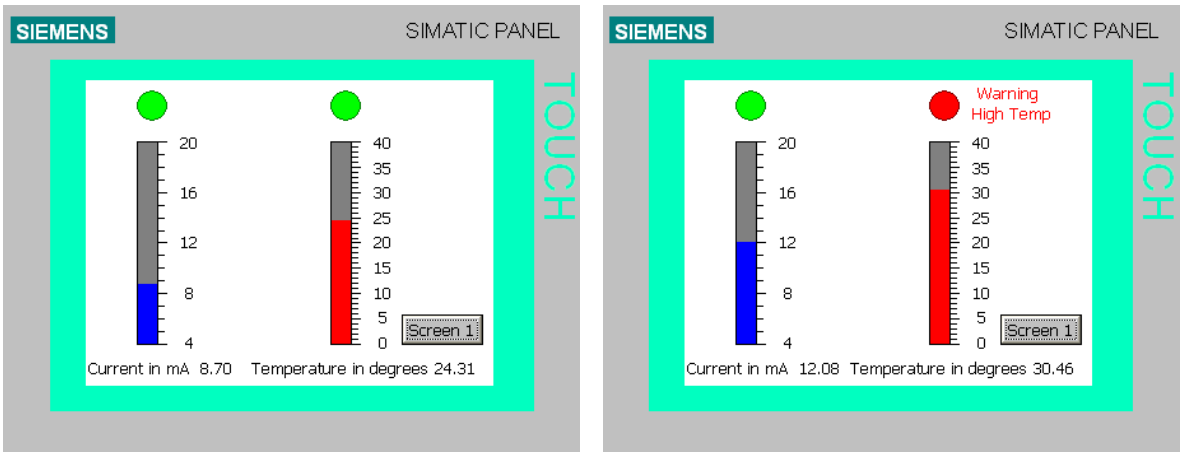

(a) Temperature below 30 degrees Celsius.

(b) Temperature above 30 degrees Celsius with the high temperature alarm active

Figure 10.10: Image of HMI panel created in WinCC Flexible.

10.3 General Discussion

10.3.1 Findings

This technique demonstrates that both a digital and an analogue signal from electrically passive FOSs, with the aid of a simple electronic circuit, can be easily connected to a digital and analog input card, respectively, on a standard industrial controller. In a commercial system, all of the electronics and electrical components could be embedded in a small optoelectronic box. Moreover, to take advantage of the benefits of FOS, and to reduce the cost of the system, many digital and analogue sensors would be multiplexed together utilising a single optoelectronic unit.

The circuitry required to make a FBG compatible with a PLC system proved to be simple and easy to implement. The final circuit designs (figures 10.1 and 10.5), which made use of 6 operational amplifiers each, could be easily implemented in a single system-on-a-chip.

The usefulness of the FBG sensor can be customized to a given application. Here, a temperature sensor was used for the analog input as a simple proof of concept, although the method and results would be consistent with many other measurands. Moreover, by matching the laser to a FBG with different spectral characteristics [279], different response curves can be realized (Figure 10.9). The response could be made steeper to give a more defined switching signal, using an FBG with a square like reflection spectrum. Alternatively, a more linear transfer function could be obtained for sensing purposes, by utilizing a broadband FBG with a linear edge, meaning the output current could be linear from 4mA to 20mA and the temperature could span a much greater range, from 0 to 100^{o}C for example.

Figures 10.4 and 10.10 demonstrate an example of the kind of information that can be provided by the PLC and displayed using a HMI. Obviously the complexity of the PLC program and the HMI will depend directly on the real application in which a system similar to this could be used; although by focusing only on the linear region of the output, no additional programming would be required to convert the current signal into the appropriate measurand.

This work is the first step in creating a PLC FOS interface by developing a digital input interface and a standard 4-20mA analogue input interface. Put simply, we have replaced a traditional electrical/electronic instrument with an optical fibre equivalent, using industry standards. To the author's knowledge, this has not been reported previously.

10.3.2 Significance

The main advantage of the approach detailed in this report is that FOS effectively become plug and play instruments with regard to current industrial controllers. All FBG interrogators on the market at present are expensive stand-alone systems that require knowledge of optical engineering. There has been some attempt to develop simpler, more compact FBG interrogators utilising smart controllers, such as field programmable gate arrays [40]. However, their penetration into mainstream industries has been extremely limited. By interfacing directly with standard industrial controllers, from an operational point of view, the control system is identical, with no need for additional training or programming.

10.3.3 Future Work

The focus of this work was to convert a single digital input and single analogue measur- and from the optical domain to the electrical domain, which could then be interpreted by a single digital and analogue input on a PLC. However, the intention of future work is to create an integrated optoelectronic interface to a PLC, for multiple FBG sensors. That is, thousands of FBGs could be multiplexed over a single fibre [280], which could then communicate with the PLC over a smart network, such as Profinet [281], as demonstrated in Chapter 11. An intensity based system capable of measuring the values of six FBG strain sensors along a single fibre utilising a broadband source and a micro-electromechanical system (MEMS) filter to interrogate the signals, has previously been reported [282]. Figure 10.11 shows an example of a single fibre meandering around a process plant, with multiple FBGs measuring different process variables that could be monitored by a PLC. In creating a smart interface for FOS, the traditional input and output rack could be completely removed, reducing the overall cost of exiting systems.

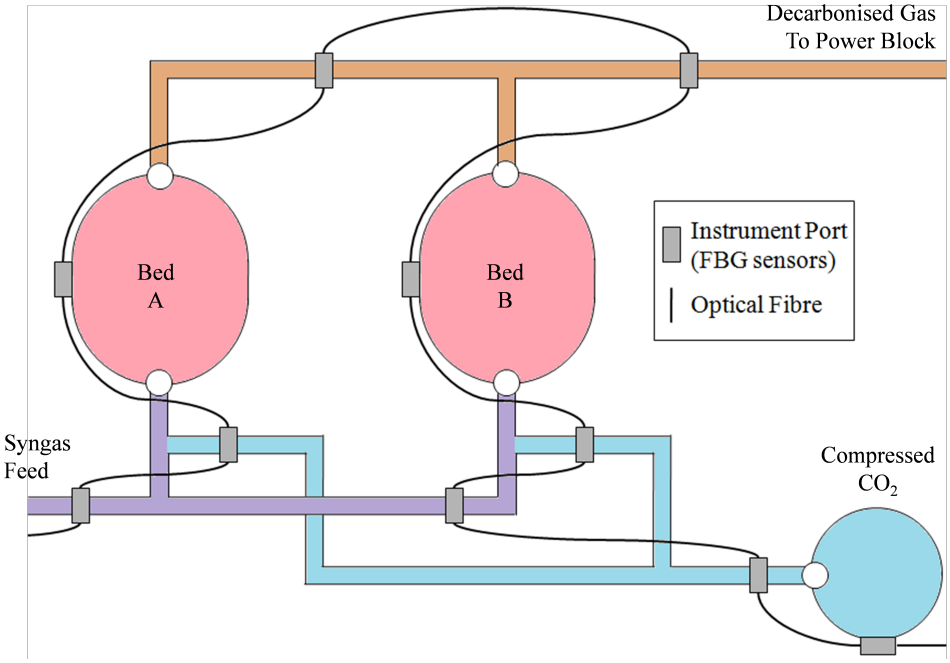

Figure 10.11: An example of a multistage industrial process monitored using multiple FBG temperature and pressure sensors, multiplexed along a single FBG cable.

10.4 Chapter Conclusion

In this chapter, the output from an in-ground FBG pressure switch connected to existing PLC digital input using a simple electronic circuit has been demonstrated. The optoelectronic circuit took in the signals from two PIN photoreceivers, differentially amplified them and then used a comparator circuit to determine if the voltage resulted in a 1 or a zero at the digital input card, which was then used to trigger an alarm that was displayed on a HMI. This demonstrates that conventional wired switches can easily be replaced with optical switches without replacing the expensive PLC hardware. In addition, an arbitrary FBG sensor has been interfaced with a PLC using the 4-20mA industry standard. The change in temperature, recorded by the FBG sensor, was displayed on the PLC's HMI as a result of an optoelectronic conversion. The optoelectronic circuit took in the signals from two PIN photoreceivers, differentially amplified them, added a DC offset, and then converted the 1 to 5V signal to the required 4-20mA, us-

ing a transconductance amplifier. These relatively simple methods enable FOS to be utilised in established process control environments, combining state-of-the-art sensing with rugged industrial controllers. In addition, we have also outlined the development of an intelligent FOS network, utilizing standard PLCs for advanced industrial automation systems in the future, based on this work.

Chapter 11

Optoelectronic Interfacing of Fibre Bragg Grating Sensors

In this chapter, a PLC FOS Interface Module (FOSIM) has been developed, in which an optical fibre is connected directly to the OFSIM located next to the PLC. The information from a FBG sensor can be sent over the existing field bus network, Profinet. Finally, a low cost optoelectronic interface for multiple FBG sensors is demonstrated. Three different transducers using off-the-shelf fibre sensors were multiplexed over the same fibre through wavelength division multiplexing. The shift in wavelength due to a change in temperature, pressure and load, was converted into a change in intensity using edge filter interrogation. Three optically mis-matched FBGs were used as edge filters for each of the transducers. A wavelength division multiplexer was used to separate the signals, which were then connected to individual photodetectors. The output voltages from the photodetectors were connected to a low cost Raspberry Pi microcontroller, where the values were converted into the appropriate measurands.

11.1 Motivation and Applications

The revenue generated from both PLC technology and optical fibre sensing technology is enormous. Siemens is a huge European based company that employs over 343,000 employees in 190 countries worldwide with a reported global revenue of over 71.9bn Euros and a net income of 5.5bn Euros in 2014 [283]. Schneider Electric reported

annual gross sales of 23.6bn Euros in 2013, with a net profit of 1.9bn Euros, up 4% on the previous year [284]. Rockwell Automation reported a revenue of $6.35bn in 2013, up 1.5% from $6.26bn in 2012 [285]. Furthermore, the distributed FOS market was US$585M in 2013 and projected to be US$1.458bn in 2018 [6]. In the five years following 2004, the security sector and process control sector increased from almost none to 10% and 5% of the total market share, respectively [153]. In recent years, FBG related product sales have had an annual growth rate of approximately 25%. By making FBG technology directly compatible with the PLC industry standards, the market potential can only increase.

This technology could benefit any client, company or organization associated with an industrial process which currently uses PLCs for control, particularly those in harsh environments. Integrating these two technologies in a simple and efficient way will result in a low cost, robust system with high sensitivity and overall improved performance. This will in turn reduce the cost for the manufacturer and the end customer of products that utilise control systems.

11.2 Programmable Logic Controller Fibre Optic Sensor Interface Module- PLC FOSIM

In order to take full advantage of the on-board intelligence of a PLC in OFS systems, a FOS interface module was designed which would send the sensor data over a standard industrial fieldbus network, potentially removing the need for the I/O rack. The optical side of the interface is based on the IDS which has been discussed in previous chapters, but will be described in more detail here. Figure 11.1 shows a circuit diagram of the IDS.

The IDS design includes 2 PIN receivers (Fujitsu FRM3Z231KT). The preamp supply and PIN bias are provided by a $\pm 5V$ supply. The power supply is internal, which uses a centre tapped 12.6V transformer to step down mains voltage. This is then half

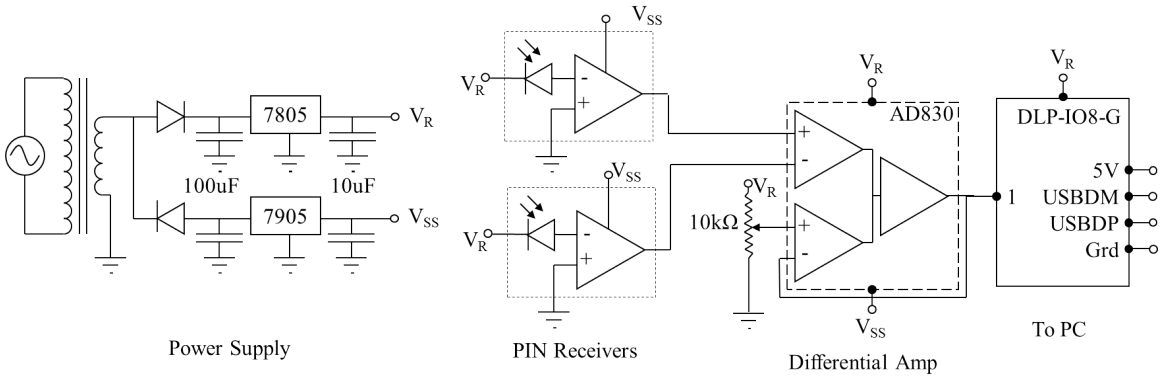

Figure 11.1: Circuit diagram of the IDS. The PIN receivers give a negative offset due to amplifier bias. The offset is removed by the difference amplifier, giving a positive or negative signal. The ADC has an internal 2.5V reference to give only positive bits.

wave rectified, filtered, and regulated. For the IDS, the output of the two receivers is differentially amplified using a high speed differential amplifier (AD830ANZ). The differential output is then digitised via an ADC (AD7827BNZ). An eight bit ADC was chosen for speed and to ensure the computer interface for the initial system was as simple as possible. The computer interface is an eight channel USB interface (DLP-IO8-G), based on a USB to serial converter (FT232R), and a microcontroller (PIC16F688).

As Profinet was the most advantageous bus topology to be used with a Siemens PLC (S7-300), it was decided that the OFSIM must be compatible with Profinet. Rather than design an interface module from scratch, a Profinet I/O module, together with an evaluation board (Anybus CompactCom), was purchased from HMS Industrial Networks [286]. This significantly reduced the development time as the module was already pre-configured with all of the necessary protocols. The Profinet I/O module was setup as a slave for the PLC and connected directly to the PLC over Profinet using an industrial Ethernet cable. The Profinet I/O module was then connected to the evaluation board using a standard 50 pin flash connector. Finally, the evaluation board was connected to the PC via a serial cable using RS232. All components communicated successfully. Figure 11.2 shows the layout of the setup.

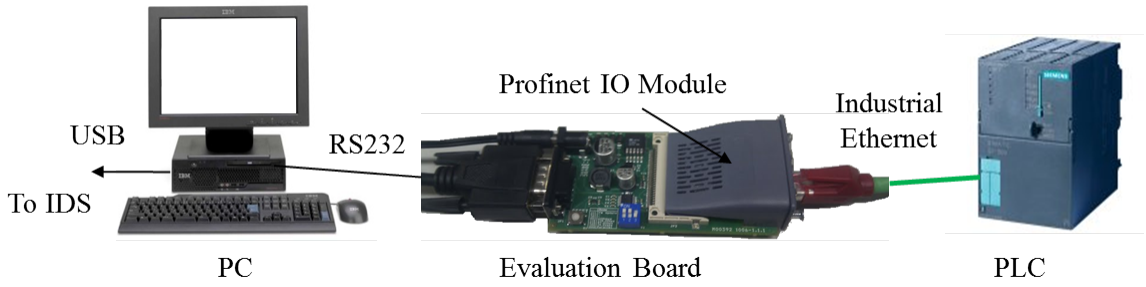

Figure 11.2: PLC FOSIM layout, showing PC, evaluation board, Profinet IO module, and PLC.

The next stage was to remove the USB interface and bypass the PC and evaluation board, and connect the output of the IDS directly to an input on the Profinet interface module for direct interpretation by the PLC. Both analogue and digital signals could be connected in this way.

The long term intention of this work is to completely remove the existing I/O rack from the PLC hardware and replace it with an optoelectronic interface module. Figure 11.3 shows the existing control system architecture and which sections could be replaced by optical components such as optical fibres and FBG sensors.

There could be as many as 1000 FBG sensors embedded in a single optical fibre [280], all transferring data to the PLC. This could be achieved by using both WDM and TDM, and encoding the address of each individual FBG within the data package which is processed by a microcontroller interface. That is, in a traditional PLC system, each instrument on the input and output is given an address, the data for each address is then poled, and sent to the PLC for monitoring and control purposes.

As well as replacing electronic I/O modules with this optical interface, power could be sent over the optical network to actuate digital outputs remotely [254]. This could be achieved by using a photonic power converter for a type of optical actuation [287]. Currently, GaAs photonic power converters can produce up to 0.5W of electrical power [288], which is enough power to actuate a small solenoid valve. Likewise a piezoelectric motor could be used to tune an additional FBG and an opto-pneumatic converter used

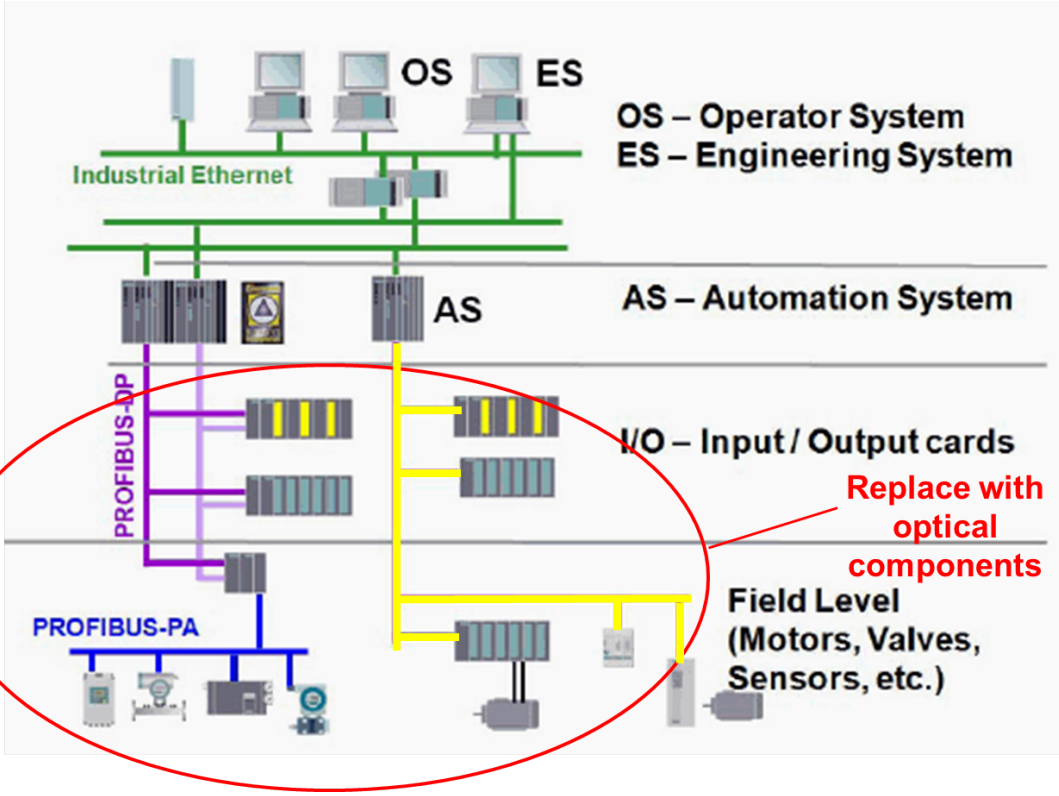

Figure 11.3: Existing control system architecture, showing which devices could be replaced by optical components in the future.

to operate a control valve, as proposed in [253]. In addition, it will also be possible to control electrical signals optically, via phototransistors. This would facilitate an almost entirely optical control system, where an optical input from an FBG sensor would drive an optical output, controlled by the PLC, and perform this type of actuation depending on the control logic. A schematic of the proposed multiplexed system is illustrated in figure 11.4. Here we see the bottom FBG is a temperature sensor, and this is coupled with a heating element, controlled by the photovoltaic power converter, receiving optical power from the 980nm laser diode. Furthermore, the system could be designed in such a way that the communication, sensing and power signals could be sent over the same fibre. It has previously been demonstrated that all three types of signals can be multiplexed on the same fibre without loss of information [276].

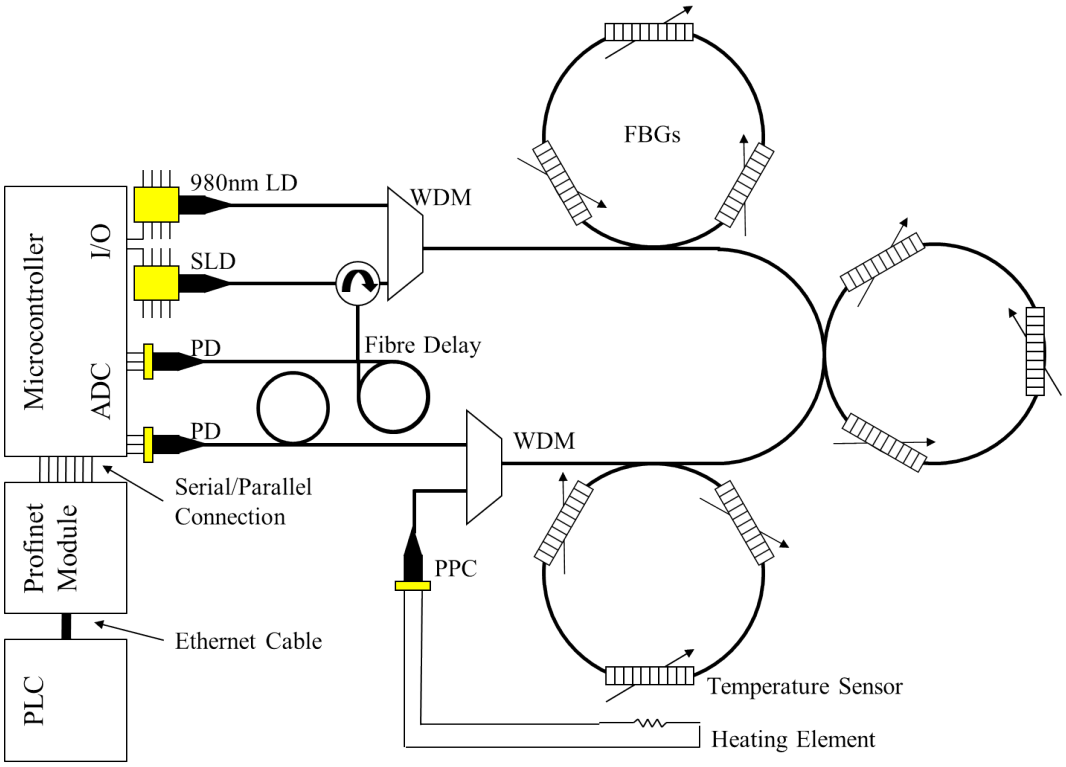

Figure 11.4: The proposed FBG WDM/TDM based intelligent optical fibre sensor network for PLC based process control.

11.3 A Simple Low Cost Optoelectronic Interface for FBG Sensors using a Raspberry Pi

Whilst interfacing FOS with standard industrial controllers is extremely important in increasing the penetration of OFS systems into mainstream industrial processes, producing a low cost interface for embedded controllers is also important. Low cost embedded controllers are being used many applications such as small scale robotics and wireless sensor networks. Integrating FOS with these controllers would enable FOS to be utilised in these applications as well as, low cost commercial systems and home automation systems.

11.3.1 Communications

The proposed communication system is designed to automatically acquire, process, and analyse sensor data from remote locations to help alleviate the time and energy required for manual monitoring. To achieve this, the system must be as reliable and self-functional as possible. The key components of this system involve:

- A Raspberry Pi (RPi) [47,289] is an ideal platform for the low cost remote sensing system due to its miniaturized size (remote deployment) and intensive computational power (required for acoustical analysis tasks).

- A low-power radio transceiver [290, 291] (Zigbee Link) can be used to transmit the sensor data from remote locations to a centralised control centre. The data may also contain alarm messages and diagnostics status to verify system operation (e.g. remaining power percentage).

11.3.2 Interfacing Multiple Fibre Optic Sensors with a Microcontroller

To demonstrate the effectiveness of a low cost optoelectronic interface, three different FOS were connected in series along a single fibre. A bare FBG (Micron Optics OS1100), acting as a temperature sensor, was immersed in water in a beaker and placed on a hot plate (Industrial Equipment and Control PTY CH2093) for heating. The diaphragm pressure transducer described in Chapter 6 and the top FBG of the load cell transducer described in Chapter 7, were both connected in series along the same sensing fibre. The sensing fibre was then connected to port 2 of a 4-port circulator (AFW CIR-4-12-L-1-2). The bottom FBG of the load cell was connected in series with a reference FBG for the temperature sensor and a reference FBG for the pressure transducer. The reference fibre was connected to port 3 of the circulator. A broadband source (DenseLight DL-BZ1-CS5254A) was connected to port 1 of the circulator and a WDM (Avanex PMC3016DCAV01PX) was used to separate the signals was connected to port 4. Three

photodetectors (Thorlabs DET01CFC) were connected to the WDM and used to convert the optical intensity reflected from the FBG pairs into voltages. The photodetectors were connected to analogue inputs on the Raspberry Pi microcontroller. The temperature, pressure and load were simultaneously varied and the output voltages were easily interpreted by a Raspberry Pi. The experimental setup is shown in figure 11.5.

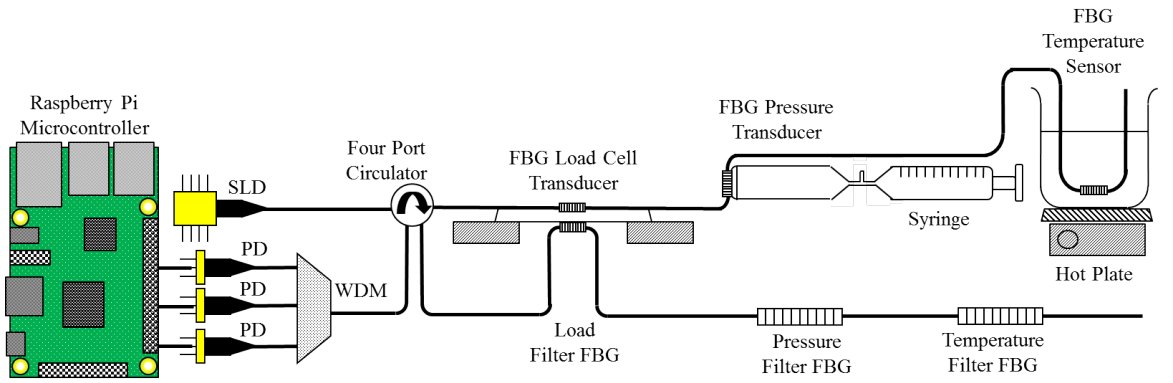

Figure 11.5: Experimental setup for multiplexing of three different FBG transducers incorporating optically mis-matched FBGs as individual linear edge filters, connected to a Raspberry Pi microcontroller.

11.3.3 Results and Discussion

Prior to performing any experiments, the reflected spectra from the sensing and reference FBGs were recorded using an OSA (Anritsu MS9001B1) to show the relative positions of each of the FBG pairs at room temperature and under no pressure or load. Figure 11.6 shows the spectra, with the temperature based FBG pair localised around 1548nm, the load cell FBG pair localised around 1552nm, and the pressure transducer pair localised around 1556nm. It can be seen that both the temperature sensor and load cell pair overlap significantly, whilst the pressure sensor pair are separated by approximately 1nm. This simply meant pressure needed to be applied before any output voltage could be recorded. As the temperature, load, and pressure were increased, the Bragg wavelength of the reflected spectra from the sensing FBGs increased, shifting from left

to right.

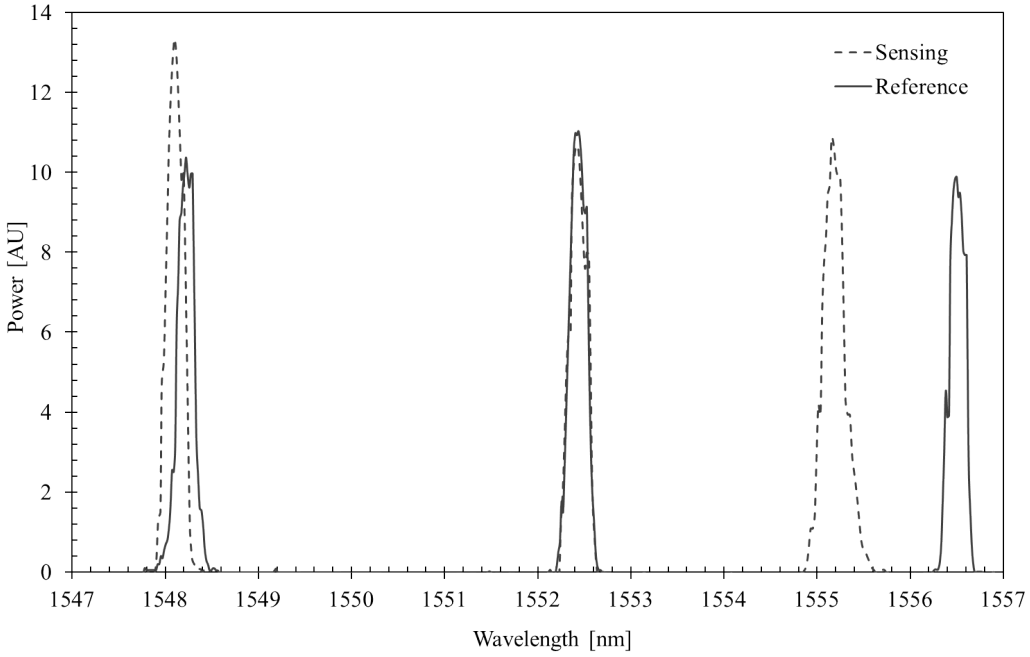

Figure 11.6: The reflected spectra from both the sensing and reference FBGs. The temperature based FBG pair are localized around 1548nm (left), the load cell FBG pair are localized around 1552nm (centre), and the pressure transducer pair are localized around 1556nm (right).

The output voltages from the temperature sensor, load cell transducer, and the pressure transducer were recorded as a function of temperature, load, and pressure, respectively. Figure 11.7 shows there is a negative linear response from the temperature sensor as the sensing FBG spectra shifted across the right side of the reference spectra. The sensitivity was recorded as $-0.06V/^oC$. Figure 11.8 shows there is a positive linear response for the pressure transducer as the sensing FBG spectra shifted across the left side of the reference spectra. The recorded sensitivity was 4.4V/kPa. Figure 11.9 shows that there is a negative linear response to load from 4kg to 8kg, again because the sensing FBG spectra shifted across the right side of the reference spectra. The sensitivity was recorded as $-0.47V/kg$

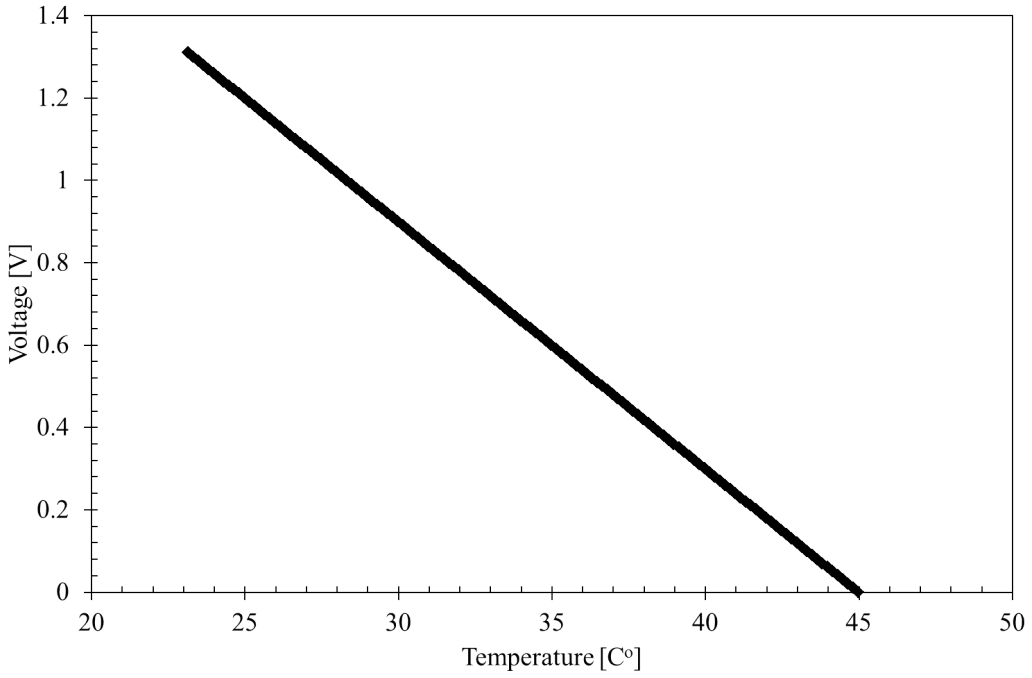

Figure 11.7: The response of the temperature sensor. The sensitivity of the sensor, as shown in the graph, is $-0.06V/C^o$.

The sensitivity of each of the transducers could be changed by modifying the physical properties of the transducers, such as having a less rigid body for the load cell to increase it's sensitivity to load, or increasing the diameter of the pressure transducer to increase it's sensitivity to pressure. The dynamic range of the transducers could be increased by using a reference FBG with a larger full-width half-maximum (FWHM), such as a chirped grating [25], although there is a trade-off between sensitivity and dynamic range.

The sensitivity of the temperature sensor used in this study was essentially fixed, as it was simply the response of the bare FBG due to a change in temperature corresponding to approximately $10pm/C^o$, which has been well documented [175]. However, the sensitivity could be changed through the development of a new temperature transducer. For example, a FBG could be bonded to a material which has a large coefficient of expansion and the strain induced wavelength shift would correspond to a change in

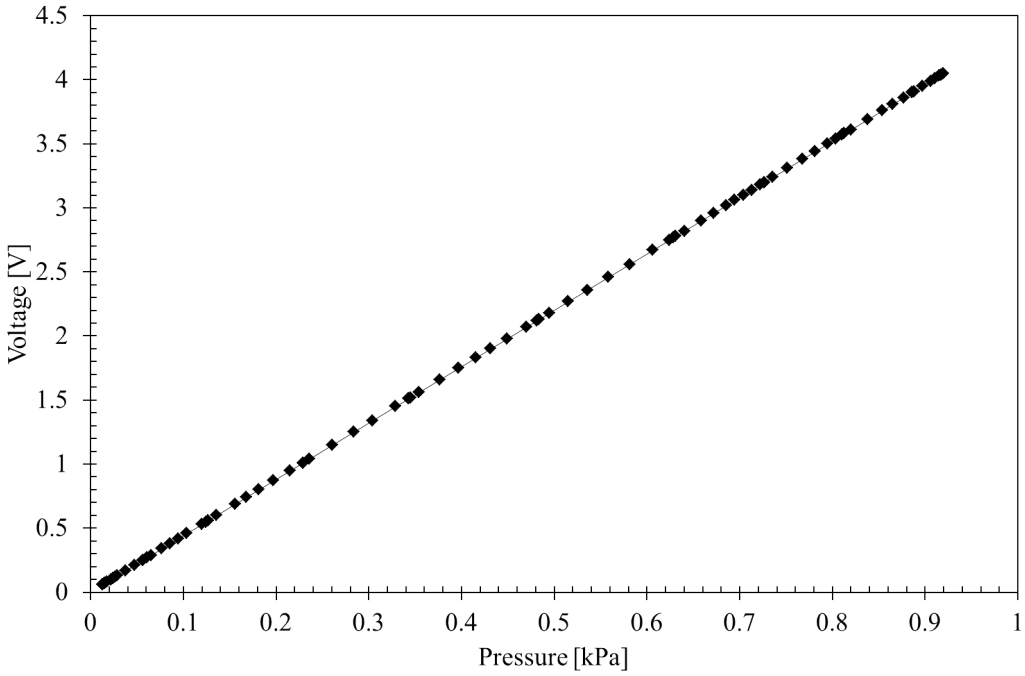

Figure 11.8: The response of the pressure transducer. The sensitivity of the transducer, as shown in the graph, is $4.4V/kPa$.

temperature, similar to the approach used in [292], although the FBG itself would have to be isolated from the temperature. However, this approach needs to be investigated in more detail in future work.

The analogue output voltage from each of the transducers could easily be recorded by a low cost microcontroller, such as a Raspberry Pi. The measured values could then be displayed by programming the linear transfer functions into the microcontroller. This low cost edge filter interrogation technique eliminates the need for an expensive stand alone commercial interrogator. Moreover, this work demonstrates that optical fibre sensors have the potential to seamlessly integrate with distributed wireless sensor networks for a range of low cost applications, with no additional complexity added in terms of programming the controllers.

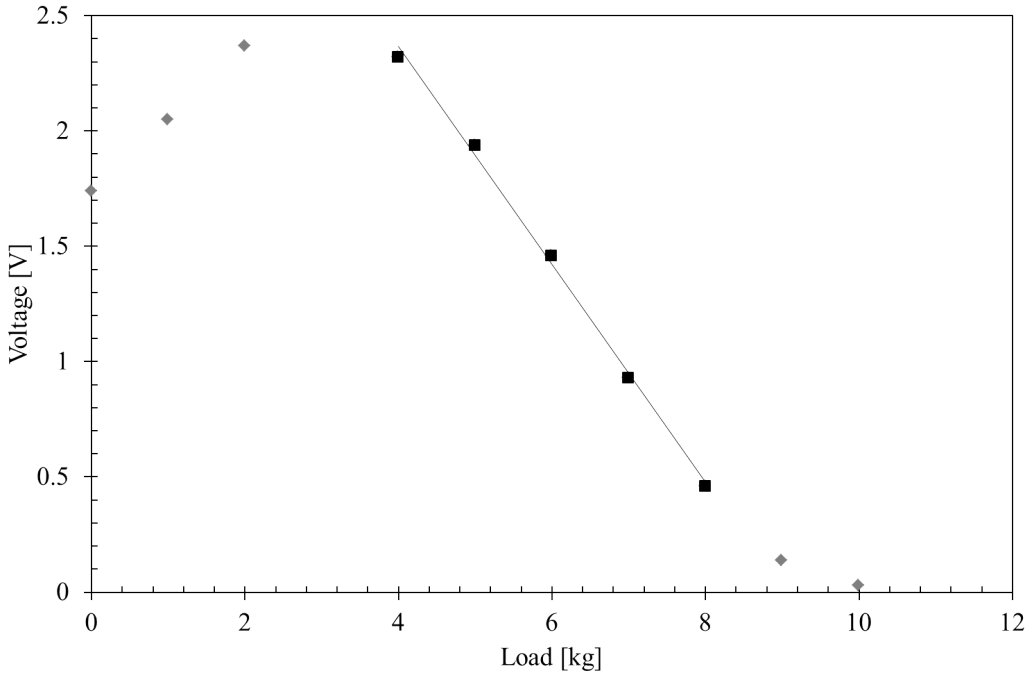

Figure 11.9: The response of the load cell transducer. The sensitivity of the transducer, as shown in the graph, is $-0.47V/kg$.

11.4 Chapter Conclusion

In conclusion, the first stage of a PLC FOSIM has been developed and implemented. It has been shown that the optical information from a FBG can be transposed into the electrical domain and connected to a PC using a USB cable. The PC was connected to an evaluation board via a serial cable using RS232. The Profinet I/O module was connected to the evaluation board using a 50 pin flash connecter. The Profinet module was then connected to the PLC via an industrial Ethernet cable using Profinet to communicate. In addition, three different optical fibre transducers, multiplexed over the same fibre, and interrogated using optically mis-matched FBGs, has been demonstrated. Further, it has been shown that the output of these transducers can easily be connected to a low cost microcontroller, with the voltage values converted into the appropriate measurand using their respective linear transfer functions. This is the first step towards the integration of distributed optical fibre sensors with wireless sensor networks.

Chapter 12

Conclusion

12.1 Findings

In conclusion, this work contributes to the development of a new generation of fibre optic sensors for physical security and mainstream industrial applications. Several different optical fibre sensing techniques have been demonstrated for use in mainstream industrial processes and physical intrusion detection systems. A specific focus on low cost transducer design and easy integration with existing control system architectures has been made, through development of fibre optic sensor optoelectronic interface modules.

The versatility of FBG sensors for physical intrusion detection systems has been explicitly demonstrated through the development of a new FBG reed switch, and through in-fence and in-ground intrusion detection. In addition, the use of FBG sensors in more esoteric applications may occur due to the realisation of strain and pressure measurements when bonded to flexible membranes. For example, it is proposed that FBGs could be used to monitor the structural integrity of large rubber dams. Moreover, a current project is investigating the use of FBG sensors in monitoring the health and displacement of rubber membranes in wave energy converters.

Within the scope of this thesis, the author has outlined two distinct techniques that may significantly improve the penetration of FBG sensing within these applications. Firstly, the development of fibre optic sensors with on-board interrogation, such as the load cell that has been proposed here. In this way, off-the-shelf fibre optic sensors could

be purchased, which have two input optical fibres, one for the sensing FBG and the other for the reference/interrogator FBG, and two output optical fibres, for multiplexing. In this case, the sensor could act as a black box, with only the sensor wavelength range known, so that several sensors could be multiplexed. Secondly, using a dual bus configuration, many different sensors with identical optical properties can be multiplexed on the same network. This creates the potential for future optical fibre sensing standards, by producing an array of transducers with the same Bragg wavelength.

The main problem with FBG sensors is their inherent sensitivity to both strain and temperature. Although there have been some complex techniques proposed in the literature to isolate these effects, here, in a quasi static applications, a co-located interrogator FBG embedded within a transducer housing, effectively removed the effect due to temperature. In the case of a temperature sensor, strain isolation can easily be achieved by ensuring the FBG is loosely bonded at one end. In addition, the possible advantages of the non-linear behaviour of FBGs have been discussed, with the aim of developing more diverse sensors which are inherently isolated from strain or temperature effects. All objectives, both primary and secondary, posed through this work have been achieved. By focusing on the requirements set by industry and not directly on the performance of the sensors, many of the issues proposed, such as integration with existing systems and being replaceable without disrupting the rest of the network, have been resolved.

12.2 Future Work

A proof of concept of FBG sensing for physical intrusion detection systems has been demonstrated, although it is anticipated that future studies will be required to establish the configuration of FBGs required for determining the location of a person. Confirmation that a person's position can be triangulated, from the difference between the intensity of the recorded acoustic emission signals through several FBGs, should be achieved using time-division multiplexing. More research on fence mounted FBGs should be performed to ensure there will be a high probability of detection with low false alarm rate.

Wavelength division and time division multiplexing techniques could be easily combined, enabling large numbers of sensors to be multiplexed in a single system. This will also reduce the cost associated with the use of a tunable laser. The use of a single superluminescent diode will facilitate the multiplexing of multiple sensors. Also, multiplexing of the different types of FBG intrusion detection sensors should be performed to demonstrate that FBG sensors have the potential to form the basis of a complete physical intrusion detection system, utilising in-ground, pressure and acoustic sensors, in-fence sensors, and in-window and door sensors, for both commercial and domestic environments. Moreover, the author proposes to develop different transducers utilising identical FBGs with the same spectral range, in conjunction with an industry partner, initially for use in water treatment and desalination plants.

An explicit investigation into the limitations of the commercial fibre optic sensor systems discussed in this thesis will also form the basis of future work, and will be addressed as commercial systems are implemented.

References

[1] E. Udd and W. B. Spillman. *Fiber Optic Sensors: An Introduction for Engineers and Scientists*. Wiley, New Jersey, USA, 2011.

[2] C. Chen, Y-S Yu, R. Yang, C. Wang, J.-C. Guo, Y. Xue, Q.-D. Chen, and H.-B. Sun. Reflective optical fiber sensors based on tilted fiber Bragg gratings fabricated with femtosecond laser. *Journal of Lightwave Technology*, 31(3):455–460, 2013.

[3] J. Luo, Y. Hao, Q. Ye, Y. Hao, and Licheng Li. Development of optical fiber sensors based on brillouin scattering and fbg for on-line monitoring in overhead transmission lines. *Journal of Lightwave Technology*, 31(10):1559–1565, 2013.

[4] D. A. Krohn. *Fiber Optic Sensors Fundamentals and Applications*. Instrument Society of America, North Carolina, USA, 1996.

[5] A. D. Kersey. A review of recent developments in fiber optic sensor technology. *Optical Fiber Technology*, 2:291–317, 1996.

[6] Light Wave Venture. 2014 photonic sensor consortium market survey report. Technical report, Photonic Sensor Consortium, 2014.

[7] MarketsandMarkets. Process automation market & instrumentation market by technology (SCADA, PLC, DCS, MES), communication (profibus, fieldbus, wireless HART, isa100), transmitter (flow, temperature, level, pressure) - analysis and forecast (2013 2018). Technical report, MarketsandMarkets, 2013.

[8] A. D. Kersey, M. A. Davis, H. J. Patrick, M. LeBlanc, K. P. Koo, C. G. Askins, M. A. Putnam, and E. J. Friebele. Fiber grating sensors. *Journal of Lightwave Technology.*, 15(8):1442–1462, 1997.

[9] B. Lee and Y. Jeong. *Fiber Optic Sensors*. Marcel Dekker, New York, USA, 2002.

[10] G. F. Smith, T. A. King, and D. Wilkins. *Optics and photonics: an introduction*. John Wiley & Sons, 2007.

[11] A. Bertholods and R. Dandliker. Determination of the individual strain-optic coefficients in single-mode optical fibers. *Journal of Lightwave Technology*, 6(1):17–20, 1988.

[12] G. Wild and S. Hinckley. Acousto-ultrasonic optical fiber sensors: Overview and state-of-the-art. *IEEE Sensors Journal*, 8(7):1184–1193, 2008.

[13] K. Pan, C.-M. Uang, F. Cheng, and F. T. S. Yu. Multimode fiber sensing by using mean-absolute speckle-intensity variation. *Applied Optics*, 33(10):2095–2098, 1994.

[14] X. Bao and L. Chen. Recent progress in distributed fiber optic sensors. *Sensors*, 12(7):8601–8639, 2012.

[15] P. Ferdinand, S. Rougeault, N. Roussel, M. Pinabiau, C. Canepa, J.-C. Da Rocha, A. Poulain, R. Blin, S. Piot, and L. Gourit. Brillouin sensing for perimetric detection: the smartfence project. In *Proceedings SPIE 22nd International Conference on Optical Fiber Sensor*, page 84219X, 2012.

[16] A. Othonos and K. Kalli. *Fiber Bragg Grating Fundamentals and Applications in Telecommunications and Sensing*. Artech House, Boston, USA, 1999.

[17] R. Kashyup. *Fiber Bragg Gratings*. Academic Press, San Diego, USA, 1999.

[18] James S Sirkis. Unified approach to phase-strain-temperature models for smart structure interferometric optical fiber sensors: part 2, applications. *Optical Engineering*, 32(4):762–773, 1993.

[19] James S Sirkis. Unified approach to phase-strain-temperature models for smart structure interferometric optical fiber sensors: part 2, applications. *Optical Engineering*, 32(4):762–773, 1993.

[20] I. Yulianti, A. S. M Supa'at, S. M Idrus, O. Kurdi, and M. R. S Anwar. Sensitivity improvement of a fibre Bragg grating pH sensor with elastomeric coating. *Measurement Science and Technology*, 23(1):015104, 2012.

[21] M. M. Werneck, R. Allil, B. A. Ribeiro, and F. V. B. de Nazaré. *Current Trends in Short- and Long-period Fiber Gratings*, chapter A Guide to Fiber Bragg Grating Sensors. InTech, 2013.

[22] M. Lai, D. Karalekas, and J. Botsis. On the effects of the lateral strains on the fiber Bragg grating response. *Sensors*, 13(2):2631–2644, 2013.

[23] S. W. James and R. P. Tatam. Optical fibre long-period grating sensors: characteristics and application. *Measurement Science and Technology*, 14(5):R49–R61, 2003.

[24] D. J. Webb, T. Allsop, H. Dobb, K. Kalli, T Earthrowl, V Mezentsev, A Gillooly, R Neal, and Ian Bennion. Sensing applications of long-period gratings in various fibre types. In *Proceedings SPIE Second European Workshop on Optical Fibre Sensors*, pages 104–107, 2004.

[25] S. Bandyopadhyay, P. Biswas, A. Pal, S. K. Bhadra, and K. Dasgupta. Empirical relations for design of linear edge filters using apodized linearly chirped fiber Bragg grating. *Journal of Lightwave Technology*, 26(24):3853–3859, 2008.

[26] Q. Wu, G. Farrell, and Y. Semenova. Simple design technique for a triangular fbg filter based on a linearly chirped grating. *Optics Communications*, 283(6):985–992, 2010.

[27] A. A. Chtcherbakov and P. L. Swart. Chirped fiber-optic Bragg grating interrogator in a multiplexed bragg grating sensor configuration. *Journal of Lightwave Technology*, 22(6):1543, 2004.

[28] Y. Zhao, Q. Wang, and H. Huang. Characteristics and applications of tilted fiber Bragg gratings. *Journal of Optoelectronics and Advanced Materials*, 12(12):2343–2354, 2010.

[29] R. Suo, X. Chen, K. Zhou, L. Zhang, and I. Bennion. 800 nm WDM interrogation system for strain, temperature, and refractive index sensing based on tilted fiber Bragg grating. *IEEE Sensors Journal*, 8(7):1273–1279, 2008.

[30] A. Iadicicco, S. Campopiano, A. Cutolo, M. Giordano, and A. Cusano. Microstructured fibre Bragg gratings: analysis and fabrication. *Electronics Letters*, 41(8):466–468, 2005.

[31] A. Cusano, A. Iadicicco, D. Paladino, S. Campopiano, A. Cutolo, and M. Giordano. Micro-structured fiber Bragg gratings. part i: Spectral characteristics. *Optical Fiber Technology*, 13(4):281–290, 2007.

[32] B. Eggleton, C. Kerbage, P. Westbrook, R. Windeler, and A. Hale. Microstructured optical fiber devices. *Optics Express*, 9(13):698–713, 2001.

[33] S. R. Blais and J. Yao. Tunable photonic microwave filter using a superstructured fbg with two reflection bands having complementary chirps. *Photonics Technology Letters*, 20(3):199–201, 2008.

[34] D. Uttamchandani and A. Othonos. Phase shifted Bragg gratings formed in optical fibres by post-fabrication thermal processing. *Optics Communications*, 127(4):200–204, 1996.

[35] R. Correia, E. Chehura, S. W. James, and R. P. Tatam. A pressure sensor based upon the transverse loading of a sub-section of an optical fibre bragg grating. *Measurement Science and Technology*, 18(10):3103, 2007.

[36] A. Cusano, D. Paladino, A. Cutolo adn A. Iadicicco, and S. Campopiano. *Fiber Bragg Graing Sensors: Research Advancements, Industrial Applications ans Market Expoitation*, chapter Photonic Bandgap Engineering in FBGs by Post Processing Fabrication Techniques. In [293], 2014.

[37] A. Cusano, A. Iadicicco, S. Campopiano, M. Giordano, and A. Cutolo. Thinned and micro-structured fibre Bragg gratings: towards new all-fibre high-sensitivity chemical sensors. *Journal of Optics A: Pure and Applied Optics*, 7(12):734, 2005.

[38] A. Cusano, A. Iadicicco, D. Paladino, S. Campopiano, A. Cutolo, and M. Giordano. Micro-structured fiber Bragg gratings. part ii: Towards advanced photonic devices. *Optical Fiber Technology*, 13(4):291–301, 2007.

[39] T. W. Verbruggen. Load monitoring for wind turbines: Fibre optic sensing and data processing. Technical Report ECN-E–09-071, Energy Research Centre of the Netherlands, 2009.

[40] W. Kunzler, Z. Zhu, R. Selfridge, S. Schultz, and M. Wirthlin. Integrating fiber Bragg grating sensors with sensor networks. In *Proceedings of IEEE AutoTest Conference*, 2008.

[41] P. Tsai, F. Sun, G. Xiao, Z.i Zhang, S. Rahimi, and D. Ban. A new fiber-Bragg-grating sensor interrogation system deploying free-spectral-range-matching scheme with high precision and fast detection rate. *IEEE Photonics Technology Letters*, 20(4):300–302, 2008.

[42] M. Lopez-Amo and J. M. Lopez-Higuera. *Fiber Bragg Graing Sensors: Research Advancements, Industrial Applications ans Market Expoitation*, chapter Multiplexing Techniques for FBG Sensors. In [293], 2014.

[43] Y. J. Rao. In-fibre Bragg grating sensors. *Meas. Sci. Technol.*, 8:355–375, 1997.

[44] J. Chen, B. Liu, and H. Zhang. Review of fiber Bragg grating sensor technology. *Frontiers of Optoelectronics in China*, 4(2):204–212, 2011.

[45] T. Kouthon and J.-D. Decotignie. Improving time performances of distributed PLC applications. In *Proceedings IEEE Emerging Technologies and Factory Automation*, volume 2, pages 656–662, 1996.

[46] W. Bolton. *Programmable Logic Controllers*. Newnes, 2009.

[47] E. Upton and G. Halfacree. *Raspberry Pi user guide*. John Wiley & Sons, 2013.

[48] J. Sarik and I. Kymissis. Lab kits using the Arduino prototyping platform. In *Proceedings IEEE Frontiers in Education Conference*, pages T3C–1, 2010.

[49] J. Axelson. *Embedded ETHERNET and Internet complete*. Lakeview Research, 2003.

[50] J.-P. Thomesse. Fieldbus technology in industrial automation. *Proceedings of the IEEE*, 93(6):1073–1101, 2005.

[51] I. Belai and P. Drahoš. The industrial communication systems profibus and PROFInet. *Applied Natural Sciences*, pages 329–336, 2009.

[52] P. Neumann and A. Poschmann. Ethernet-based real-time communications with PROFINET IO. *WSEAS Transactions on Communications*, 4(5):235–245, 2005.

[53] T. Ozkul. *Data acquisition and process control using personal computers*. Marcel Dekker, Inc., 1996.

[54] J. Liu, Y. Fang, and D. Zhang. PROFIBUS-DP and HART protocol conversion and the gateway development. In *Proveedings IEEE Industrial Electronics and Applications*, pages 15–20, 2007.

[55] T. G. Giallorenzi, J. A. Bucaro, A. Dandridge, G. H. Sigel, J. H. Cole, S. C. Rashleigh, and R. G. Priest. Optical fiber sensor technology. *IEEE Transactions on Microwave Theory and Techniques*, 30(4):472–511, 1982.

[56] K. Bohnert, H. Brandle, M. G. Brunzel, P. Gabus, and P. Guggenbach. Highly accurate fiber-optic DC current sensor for the electrowinning industry. *IEEE Transactions on Industry Applications*, 43(1):180–187, 2007.

[57] D. F. Nelson, D. A. Kleinman, and K. W. Wecht. Vibration-induced modulation of fiberguide transmission. *Applied Physics Letters*, 30(2):94–96, 1977.

[58] J. H. Cole, R. L. Johnson, and P. G. Bhuta. Fiber-optic detection of sound. *The Journal of the Acoustical Society of America*, 62(5):1136–1138, 1977.

[59] J. A. Bucaro, H. D. Dardy, and E. F. Carome. Fiber-optic hydrophone. *The Journal of the Acoustical Society of America*, 62(5):1302–1304, 1977.

[60] K. O. Hill, Y. Fujii, D. C. Johnson, and B. S. Kawasaki. Photosensitivity in optical fiber waveguides: Application to reflection filter fabrication. *Applied Physics Letters*, 32(10):647–649, 1978.

[61] G. Meltz, W. W. Morey, and W. H. Glenn. Formation of Bragg gratings in optical fibers by a transverse holographic method. *Optics Letters*, 14(15):823–285, 1989.

[62] W. W. Morey, G. Meltz, and W. H. Glenn. Fiber optic Bragg grating sensors. In *Proceedings SPIE Fiber Optic and Laser Sensors VII*, volume 1169, pages 98–107, 1990.

[63] A. Kersey. Multiplexed Bragg grating fiber sensors. In *Proceedings IEEE Lasers and Electro-Optics Society Annual Meeting*, volume 2, pages 153–154, 1994.

[64] I. M. Perez, H. Cui, and E. Udd. Acoustic emission detection using fiber Bragg gratings. In *Proceedings SPIE 8th Annual International Symposium on Smart Structures and Materials*, pages 209–215, 2001.

[65] R. L. Barnard. *Intrusion Detection Systems, 2nd edition.* Butterworth, Massachusetts, USA, 1988.

[66] R. L. Pearson. *Electronic Security Systems A Manager's Guide to Evaluating and Selecting System Solutions.* Elsevier, Oxford, UK, 2007.

[67] Y. Lee, J. Kim, and C.-M. Kyung. Energy-aware video encoding for image quality improvement in battery-operated surveillance camera. *Transactions on Very Large Scale Integration (VLSI) Systems*, 20(2):310–318, 2012.

[68] A. Catalano, F. A. Bruno, M. Pisco, A. Cutolo, and A. Cusano. An intrusion detection system for the protection of railway assets using fiber Bragg grating sensors. *Sensors*, 14(10):18268–18285, 2014.

[69] J. D. Montegomery and F. W. Dixon. Fiber optics in security systems. In *Proceedings 1981 Carnahan Conference on Crime Countermeasures*, pages 121–124, 1981.

[70] D. H. Rowe. Fiber optic line sensors. In *Proceedings 1983 Carnahan Conference on Crime Countermeasures and Security*, pages 9–12, 1983.

[71] M. D. Robertson and J. A. Rarick. Application of fiber optics technology to physical security. In *Proceedings 1984 Carnahan Conference on Security Technology*, pages 183–186, 1984.

[72] C. Y. Leung and I. F. Chang. Optical fiber line-sensor based on intermodal interference. In *Proceedings SPIE*, volume 813, pages 365–366, 1987.

[73] C. Y. Leung, C. H. Huang, and I. F. Chang. Optical fiber security system: a field test report. In *Procedeings SPIE*, volume 838, pages 365–371, 1987.

[74] J. Wu and C. Leung. An optical fiber multisensor network for security applications. In *Proceedings Security Technology International Carnahan Conference on Security Technology*, pages 271–280, 1991.

[75] J. K. Lynn. Smart sensor systems for outdoor intrusion detection. In *Proceedings 1988 Carnahan Conference on Security Technology: Electronic Crime Countermeasures*, pages 65–68, 1988.

[76] R. R. Nason, D. E. Snyder, and J. A. Milloy. Cost effective fiber optic system design. In *Proceedings 1988 Carnahan Conference on Security Technology: Electronic Crime Countermeasures*, pages 45–49, 1988.

[77] R. W. Schwalm. Use of fiber optic equipment for security. In *Proceedings 1988 Carnahan Conference on Security Technology: Electronic Crime Countermeasures*, pages 79–81, 1988.

[78] G. B. Cogdell. Fiber optic sensors for intruder detection. In *Proceedings 1988 IEEE International Carnahan Conference on Security Technology: Crime Countermeasures*, pages 19–23, 1988.

[79] J. P. Hazan, M. Steers, G. Delmas, and J. L. Nagell. Buried optical fibre pressure sensor for intrusion detection. In *Proceedings 1989 International Carnahan Conference on Security Technology*, pages 149–154, 1989.

[80] G. Kotrotsios and O. Parnaux. A distributed optical fiber alarm system of very high dynamic range. In *Proceedings IEEE 1989 International Carnahan Conference on Security Technology*, pages 155–158, 1989.

[81] D. Skogmo and B. Black. A fiber optic barrier integrity monitor. In *Proceedings Security Technology International Carnahan Conference on Security Technology*, pages 19–25, 1990.

[82] B. Griffiths. Fiber optic sensors, systems and applications in physical security. In *Proceedings International Carnahan Conference on Security Technology*, pages 13–17, 1990.

[83] B. Griffiths. Developments in and applications of fibre optic intrusion detection sensors. In *Proceedings International Carnahan Conference on Security Technology*, pages 325–330, 1995.

[84] C. Bryson and I. Hawkes. Interferometric sensor system for security applications. In *Proceedings SPIE*, volume 2360, pages 485–488, 1994.

[85] C. Bryson and I. Hawkes. Fibre optic sensor system for integrated perimeter protection. In *Proceedings European Convention on Security and Detection*, pages 188–192, 1995.

[86] J. Park and H. F. Taylor. Fiber optic intrusion sensor. In *Proceedings SPIE*, volume 2895, pages 214–221, 1996.

[87] J. Park, W. Lee, and H. F. Taylor. Fiber optic intrusion sensor with the configuration of an optical time-domain reflectometer using coherent interference of Rayleigh backscattering. In *Proceedings SPIE Photonics China'98*, pages 49–56, 1998.

[88] J. Bush, C. A. Davis, P. G. Davis, A. Cekorich, and F. P. McNair. Buried fiber intrusion detection sensor with minimal false alarm rates. In *Proceedings SPIE Photonics East'99*, pages 285–295, 1999.

[89] W. M. Ciurpapinski and A. Maciejak. Localisation of the disturbance place in a distributed fiber optic sensor. In *Proceedings SPIE*, volume 3054, pages 47–49, 1997.

[90] M. Szustakowski and W. M. Ciurpapinski. Fibre optic distributed sensors. In *Proceedings SPIE*, volume 3054, pages 12–17, 1997.

[91] M. Szustakowski, W. Ciurapiriski, N. Palka, and M. Zyczkowski. Recent development of fiber optic sensors for perimeter security. In *Proceedings IEEE 35th International Carnhan Conference on Security Technology*, pages 142–148, 2001.

[92] M. Szustakowski, M. Zyczkowski, W. Ciurapiriski, and N. Palka. Sensitivity of perimeter sensor based on Sagnac interferometer. In *Proceedings SPIE*, volume 5576, pages 319–323, 2004.

[93] M. Szustakowski and M. Zyczkowski. Fiber optic sensors for perimeter security with intruder localization. In *Proceedings SPIE*, volume 5576, pages 59540C–1–59540C–15, 2005.

[94] M. Zyczkowski and W. Ciurapiriski. Fibre optic sensor with disturbance localization in one optical fibre. In *Proceedings SPIE*, volume 6585, pages 65851K–1–65851K–8, 2007.

[95] M. Kondrat and M.Zyczkowski. Perturbation place localization by the use of two-interferometer fibre optic system. In *Proceedings SPIE*, volume 6608, pages 66081O–1–66081O–5, 2007.

[96] M. Zyczkowski, W. Ciurapiriski, and M. Szustakowski. Preparation and characterization technique for linear disturbance localization in fibre optical sensor. In *Proceedings SPIE*, volume 6736, pages 67360C–1–67360C–9, 2007.

[97] M. Zyczkowski. Intruder localization and identification in fiber optic systems. In *Proceedings SPIE*, volume 7119, pages 71190L–1–71190L–12, 2008.

[98] M. Życzkowski. The fiber-optic sensor for the museum collections protection. *Acta Physica Polonica A*, 122(5):933–937, 2012.

[99] M. Życzkowski. Modalmetric fiber optic sensor for security of collections. *Acta Physica Polonica A*, 124(3):428–431, 2013.

[100] M. Życzkowski. The use of fiber optic sensors for the direct, physical protection of museums and cultural heritages. In *Proceedings SPIE Security + Defence*, page 89010N, 2013.

[101] M. Życzkowski. Improvement of sensitivity for hybrid fiber optic sensor for application in perimeter protection and cultural heritages. In *Proceedings SPIE 8794, Fifth European Workshop on Optical Fibre Sensors*, pages 89740U–1–89740U–6, 2013.

[102] M. Zyczkowski, M. Karol, P. Markowski, and M. Napierała. Simple fiber optic sensor for applications in security systems. In *Proceedings SPIE Security+ Defence*, page 92480B, 2014.

[103] M. Maki and F. Kapounek. Intellifiber^{TM}- the next generation fiber optic fence sensor. In *Proceedings IEEE 35th International Carnhan Conference on Security Technology*, pages 128–135, 2001.

[104] M. C. Maki and J. K. Weese. Intellifiber^{TM}: fiber optic fence sensor developments. In *Proceedings IEEE 37th International Carnhan Conference on Security Technology*, pages 17–22, 2003.

[105] M. C. Maki and J. K. Weese. Fiber optic fence sensor developments. *IEEE Aerospace and Electronic Systems Magazine*, 19(2):8–13, 2004.

[106] M. C. Maki, A. Brydges, and J. Labelle. Intellifiber^{TM}: fence sensor installation on alternative fence constructions. In *Proceedings IEEE 38th International Carnhan Conference on Security Technology*, pages 156–163, 2003.

[107] R. Crickmore, P. Nash, and J. Wooler. Fibre optic security systems for land and sea based applications. In *Proceedings SPIE*, volume 5611, pages 79–86, 2004.

[108] J. Wooler and R. Crickmore. Fibre optic seismic intruder detection. In *Proceedings SPIE*, volume 5855, pages 278–281, 2005.

[109] M. Kezmah, D. Donlagic, and B. Lenardic. Low cost security perimeter based on a Michelson interferometer. In *Proceedings IEEE Sensors Conference*, pages 1139–1142, 2009.

[110] S. Mahmoud and J. Katsifolis. A real-time event classification system for a fibre-optic perimeter intrusion detection system. In *Proceedings SPIE*, volume 7503, pages 75031P–1–75031P–4, 2009.

[111] S. Mahmoud and J. Katsifolis. Performance investigation of real-time fiber optic perimeter intrusion detection systems using event classification. In *Proceedings IEEE International Carnahan Conference on Security Technology*, pages 387–389, 2010.

[112] S. S. Mahmoud, Y. Visagathilagar, and J. Katsifolis. Real-time distributed fiber optic sensor for security systems: Performance, event classification and nuisance mitigation. *Photonic Sensors*, 2(3):225–236, 2012.

[113] H. Yan, G. Shi, Q. Wang, and S. Hao. Identification of damaging activities for perimeter security. In *Proceedings IEEE International Conference on Signal Processing Systems*, pages 162–166, 2009.

[114] T. Lan, C. Zhang, L. Li, G. Luo, and C. Li. Perimeter security system based on fiber optic disturbance sensor. In *Proceedings SPIE*, volume 6830, pages 68300J–1–68300J–6, 2007.

[115] A. McAulay and J. Wang. A Sagnac interferometer sensor system for intrusion detection and localization. In *Proceedings SPIE*, volume 5435, pages 114–119, 2004.

[116] T. Kumagai, A. Ogura, W. Ohnuki, K. Tan, and T. Sato. Optical intrusion detection sensor with polarisation maintaining fiber. In *Proceedings AIP 1st workshop on Specialty Optical Fiber and Their Applications*, volume 1055, pages 46–49, 2008.

[117] T. Kumagai, S. Sato, W. Ohnuk, and T. Nakamura. Fiber-optic intrusion detection sensor for physical security system. In *Proceedings SPIE*, volume 7753, pages 775331–1–775331–4, 2011.

[118] T. Kumagai, S. Sato, and T. Nakamura. Fiber-optic vibration sensor for physical security system. In *Proceedings IEEE International Conference on Condition Monitoring and Diagnosis*, pages 1171–1174, 2012.

[119] X. Li, Q. Sun, and J. Wo. Hybrid TDM/WDM based fiber-optic sensor network for perimeter intrusion detection. In *Proceedings SPIE*, volume 7753, pages 77532V–1–77532V–7, 2011.

[120] Y. Wu, P. Bian, B. Jia, and Q. Xiao. A novel Sagnac fiber optic sensor employing time delay estimation for distributed detection and location. In *Proceedings SPIE Security+ Defence*, page 88960A, 2013.

[121] K. Choi. Optical fiber speckle sensor for wire net fence application. In *Proceedings SPIE*, volume 6041, pages 60412T–1–760412T–6, 2005.

[122] R. Arnaoudov, W. Bock, R Militiev, Y. Angelov, and T. Eftimov. Performance evaluation of a few- and multi-mode fiber-optic perimeter sensor. In *Proceedings IEEE Instrumentation and Measurement Technology Conference*, pages 1–5, 2007.

[123] I. Kwon, D. Seo, C. Kim, and D. Yoon. Two step signal processing of optical fibre mesh for intruder detection. In *Proceedings SPIE*, volume 6945, pages 69451P–1–69451P–9, 2008.

[124] F. Blackmon and J. Pollock. Blue rose perimeter defense and security system. In *Proceedings SPIE*, volume 6201, pages 620123–1–620123–9, 2006.

[125] V. Vdovenko and B. Gorshkov. Fiber optic intrusion sensing based on coherent optical time domain reflectometry. In *Proceedings SPIE*, volume 6733, pages 673321–1–673321–9, 2007.

[126] B. G. Gorshkov, V. M. Paramonov, A. S. Kurkov, and A. T. Kulakov. Phase-sensitive fiber reflectometer for distributed external disturbance sensors. *Lightwave Russian Edition*, 4:47–49, 2005.

[127] B. G. Gorshkov, V. M. Paramonov, A. S. Kurkov, A. T. Kulakov, and M. V. Zazirny. Distributed sensor of external disturbance based on phase-sensitive fiber reflectometer. *Quantum Electronics*, 36:963–966, 2005.

[128] K. N. Choi, J. C. Juarez, and H. F. Taylor. Distributed fiber-optic pressure/seismic sensor for low-cost monitoring of long perimeters. In *Proceedings SPIE*, volume 5090, pages 134–141, 2003.

[129] J. C. Juarez, E. W. Maier, K. N. Choi, and H. F. Taylor. Distributed fiber-optic intrusion sensor system. *Journal of Lightwave Technology*, 23(6):2081–2087, 2005.

[130] J. C. Juarez and H. F. Taylor. Distributed fiber optic intrusion sensor system. In *Proceedings Optical Fiber Communication Conference*, volume 4, pages 3–5, 2005.

[131] J. C. Juarez and H. F. Taylor. Distributed fiber optic intrusion sensor system for monitoring long perimeters. In *Proceedings SPIE*, volume 5778, pages 692–703, 2005.

[132] J. C. Juarez and H. F. Taylor. Polarization discrimination in a phase-sensitive optical time-domain reflectometer intrusion-sensor system. *Optics Letters*, 30(24):3284–3286, 2005.

[133] J. C. Juarez and H. F. Taylor. Field test of a distributed fibero-optic intrusion sensor system for long perimeters. *Applied Optics*, 46(11):1968–1971, 2007.

[134] C. Madsen, T. Bae, and R. Atkins. Long fiber-optic perimeter sensor: signature analysis. In *Proceedings Photonic Applications, Systems and Technology Conference*, 2007.

[135] C. Madsen, T. Bae, and T. Snider. Intruder signature analysis from a phase-sensitive distributed fiber-optic perimeter sensor. In *Proceedings SPIE*, volume 6770, pages 67700K–1–67700K–6, 2007.

[136] C. Madsen, T. Snider, R. Atkins, and J. Simcik. Real-time processing of a phase sensitive distributed fiber optic perimeter sensor. In *Proceedings SPIE*, volume 6943, pages 694310–1–694310–8, 2008.

[137] Y. J. Rao, J. Z. Li, Z. L. Ran, and K. L. Xie. Distributed intrusion detection based on combination of ϕ-ODTR and POTDR. In *Proceedings SPIE*, volume 7004, pages 700461–1–700461–4, 2008.

[138] Y. J. Rao, J. Luo, Z.-L. Ran, J.-F. Yue, X-D Luo, and Z. Zhou. Long-distance fiber-optic ϕ-OTDR intrusion sensing system. In *Proceedings SPIE 20th International Conference on Optical Fibre Sensors*, page 75031O, 2009.

[139] F. Peng, Z. Wang, Y. J. Rao, and X.-H. Jia. 106km fully-distributed fiber-optic fence based on P-OTDR with 2nd-order Raman amplification. In *Proceedings OSA National Fiber Optic Engineers Conference*, pages JW2A–22, 2013.

[140] H. Wu, Y. Rao, S. Li, X. Lu, and Y. Wu. A novel FBG-based fence with high sensitivity and low nuisance alarm rate. In *Proceedings SPIE 21st International Conference on Optical Fibre Sensors (OFS21)*, page 77537R, 2011.

[141] H. Wu, X. Lu, S. Li, Y. Wu, and Y. Rao. Real-time activity identification in a smart FBG-based fiber-optic perimeter intrusion detection system. In *Proceedings SPIE 22nd International Conference on Optical Fiber Sensor*, page 84215B, 2012.

[142] H. J. Wu, S. S. Li, X. L. Lu, Y. Wu, and Y. J. Rao. A cost effective FBG-based security fence with fire alarm function. In *Proceedings SPIE Asia Pacific Optical Sensors Conference*, page 835134, 2012.

[143] H. Wu, X. Xie, H. Li, X. Li, Y. Wu, Y. Gong, and Y. Rao. A novel fiber-optical vibration defending system with on-line intelligent identification function. In *Proceedings SPIE Asia Pacific Optical Sensors Conference*, page 89241P, 2013.

[144] Y. J. Rao. Applications of advanced optical fiber sensors at UESTC. In *Proceedings SPIE Asia Pacific Optical Sensors Conference*, page 835102, 2012.

[145] H. Wu, Z. Wang, F.i Peng, Z. Peng, X. Li, Y. Wu, and Y. Rao. Field test of a fully distributed fiber optic intrusion detection system for long-distance security monitoring of national borderline. In *Proceedings SPIE 23rd International Conference on Optical Fiber Sensors*, page 915790, 2014.

[146] A. Klar and R. Linker. Feasibilty study of the automated detection and localization of underground tunnel excavation using Brillouin optical time domain reflectometer. In *Proceedings SPIE*, volume 7316, pages 7316–1–7316–12, 2009.

[147] D. Jia, N. Fang, L. Wang, and Z. Huang. Distributed fiber optic in-line intrusion sensor system. In *Proceedings Microwave Conference*, pages 608–611, 2008.

[148] N. Fang, L. Wang, D. Jia, C. Shan, and Z. Huang. Walking intrusion signal recognition method for fiber fence system. In *Proceedings Communications and Photonics Conference and Exhibition*, pages 1–6, 2009.

[149] M. Lu, N. Fang, L. Wang, Z. Huang, and X. Sun. DAQ application of PC oscilloscope for chaos fiber-optic fence system based on labVIEW. In *Proceedings IEEE Communications and Photonics Conference and Exhibition*, pages 1–8, 2011.

[150] Y. Wang, Z. Li, and Z. Jiang. An improved distributed optical fiber sensor (DOFS) for monitoring long-distance buried oil pipeline leakage and intrusion. In *Proceedings 4th IEEE Conference on Industrial Electronics and Applications (ICIEA)*, pages 318–320, 2009.

[151] H. Okazaki, M. Nishiyama, and K. Watanabe. Specific vibration frequency detection based on hetrocore fiber optic sensing for security. In *Proceedings IEEE International Workshop on Robotic and Sensors Environments*, pages 53–57, 2009.

[152] A. H. Morshed. Intensity-based optical fiber intrusion detector. *Optical Engineering*, 51(3):034402–1, 2012.

[153] A. Mendez. Fiber Bragg grating sensors: a market overview. In *Proceedings SPIE Third European Workshop on Optical Fibre Sensors*, page 661905, 2007.

[154] V. V. Spirin, M. G. Shlyagin, S. V. Miridonov, R. Lopez, I. M. Borbon, and P. L. Swart. Localization of a loss-inducing perturbation for a fiber optic alarm-condition sensor using an un-modulated light source. In *Proceedings IEEE 15th Optical Fiber Sensors Conference Technical Digest*, pages 423–426, 2002.

[155] Y. Zhang, S. Li, Z. Yin, and H.Cui. Unattended ground sensor based on fiberBragg grating technology. In *Proceedings SPIE*, volume 5796, pages 133–140, 2005.

[156] J. Dorleus, Y. Zhang, J. Ning, T. Koscica, H. Li, and HL Cui. A fiber optic seismic sensor for unattended ground sensing applications. Technical report, DTIC Document, 2009.

[157] Y. Zhang, J. Ning, T. Koscia, H. Li, and H Cui. A fiber optic seismic sensor for unattended ground sensing applications. *International Test and Evaluation Association Journal*, 30:455–460, 2009.

[158] Q. Jiang, Y. J. Rao, and D. H. Zeng. A fiber-optical intrusion alarm system based on quasi-distributed fiber Bragg grating sensors. In *Proceedings Optical Fiber Sensors Conference*, pages 1–5, 2008.

[159] J. Hao, B. Dong, P. Varghese, J. Phua, and S. F. Foo. An armored-cable-based fiber Bragg grating sensor array for perimeter fence intrusion detection. In *Proceedings SPIE Photonics and Optoelectronics Meetings*, page 83320B, 2011.

[160] A. Catalano, F. A. Bruno, M. Pisco, A. Cutolo, and A. Cusano. Intrusion detection system for the protection of railway assets by using fiber Bragg grating sensors: a case study. In *Proceedings IEEE Third Mediterranean Photonics Conference*, pages 1–3, 2014.

[161] S. Allwood, G.and Hinckley and G. Wild. Optical fiber Bragg grating based intrusion detection systems for homeland security. In *Proceedings IEE Sensors Applications Symposium*, pages 66–70, 2013.

[162] G. Allwood, G. Wild, and S. Hinckley. Fibre optic acoustic sensing for intrusion detection systems. In *Proceedings Acoustics 2011: Breaking New Ground*, pages 89–1–89–6. Australian Acoustical Society, 2011.

[163] G. Allwood, G. Wild, and S. Hinckley. In-ground optical fibre Bragg grating pressure switch for security applications. In *Proceedings SPIE Asia Pacific Optical Sensors Conference*, page 83510N, 2012.

[164] G. Allwood, G. Wild, and S. Hinckley. Programmable logic controller based fibre Bragg grating in-ground intrusion detection system. In *Proceedings 4th Australian Security and Intelligence Conference*, pages 1–8. Security Research Centre, Edith Cowan University, Perth, Western Australia, 2011.

[165] G. Allwood, A. Qandour, S. Hinckley, and Graham Wild. A simple low cost optoelectronic interface for FBG sensors using a raspberry pi. In *Presented at Conference on Optoelectronic and Microelectronic Materials and Devices*, pages 1–4, 2014.

[166] J. A. Sadler. Fibre optic security system, September 29 1981. US Patent 4,292,628.

[167] C. D. Butter. Einbruchssicherungseinrichtung mit einer detektorleitung burglar alarm device with a detector circuit, October 9 1980. DE Patent App. DE19,803,011,052.

[168] J. B. Lamont. Fiber Bragg grating perimeter security system, May 7 2013. US Patent 8,436,732.

[169] R. Willsch, W. Ecke, and G. Schwotzer. Spectrally encoded optical fibre sensor systems and their application in process control, environmental and structural monitoring. In *Proceedings SPIE Congress on Optics and Optoelectronics*, page 59520I, 2005.

[170] R. Willsch, W. Ecke, and H. Bartelt. Optical fiber sensor research and industry in Germany: review and outlook. In *Proceedings SPIE 21st International Conference on Optical Fibre Sensors*, pages 775302–775302, 2011.

[171] P. Lefebvre, A. Vincelette, C. Beaulieu, and P. Ficocelli. Automated manufacturing of fiber Bragg grating arrays. In *Proceedings OSA Optical Fiber Sensors*, page ThE27, 2006.

[172] Electronicast. Fiber optic sensors global market forecast & analysis. Technical report, EletroniCast Consultants, 2014.

[173] BCC Research. Fiber optic sensors: Global markets. Technical report, BCC Research LLC, 2014.

[174] BCC Research. Fiber optic sensors: Global markets. Technical report, BCC Research LLC, 2011.

[175] M. G. Xu, J.-L. Archambault, L. Reekie, and J. P. Dakin. Discrimination between strain and temperature effects using dual-wavelength fibre grating sensors. *Electronics Letters*, 30(13):1085–1087, 1994.

[176] Y. J. Rao, L. Zhang, I. Bennion, A. B. Lobo Ribeiro, and D. A. Jackson. Combined spatial-and time-division-multiplexing scheme for fiber grating sensors with drift-compensated phase-sensitive detection. *Optics Letters*, 20(20):2149–2151, 1995.

[177] Y. J. Rao, D. J. Webb, D. A. Jackson, L. Zhang, and I. Bennion. In-fiber Bragg-grating temperature sensor system for medical applications. *Journal of Lightwave Technology*, 15(5):779–785, 1997.

[178] V. R. Mamidi, S. Kamineni, L. N. S. P. Ravinuthala, S.i S. Madhuvarasu, V. R. Thumu, V. R. Pachava, and K. Putha. Fiber Bragg grating-based high temperature sensor and its low cost interrogation system with enhanced resolution. *Optica Applicata*, 44(2), 2014.

[179] J. Canning, M. Stevenson, K. Cook, M. Aslund, W. Ecke, R. Willsch, H. Bartelt, H. J. Kalinowski, L. Grabarski, V. Oliveira, C. Martelli, A. Braga, N. Groothoff, and G. D. Peng. Optical fibre Bragg gratings for high temperature sensing. In *Proceedings SPIE 20th International Conference on Optical Fibre Sensors*, page 75032N, 2009.

[180] M. A. Romero, A. Calligaris Jr, and M. T. C. Silva. A fiber-optic Bragg-grating temperature sensor for high-voltage transmission lines. In *Proceedings IEEE Microwave and Optoelectronics Conference: Linking to the Next Century*, volume 1, pages 34–38, 1997.

[181] H. Lee, Z. Jin, and M. Song. Investigation of fiber Bragg grating temperature sensors for applications in electric power systems. In *Proceedings SPIE Photonics Asia*, pages 579–584, 2005.

[182] M. Kim, J.-H. Lee, J.-Y. Koo, and M. Song. A study on internal temperature monitoring system for power transformer using pptical fiber Bragg grating sensors. In *Proceedings IEEE International Symposium on Electrical Insulating Materials*, pages 163–166, 2008.

[183] Y. Cheng, X. Tian, J. Jiang, and C. Li. Using fiber Bragg grating sensor on ice monitoring on electric power transmission lines, part i: the measurement of the temperature. In *Proceedings IEEE High Voltage Engineering and Application*, pages 256–259, 2010.

[184] P. Wang, J. Liu, F. Song, and H. Zhao. Quasi-distributed temperature measurement for stator bars in large generator via use of fiber Bragg gratings. In *Proceedings IEEE 6th International Forum on Strategic Technology*, volume 2, pages 810–813, 2011.

[185] K. de Morais Sousa, A. A. Hafner, M. Crespim, J. Somenzi, V. de Oliveira, H. J. Kalinowski, and J. C. C. da Silva. Fiber Bragg grating sensing applications in

temperature monitoring of three-phase induction motors. In *Proceedings IEEE Microwave & Optoelectronics Conferencel*, pages 862–866, 2011.

[186] M. M. Werneck, R. C.s Allil, and B. A Ribeiro. Calibration and operation of a fibre Bragg grating temperature sensing system in a grid-connected hydrogenerator. *Science, Measurement & Technology*, 7(1):59–68, 2013.

[187] M. G. Xu, L. Reekie, Y. T. Chow, and J. P. Dakin. Optical in-fibre grating high pressure sensor. *Electronics Letters*, 29(4):398–399, 1993.

[188] M. G. Xu, H. Geiger, and J. P. Dakin. Fibre grating pressure sensor with enhanced sensitivity using a glass-bubble housing. *Electronics Letters*, 32(2):128–129, 1996.

[189] Y. Liu, Z. Guo, Y. Zhang, K. S. Chiang, and X. Dong. Simultaneous pressure and temperature measurement with polymer-coated fibre Bragg grating. *Electronics Letters*, 36(6):564–566, 2000.

[190] Y. Zhang, D. Feng, Z. Liu, Z. Guo, X. Dong, K. S. Chiang, and B. C. Chu. High-sensitivity pressure sensor using a shielded polymer-coated fiber Bragg grating. *IEEE Photonics Technology Letters*, 13(6):618–619, 2001.

[191] L. Liu, H. Zhang, Q. Zhao, Y. Liu, and F. Li. Temperature-independent FBG pressure sensor with high sensitivity. *Optical Fiber Technology*, 13(1):78–80, 2007.

[192] W. T. Zhang, F. Li, Y. L. Liu, and L. H. Liu. Ultrathin FBG pressure sensor with enhanced responsivity. *Photonics Technology Letters*, 19(19):1553–1555, 2007.

[193] W. Zhang, F. Li, and Y. Liu. Fiber Bragg grating pressure sensor with ultrahigh sensitivity and reduced temperature sensitivity. *Optical Engineering*, 48(2):024402, 2009.

[194] D. Song, J. Zou, Z. Wei, S Yang, and H. Cui. High-sensitivity pressure sensor based on fiber Bragg grating and metal bellows. In *Proceedings SPIE*, volume 7316, 2009.

[195] H. Ahmad, S. W. Harun, W. Y. Chong, M. Z. Zulkifli, M. M. M. Thant, Z. Yusof, and P. Poopalan. High-sensitivity pressure sensor using a polymer-embedded FBG. *Microwave and Optical Technology Letters*, 50(1):60–61, 2008.

[196] H. Ahmad, W. Y. Chong, K. Thambiratnam, M. Z. Zulklifi, P. Poopalan, M. M. M. Thant, and S. W. Harun. High sensitivity fiber Bragg grating pressure sensor using thin metal diaphragm. *IEEE Sensors Journal*, 9(12):1654–1659, 2009.

[197] J. Huang, Z. Zhou, X. Wen, and D. Zhang. A diaphragm-type fiber Bragg grating pressure sensor with temperature compensation. *Measurement*, 46(3):1041–1046, 2013.

[198] J. Huang, Z. Zhou, D. Zhang, and Q. Wei. A fiber Bragg grating pressure sensor and its application to pipeline leakage detection. *Advances in Mechanical Engineering*, 2013, 2013.

[199] V. R. Pachava, S. Kamineni, S. S. Madhuvarasu, and K. Putha. Enhanced sensitivity of FBG pressure sensor using thin metal diaphragm. In *Proceedings OSA International Conference on Fibre Optics and Photonics*, pages TPo–20, 2012.

[200] V. R. Pachava, S. Kamineni, S. S. Madhuvarasu, and K. Putha. A high sensitive FBG pressure sensor using thin metal diaphragm. *Journal of Optics*, 43(2):117–121, 2014.

[201] Y. Xiong, J. He, W. Yang, L. Sheng, W. Gao, and Y. Chen. Research on FBG pressure sensor of flat diaphragm structure. In *Proceedings IEEE, International Conference on Measurement, Information and Control (MIC)*, pages 787–790, 2012.

[202] W. J. Bock, J. Chen, P. Mikulic, and T. Eftimov. A novel fiber-optic tapered long-period grating sensor for pressure monitoring. *Transactions on Instrumentation and Measurement*, 56(4):1176–1180, 2007.

[203] C. Yan, E. Ferraris, T Geernaert, F Berghmans, and D Reynaerts. Development of flexible pressure sensing polymer foils based on embedded fibre Bragg grating sensors. *Procedia Engineering*, 5:272–275, 2010.

[204] C. Yan, E. Ferraris, and D. Reynaerts. A pressure sensing sheet based on optical fibre technology. *Procedia Engineering*, 25:495–498, 2011.

[205] Y. S. Hsu, L. Wang, W.-F. Liu, and Y. J. Chiang. Temperature compensation of optical fiber Bragg grating pressure sensor. *Photonics Technology Letters*, 18(7):874–876, 2006.

[206] C. Wu, Y. Zhang, and B.-O. Guan. Simultaneous measurement of temperature and hydrostatic pressure using Bragg gratings in standard and grapefruit microstructured fibers. *IEEE Sensors Journal*, 11(2):489–492, 2011.

[207] G. Rajan, B. Liu, Y. Luo, E. Ambikairajah, and G.-D. Peng. High sensitivity force and pressure measurements using etched singlemode polymer fiber Bragg gratings. *IEEE Sensors Journal*, 13(5):1794–1800, 2013.

[208] T. Guo, Q. Zhao, Q. Dou, H. Zhang, L. Xue, G. Huang, and X. Dong. Temperature-insensitive fiber Bragg grating liquid-level sensor based on bending cantilever beam. *Photonics Technology Letters*, 17(11):2400–2402, 2005.

[209] K.-R. Sohn and J.-H. Shim. Liquid-level monitoring sensor systems using fiber Bragg grating embedded in cantilever. *Sensors and Actuators A: Physical*, 152(2):248–251, 2009.

[210] C.-W. Lai, Y.-L. Lo, J.-P. Yur, and C.-H. Chuang. Application of fiber Bragg grating level sensor and fabry-perot pressure sensor to simultaneous measurement of liquid level and specific gravity. *IEEE Sensors Journal*, 12(4):827–831, 2012.

[211] L. Meng, Y. Liu, and T. Wang. A novel liquid level monitoring sensor system using a fiber Bragg grating. In *Proceedings IET International Conference on Smart and Sustainable City*, pages 145–148, 2013.

[212] Y. Dai, Q. Sun, J.i Wo, X. Li, M. Zhang, and D. Liu. Highly sensitive liquid-level sensor based on weak uniform fiber Bragg grating with narrow-bandwidth. *Optical Engineering*, 51(4):044401, 2012.

[213] K. Fukuchi, S. Kojima, Y.i Hishida, and A. Hongo. Optical water-level sensing systems using fiber Bragg grating. In *Proceedings SPIE Photonics Asia*, pages 54–61, 2002.

[214] D. Sengupta, M. S. Shankar, P. V. Rao, P. S. Reddy, R. L. N. S. Prasad, P. Kishore, and K. Srimannarayana. Temperature compensated liquid level sensor using FBGs and a bourdon tube. In *Proceedings SPIE Asia Communications and Photonics*, page 83110R, 2011.

[215] S. Khaliq, S. W. James, and R. P. Tatam. Fiber-optic liquid-level sensor using a long-period grating. *Optics Letters*, 26(16):1224–1226, 2001.

[216] B. Yun, N. Chen, and Y. Cui. Highly sensitive liquid-level sensor based on etched fiber Bragg grating. *Photonics Technology Letters*, 19(21):1747–1749, 2007.

[217] C. Mou, K. Zhou, L. Zhang, and I. Bennion. Thermal insensitive optical liquid level sensor based on excessively tilted fibre Bragg grating. In *Proceedings OSA Asia Optical Fiber Communication and Optoelectronic Exposition and Conference*, page SuR5, 2008.

[218] C. Mou, K. Zhou, Z. Yan, H. Fu, and L Zhang. Liquid level sensor based on an excessively tilted fibre grating. *Optics Communications*, 305:271–275, 2013.

[219] B. Gu, W. Qi, Y. Zhou, J. Zheng, P. Shum, and F. Luan. High-performance reflective liquid level sensor based on titled fiber Bragg grating inscribed in the thin-core fiber. In *Proceedings OSA Optical Fiber Communication Conference*, pages Th2A–34, 2014.

[220] Y. Zhao, K. Chen, and J. Yang. Novel target type flowmeter based on a differential fiber Bragg grating sensor. *Measurement*, 38(3):230–235, 2005.

[221] P. Lu and Q. Chen. Fiber Bragg grating cantilever sensor system for fluid flow monitoring with temperature compensation. In *Proceedings SPIE 21st International Conference on Optical Fibre Sensors (OFS21)*, page 77538L, 2011.

[222] W. Yao, W. Peng, X. Zhang, X. Zhou, and Y. Liu. Self-compensating fiber optic flow sensor based on dual fiber Bragg gratings. In *Proceddings SPIE 6th International Symposium on Advanced Optical Manufacturing and Testing Technologies (AOMATT 2012)*, page 84181U, 2012.

[223] I. Latka, T. Bosselmann, W. Ecke, and M. Willsch. Monitoring of inhomogeneous flow distributions using fibre-optic Bragg grating temperature sensor arrays. In *Proceedings SPIE Photonics Europe*, page 61892G, 2006.

[224] L. J. Cashdollar and K. P. Chen. Fiber Bragg grating flow sensors powered by in-fiber light. *IEEE Sensors Journal*, 5(6):1327–1331, 2005.

[225] P. Caldas, P. A. S. Jorge, G. Rego, O. Frazão, J. L. Santos, L. A. Ferreira, and F. Araújo. Fibre optic hot-wire flowmeter based on a metallic coated hybrid LPG-FBG structure. In *Proceedings SPIE Fourth European Workshop on Optical Fibre Sensors*, page 76530B, 2010.

[226] P. Caldas, P. AS Jorge, G.r Rego, O. Frazão, J. L. Santos, L. A. Ferreira, and F. Araújo. Fiber optic hot-wire flowmeter based on a metallic coated hybrid long period grating/fiber Bragg grating structure. *Applied Optics*, 50(17):2738–2743, 2011.

[227] L. Rodriguez-Cobo, M. A. Quintela, M. Lomer, A Cobo, and J. M. Lopez-Higuera. Pipe flow speed sensor based on fiber Bragg gratings. In *Proceedings SPIE 22nd International Conference on Optical Fiber Sensor*, page 84214E, 2012.

[228] P. Salgado, M. L Filograno, F. D Senent, and P. Corredera. Non-intrusive measurement of internal pressure and flow in pipelines using fiber Bragg grating. In *Proceedings SPIE Photonics North*, page 89151J, 2013.

[229] Q. Jiang and F. Gao. Simulation and design of a fiber Bragg grating flow sensor. In *Proceedings SPIE Sixth International Symposium on Precision Mechanical Measurements*, page 89162M, 2013.

[230] C. R. Zamarreñoa, C. Martellib, V. H. V. Baroncinib, E. N. dos Santosb, M. J. da Silvab, R. E. M. Moralesc, I. R. Matiasa, and F. J. Arreguia. Optical fiber Bragg grating mesh for multiphase flow sensing. In *Proceedings SPIE Vol*, volume 9157, pages 91578U–1, 2014.

[231] C. R. Zamarreño, F. J. Arregui, I. R. Matias, C. Martelli, V. H. V. Baroncini, E.N dos Santos, M. J. da Silva, and R. E. M. Morales. Fluid turbulence monitoring by means of FBG mesh. *IEEE Sensors Journal*, pages 1150–1152, 2014.

[232] G. Meltz, W. W. Morey, and J. R. Dunphy. Fiber Bragg grating chemical sensor. In *Proceedings SPIE Chemical, Biochemical, and Environmental Fiber Sensors III*, pages 350–361, 1992.

[233] P. Lu, L. Men, and Q. Chen. Polymer-coated fiber Bragg grating sensors for simultaneous monitoring of soluble analytes and temperature. *IEEE Sensors Journal*, 9(4):340–345, 2009.

[234] A. Richter, G. Paschew, S. Klatt, J. Lienig, K-F Arndt, and H-J P Adler. Review on hydrogel-based pH sensors and microsensors. *Sensors*, 8(1):561–581, 2008.

[235] J. Cong, X. Zhang, K. Chen, and J. Xu. Fiber optic Bragg grating sensor based on hydrogels for measuring salinity. *Sensors and Actuators B: Chemical*, 87(3):487–490, 2002.

[236] O. Frazão, D. A. Pereira, J. L. Santos, I. Dias, J. M. Dias, N. Vaz, M. Teixeira, A. Quintela, J. Ferreira, L. A. Ferreira, and F. M. Araujo. Industrialization of advanced optical technologies for environmental monitoring. *Clean Technologies and Environmental Policy*, 12(1):65–73, 2010.

[237] K. V. Madhav, R. K. Kumar, T. Srinivas, and S. Asokan. Fiber Bragg grating magnetic field sensor. In *Proceedings 23rd IEEE Instrumentation and Measurement Technology Conference*, pages 2042–2044, 2006.

[238] Y. Zhu, P. Shum, C. Lu, B. M. Lacquet, P. L. Swart, and S. J. Spammer. Temperature-insensitive fiber Bragg grating accelerometer. *Photonics Technology Letters*, 15(10):1437–1439, 2003.

[239] B.-O. Guan, H.-Y. Tam, and S.-Y. Liu. Temperature-independent fiber Bragg grating tilt sensor. *Photonics Technology Letters*, 16(1):224–226, 2004.

[240] R. A. Perez-Herrera and M. Lopez-Amo. Fiber optic sensor networks. *Optical Fiber Technology*, 19(6):689–699, 2013.

[241] R. W. Fallon, L. A. Everall, L. Zhang, and I. Bennion. Multiple-strain-sensor interrogation with an asymmetric grating. In *Proceedings of IEEE Lasers and Electro-Optics Conference Technical Digest*, pages 423–424, 1998.

[242] A. A. Chtcherbakov and P. L. Swart. Chirped fiber-optic Bragg grating interrogator in a multiplexed Bragg grating sensor configuration. *Journal of lightwave technology*, 22(6):1543, 2004.

[243] C.-C. Ye, S. E. Staines, S. W. James, and R. P. Tatam. A polarization-maintaining fibre Bragg grating interrogation system for multi-axis strain sensing. *Measurement Science and Technology*, 13(9):1446, 2002.

[244] S. Abad, F. M. Araújo, L. A. Ferreira, J. L. Santos, and M. López-Amo. Bragg-grating interrogation scheme using spectral filtering and amplitude-to-phase optical conversion. In *Proceedings IEEE 15th Optical Fiber Sensors Conference Technical Digest*, pages 103–106, 2002.

[245] J. S. Roths, C. Kuttler, and C. Gerz. robust interrogation system for fiber Bragg grating sensors. In *Proceedings Lasers and Electro-Optics Europe*, page 461, 2005.

[246] R. Beccherelli, L. De Sio, C. Umeton, D. Donisi, A. d'Alessandro, and M. A. Caponero. Fiber Bragg grating interrogation system based on a novel integrated optical filter. In *Proceedings IEEE Sensors*, pages 140–143, 2008.

[247] P. Tsai, F. Sun, G. Xiao, Z.i Zhang, S. Rahimi, and D. Ban. A new fiber-Bragg-grating sensor interrogation system deploying free-spectral-range-matching scheme with high precision and fast detection rate. *Photonics Technology Letters*, 20(4):300–302, 2008.

[248] J. Villatoro, V. Finazzi, V. P Minkovich, and G. Badenes. Compact all-fiber interrogation unit for FBG sensors. In *Proceedings OSA Optical Fiber Communication Conference*, page OWO4, 2008.

[249] W. Kunzler, Z. Zhu, R. Selfridge, S. Schultz, and M. Wirthlin. Integrating fiber Bragg grating sensors with sensor networks. In *Proceedings IEEE AUTOTEST Conference*, pages 354–359, 2008.

[250] W. Kunzler, J Newmann, D. Wilding, Z. Zhu, T. Lowder, R. Selfridge, and St. Schultz. Advanced FBG sensing through rapid spectral interrogation. In *Proceedings SPIE*, volume 6933, page 69330D, 2008.

[251] P. Orr and P. Niewczas. Polarization-switching FBG interrogator for distributed point measurement of magnetic field strength and temperature. *IEEE Sensors Journal*, 11(5):1220–1226, 2011.

[252] B. D. Hockaday and J. P. Waters. Direct optical-to-mechanical actuation. *Applied Optics*, 29(31):4629–4632, 1990.

[253] M. Mahmoud. Modelling of all optical control systems based on fiber Bragg gratings technology. In *Proceedings IEEE American Control Conference*, volume 4, pages 3353–3357, 2003.

[254] G. Allwood, G. Wild, and S. Hinckley. Power over fibre: material properties of homojunction photovoltaic micro-cells. In *Proceedings Sixth IEEE International Symposium on Electronic Design, Test and Application*, pages 78–82, 2011.

[255] E. Oliva, F. Dimroth, and A. W. Bett. GaAs converters for high power densities of laser illumination. *Progress in Photovoltaics: Research and Applications*, 16(4):289–295, 2008.

[256] S. J. Wojtczuk. Long-wavelength laser power converters for optical fibers. In *Proceedings IEEE 26th Photovoltaic Specialists Conference*, pages 971–974, 1997.

[257] J.-G. Werthen. Powering next generation networks by laser light over fiber. In *Proceedings OSA Optical Fiber Communication Conference*, page OWO3, 2008.

[258] Z. Ping, P. Shiyong, and L. Yong. The research on the network optical fiber sensor of the surface temperature measurement for a large rotor based on IEEE1451.2. In *Proceedings IEEE 8th International Conference on Electrical Machines and Systems*, volume 3, pages 2434–2436, 2005.

[259] Z. Ping, P. Shiyong, C. Changju, and R. Yinlu. Research on a networked optical fiber temperature sensor of large power transformer windings. In *Proceedings IEEE International Conference on Industrial Informatics*, pages 515–518, 2006.

[260] Y. Zhang. Real-time monitoring of the security for the large construction with wireless FBG sensor network. In *Proceedings IEEE International Conference on E-Business and E-Government*, pages 1–4, 2011.

[261] G. Wild, S. Hinckley, and P. Janzs. A transmit reflect detection system for fiber Bragg grating photonic sensors. In *Proceedings SPIE*, volume 6801, 2008.

[262] G. Wild and S. Hinckley. An intensiometric detection system for fibre Bragg grating sensors. In *Proceedings IEEE Australian Conference on Optical Fibre Technology*, page 2, 2008.

[263] G. Wild, G. Swan, and S. Hinckley. A fibre bragg grating based reed switch for intrusion detection. In *Conference on Lasers and Electro-Optics/Pacific Rim*, page C1080. Optical Society of America, 2011.

[264] S. M. Melle, K. Liu, and R. M. Measures. A passive wavelength demodulation system for guided-wave Bragg grating sensors. *IEEE Photonics Technology Lettters.*, 4(5):516–518, 1992.

[265] P. Vengal Rao, K. Srimannarayana, M. S. Shankar, P. Kishore, and S. R. Prasad. Enhanced sensitivity of FBG pressure sensor using thin metal diaphragm. In *Proceedings of OSA, International Conference on Fiber Optics and Photonics*, 2012.

[266] P. Vengal Rao, K. Srimannarayana, M. Sai Shankar, and P. Kishore. A high sensitive FBG pressure sensor using thin metal diaphragm. *Journal of Optics*, 43(2):117–121, 2014.

[267] PASCO Scientific. PASCO stress strain apparatus instruction manual ap-8214A. Technical report, PASCO Scientific.

[268] S. Timoshenko and S. Woinosky-Krieger. *Theory of plates and shells*. McGraw Hill Clasic Textbook Reissue, USA, 1987.

[269] Z. Feng, Q. Wang, and K. Shida. Design and implementation of a self-validating pressure sensor. *IEEE Sensors Journal*, 9(3):207–218, 2009.

[270] G. Wild and S. Richardson. Numerical modeling of intensity-based optical fiber Bragg grating sensor interrogation systems. *Optical Engineering*, 52(2):1–9, 2013.

[271] V. P. Benjamin, K. N. Madhusoodanan, P. Vinod, and P. Radhakrishnan. A novel fiber Bragg grating sensor for measuring weight. In *Proceedings IEEE India Conference*, pages 1–3, 2011.

[272] T. Matsumura, K. Nakamura, and S. Ueha. A load cell using an optical fiber bragg grating with inherent mechanical temperature compensation. In *Proceedings IEEE Optical Fiber Sensors Conference Technical Digest*, pages 347–350, 2002.

[273] R. B. Wagreich, W. A. Atia, H. Singh, and J. S. Sirkis. Effects of diametric load on fibre Bragg gratings fabricated in low birefringent fibre. *Electronics Letters*, 32(13):1223–1224, 1996.

[274] F. Urban, J. Kadlec, R. Vlach, and R. Kuchta. Design of a pressure sensor based on optical fiber Bragg grating lateral deformation. *Sensors*, 10(12):11212–11225, 2010.

[275] B. J. C. Birch. *Simulation of fibre Bragg grating (FBG) reflection spectrums using OptiGrating*. PhD thesis, University of Southern Queensland, 2013.

[276] G. Wild, G. Allwood, and S. Hinckley. Distributed sensing, communications, and power in optical fibre smart sensor networks for structural health monitoring. In *Proceeding IEEE Sixth International Conference on Intelligent Sensors, Sensor Networks and Information Processing*, pages 139–144, 2010.

[277] L. Jiansheng, L. Zhang, J.and Xin, and Z. Zheng. Study on multiplexing ability of identical fiber Bragg gratings in a single fiber. *Chinese Journal of Aeronautics*, 24(5):607–612, 2011.

[278] C. Bejan, M. Iacob, and G. Andreescu. SCADA automation system laboratory, elements and applications. In *Proceedings 7th Int. Symp. Intelligent Systems and Informatics*, pages 181–186, 2009.

[279] K. Wen, L. Yan, W. Pan, and B. Luo. Design of fibre Bragg gratings with arbitrary reflective spectrum. *Optical Engineering*, 50(5):054003, 2011.

[280] L. C. S. Nunes, B. S. Olivieri, C. C. Kato, L. C. G. Valente, and A. M. B. Braga. FBG sensor multiplexing system based on the TDM and fixed filters approach. *Sensors and Actuators A: Physical*, 138(2):341–349, 2007.

[281] M. Popp and P. Wenzel. PROFInet linking worlds. In *Proceedings 8th IEEE Int. Conf. Emerging Technologies and Factory Automation*, volume 2, page 519512, 2001.

[282] W. R. Allan, Z. W. Graham, J. R. Zayas, D. P. Roach, and D. A. Horsley. Multiplexed fiber Bragg grating interrogation system using microelectromechanical fabry-perot tunable filter. *Sensors*, 9(8):936943, 2009.

[283] Siemens. Siemens annual report 2014. Technical report, Siemens, 2014.

[284] Schneider Electric. Schneider electric financial and sustainable development annual report 2013. Technical report, Schneider Electric, 2013.

[285] Rockwell Automation. Rockwell automation 2013 annual report and form 10-k. Technical report, Rockwell Automation, 2013.

[286] HMS Industrial Networks. Anybus compactcom profinet io 2-port. Technical report, HMS Industrial Networks, 2011.

[287] W. W. Ng, K. Nakano, Y. Z. Liu, and P. Daniel. A monolithic GaInAsP/InP photovoltaic power converter. *Trans. Electron Devices*, 29:14491454, 1982.

[288] JDS Uniphase. 12 v photovoltaic power converter. Technical report, JDS Uniphase, 2006.

[289] G. Coley. Beaglebone black system reference manual, 2013.

[290] ZigBee Alliance. IEEE 802.15. 4, zigbee standard. *On http://www.zigbee.org*, 2009.

[291] J. A. Gutierrez, E. H. Callaway, and R. L. Barrett. *Low-rate wireless personal area networks: enabling wireless sensors with IEEE 802.15. 4*. IEEE Standards Association, 2004.

[292] G.-C. Lin, L. Wang, C. C. Yang, M. C. Shih, and T. J. Chuang. Thermal performance of metal-clad fiber bragg grating sensors. *Photonics Technology Letters*, 10(3):406–408, 1998.

[293] A. Cusano, A. Cutolo, and J. Albert. *Fiber Bragg Graing Sensors: Research Advancements, Industrial Applications ans Market Expoitation*. Bentham Science, Sharjah, UAE, 2014.